Competitive Interactions Between Copper(II) ions, Thiomolybdates, and some Biological Ligands

A Thesis Submitted to the College of
Graduate Studies and Reasearch
In Partial Fulfillment of the Requirements
For the Degree of Doctor of Philosophy
In the Department of Chemistry
University of Saskatchewan
Saskatoon

By

Emmanuel Kobina Quagraine
Fall 2002

PERMISSION TO USE

In presenting this thesis in partial fulfillment of the requirements for a Postgraduate degree from the University of Saskatchewan, I agree that the Libraries of this University may make it freely available for inspection. I further agree that permission for copying of this thesis in any manner, in whole or in part for scholarly purposes may be granted by the professor who supervised my thesis work or, in his absence, by the Head of the Department or the Dean of the College in which my thesis work was done. It is understood that any copying or publication or use of this thesis or parts thereof for financial gain shall not be allowed without my written permission. It is also understood that due recognition shall be given to me and to the University of Saskatchewan in any scholarly use which may be made of any material in my thesis.

Request for permission to copy or to make other use of material in this thesis in whole or part should be addressed to:

Head of the Department of Chemistry
University of Saskatchewan
110 Science Place
Saskatoon, Saskatchewan
S7N 5C9
CANADA.

ABSTRACT

Thiomolybdates formed in the rumen have been implicated in copper deficiency in ruminants. However, the chemical basis of the interaction between the individual thiomolybdates and both dietary and systemic copper is poorly understood. Which particular thiomolybdate(s) are formed in the rumen has also been an issue of contention. In part, these problems can be ascribed to lack of availability of synthesized thiomolybdates of known purity.

The main objective of this study was to determine the chemical mechanism by which thiomolybdates render Cu(II) unavailable for utilization in ruminants, particularly cattle.

In the thesis, facile methods are described for the preparation of ammonium dithiomolybdate and tetrathiomolybdate, and of cesium monothiomolybdate and trithiomolybdate. The methods involve successive replacement of the oxygen atoms in sodium molybdate by sulfur atoms using ammonium sulfide. This is the first time the cesium salt of the monothiomolybdate has been reported in pure form. Previous studies in the literature have assumed purity of the thiomolybdates based on elemental analysis; this is not sufficiently discriminating. A more thorough analysis, based on multi-wavelength analyses of the UV/visible spectra of the products, and of mixtures, was used to determine the actual purity of these samples. Discrepancies in previously published spectra for these materials can now be ascribed to unrecognized variations in purity. It is also possible to judge the performance of previously published purification methods of these materials.

The relative proportions of the different thiomolybdates formed under conditions simulating those within the rumen fluid of ruminants prone to copper deficiency have been measured from UV/visible spectra data. Pure synthesized thiomolybdates have also been used to study spectrophotometrically the interactions between the thiomolybdates and Cu(II) in the presence and absence of some inorganic

ligands, low molecular mass complexing agents and bovine serum albumin, in aqueous solutions.

Some small peptides (His-Lys, Thr(Ac)-His-Lys and Asp-Thr(Ac)-His-Lys) were synthesized and characterized and employed as models to study the influence of bovine serum albumin, the main protein for transporting "exchangeable" copper in the blood plasma, on the Cu(II)-thiomolybdate interactions. ^{1}H NMR was used to study the acid-base behaviour of these peptides and their complexation with Cu(II) in H_2O. Changes in the chemical shifts of these peptides were obtained as a function of pH and from these, reliable K_a values have been established. Probable binding sites of Cu(II) and the relative strengths of binding to these peptides are also discussed.

To investigate the possible 3-way interaction between bovine serum albumin, Cu(II) and thiomolybdates, both ^{1}H NMR and UV/visible spectroscopy were used to study the ternary complexation between the peptide models, Cu(II) and thiomolybdates. The results show clearly that ternary complexes, which are poorly soluble in water, are formed between these three species. It was not possible to come to a definite conclusion about the structure of the ternary complex. However, results seem to suggest a core unit where the peptide binds Cu in the +1 state via the terminal amino N, the imidazole N-3 nitrogen and two sulfur atoms from the thiomolybdate. Polymerization of this core unit seems to occur, especially for the interaction involving the tetrathiomolybdate.

Throughout the studies it was noted that tetrathiomolybdate behaved differently from the other thiomolybdates in several respects: stability in aqueous solutions; the kinetics of the interactions with Cu(II); the stability of the resulting products from the interaction with copper(II); the formation of insoluble products and/or polymerization of the core units of the ternary complex initially formed.

ACKNOWLEDGMENTS

I would first like to thank God who works in man to will and to do what is good. To my supervisor, Dr. R. S. Reid, I wish to say big Thanks for all the patience, assistance, support and guidance throughout the course of this study. His criticisms and suggestions were very instrumental in the successful completion of this work.

I would also like to thank the other members of my supervisory committee for their helpful suggestions and discussions: Dr. R. G. Sutherland, Dr. H.-B. Kraatz, Dr. M. Singh (chairman of the committee), Dr. D. A. Christensen, and Dr. S. G. Urquhart.

The assistance given by Dr. K. Brown, Mr. K. Thoms, and Mr. B. Wilson in collecting various analytical data was really appreciated.

I gratefully acknowledge the help and encouragement of the past and present members of the group: Miss. M. Budu, Miss A. Dahl, Dr. M. A. Attaelmannan, Mr. K. Wong, Mr. D. Thome, Mr. M. T. Bagonluri and Mr. J. Essilfie-Dughan. I also wish to thank the many friends in Saskatoon, who are too numerous to mention, in particular Dr. S. Abaidoo, Dr. Y. Adu-Gyamfi, Mr. W. Pearson, Mr. S. Gyepi-Garbrah, Mr. F. Appoh, Mr. G. Quainoo and Miss I. Bediako.

To my wife Janet and my children, Emmanuel (Jr), Theresa, Theodocia and Eunice, I dearly appreciate your various sacrifices that were very instrumental in the completion of this thesis.

The financial support of the University of Saskatchewan, The Department of Chemistry, The College of Graduate Studies and The Agricultural Development Fund (ADF) of the Province of Saskatchewan is gratefully acknowledged.

To

My beloved, hardworking wife, Janet and my cooperating children: Emmanuel, Theresa, Theodocia and Eunice.

TABLE OF CONTENTS

LIST OF TABLES

LIST OF FIGURES

LIST OF ABBREVIATIONS

a_x	Activity of species x
A_x	Absorbance of species x
acac	acetylacetone
Ala	Alanine
Arg	Arginine
Asn	Asparagine
Asp	Aspartic acid
bipy	2, 2?bipyridine
Boc	t-Butoxycarbonyl
Bp	dihydrobis(3,5-dimethylpyrazoyl)borate
Bpoc	Biphenylisopropyloxycarbonyl
BSA	Bovine serum albumin
^{13}C NMR	carbon-13 nuclear magnetic resonance
CSA	Canine serum albumin
COSY	Correlation spectroscopy
DCC	1,3-Dicyclohexylcarbodiimide
DCM	Dichloromethane
DM	Dry matter
DSS	Sodium dimethyl –2-silapentane-5-sulphonate
DMSO	Dimethyl sulphoxide
DMF	Dimethyl formamide
DNP	Dinitrophenyl
dtc	dithiocarbamate
E^0	Standard Reduction Potentials vs NHE
EDC	1-(3-dimethylaminopropyl)-3-ethyl-carbodiimide hydrochloride
EDTA	Ethylenediaminetetraacetic acid
en	1,2-ethanediamine (ethyelendiamine)
ESMS	Electrospray mass spectroscopy
Et	Ethyl

EXAFS	Extended X-ray Absorption Fine Structure
Exp	Experimental
FAB	Fast-atom bombardment
F-moc	Fluorenylmethoxycarbonyl
GIT	Gastro-intestinal tract
HOBt	N-hydroxybenzotriazole
HOMO	Highest occupied molecular orbital
HOSu	N-hydroxysuccinimide
hr	Hour(s)
HSA	Human serum albumin
Hz	Cycles per second
I	Ionic strength
I	Nuclear spin quantum number
IR	Infrared
K_a	Acid dissociation constant
K_f	Formation constant
K_{sp}	Solubility constant
KHP	Potassium hydrogen phthalate
LMM	Low molecular mass
LUMO	Lowest unoccupied molecular orbital
Me	Methyl
M	Molarity = moles solute/L solution
MHz	MegaHertz
min	Minute(s)
m**M**	Millimolar
^{95}Mo NMR	Molybenum-95 nuclear magnetic resonance
N	Natural abundance
NBA	m-Nitrobenzyl alcohol
NEXAFS	Near Edge X-ray Absorption Fine Structure
NHE	Normal Hydrogen Electrode
NIST	National Institute of Standards and Technology

NMR	Nuclear magnetic resonance
Obs	observed
pH	Negative log of the hydrogen ion activity (see Section 1.11.1.1 for details)
Ph	Phenyl
phen	1,10-phenanthroline
pK_a	Negative log of the acid dissociation constant
pK_w^c	Negative log of the concentration autoionisation constant for H_2O
ppm	Parts per million
ppb	Parts per billion
Pr	Propyl
PSA	Pig serum albumin
Pz	Pyrazoyl
R	Residual factor
R^2	Correlation coefficient
RSA	Rat serum albumin
S	Square root of the sum of squares factor
T	Tesla
T_1	Spin-lattice relaxation time
T_2	Spin-spin relaxation time
TBAF	Tetrabutylammonium fluoride
TFA	Trifluoroacetic acid
TM	Thiomolybdate
TM1	Monothiomolybdate ($MoSO_3^{2-}$)
TM2	Dithiomolybdate ($MoS_2O_2^{2-}$)
TM3	Trithiomolybdate (MoS_3O^{2-})
TM4	Tetrathiomolybdate (MoS_4^{2-})
TLC	Thin layer chromatography
Tosyl	p-Toluene sulfonyl
Trityl	triphenylmethyl
UV	Ultraviolet

XPS	X-ray Photoelectron Spectroscopy
XANES	X-ray Absorption Near Edge Structure
Z	Benzylcarbonyl
z_x	Charge of the ion x
α_x	Molar fraction of species x
ε	Molar absorptivity
δ	Chemical shift
λ	Wavelength
μ	Micro
ΔG^o	Change in the free energy per mole
^oC	Degree celsius

1. INTRODUCTION

1.1 CHEMICAL PROPERTIES OF COPPER

Copper (Cu), element 29, is a member of the first transition series and therefore can form colored complexes due to partially filled 3d orbitals. The configuration in the ground state is $[Ar]3d^{10}4s^1$. As expected for a typical transition element, Cu is a metal; can serve as a catalyst (e.g. in the oxidation of organic molecules by O_2); exists in a variety of oxidation states ranging from 0 in the metal to +4; and gives rise to ions which readily form complexes, yielding an extensive variety of coordination compounds (87H, 81J). By far the most common oxidation states for Cu are the +1 and the +2 states. The +3 state is not common and the +4 state (e.g. $Cs_2[CuF_6]$) extremely limited (87H).

1.1.1 Redox Properties

Most Cu(I) compounds are readily oxidized to Cu(II) compounds (99CW). The redox properties of Cu(I)/Cu(II) systems are associated with three principal processes (87H): (a) electrolytic oxidation or reduction (Equation 1.1) (b) disproportionation (Equation 1.2) and (c) the oxidation of Cu(I) with O_2 to yield H_2O ultimately (Equation 1.3).

$$Cu^0 \overset{-e^-}{\rightleftharpoons} Cu^+ \overset{-e^-}{\rightleftharpoons} Cu^{2+} + e^- \quad \textbf{(1.1)}$$

$$2Cu^+ \rightleftharpoons Cu^{2+} + Cu^0 \quad \textbf{(1.2)}$$

$$4Cu^+ + O_2 + 4H^+ \longrightarrow 2H_2O + 4Cu^{2+} \quad \textbf{(1.3)}$$

According to the Franck-Condon principle, there must be no movement of the nuclei during the time of electron transfer. Consequently, when a copper ion in a complex undergoes oxidation or reduction, the geometry of the complex species $[Cu^{I}L_n]$ and $[Cu^{II}L_n]$ (where L is a ligand), must be essentially the same before and after the reaction (87H). The only coordination number common to both +1 and +2 states of Cu is four (see Section 1.1.2). However, Cu(I) four-coordinate complexes typically have a reasonably regular tetrahedral geometry, while four-coordinate Cu(II) complexes usually have a compressed tetrahedral geometry or a square planar geometry. Consequently, rearrangement of geometry must occur either before or after electron transfer. The reverse is true; alteration of geometry may facilitate redox processes. For instance, bis-chelates frequently adopt square planar coordination, but are readily forced out of plane by steric hindrances between ligand molecules, leading to modification of their redox properties (81J).

As with any other cation with variable oxidation states, the redox properties of Cu are strongly influenced by the ligands, their disposition in space, and the solvent (81J). Reduction potential (E^0) values, which relate to the ease of reduction, have been reported for various Cu(II)/Cu(I) systems in terms of the ligands present in the complex, (81J). The higher the E^0 the more stable the Cu(I) complex. Conversely, the lower the E^0 the more stable the Cu(II) complex. In general reducing (soft) ligands such as CN^-, I^- and 1,10-phenanthroline (phen) produce the more positive E^0 values and stabilize the Cu(I) state, while hard Lewis acids like ethylenediamine (en) produce very negative E^0 values (81J, 87Ha). For Cu chelates, nonplanar complexes have been found to be easier to reduce than planar complexes;for the latter, the ease of reduction was in the order $N_4 < N_2O_2 < N_2S_2$ (87H).

Due to the sharing between Cu(II) and Cu(III) of square planar coordination geometry, Cu(III)-Cu(II) redox processes are also possible (81J). The +3 state, although not common, is extensively invoked as an intermediate oxidation state in mechanistic studies, especially those involving amino acid species (87H). Cu(III)-peptide complexes are now well known and reduction potentials (E^0) that range from

0.37 to 1.0 V (vs NHE) have been observed. The lower the E^0 value the more stable is the Cu(III)-peptide complex; one low potential Cu(III) complex was sufficiently stable to permit the determination of its crystal structure (83DR). Cu(III)-peptide complexes involving peptides with Histidine(His) at the third position from the amino terminal are reported to undergo rapid oxidative decarboxylation (95MS, 97MF).

1.1.2 Spectroscopic Properties and Coordination Geometry

Cu(I), having a closed shell configuration, $[Ar]3d^{10}$, is diamagnetic. Since it has no vacant d orbitals, it cannot undergo d-d transitions, as observed for Cu(II) (see below). Hence, Cu(I) compounds are usually colorless. However, there are some that are colored, due to charge-transfer transitions (both ligand to metal charge transfer (LMCT) and metal to ligand charge transfer (MLCT)) or intraligand-orbital transitions (81J, 99CW). Although the intraligand-orbital transitions do not involve the metal center directly, any intra-ligand absorptions are often strongly modified on complexing the ligand to the metal center (81J).

The single unpaired electron in the case of Cu(II)($[Ar]3d^9$) makes it paramagnetic. Cu(II) compounds therefore show EPR (electron paramagnetic resonance) signals, and in nuclear magnetic resonance (NMR) spectroscopy the binding of Cu(II) to ligands results in paramagnetic linebroadening and shift effects for the ligand resonances (see Section 1.12.7 for details).

Cu(II) complexes show d-d transitions, that is, they exhibit a spectrum, which is due to transition of electrons from a lower d orbital to a higher d orbital. Such d-d transition is as a consequence of light absorption in the visible region of electromagnetic spectrum (~ 400 to 800 nm) and that is the original of color to partially filled d orbitals where such transitions are possible. Virtually all Cu(II) complexes or compounds are blue or green in color (99CW). The d-d spectra, although composed of broad, overlapping bands, yield considerable information concerning coordination and site symmetry. The d-d transitions are formally forbidden by the Laporte selection rule

($\Delta l = \pm 1$). One reason that may explain why d-d transitions are nevertheless observed is the possible interaction between electronic states and an appropriate vibrational state of the molecule, leading to a vibronic (vibrational-electronic) admixture of states. For such an interaction, it is possible for a non-symmetric vibration of an excited electronic state to give this electronic state a component of the proper symmetry to combine with the initial electronic state. This effect is usually small, and explains the color of $[Cu(H_2O)_6]^{2+}$, for example (81J).

Another reason that may explain why the supposedly forbidden d-d-transition is observed is the removal of the center of symmetry by the coordination sphere itself (i.e., the distortion of the coordination site).

In an electrostatic field due to a set of ligands with octahedral symmetry, the 5d orbitals (which are energetically equivalent in a "free" spherically symmetrical transition metal ion), split into two set of degenerate orbitals, e_g (d_{x2-y2}, d_{z2}) and t_{2g} (d_{xy}, d_{xz} and d_{yz}). Other splittings are observed in ligand fields of different symmetries (i.e tetragonal distortion, square planar, flattened tetrahedron and tetrahedral), as shown in Figure 1.1.

The lowering of the symmetry as discussed above can result from Jahn Teller effects. The Jahn-Teller theorem requires that any nonlinear system with an electronically degenerate ground state will undergo geometrical distortion, i.e. a lowering of the symmetry to remove the orbital degeneracy (87H, 97KS). With Cu(II) and any other d^9 system, the octahedral configuration is unstable because of the ambiguity which results from incomplete occupation of the e_g degenerate orbital (Figure 1.1B). The majority of 6-coordinated octahedral Cu(II) complexes therefore involve elongated tetragonal distortion resulting from having the odd electron in the d_{x2-y2} orbital after splitting the e_g degenerate orbital to two non-degenerate orbitals d_{x2-y2} and d_{z2} (see Figure 1.1). The elongation is along one four-fold axis, so that there is a planar array of tetragonal structure (Figure 1.1C). In the extreme case of this distortion, of course, the elongation leads to a square planar coordination (Figure. 1.1D).

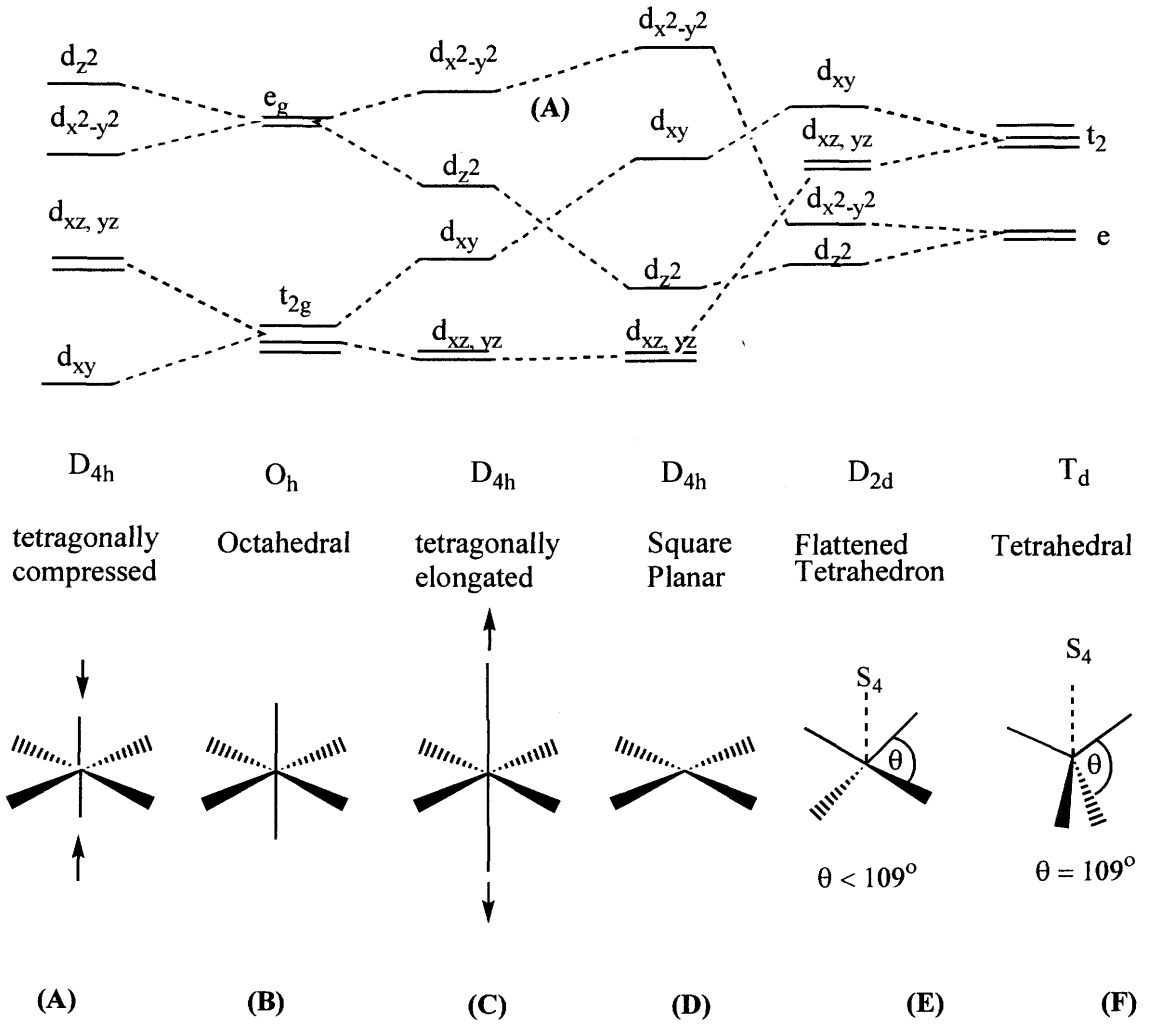

Figure 1.1: Correlation diagram showing splitting of the d orbitals in electrostatic fields arising from some common stereochemistry (81J, 87H).

There are also Cu(II) complexes with compressed tetragonal octahedral structure as shown in Figure 1.1A. The compressed tetragonal distorted octahedron results from having the odd electron in the d_{z^2} orbital. The d^9 configurations of Cu(II) therefore subject its complexes to Jahn-Teller distortion if placed in an environment of cubic (i.e. regular octahedral or tetrahedral) symmetry (99CW) (See Section 1.1.3 for details). For Cu(I) with a d^{10} configuration, all the d orbitals are filled in all the common stereochemistry shown in Figure 1.1. Hence regular octahedral (Figure 1.1B) and tetrahedral (Figure 1.1F) symmetry are possible as discussed in Section 1.1.3.

Cu(III), having a ground state electronic configuration of $[Ar]3d^8$, is unaffected by Jahn-Teller distortion effects.

1.1.3 Coordination Properties

Cu(I) is unstable in aqueous solution, being readily oxidized by O_2 to Cu(II). Cu(I) ions readily form complexes in which the cation serves as a Lewis acid and the ligand as a Lewis base. Cu(I) is classified as a soft acid, forming a wide range of complexes with halides (Cl^-, Br^- and I^-), S, P and N ligands. Although it would be predicted that P is a better soft base than N, more Cu(I) complexes involving N as a ligand have been characterized crystallographically than P complexes (87H). The reducing properties of S, P and I^- ligands, and the ready reduction of Cu(II) ion to stable Cu(I) species with these ligands, accounts for their dominance in Cu(I) complexation chemistry. The Cu(I) cation can form a number of complexes with coordination numbers 2, 3 and 4 (81J, 87H). The 2-coordinated complexes are less common (81J). The most common coordination number is 4 and the geometry is essentially tetrahedral. The 3-coordinated complexes are trigonal planar (81J).

Cu(II), on the other hand, is classified as a borderline hard acid; N-type, O-type, and Cl^- ligands dominate its chemistry, although a fair number of complexes with S ligands are known (98A). With the Cu(II) cation, the hard base function of the ligands is complicated by the tendency to reduce Cu(II) to Cu(I) by even mild reducing ligands, unless the Cu(II) is stabilized by complex formation. In common with most first-row transition metal(II) cations, the coordination number 2 is rare, except for gaseous phase compounds. Cu(II) readily forms coordination complexes involving mainly the coordination numbers 4, 5, and 6. These complexes are mostly distorted due to the Jahn-Teller effect, as discussed in Section 1.1.2.

Thus, even near regular tetrahedral geometry is unknown, and instances of regular octahedral geometry are rare, as mentioned in Section 1.1.2. The majority of

6-coordinated Cu(II) complexes involve elongated tetragonal or rhombic octahedral structure, with a few involving a compressed tetragonal (or rhombic) octahedral structure.

5-coordinated Cu(II) complexes generally involve distorted square pyramidal and distorted trigonal bipyramidal stereochemistry. In the distorted square pyramidal geometry there is both an elongation of the four-fold axis and a trigonal in-plane distortion or, less frequently, a tetrahedral distortion. It rarely involves a regular square pyramidal stereochemistry (87H). Regular trigonal bipyramidal geometry can occur but is more frequently distorted towards square pyramidal geometry.

The 4-coordinate Cu(II) complexes have either tetrahedral geometry, which involves significant compression along the S4 symmetry axis (Figure 1.1E), and regular square planar geometry (Figure 1.1C). Even the latter often involves a slight tetrahedral distortion (87H).

1.2 THE CHEMISTRY OF THIOMOLYBDATES (TMs)

Molybdenum (Mo), element 42, is a member of the second transition series, and exhibits many properties which are due to its partially filled 4d orbitals.For instance, it can exist in variable oxidation states, can play catalytic roles and can form colored complexes.

Mo is a group 6 element and hence its highest oxidation state is +6. Mo has a wide variety of stereochemistries in addition to the variety of oxidation states (from -2 to +6), so its chemistry is among the most complex of the transition elements (99CW). The stereochemistries of Mo compounds in the various oxidation states are well outlined by Cotton et al. (99CW) and complexes of coordination numbers 4 to 9 are all known. The Mo compound stereochemistries which are relevant to this study will be discussed below. These include the tetrahedral geometry of MoS_4^{2-} and the cluster compounds from the reaction of the thiomolybdates with Cu.

Mo has long been known for its biological activity. It is well known for its function in the nitrogenase enzyme, which is responsible for the reduction of atmospheric N_2 to NH_3 and its derivatives. It is also well known in enzymes for the reduction of nitrates and in other biological process (99CW).

Many Mo oxides are known that include simple ones such as molybdenum(VI) oxide (MoO_3), molybdenum(IV) oxide (MoO_2) and more complex ones such as Mo_8O_{23}. Mo sulfides are well known; in fact, Mo occurs chiefly in nature as molybdenite (MoS_2). Other sulfides such as MoS_3, MoS_4, Mo_2S_5 and Mo_2S_3 are also known. The molybdate ion MoO_4^{2-}, which contains Mo(VI), can be obtained from solutions of MoO_3 in aqueous alkali. MoO_4^{2-} is the most stable soluble form of Mo found in nature (in sea water) (97KS). When solutions of molybdates are made weakly acidic, polymeric anions (e.g. $Mo_2O_7^{2-}$) are formed (see Section 1.2.4). In strongly acidic solutions, substances often called molybdic acids (e.g. $HMoO_4^-$, $Mo(OH)_6$) are formed (99CW). Both molybdic acids and the salts of MoO_4^{2-} or $Mo_2O_7^{2-}$ have been reacted with different sources of sulfides to form various thiomolybdates (TMs) as discussed in the next section.

1.2.1 Previous approaches to Thiomolybdate Synthesis

In the early 19th century Berzelius (1826B) reported the formation of $(NH_4)_2MoS_4$ by evaporating a solution of molybdic acid in ammonium sulfide, and later Debray described the formation of $(NH_4)_2MoO_2S_2$ by treating ammonium molybdate with ammonium sulfide (22M). However, the true composition of the products was not established until fairly recently (81MD). Other sulfides have also been reacted with molybdate or polymolybdates (i.e. MoO_4^{2-} and $Mo_2O_7^{2-}$) salts to prepare one or more of the thiomolybdate anions, $MoO_xS_{4-x}^{2-}$, (hereafter referred to as TMs; TM1, TM2, TM3 and TM4 respectively for mono-, di-, tri-, and tetra-thiomolybdate). These include the use of hydrogen sulfide (H_2S) (22M, 81MD, 69ARD, 80HS, 83MF, 00EH, 00L), sodium hydrogen sulfide, NaSH (22M) and sodium sulfide, Na_2S (80CL). In the latter case, the presence of these species was only inferred from buffered solutions at pH 7.

In some cases, H_2S was also used in addition to the Na_2S (87WM, 84HL, 88WM). TM1 (MoO_3S^{2-}) is said to be difficult to isolate (81MD, 80CL, 80HS, 00L, 00EH), and various workers have attempted in vain to produce salts of this anion (81MD). The presence of this anion has therefore been mainly inferred from analysis of aqueous reaction mixtures containing low S: Mo ratios (80CL, 80HS, 00EH).

On the basis of qualitative observations, Müller et al. (81MD) concluded that H_2S and not S^{2-} might be involved in the formation reactions. However, Harmer et al. have proposed HS^- as the most likely nucleophile (80HS). The first and second acid dissociation constants of H_2S are respectively 1.6×10^{-7} and 4.0×10^{-13} (79WL). Thus, whether sulfur (S) is originally added as H_2S, HS^- or S^{2-}, in aqueous solutions at all moderate pH values a significant population of HS^- is present. In fact, all syntheses reported appear to buffer the pH in this range.

Harmer and Sykes (80HS) have observed that the rate of formation of TMs from the sequential displacement of O^{2-} with S^{2-} depends on $[H^+]$. The reverse reaction (hydrolysis) was found to be $[H^+]$ independent at pH > 8. Based on these observations and other trends in their kinetic study of TM formation and hydrolysis, they proposed a mechanism for the sequential displacement of O^{2-} (in oxy(thio)molybdate) where these are first protonated before HS^- acts as a nucleophile as shown in Scheme IA. The prior protonation leads to a subsequent weakening of the Mo-O. An associative type mechanism is presumed. The reverse reaction is also assumed to be an associative process, involving an incoming H_2O as also shown in Scheme IA, where an opportunity is provided for proton transfer to the departing S^{2-}. Harmer and Sykes (80HS) also observed that at lower pHs (3.6-5.6), the hydrolysis of TM3 was $[H^+]$- dependent as opposed to what was observed at higher pHs as mentioned above. They hence suggested an alternative mechanism where H_2S was presumed to be the nucleophile as shown in Scheme IB. This pathway is therefore relevant only at lower pHs (< 6) only.

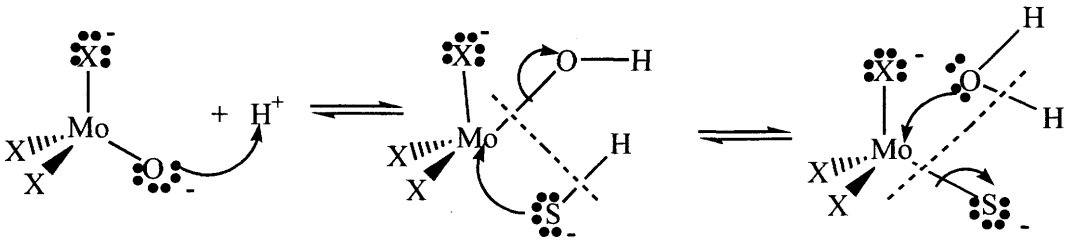

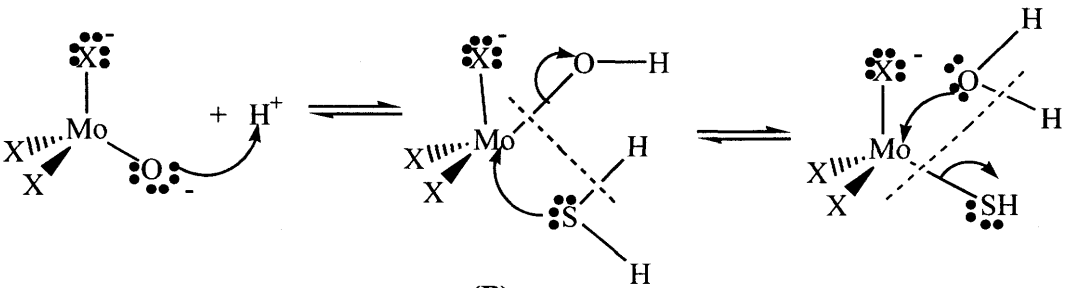

Scheme I

The reaction between MoS_3 and aqueous alkali hydroxides is also known to form TM4 (MoS_4^{2-}) and other TMs. The reactions between MoS_9^{2-} with twice the molar amount of $[SCH_2CH_2S]^{2-}$ also form TM4 (92BC).

1.2.2 Electronic and Spectroscopic Properties of Thiomolybdates

Prediction from the Lewis structure and the valence shell electron-pair repulsion (VSEPR) theory suggest that TMs ($MoO_xS_{4-x}^{2-}$ x = 0 to 3) have a tetrahedral geometry, with two M=S (or O) bonds, and two Mo-S (or O) bonds where each of the two singly bonded S (or O) carries one formal negative charge as shown below.

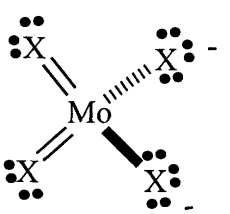

x = O or S

It is obvious that the electrons are not as localized as shown in the Lewis structure above, therefore more resonance structures are expected. The overall effect is to have bond orders of about 1.5 and a 0.5 negative charge on each X.

There are three remarkable and somehow related features of the TMs (00L):

1. The Mo-S bond lengths that have been determined are all similar, 2.15-2.18 Å and between those of double and single bonds (81MD).
2. All the metal centers are in their highest oxidation states (based on EPR (84CBa, 98EL)) despite being coordinated to the strongly reductive S^{2-} ions.
3. The S 3p and the Mo 4d orbital energies are close (98C).

The first feature suggests a π character in the Mo-S bonds as also suggested from molecular orbital calculations (81MD, 00L) and the simple Lewis structure. Similarly, the Mo-O bonds have π character (81MD). Electron delocalisation through π bonding may explain why the TMs do not undergo a spontaneous internal redox reaction. The third feature accounts for the origin of the strong colors of TMs as the S to Mo charge transfer bands (discussed in greater detail in the next paragraph) are of relatively low energy and lie in the visible region. The three features jointly account for the diversity in structural and reactivity characteristics of TMs and the complexes derived from them, as discussed in Sections 1.2.2 to 1.2.6.

The electronic transitions of TMs at low energies are all ligand to metal charge transfer (LMCT) transitions from S^{2-} to Mo (81MD, 00L). See Figure 1.2 for the correlation energy diagram for TM4 (81MD). The molecular orbitals of TM4 (T_d symmetry) that are involved in electronic transitions above 200 nm are the filled $3t_2$, $1t_1$ (HOMO), the empty 2e* (LUMO) and the $4t_2$* orbitals (81MD, 88VK). The $1t_1$ level is a pure S orbital and the $3t_2$ level is largely composed of S orbitals (~90%) with a minor contribution by the Mo (~10%). The empty molecular orbitals 2e* and $4t_2$*, antibonding with respect to Mo-S interaction, are composed of comparable portions of metal and ligand orbitals (88VK).

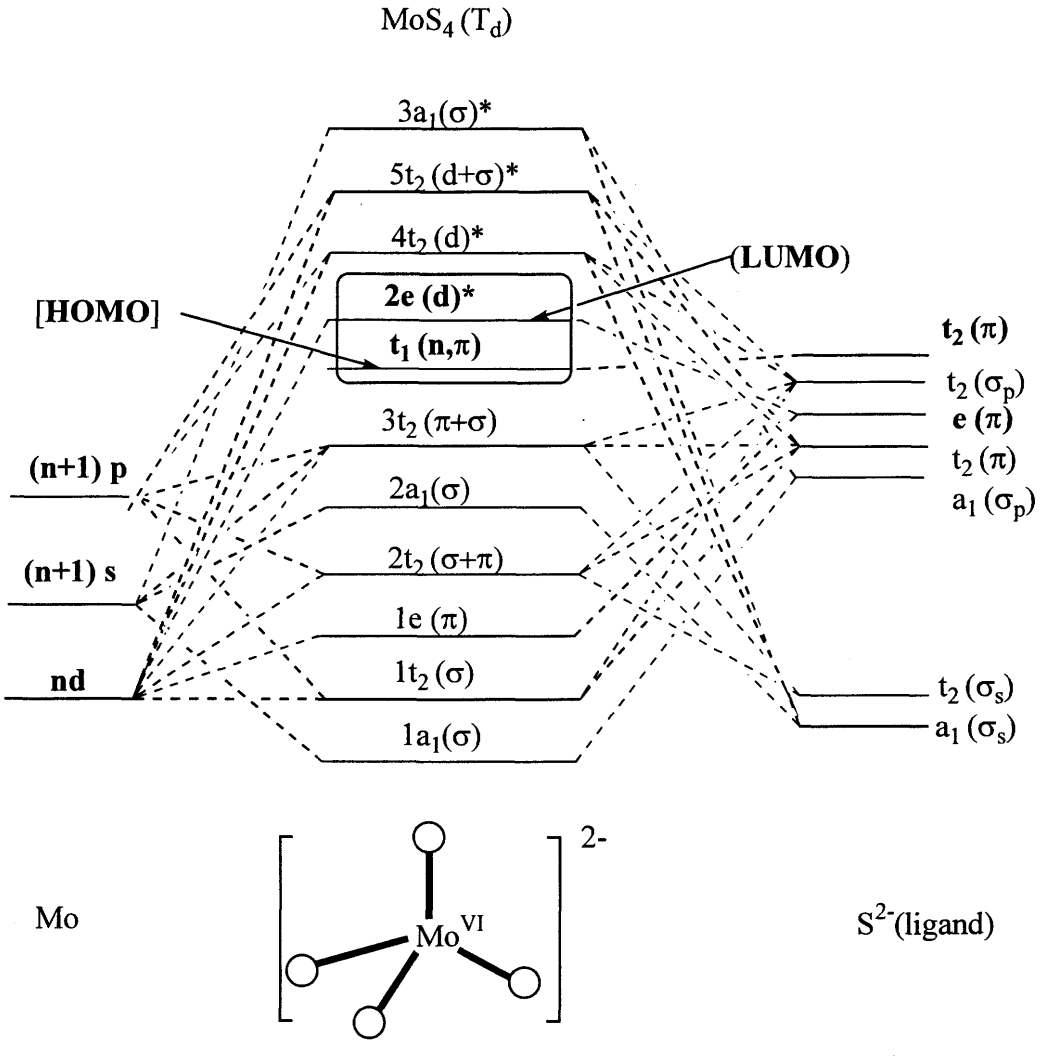

Figure 1.2: Simplified molecular orbital scheme for TM4 with T_d symmetry (81MD)

Figure 1.3 shows the electronic spectrum of TM4 (see Chapter 2 for details). Three bands are seen, labelled ν_1 through ν_3. There is a general consensus on assigning the longest wavelength band, at $\lambda_{max} = 468$ nm to the $1t_1 \rightarrow 2e^*$ transition. The ordering of the higher-energy transitions ($1t_1 \rightarrow 2e^*$, $3t_2 \rightarrow 2e^*$, $1t_1 \rightarrow 4t_2^*$) is uncertain (92BC, 81MD, 88VK, 89EA), although opinion seems to skew towards the order above for the ν_1, ν_2, and ν_3 bands respectively (81MD, 84SM, 87MD).

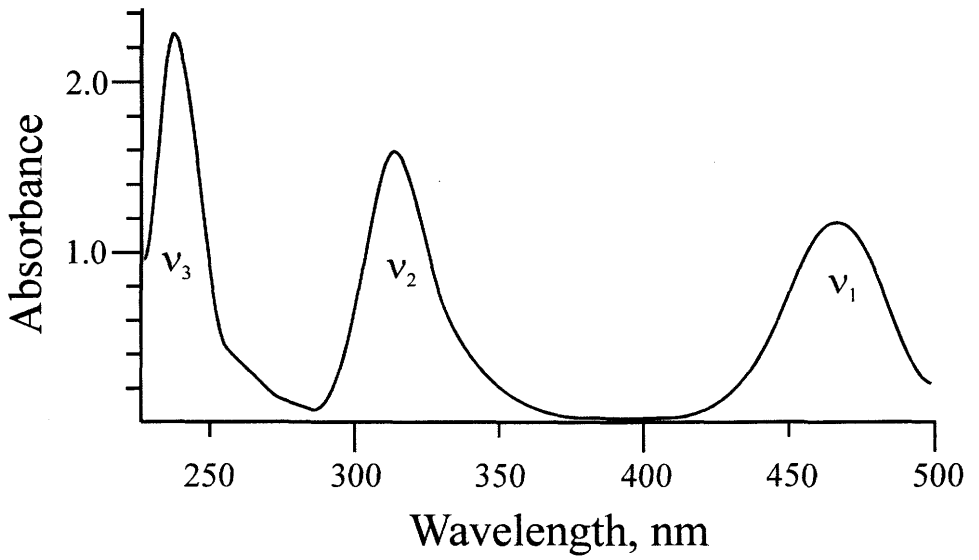

Figure 1.3: UV/visible spectrum of tetrathiomolybdate (TM4).

Symmetry for the (thio)molybdates is T_d for TM4, C_{3v} for TM3, C_{2v} for TM2 C_{3v} for TM1 and T_d for molybdate ("TM0"). Since both C_{3v} and C_{2v} symmetry groups are subgroups of T_d, a correlation of the transformed orbitals in those symmetries to their corresponding T_d orbitals can be made (89EA). For TM3, the nine p orbitals of S atoms will be resolved into 3E, $2A_2$, and A_1 sets while the three p orbitals of the O atom will be resolved into E and an A_1 set. Because of the relative energies of the p orbitals of free S and O, molecular orbitals that contain preponderant O (p) character will be lower in energy than those containing preponderant S (p) character. As in the case for TM4, the longest wavelength band of TM3 can be unambiguously assigned to $\pi(S) \rightarrow$ d (Mo) (or $a_2 \rightarrow$ e) transition. Assignments for TM2 ($MoO_2S_2^{2-}$) and TM1 (MoO_3S^{2-}) are not fully resolved, since calculated wavelengths based on such assignment vary significantly from those observed (89EA).

The TMs and their complexes have been extensively investigated by IR and Raman spectroscopy, especially in respect of their Mo-O and Mo-S stretching vibrations, which occur in the ranges 780-1100 and 400-510 cm^{-1}, respectively (73DM, 87G). Other reported vibrations include; δ (OMoO), δ (SMoS), and δ (OMoS) in the

ranges 280-350, 170-200 and 230-290 cm^{-1} respectively (where δ refers to bending vibrational modes).

For the free TM4 ion four vibrational modes are expected: $\Gamma\ (T_d) = A_1 + E + 2F_2$. All four (i.e. A_1, E, F_2 and $*F_2$, the asterisk being used only to distinguish the two F_2 vibrational modes) are Raman-active and have been observed in DMSO at 458, 184, 472 and 184 cm^{-1} and assigned accordingly as ν_s(MoS), δ (SMoS), ν_{as}(MoS) and δ(SMoS) (73DM). ν_s and ν_{as} refer to symmetrical and asymmetrical stretching vibrations, respectively. A_1 and E, which respectively are nondegerate and doubly degenerate, are both IR-forbidden. In solid compounds, TM4 may have a lower symmetry, leading to splitting of E, and the two triply degenerate modes F_2 and $*F_2$ and consequently making the A_1 and E vibrational modes IR active (92BC). For the Mo-S stretching mode of the TM4 IR spectrum, the symmetric (ν_s) and the asymmetric (ν_{as}) stretching have been observed at 458 cm^{-1} and 472 cm^{-1} respectively, in agreement with the Raman spectrum (73DM, 81MD, 94LN). The vibrational modes for the other 3 TMs, as reported by Diemann and Müller (73DM), are summarized in Table 1.1 below.

Table: 1.1: Vibrational frequencies of TM3, TM2, and TM1 (in cm^{-1}). ν_s, ν_{as}, δ_s, and δ_{as} refer to respectively to symmetric stretching, asymmetric stretching, symmetric bending, asymmetric bending.

	TM3 (C_{3V})	TM2 (C_{2V})	TM1 (C_{3v})
ν_s(MoO)	862	867	882
ν_s(MoS)	461	451	475
δ_s (OMoO)	-	310	331
δ_s (SMoS)	183	200	-
ν_{as}(MoO)	-	842	833
ν_{as}(MoS)	470	471	-
$\delta_{as}(MoO_3)$	-		314
$\delta_{as}(MoS_3)$	183		-
2δ(OMoS)		248 & 270	

1.2.3 Stability of Thiomolybdates

TMs are not very stable in aqueous solution, especially at low pH. The stability decreases with increasing O content (81MD). Hence, the lower S containing TMs (i.e. TM1 and TM2) are less stable. Under oxygen-free nitrogen atmosphere TM4 aqueous solution was found to be stable up to 1 day at 38°C while TM3 showed a 33% decrease in overall absorbance in the first 3 hr (80CL). An aqueous solution of TM4 even under normal conditions can be stable over 2.5 hr at 25°C (82CL).

The stabilities of the TMs in solution are said to depend on the presence (or absence) of O_2 (92BC). TMs are more stable at alkaline pH (22M, 87WM). The half-life, $t_{½}$ for the hydrolysis of TM4 in anaerobic 0.2 **M** sodium phosphate buffer (pH 12) is ~ 170 hr at 25°C (87AK). The stabilities of the TMs in solution may depend on three processes (80HS, 92BC, 81MD):

1. Hydrolysis to form "lower "TMs (those containing less sulfur).
2. Decomposition at high acidity, with precipitation of MoS_3 (80HS, 68SJ) and (probably) MoS_2 (80HS). The formation of the polymeric species "$Mo_2S_7^{2-}$" and "$Mo_4S_{13}^{2-}$" on acidification of TM4 has also been suggested on the basis of conductometric titrations (68SJ), although this claim has not been substantiated (see Section 1.2.4. for details).
3. Decomposition caused by intramolecular redox processes (see Section 1.2.4 for more details).

In unsealed or partially sealed containers the final product for the hydrolysis reaction is MoO_4^{2-} (79WL). This is because any sulfide formed is in acid-base equilibrium with a small amount of H_2S, which can be irretrievably lost by evaporation and thus "pull" the system towards complete reaction.

However, in a closed vessel, higher TMs may be formed, presumably by reaction with the HS- previously liberated by TM hydrolysis. For instance, TM2 can be formed from TM1, and TM3 can be formed from TM2 in aqueous solution over longer periods of time (80CL). The net effect is S atom transfer from one original TM ion to

another, to give both the higher and lower TM, i.e. TM1 gives TM2 and TM0, TM2 gives TM3 and TM1, etc. (80CL).

Generally, the ammonium salts of TMs are relatively unstable as compared to other cationic salts of TMs (81MD). However, freshly prepared solid $(NH_4)_2MoS_4$ can be stored indefinitely in a dry inert atmosphere. Heating of $(NH_4)_2MoS_4$ leads to decomposition to give NH_3 , H_2S and MoS_3. Under N_2, $(Et_4N)_2MoS_4$ is reported to be stable up to 180^0C (92BC). The mechanism of decomposition of $(NH_4)_2MoO_2S_2$ is complex, and the original assumption that $MoOS_2$ is formed as an independent compound has not been clearly confirmed (81MD).

1.2.4 Polythiomolybdates

Despite the great deal of research done on condensations in aqueous solutions of oxometalates in general, there has been little such work in the field of thiometalates (81MD). The condensation reactions subsequent to protonation of thiometalates ions, including TMs, takes place at lower pH values than those of the corresponding oxoanions, since the proton affinity of S is appreciably lower than that of O (87DM). The acid dissociation constant pK_a value of H_2O for instance is 15.7 whereas that of H_2S is 7 (81HS). In fact from known acid dissociation pK_a values, it has been estimated on the basis of pK_a 3.47 for MoO_4H^- that the pK_a of the sulfide that corresponds to this species should be ca. –5 (i.e. extremely small) (81HS). This estimation, although possibly exaggerated, nevertheless points to the fact that the S atoms in TMs are protonated only at lower pH than the O atoms.

Investigation of the condensation behavior of TMs is difficult, since various complex processes are involved. For example, no definite condensation product has yet been isolated from an ***aqueous*** solution containing TM4. The $[Mo_3S_9]^{2-}$ ion, whose two plausible Lewis structures are shown in Figure 1.4, could not be obtained directly from an ***aqueous*** solution but was prepared by heating a solution of $(NH_4)MoS_4$ in an organic solvent (81MD).

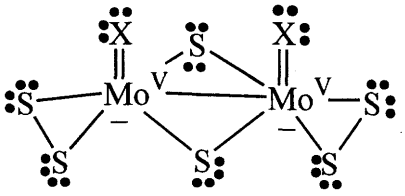

$[Mo_2X_2S_2(S_2)_2]^{2-}$; X = O or S

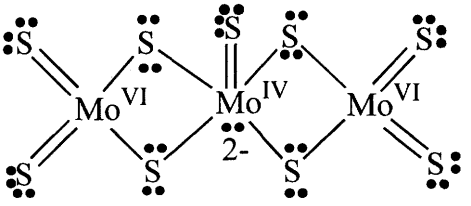

$(Mo_3S_9^{2-})$

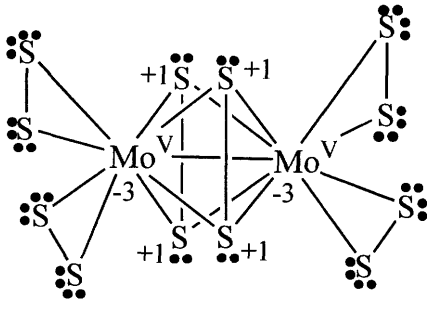

$[Mo_2(S_2)_6]^{2-}$

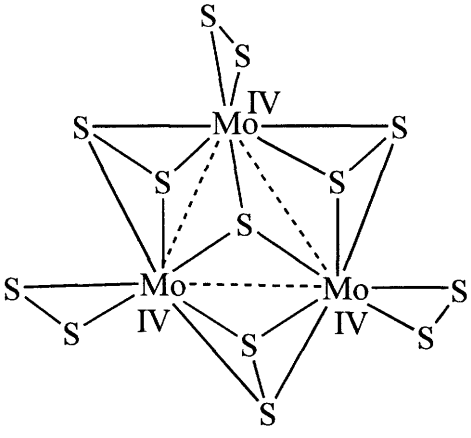

$(Mo_3S_{13}^{2-})$

Figure 1.4: Lewis structures for some polythiomolybdates consistent with reported crystallographic data on $[Mo_2S_7O]^{2-} = [Mo_2OS(\mu\text{-}S_2)(S_2)_2]^{2-}$ (85XM), $[Mo_2S_6O_2]^{2-} = [Mo_2O_2(\mu\text{-}S_2)(S_2)_2]^{2-}$ (79RM), $[Mo_2S_8]^{2-} = [Mo_2S_2(\mu\text{-}S_2)(S_2)_2]^{2-}$ (84PH,92BC), $[Mo_2S_{12}]^{2-}$ (78MN, 92BC), $[Mo_3S_9]^{2-}$ (92BC), and $[Mo_3S_{13}]^{2-}$ (92BC).

Although it was claimed "$[Mo_2S_7]^{2-}$" and "$[Mo_4S_{13}]^{2-}$" could be formed on adding HCl to Na_2MoS_4 solutions in ***water*** to give pH values of 4.5 and 2.8 respectively (68SJ), such claims could not be substantiated by Simpson and Mills (82SMa), who instead observed the formation of insoluble MoS_3 under similar conditions. However, addition of 2 **M** HCl to aqueous solution of ~ 0.16 **M** $(NH_4)_2MoS_4$ (TM4) to obtain a reaction mixture of approximate mole ratio 1:2 (HCl:TM4), caused the precipitation of a dark red solid $(n\text{-}Bu_4N)_2Mo_2OS_7$) in the presence of $n\text{-}Bu_4NBr$ (85XM, 92BC). The structure of the $[Mo_2OS_7]^{2-}$ anion was determined by crystallography (85XM) and is isostructural to both $[Mo_2O_2S_2(S_2)_2]^{2-}$ and $[Mo_2S_4(S_2)_2]^{2-}$ (i.e. $[Mo_2S_8]^{2-}$), which are

discussed below. See Figure 1.4 for the Lewis structure in consistence to the crystallographic data for these three polythiomolybdate complexes (79RM, 85XM, 92BC). A photometric study during gradual acidification suggested that the reaction involves an intermediate hydrolysis to TM3 (85XM).

The oxothiomolybdates (TM1, TM2 and TM3) should show a greater tendency toward condensation than TM4, due to the higher proton affinity of O over S (see earlier part of this section for details). The $[Mo_2O_2S_2(S_2)_2]^{2-}$ anion, isostructural to $[Mo_2OS_7]^{2-}$ as mentioned above (see Figure 1.4), was isolated upon heating an aqueous solution of TM2 to boiling. In the reaction an $(S_2)^{2-}$ ligand is generated by oxidation of two S^{2-} ligands with the reduction of Mo from + 6 to + 5 state (79RM, 87MD). Two S^{2-} sulfur bridges are formed, maintaining two terminal O^{2-} as shown in Figure 1.4. The distance between the two Mo atoms in the $[Mo_2O_2S_2(S_2)_2]^{2-}$ anion as revealed by the crystallographic studies indicate a distance of 2.825 Å. Crystallographic data for the isostructural $[Mo_2S_8]^{2-}$ discussed below indicate a Mo to Mo separation close to this value, (2.821 Å) . The value in $[Mo_2OS_7]^{2-}$ (see above) is 2.811 Å. Such bond separations, according to Xin et al. (85XM) are common to Mo(V)-Mo(V) dimers and indicative of a single Mo-Mo bond as shown in Figure 1.4. Furthermore, the average bond distance 2.111 Å (85XM) for the apical Mo to S in the two isostructural complexes of $[Mo_2O_2S_2(S_2)_2]^{2-}$ is shorter than the typical separation for an Mo-S single bond of ~ 2.4 Å for Mo bonded to an S_2^{2-} group , ~ 2.2 Å for a Mo bonded to S^{2-} bridging atom, and ~ 2.5 Å for Mo bonded to terminal S^{2-} (85XM, 92BC). This suggests a double bond (i.e. Mo=X) and not a single bond for the apical Mo linkage to X. The formal charges will therefore not be on the X atoms as would be expected if the Mo-X bond were single but rather on the two Mo central atoms as shown as accordingly in Figure 1.4.

As should be expected based on the discussion earlier in this section, the initial step of the "condensation" reaction of TM2 to $[Mo_2O_2S_2(S_2)_2]^{2-}$ anion is the protonation at the oxygen, which favors both the condensation as well as the intramolecular redox reaction (79RM). What will be the source of the H^+? The reaction, which was

performed in aqueous solution, was observed to be strongly dependent upon temperature, and hence the formation of H_2S will be inevitable, serving as a source of H^+ upon dissociation in water (see Section 1.2.1 for the K_a values of H_2S). Also, note that the protonation at the oxygen decreases the Mo-O π character, and consequently the oxidizing action and the tendency of the Mo central atom to coordinate increases. Recall from Section 1.2.2 that the stability of the TMs with Mo maintaining the +6 state despite being bonded by the highly reductive S^{2-} is attributed to the π character in the Mo-O or M-S bonds. In fact, the presence of protons has been observed to be necessary for the condensation reactions of TMs in general leading to the polythiomolybdates (88CA).

More recently, an alternative means of preparing polythiomolybdates has emerged, which features lower metal oxidation states and oxidized S ligands such as the persulfide (S_2^{2-}) ion (84GH, 92BC). Mo-Mo and S-S bonding and their interrelationships are a dominant feature of the chemistry of these polythiomolybdates (92BC). The clearest demonstration of this interrelationship is the reaction of TM4 and organic disulfides to form $Mo_2S_8^{2-}$ (structure is isostructural to $Mo_2O_2S_6^{2-}$), involving reduction of Mo (from Mo^{VI} to Mo^{V}), production of (S_2^{2-}) ions and the formation of the Mo-Mo bond (84PH, 90CH):

$$2\ [MoS_4]^{2-} + RSSR \rightarrow [Mo^{V}_2S_4(S_2)_2]^{2-} + 2RS^- \qquad \textbf{(1.4)}$$

An internal (intramolecular) electron transfer from S to Mo induced by the external oxidant, e.g. by organic disulfides, organic diselenides or elemental sulfur (S_8) (84PH, 85PH, 88CA, 89CT, 90CH, 98C, 00L) has been proposed to be the mechanism, since the presence of external oxidants is essential in ensuring the formation of the polythiomolybdates (88CA). In fact, the overall rate of reaction has been found (in the case of the organic disulfides as the external oxidants) to be dependent on the electron-withdrawing properties of the disulfide used (90CH). By using diphenyl diselenide, PhSeSePh as the external oxidant, the same $[Mo^{V}_2S_4(S_2)_2]^{2-}$ is produced (84PH), suggesting that all of the S atoms in the product come from TM4. In this case the

external oxidant, PhSeSePh, takes up two electrons and each of the two Mo atoms takes up one electron (84PH). This therefore requires the donation of four electrons, which come from the conversion of S^{2-} (in TM4) to S_2^{2-} (in polythiomolybdate) (84PH, 00L):

$$4S^{2-} \rightarrow 2S_2^{2-} + 4\ e^- \qquad \textbf{(1.5)}$$

This mechanism accounts for reactions between higher valent molybdenum sulfur compounds with external oxidants to produce a *lower* valent molybdenum compounds, which appears at first sight to be unusual (90CH).

TM4 reactions with polysulfides (S_x^{2-}; $x \geq 2$) to form polythiomolybdates are also well documented, both in aqueous and non-aqueous solutions (92BC). Thus, a reaction between $(NH_4)_2MoS_4$ and ammonium polysulfides in aqueous solution (78MN) for 12 days, and the heating of $(PPh_4)_2MoS_4$ in DMSO with a methanolic polysulfide solution, both yield the dimeric species, $[Mo_2S_{12}]^{2-}$, which involves S_2^{2-} ligands as shown in Figure 1.4. The structure of the $[Mo_2S_{12}]^{2-}$ anion as elucidated by a single-crystal X-ray diffraction analysis of $(NH_4)_2[Mo_2S_{12}].2H_2O$ indicates that the compound exists as two discrete crystallographically independent ions, both with exact C_2 symmetry. One anion has its twofold axis through the Mo-Mo bond and the other anion perpendicular to the Mo-Mo bond (92BC). $(NH_4)_2[Mo_2S_{12}].2H_2O$ is diamagnetic (92BC), suggesting there are no unpaired electrons. The magnetic property and the Mo-Mo separation of 2.827 Å, which is approximately the same as that of the other dimers discussed above, suggest a central Mo-Mo single bond. The S and Mo XPS data are consistent with an effective negative charge of ~ 2 of the disulfido ligands (92BC). The decrease in the Mo 3d binding energies from (232.1 eV) TM4 to (230.3 eV) $[Mo_2S_{12}]^{2-}$ agrees with a change in the Mo oxidation state from +6 to +5 (82MJ). As shown in Figure 1.4, in $[Mo_2S_{12}]^{2-}$ each Mo(V) is coordinated "side on" by four S_2^{2-} groups, two of which are bridging and two terminal.

Other polythiomolybdates, such as the trimeric species, $Mo_3S_{13}^{2-}$, which has the three central Mo in the + 4 states have also been formed from the reaction of TM4 with

polysulfides (81MD, 92BC, 00L). The crystal structure indicates that the three Mo atoms are at the vertices of an equilateral triangle with a unique S atom above the center. There are also bridging as well as terminal S_2^{2-} which lie below and above the Mo_3 plane: $[Mo_3(\mu_3\text{-}S)(\ (\mu_2\text{-}S_2)_3(S_2)_3]^{2-}$. The average Mo-Mo bond distance was 2.725 Å, only a little shorter that the Mo(V)-Mo(V) bond distances of the dimeric species discussed above.

Alkyl halides have also been used in organic solvents (e.g. acetonitrile) to react with TM4 in forming polythiomolybdates (95BW, 01KW). The reaction goes through the intermediate anion $[MoS_3(SR)]^-$ (R = alkyl group), where the Mo-S bond breaks to yield alkyl sulfides, alkyl thiols, and polythiomolybdates such as $Mo_3S_9^{2-}$ above (01KW). In water, TM4 salts with organic cations (but not the NH_4^+ salt), have been identified to be involved in a sulfur transfer reaction with alkyl halides to yield the corresponding alkyl disulfides and not polythiomolybdates (97IP).

1.2.5 TM interaction with Cysteine and other RSH containing reagents

Cysteine has been shown to react readily with molybdate in water to form $Mo^V_2O_4(Cys)_2^{2-}$ as shown below (70KMa, 77OS).

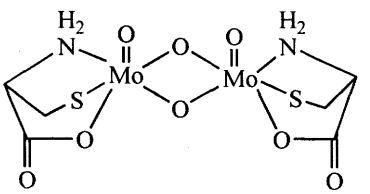

$[Mo^V_2O_4(Cys)_2]^{2-}$

When H_2S is passed in an aqueous solution of the complex $[Mo_2O_4(Cys)_2]^{2-}$, it produces the complex $[Mo_2S_2\,O_2(Cys)_2]^{2-}$ which has the bridging O replaced by bridging S atoms. This reaction presumably involves initially the protonation of the bridging O followed by elimination of H_2O. The mechanism prior to the S- bridging of the two monomers may be similar to that of the sequential replacement of O with S in TMs (Section 1.2.1).

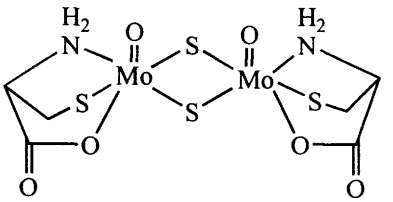

$[Mo^{V}_2O_2S_2(Cys)_2]^{2-}$

When cysteine methyl ester ($HSCH_2CH(NH_2)COOMe$) is added to a reaction mixture of H_2S and sodium molybdate, $[Mo^{V}_2S_2O_2(SCH_2CH(NH_2)COOMe)_2]$ is obtained (70KMa, 77OS).

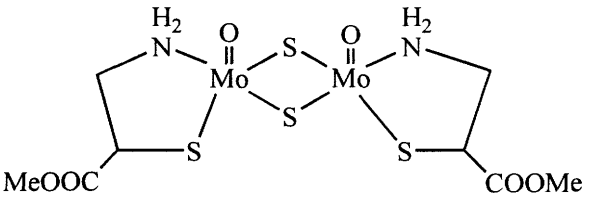

$[Mo^{V}_2S_2O_2(SCH_2CH(NH_2)COOMe)_2]$

The reaction mixture of the H_2S and the molybdate can lead to the formation of any of the TMs (see Section 1.2.1) or mixtures of them. The presence of the O atoms bonded to Mo in $[Mo^{V}_2S_2O_2(SCH_2CH(NH_2)COOMe)_2]$ seems to exclude TM4 as the main product formed from the reaction between H_2S and the molybdate. It is perhaps TM3 or TM2, which is the dominant species in the reaction mixture, and which consequently react with the cysteine methyl ester to give $Mo^{V}_2S_2O_2(SCH_2CH(NH_2)COOMe)_2^{2-}$. If this is the case, then a reaction of TM4 with cysteine methyl ester will yield $Mo^{V}_2S_4(SCH_2CH(NH_2)COOMe)_2^{2-}$ (i.e. the replacement of the axial O atoms with S atoms).

MoO_4^{2-} reacts with 2 equivalents of 2-aminoethanethiol hydrochloride, $HS(CH_2)_2NH_2.HCl$ to yield the product $Mo^{VI}O_2(S(CH_2)_2NH_2)_2$ (70KM) and presumably two mole equivalents of water. However, passing of H_2S through the reaction mixture produced different compounds, whose molecular formulae were determined as; $Mo_5O_9S_3(S(CH_2)_2NH_2)_6$, $Mo_4O_3S_6(S(CH_2)_2NH_2)_5$, and $Mo_3OS_5(S(CH_2)_2NH_2)_4$.

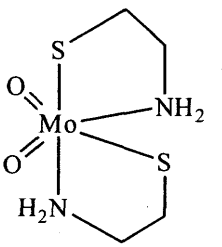

$(Mo^{VI}O_2(S(CH_2)_2NH_2)_2)$

It seems from all the reactions above that the reaction of cysteine (or thiols in general) with molybdates or oxythiomolybdates involves the elimination of water via the initial protonation of an O atom of these molybdenum species, in a similar manner to that discussed in Section 1.2.1, only replacing HS^- or H_2S with RS^- or RSH in the mechanistic steps. This may be the means by which the thiolate group binds the oxyTMs or molybdates in the first place, before any other coordination to the TMs and subsequent bridging of monomers in some cases. In fact, none of the products discussed above suggests directly the involvement of TM4, since all the products at least appear to have one original Mo-O bond. A possible reaction with TM4 as alluded to above, will also involve protonation of an S atom of the TM4, which will lead eventually to the elimination of H_2S (instead of H_2O in the case of molybdate). Actually, in the case of the oxyTMs the protonation of both the O and the S can occur.

Both human serum albumin (HSA) and bovine serum albumin (BSA) have one free cysteine –SH (Section 1.6). Binding to BSA by the TMs and/or MoO_4^{2-} has been investigated by various techniques including UV/visible spectral difference (87WM), a membrane filtration method (87WM, 87CLa), ^{95}Mo spectroscopy (85BG), equilibrium dialysis (83AS), and polarography (83AS). The binding has been identified to be weak (87CLa), and depends on pH and ionic strength (87WM). TM3 also binds to BSA and also to Canine Serum Albumin (CSA), although the influence of pH on the two interactions seems to be different (87WM). The dependence of the interaction on ionic strength suggests that the TM ion binds via ionic interactions to the protein and not via covalent disulfide bond formation (87CLa). The location of the binding site of MoO_4^{2-} and the TMs to albumin is still unknown.

1.2.6 Multicenter Metal Complexes with TMs as Ligands

The formation of bis(thiomolybdate) complexes (see below) from the reaction between TMs and various divalent transition metal cations in solution (e.g. in H_2O) are well established (81MD, 87MD). Complexes of d^8 metal ions (Ni(II), Pt(II), Pd(II)) show square planar geometry at the d^8 metal centers (80CP, 87G) while other metal ions

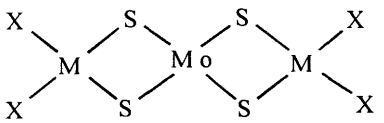

X = O, S

M = Fe, Co, Ni, Pd, Zn, Cd, Hg

such as Co(II) form tetrahedral geometry. The reaction of Fe^{2+} and TM4 in H_2O is more complicated, giving variable products whose composition depends on the nature of the precipitation conditions (81MD). (This reaction is of biological interest, since the FeMoco unit of the enzyme nitrogenase contains Fe-S-Mo clusters implicated for the binding and the reduction of N_2 to NH_3). The reaction between Cu(II) and TM4 ions, which is also of considerable biological relevance, and which forms the basis of the studies reported in this thesis, likewise forms variable products whose actual composition also depends on the reaction conditions. Factors such as the ratios of the reactants and the nature of the solvent have been reported to influence substantially the final products formed (00L). See Table 1.2.

The syntheses and crystallographic characterization of various polymeric M*-Mo-S (M* = Cu(I), Ag (I), Au(I)) compounds in the presence or absence of other ligands have been described extensively in the literature (84SM, 80MB, 81MD, 83MD, 87DM, 98LT, 98LK, 98C, 88MP). Hereafter, the various products formed from the reaction of Cu salts with TMs where the TMs bind at least one Cu atom via S bridge(s) will generally be called "Cu-(S)-Mo-S adducts" or "Cu-(S)-Mo-S complexes". The term "Cu-(S)-Mo-S clusters" is however reserved for such species formed from the reaction between Cu salts and TM with at least three-metal centers, that is, where the TM as a unit, acts as a bridging ligand between Cu atoms, coordinating via the S atoms.

Table 1.2: Examples of compounds isolated from the interaction of Cu^{n+} (n =1 or 2) salts and TM4, TM3 or TM2 in different solvents when co-ligands are present or absent.

Formulae	Reactants (solvents in parenthesis)	Structural Type	Ref.
$[NH_4CuMoS_4]$	CuS + ***TM4*** (H_2O)	Polymeric linear chain	70Br
$(PPh_3)_3Cu_2MoS_4$	4:1 CuS + ***TM4*** + PPh_3 in DMF (H_2O + DMF)	[a]L-trinuclear	81MD 92BC
$Cu_3MoS_3Cl(PPh_3)_3S$	2:1:3 $CuCl_2$ + ***TM4*** + PPh_3 in CH_2Cl_2 (H_2O + CH_2Cl_2)	cubane-like	83MB
$[(CuCl)_3MoS_4]^{2-}$	3:1 CuCl + ***TM4*** (MeCN)	Chair form	84MS 87G
$[(CuCl)_3MoS_4]^{2-}$	4:1 CuCl + ***TM4*** (Me_2CO)	polymeric (bridging Cl^- and S^{2-})	87G
$[Cu_{10}Cl_{12}MoS_4]^{2-}$	10:1 CuCl + ***TM4*** (acac + DMSO)	polymeric (bridging Cl^- and S^{2-})	96WH
$[(CuCN)S_2MoS_2]^{2-}$	1:1 $Cu(CN)_2^-$ or $Cu(CN)_3^{2-}$+ ***TM4*** (H_2O)	L-binuclear	84GH
$[(CuCN)S_2MoS_2]^{2-}$	1:1 CuCN + ***TM4*** (MeCN+ CH_2Cl_2)	L-binuclear	81MDa 87MD
$[(CNCu)S_2MoS_2\ CuCN]^{2-}$	2:1 $Cu(CN)_2^-$ or $Cu(CN)_3^{2-}$+ ***TM4*** (H_2O)	L-trinuclear	84GH
$[(SCN\text{-}Cu)S_2MoS_2\ Cu\text{-}NCS]^{2-}$	1.5:1:1.5 CuCl + ***TM4*** + NH_4 SCN (Me_2CO)	L-trinuclear	87PMa
$[(CNCu)MoS_4\ Cu(CN)_3]^{2-}$	2:1 CuCN + ***TM4*** (MeCN + CH_2Cl_2)	polymeric	81MDa 87MD
$[(o\text{-phen})CuS_2MoS_2]^-$	1:1:1 CuSCN + ***TM4*** + o-phen (-)	L-binuclear	84SM 92BC
$[(o\text{-phen})CuS_2MoS_2\ (o\text{-phen}]$	2:1:2 CuSCN + ***TM4*** + o-phen (-)	L-trinuclear	84SM 92BC

Table 1.2 continued

$Cu(Me_2dtc)_2\,MoS_4\,]^{2-}$ dtc = dithiocarbamate	3:1:4:4 CuCl + ***TM4*** + Me_2dtcNa+ C_5H_9SNa (MeCN)	L-trinuclear	97ZH
$(NH_4)_2\,CCuS_2MoS_2CuC$	1:1 Cu_2C_2 + ***TM4*** (EtOH)	Polymeric linear chain	(92ST)
$[(CuNCS)_4MoS_4]^{2-}$	3:1:3 CuCl +***TM4*** + KSCN (Me_2CO + MeCN)	[b] Polymeric dianions	88MP
$Cu_3MoS_3Cl(PPh_3)_3O$	2:1:3 $CuCl_2$ + ***TM3*** + PPh_3 in CH_2Cl_2 (H_2O + CH_2Cl_2)	cubane-like	83MB
$[(CuCN)MoOS_3]^{2-}$	1:1:3 $CuSO_4$ + ***TM3*** + KCN (H_2O)	L-binuclear	84GH
$[(CuCl)_3MoOS_3]^{2-}$	3:1 CuCl + ***TM3*** (organic solvents)	Incomplete cubane-like	83MS
$CuPPh_3Cu(PPh_3)_2\,MoOS_3$. $0.8CH_2Cl_2$	3:1 CuCN + ***TM3*** + PPh_3 (H_2O + CH_2Cl_2)	Butterfly	83MS
$[Mo_4Cu_{10}S_{16}O_3]^{4-}$	2:1:2.5 CuBr +***TM3*** + Li_2S (DMF + H_2O)	[c] Incomplete cubane,	98GS
$[Mo_4Cu_4S_{12}O_4]^{4-}$	1:1:1 $Cu(NO_3)_2$ + ***TM2*** + Et_2NBH_4 (MeCN)	[d] Square-type	96HW
$MoS_3OCu_2(PPh_3)_3$	$Cu(PPh_3)_3Cl$ + ***TM2*** (MeCN)	Cubane-like	92CL
$[Mo_2\,Cu_5\,S_6O_2(S_2CNEt_2)_3]^{2-}$	CuCl + PPh_4Br + ***TM2*** + Na_2 S_2CNEt_2 (DMF)	[e] 2 Defective cubane-like units	92CL

a. L = linear;
b. The linked $(CuNCS)_4MoS_4$ fragments form zig-zag chains extending along screw axes and these infinite chains are held together by similar –$Cu(NCS)_2$-Cu linkages;
c. Also contains 1 trigonal prism-type Cu_3MoS_4, and two butterfly-type Cu_2MoS_3O;
d. Can be viewed as two butterfly-type of $[CuOMoS_3Cu]$ fragments bridged by two bidendate $[MoOS_3]^{2-}$ groups;
e. Consists of two defective cubane-like units $OMoS_3Cu_2$ and $OMoS_3Cu_3$ linked by two Cu-S bonds and two bridging $S_2CNEt_2^-$ ligands.

In the absence of any co-ligands, polymeric products such as $(NH_4)CuMoS_4$, whose structure indicate alternate S-linked Cu(I) and Mo(VI) centers (i.e. Cu(S)-Mo-S linear clusters), are formed in aqueous solutions. Prevention of such polymerization has been achieved in reactions involving Cu(I) and TM4 in the presence of co-ligands such as phosphine, cyanide, and some N- donor ligands, in both aqueous and non-aqueous solution (Table 1.2) as well as in the solid state (81MD, 83MB, 84SM, 87MD, 98LT). The co-ligands serve as "capping groups" on the Cu atoms, preventing attachment of further TM moieties and hence further polymerization.

The types of structures formed in the presence of co-ligands include trinuclear complexes where each pair of the metal (M*) is connected via doubly bridging TM4, central cubane-type units where the TM ligand is triply bridging, and prismatic types of cage structure where the TM ligands acts as a quadruple bridge. Since these compound types have a comparable formation tendency, different compounds can easily co-exist in a given reaction; slight variations of the concentrations of the reactants can shift the equilibrium strongly in favor of one of the possible products (87MD). For instance, from the reaction of Cu(I), TM4 and CN^- several different species could be isolated (Table 1.2): a polymeric complex with a core unit $[NCCuS_2MoS_2Cu(CN)_2]^{2-}$, $[NCCu(MoS_4)CuCN]^{2-}$ and $[NCCu\text{-}MoS_4]^{2-}$ (87MD).

TM ligands coordinate via the sulfur atoms to the soft cations M* above. Consistent with this, trinuclear complexes involving doubly bridging TMs to form linear structures using TM3 could not be prepared (81MD, 87MD), although compounds of the binuclear linear structures have been prepared (Table 1.2). In fact, to date, it does not seem that any of the oxyTMs (TM1, TM2, and TM3) has been used to prepare polymeric linear chains of Cu-(S)-Mo-S clusters. The particular TM involved in the interaction is very important, as the Cu(I) has little tendency to bind oxo functions (84GH). Any O atoms in a TM ligand therefore act as terminal groups in the Cu-(S)-Mo-S clusters (94HL). It is clear from Table 1.2 that the oxy-TMs form mainly complexes of the cubane-like shape, whereas TM4 is more versatile, having the capability of forming a wide array of structures. For instance, 3:1 CuCl:TM in organic

solvents forms a compound with an incomplete cubane-like structure in the case of TM3, but in the case of TM4 forms a compound with a chair-form configuration (Table 1.2). For similar reasons, a butterfly shaped compound (incomplete cubane) is observed for the trinuclear species $[(Ph_3P)_3Cu_2(MoS_3O)]$ but a linear structure is observed for the TM4 analog $[(Ph_3P)_3Cu_2(MoS_4)]$.

Most of the Cu complexes described above are formed in the presence of organic solvents. Since the product isolated is dependent on the solvent (00L), such reactions may not be relevant to an understanding of physiological (i.e., aqueous) Cu-Mo interactions. Claims that Cu-TM complexes flanked by N (and not P)-donor ligands may act as close models for a biological situation, because N is a potential donor site in most proteins, would only be valid when the reaction is being performed in aqueous media. Hence, the polymeric Cu(I) compounds derived from the interaction of Cu(II) with TM4 in aqueous solutions such as $NH_4Cu(MoS_4)$ (already discussed above) and others like Cu_2MoS_4 isolated as 1,10-phenanthroline (phen) complex from the reaction of CuS and TM4 in aqueous solution (84SM) may be better models for biological situations.

The Cu:Mo ratio identified for the linear polymeric species from the interaction of Cu(II) with TM4 in water described in the preceding section is 1:1. However, the reaction between CuS and TM4 in mixtures of varied reacting proportions (1:1, 2:1, 3:1 and 4:1) and the subsequent isolation of the 1,10-phenanthroline and triphenyl-phosphine complexes, all in aqueous solution show a high tendency for the formation of the core unit $\{CuS_2\,MoS_2Cu\}$, i.e., a Cu:Mo stoichiometry of 2:1 (84SM). The presence of co-ligands such as the two just mentioned, which terminate the polymerization of the Cu-(S)-Mo-S core unit, has also led to the formation of a large number of discrete Cu-(S)-Mo-S cluster compounds of varying compositions depending on the reaction conditions (00L), as shown in Table 1.2. Compounds for which 1 to 6 Cu atoms occupy the six edges of the tetrahedral TM4 (MoS_4^{2-}) (e.g. $[MoS_4(CuCl)_6Cl_2]^{4-}$, with Cu:Mo ratio of 6:1) have been reported for the reaction between CuCl and TM4 (96WH). In fact, a quite recently reported polynuclear Mo-Cu cluster, $(Et_4N)[MoS_4Cu_{10}Cl_{12}]$,

consisting of a tetrahedral MoS_4 core encapsulated by octahedral Cu_6 and tetrahedral Cu_4 arrays of Cu(I) atoms represents a further addition of CuCl to $[MoS_4(CuCl)_6Cl_2]^{4-}$ to form a complex of higher Cu:Mo ratio than 6 (96WH).

The metal centers Cu and Mo and the S (bridging and terminal) ligands of the Cu-(S)-Mo-S complexes can each exist in more than one oxidation state. The S can be in the oxidation states S^{2-}, S_2^{2-} and S_4^{2-}. The oxidation state of Mo in the unreacted TM is +6, which can be reduced to lower oxidation states in the Cu-(S)-Mo-S clusters. The Cu can also be in the +2 or the +1 state.

There seems to be a general agreement that the oxidation state of Cu in the clusters is +1, irrespective of whether the Cu source in the reactant was originally in the +2 or +1 state (see Tables 1.2 and 1.3). The Mo state has however been reported either in the +6 state or the +5 state (Table 1.3).

Table 1.3: The Mo and Cu oxidation states in some Cu-(S)-Mo-S clusters reported in literature.

Compound	Mo	Cu	Ref
$[Cu_{12}Mo_8S_{32}]^{4-}$	+6	+1	98GD
$(NH_4)_n(CuMoS_4)_n$	+6	+1	86LP
$[PhSCuS_2MoS_2]^{2-}$	+6	+1	83AG
$[PhSCuS_2MoS_2CuSPh]^{2-}$	+6	+1	83AG
$(PipH)[CuMoS_4]$	+6	+1	94LN
$(PPh_4)[CuMoS_4]$	+6	+1	94LN
$Cu_{1.6}MoS_4X_y$ ($x = Cl^-, Br^-$, $y = 1$)	+5	+1	00L
$CuMoS_4O_x$ ($x = 2$-3)	+5	+1	86LP

The induced internal redox reaction discussed in Section 1.2.4 for the formation of polythiomolybdates has also been proposed to occur for the reaction of Cu(II) halide or sulfate with TM4 in aqueous solution to form $Cu_{1.6}MoS_4X_y$ ($X = Cl^-, Br^-$, $y = 1$; $X = SO_4^{2-}$, $y = 0.5$) (86LP, 98EV, 00L). A reaction similar to that shown in Equations 1.4

and 1.5 (Section 1.2.4) were presumed to occur, with Cu(II) serving as the external oxidant in the place of the disulfide. The two electrons required to reduce Cu(II) to Cu(I) and Mo(VI) to Mo(V) are expected to originate from the oxidation of S^{2-} to persulfide (S_2^{2-}). Reaction of Cu(II) with the oxythiomolybdates (TM2 and TM3) has also been identified to lead to mutual reduction to Cu(I) and Mo(V) from the EPR spectra of the products (00L).

1.2.7 Characterization of Cu-(S)-Mo-S Complexes

1.2.7.1 UV/visible Spectrosocopy

The reduction in symmetry due to complex formation often leads to the broadening and splitting of the UV/visible bands. In the majority of the d transition metal complexes, the lowest band is red-shifted by an amount which is dependent both upon the nature of the transition metal and the number of such metals bound per TM ligand (87G).

In the case of Cu(II) or Cu(I) interaction with TM4, the electronic spectra of the Cu-(S)-Mo-S complexes formed show characteristic absorption bands whose positions are roughly comparable to those of unreacted TM4 (84SM) (Table 1.4). All the three lowest energy bands, i.e.ν_1, ν_2 and ν_3 (Section 1.2.2) have been reported to shift to longer wavelengths (red-shift) (83AG, 84SM, 84GH, 92ST), despite an earlier report that the ν_2 was unaffected (81MD). See Table 1.4 for details. These shifts of these bands from those of TM4 indicate strong Cu-TM4 interactions due to charge transfer (92ST). The ν_2 red shifts in trinuclear species are more pronounced than those of the corresponding dinuclear species (84SM). For instance, the trinuclear species [(phen)Cu(μ-S)$_2$Mo(μ-S)$_2$Cu)[(phen)] and [(PhSCu(μ-S)$_2$Mo(μ-S)$_2$CuSPh] show their ν_2 bands at 375 and 370 nm respectively, whereas the dinuclear analogues show their respective ν_2 bands at 338 and 350 nm (Table 1.4).

Table 1.4: UV/visible and IR spectra of Cu-(S)-Mo-S complexes formed from TM4 interactions with Cu^{n+} (n =1 or 2) complexes

Compound (reference)	λ max (nm)			Mo-S vibrations (cm^{-1})	
	ν_1	ν_2	ν_3	$\nu(Mo\text{-}S)_b$	$\nu(Mo\text{-}S)_{term}$
$(NH_4)_2MoS_4$ (00L)	[f]465	[f]316	[f]241	-	472
$[CNCuMoS_4]^{2-}$ (81MD, 84GH, 87MD)	[g]471, [h]472	[g]3.19, [h]317	[h]247	452,410	500,486
$[(CNCu)_2MoS_4]^{2-}$ (84GH)	[g]492	[g] 340(sh)	-	434, 432	480,475
$[PhsCuS_2MoS_2]^{2-}$ (83AG)	[h]480	[h]350(sh)	[h]286	440	491
$[PhSCuS_2MoS_2CuSPh]^{2-}$ (83AG)	[g]495	[h]370	[h]284	462	471
$(PPh_4)[(o\text{-phen})CuS_2MoS_2]$ (84SM)	495	338	260	448,425	499,488
$[(o\text{-phen})CuS_2MoS_2\ CuS_2(o\text{-phen})]$ (84SM)	495	375	258	460	-
$(NH_4)_2\ CCuS_2MoS_2CuC$ (92ST)	490	330	250	455	-
$(NH_4)_2\ MoS_4Cu_2C_2\ (py)_2$ (92ST)	478	335	255	460	510
$(NH_4)_2\ MoS_4Cu_2C_2$ (o-phen) (92ST)	480	340	285	460	495
$(NH_4)_2\ MoS_4Cu_2C_2$ (o-phen) (bipy) (92ST)	470	335	262	460	495
$(NEt_4)_2[(CuNSC)_4MoS_4]$ (88MP)	[g]510	[g]360(sh)	-	458,447	-
$(PPh_4)_2[(CuNSC)_4MoS_4]$ (87PMa)	[g]504	[g]360(sh)	-	454	-

f. solvent = H_2O;
g. solvent = DMF;
h. solvent = MeCN. The solvents used for the other λ_{max} determination were not indicated in the literature.

1.2.7.2 Raman and IR Spectroscopy

Raman and infrared spectroscopy have also been used to obtain information about the symmetry at the Mo atom in solid samples. An IR band in the range 510 – 480 cm^{-1} and another in the range 460 – 430 cm^{-1} characterize the presence of terminal sulfido groups and bridging sulfido groups, respectively, in Cu-(S)-Mo-S complexes (92ST). Table 1. 4 also shows these characteristic IR bands for some examples of Cu-Mo-S cluster compounds as compared to $\nu(Mo\text{-}S)_{term}$ = 472 cm^{-1} for unreacted TM4.

1.2.7.3 ^{95}Mo NMR Spectroscopy

Discussions of the principles behind using ^{95}Mo-NMR as an analytical tool for Mo-containing species are deferred to Section 1.3.4.

The ^{95}Mo NMR resonances of the $[(XCu)_nMoS_4]^{2-}$ anions where X = SPh, I, Br, Cl are more shielded than that of TM4. As discussed in Section 1.3.4, the ^{95}Mo chemical shifts of the ammonium salt of TM4 in various solvents were: H_2O, 2258; MeOH, 2230; MeCN, 2207; DMF, 2192; DMSO, 2176 ppm. Each successive addition of a CuX moiety to the MoS_4^{2-} core in DMF results in a monotonic decrease in the chemical shift of the Mo nucleus by 200-400 ppm (84ME). The ^{95}Mo NMR spectra of $[MoCu_{10}S_4Cl_{12}]^{4-}$ in DMSO shows a resonance at 505 ppm.

The ^{95}Mo NMR resonances of the $[(XCu)_nMoS_4]^{2-}$ anions are much broader than that of TM4. An increase in the ^{95}Mo relaxation rate caused by coupling to a rapidly relaxing neighboring quadrupolar nucleus (^{63,65}Cu, I = 3/2) and the increased molecular mass of the Cu-(S)-Mo-S clusters can both contribute to line broadening (84ME), as discussed in Section 1.3.4. Although the peaks generally broadened with an increase in the number of Cu atoms in the complexes (n) (from 1 to 4), no simple correlation was found between n and the linewidth. The ^{95}Mo linewidths of $[(CuCl)_4MoS_4]^{2-}$ ions were substantially broader (~ 1400 Hz) as compared to the case when n = 3 (~ 200 Hz). This

huge difference may be accounted for by the polymeric nature and hence the large size of the former as compared to the smaller size of the $[(CuCl)_3MoS_4]^{2-}$ anion with the chair-conformation. The quadrupolar nature of ^{95}Mo itself was not discussed, but considering the fact that $[(CuCl)_3MoS_4]^{2-}$ anion is of a lower symmetry round the Mo than the TM4, that could also be a contributing factor for observing broader peaks in the former than the latter (see Section 1.3.4). However, the quadrupolar effects of ^{95}Mo may be discounted in comparing TM4 to $[(CuCl)_4MoS_4]^{2-}$, since there is no substantial decrease in symmetry around Mo in the two species.

Apart from the $[(XCu)_nMoS_4]^{2-}$ cluster systems, ^{95}Mo NMR spectra of a variety of Cu-(S)-Mo-S cluster compounds have been determined and are summarized in Table 1.5. The chemical shifts of $(NH_4)_2MoS_4$ given in Section 1.3.4 are also given for comparison. Those of TM2 in D_2O and MeCN have also been shown for comparison.

Table 1.5: ^{95}Mo NMR chemical shifts (ppm with reference to MoO_4^{2-} peak at 0 ppm) of the Cu-Mo-S compounds formed from the interactions of Cu^{n+} (n=1 or 2) with a) TM4 b) TM3 and c) TM2

Complex	Solvent	δ (ppm)	Ref.
TM3	D_2O	1654	84GH
TM3	MeCN	1587	84GH
TM2	D_2O	1066	84GH
TM2	MeCN	964	84GH
(a) $(Pr_4N)_2[MoS_4CuSPh]$	MeCN/DMSO	1902	97ZH
(a) $(Pr_4N)_2[MoS_4(CuSPh)_2]$	MeCN/DMSO	1702	97ZH
(a) $(Et_4N)_2[(MoS_4CuMe_2dtc)_2]$	DMSO	1631	97ZH
(a) $(Et_4N)_2[(MoS_4CuEt_2dtc)_3]$	DMSO	1296	97ZH
(b) $[(n\text{-}Bu)_4N]_4\ [Cu_{10}Mo_4S_{16}O_3]$	DMF	1224, 877, 481	98GS
(b) $[(n\text{-}Bu)_4N]_4\ [Cu_{10}Mo_4S_{18}O]$	DMF	1547, 1216, 1154	98GS
(c) $[Et_4N]_4\ [Cu_4Mo_4S_{12}O_4]$	DMSO	999	96HW

1.3 TECHNIQUES EMPLOYED TO CHARACTERIZE THE PURITY OF THIOMOLYBDATES

1.3.1 Elemental Analysis

Assessment of the purity of these products (80CL, 80HS, 83MF, 82ML, 89GL, 84LP, 83EM) has typically been based either on elemental analysis or on comparison of the measured UV/visible spectra to any of those available in the literature. However, neither of these approaches is discriminating enough to determine the degree of cross-contamination of the various TMs by each other. Satisfactory elemental analysis is a necessary but not sufficient condition for establishing purity. It should be recognized that an equimolar mixture of TM2 and TM4 would have exactly the same elemental analysis as that of pure TM3.

1.3.2 Ultraviolet Spectroscopy

As discussed above, all the TMs have strong and characteristic UV/visible absorption spectra. The spectra reported in literature (81MD, 80CL, 87WM, 84HL, 88WM, 69AR, 80HS, 83MF, 00EH, 00L) for the synthesized materials agree reasonably well in overall appearance. However, details (electronic spectral absorption maxima (λ_{max}) and molar absorptivities (ε)) show a lack of consistency between the various studies (see Section 2.3.3 for details). This is especially pronounced for "TM3" and "TM2".

The inherent problem is in deciding which of the several published spectra should be used as the standard. Beer's Law has been employed to calculate the levels of some TMs in synthesized materials (79WL, 61BT) from the absorption maxima measurements of two or three peaks. The ratios of the intensities of some peaks have also been proposed as criteria to assess the purity of TMs (83MF). Such approaches have some validity, but one of the main reasons for the studies reported in this thesis is that they have not hitherto been applied rigorously enough. For instance, the uncertainty

in λ_{max} and ε values are rarely defined. Calculations are typically done using only two or three wavelengths. However, the UV bands for all four TMs overlap in most cases, so such an approach is obviously inadequate. McDonald et al. (93MF) reported that the presence of TM4 in TM3 salts could be inferred by comparing the ratio of the intensity of the peaks at 395 and 457 nm (as observed by their group) to an 'expected' ratio of 4.6. A lower value for this ratio was said to be an indication of contamination by TM4.

1.3.3 Infrared Spectroscopy

A combination of infrared and UV/visible spectroscopy has been used to determine the purity of various TMs (83MF, 00L). Diemann and Müller (73DM), in a classic review, provided a compilation of such data, from which such assessment was made (see Section 1.2.2). Hence, the absence of extra bands has been used as criteria for identifying the purity of the TMs (82SMa). The positions of the M=S and the M=O bands in the solid state IR spectra of the TMs are dependent on the associated cation as well as the solvent (83MF, 92BC, 00L), and also the bands for individual TMs virtually overlap in most cases, even when the associated cations and the solvent used are the same. Hence TM characterization, especially in the determination of the level of cross-contamination, based solely on such comparison of IR data with those in literature, may not be a straightforward issue and should be handled with much understanding and care.

1.3.4 ^{95}Mo NMR

The ^{95}Mo nucleus gives indifferent sensitivity in NMR experiments. There are two main reasons:

1. *Low receptivity*. In general terms, NMR signal intensities (receptivity) are proportional to $\gamma^3 NI(I+1)$, where γ is the magnetogyric ratio, N the natural abundance of the isotope and I the nuclear spin quantum number (85ME). The ^{95}Mo nucleus has a low receptivity as compared to the commonly used ^{1}H and ^{13}C.
2. *Nuclear electric quadrupole moment*. For any nuclei with $I > 1/2$, the nuclear

charge distribution is no longer spherical and the nucleus will possess an electric quadrupole moment (87SH). ^{95}Mo has $I = 5/2$ and therefore possess an electric nuclear quadrupole moment, Q, which can couple to the local electric gradient, q, providing a mechanism of rapid relaxation. This leads to large linewidths and low resolution (85ME). For molecules rotating rapidly and whose motion is isotropic with correlation time τ_c, the linewidth is given by Equation 1.6

$$\nu_{1/2} = \frac{3\pi}{10}\left(\frac{(2I+3)}{I^2(2I-1)}\right)\left(\frac{e^2 q_z Q}{h}\right)^2\left(1+\frac{\eta^2}{3}\right)\tau_c \qquad \textbf{(1.6)}$$

where η is the asymmetry parameter for q ($\eta = (q_y - q_x)/q_z$).

Hence, the linewidth is dependent on the symmetry of the studied species. The more symmetric the molecule, the sharper the linewidth. Thus the half bandwidth ($W_{1/2}$) of molybdate (TM0) and TM4 (both having a T_d symmetry) are both small: 0.5 and 0.3 Hz, respectively. The TM2 possessing a C_{2v} symmetry has a larger $W_{1/2}$ of 2.8 Hz. The $W_{1/2}$ of TM1 and TM3 (both with a symmetry of C_{3v}) are respectively 10 Hz and 0.7 Hz. The origin of the substantial difference in ^{95}Mo NMR linewidths between these two TMs of the same point group is unclear.

Lutz et al. (77LN) recommended the NMR approach for the quantitative and qualitative analysis of TM solutions. The intensities of ^{95}Mo NMR signals could be used to determine the level of cross-contamination of the various TMs. The utilization of this technique for quantitative measurements has however not been routine, probably because of the following reasons:

1) the relatively high background noise makes it difficult to establish the presence or absence of cross contamination by the other TMs to an acceptable confidence level.

2) The amount of TM required for ^{95}Mo-NMR analysis is larger than that needed by, for instance, UV/visible spectroscopy.

3) The length of time required to acquire NMR spectrum of acceptable signal to noise ratio is sometimes long enough for possible hydrolysis of the TMs, especially TM1 and TM2 to become an issue (77LN).

1.3.5 X-ray Crystallography

Several attempts to solve the crystal structures of the salts of the TMs have been made, notably by Müller and co-workers, who reported unit cell dimensions and space group determinations for TM2 and TM3 salts (68MD, 69MD, 70MD, 70KM). Other workers have reported some structural information also on TM4 salts (64SS, 73LC). None of these workers actually solved the crystal structure of these salts, but recently crystal structures of different TM salts of TMs have been solved. The ammonium salts of TM4 and TM2 and the cesium salts of TM1 and TM3, synthesized by the approach described in this thesis (Section 2.2.3) or by a slightly modified synthesis, were solved by Thome (01T). The X-ray structures of the ethylenediammonium (01SV), cesium (95RD) and rubidium (99EN) salts of TM4 have also been solved. The TM4 salt structures from all these authors show the TM anions to be tetrahedral. Interestingly, the Mo-S bond lengths and angles of TM4 are almost perfect for complexation to Cu(I), to give just the right geometry- i.e. ~ zero ring strain (01T). This may explain the strong affinity of TM4 in binding Cu(I) as compared to the oxyTMs (see Section 1.2.6)

1.4 THE USE OF SPREADSHEETS IN NON-LINEAR REGRESSION ANALYSIS

The majority of programs used to estimate formation constants are based on least squares refinement procedures. In these procedures, the simultaneous optimization of unknown parameters is achieved through the minimization of the error square sum, R(92G, 96RK):

$$R = \Sigma_i w_i [y_{i(meas)} - y_{i(calc)}]^2 \qquad \textbf{(1.7)}$$

where $y_{i(meas)}$ is the ith experimentally measured value of the dependent variable, $y_{i(calc)}$ is the corresponding value assuming a mathematical "model" for the dependence of y on the independent variable, i.e. $y_i(calc) = f(x_i, a_1, a_2, \ldots a_k)$, and w_i are weighting factors

that depend on the distribution of random errors in the dependent and independent variables. The standard deviation of measured y values from calculated is given by

$$S = \sqrt{\{(\Sigma_i[y_{i(meas)}-y_{i(calc)}]^2)/(N-1)\}} \quad \textbf{(1.8)}$$

For equal weights in the regression, this reduces to $S = \sqrt{\{R/(N-1)\}}$

The regression may be termed linear or non-linear depending on the algebraic equation (the "model") relating the value of the dependent variable, y, to those of the parameters, a_1, a_2, ...a_k and of the independent variable x. For example, a model based on Beer's law might be written as:

$$A_i = ac_i + b \quad \textbf{(1.9)}$$

where A_i is the absorbance (dependent variable) at concentration c_i of an absorbing chemical species and b is a constant background signal. The parameter $a = \varepsilon l$, where ε is the molar absorptivity and l is the path length. Equation 1.9 is a **linear model** because the dependent variable A is a linear function of the model parameters a and b (i.e. does not contain higher powers of these parameters, or contain them multiplied together), **not** because the equation describes a straight line. A model need not involve a straight line to be linear (96RK).

Most models encountered in nature are non-linear. In many cases, it is possible to linearize a non-linear model (96RK, 65W). However, since this will require a variable transformation it is necessary to consider how linearization of the model changes the distribution of errors in the dependent variable (y) and the independent variable (x). It must be determined whether unweighted linear regression remains applicable after linearization, since this has been illustrated in some cases to be otherwise (96RK). The approach therefore introduces biases that are dependent on the model (97ZA). Despite the caution, linearization of non-linear data is becoming ever more strongly entrenched with the availability of spreadsheet programs that are able to

linearize data and generate a linear least squares fit with only a few strokes (97ZA).

The principle of least squares regression is based on the major premise that the best values of the parameters to be determined will be when R (Equation 1.7) is at a minimum value. The power of spreadsheet programs like Excel, mathematical engines like Mathcad, and other computer programs, make it possible to extract information directly from processed data through the use of non-linear curve fitting and render the linearization approach inappropriate in most cases. To determine unknown parameters, an initial intelligent guess is made for these parameters, and by using iterative procedures these values are varied till one gets the minimum residual (R). This approach, using Excel and/or Sigmaplot spreadsheets, has been used to compute speciation in solutions containing Cu(II) and Lysine (96AR), and has also been reported for calculating pK_a and the chemical shifts for the individual species of amino acids and peptides (98RA, 98A, 01QK). Spreadsheet approaches (97DH) are more convenient than using other computer programs, in that these programs require the use of a computer language to enter the equation into the program, and that subroutine (or program) must be compiled each time a new problem with a different equation, however slight, is addressed (97L).

1.5 COPPER PROTEINS AND THEIR BIOCHEMICAL FUNCTIONS

Cu and its salts are highly toxic to lower organisms, and also poisonous to man when in large quantities, but at a much lower concentration Cu is an essential constituent of proteins and enzymes. As a trace metal, it is present in tissues and fluids at parts per million (ppm) or parts per billion (ppb) concentrations (87H).

1.5.1 Biochemical Functions

Cu is involved in both enzymatic and non-enzymatic roles in animals. The non-enzymatic roles include angiogenesis, neurohormone release, oxygen transport, and the regulation of genetic expression (97H). Enzymatic reactions include systems that

generate oxidative energy, oxidize ferrous iron, synthesize neurotransmitters, supply pigment to hair and skin, give strength to bones and arteries, assure competence of the immune system, and stabilize the matrices of connective tissues (97H). Detailed descriptions of these proteins and their function(s) have been published elsewhere (87Ha, 91L, 97H, 99T) and will not be duplicated in this thesis.

Examples of some common cuproenzymes include; Ferroxidases which catalyzes the oxidation of Fe(II)), Cu/Zn Superoxide Dismutase (SOD) which protects intracellular components from oxidative damage by converting the superoxide radical to hydrogen peroxide and molecular oxygen, Cytochrome C Oxidase *which* permits formation of adenosine triphosphate (ATP) in mitochondrial energy production and Copper Amine oxidases which catalyzes the oxidative deamination of primary amino groups of several biogenic amines in the presence of molecular oxygen (95BM). Lysyl oxidase is a special class of copper amine oxidase that catalyzes the deamination of Lys residue in peptides to form peptidyl α-aminoadipic-δ-semialdehyde residues, the aldehyde derivative (97H). The formed peptidyl aldehyde can then condense with neighboring amino groups or peptidyl aldehydes to form the covalent crosslinkages found in collagen and elastin (02KB).

1.5.1.1 Non-Enzymatic Copper Proteins

In the previous section the proteins that need Cu to perform their enzymatic roles were discussed. There are also many other proteins that are involved in the absorption and distribution of Cu to the various enzymes, and excretion of Cu in living organisms (95BM).

Once Cu is digested, its further uptake is controlled by serum albumin, circulating in the blood, that delivers it to the liver (91FW). Albumin is the most abundant protein in serum (40 - 50 g L^{-1}, 6.2 –7.7 x 10^{-4} **M**) (95HS, 97HS, 98CM, 99SKa). Detailed discussion of this protein and its Cu-binding properties is provided in Sections 1.6 and 1.7. Serum transferrins are also thought to be involved in Cu transport,

but to a far lesser extent than albumins (97H, 99T). Metallothioneins (MTs), a class of Cys-rich proteins is also known to coordinate with high levels of Cu (02MH) and therefore in the liver, the kidney and the intestines Cu is found primarily bound to MTs (91S, 87Ha, 80B, 77U).

1.5.2 Copper Deficiency

Symptoms of Cu deficiency include connective tissue weakness, anemia and loss of pigmentation. These are normally associated with defects in particular cuproenzyme(s) as a result of lack of Cu, thereby leading to the loss of their catalytic effectiveness. The symptoms observed often fit the function(s) of the failing enzyme in question (97H). Copper deficiency is often a problem for cattle. Acute deficiency is characterized by clinical signs such as diarrhea, anemia, stiffness of gait, infertility, loss of hair color and severe growth retardation (78M, 91S).

Cu deficiency can be caused by inadequate Cu intake (***primary Cu deficiency***) or by the presence of an antagonist in the diet (***secondary Cu deficiency***) (96WS). A variety of substances can cause secondary deficiency. The metals Cd, Hg, Ag, and Zn interfere with Cu metabolism, probably by competing for Cu-binding sites in proteins (87HL). Several other minerals, such as Fe, Se, Pb and Ni, have been shown to interfere with Cu metabolism (89GB). Ascorbic acid, which is known to improve intestinal absorption of Fe by reducing Fe(III) to Fe(II) to form more soluble complexes, is said to depress the intestinal absorption of Cu (77U, 87HL). Sulfide (S^{2-}) ion is a well known inhibitor of Cu absorption, since it gives rise to insoluble Cu(II)S (87HL).

Bovine Cu deficiency is said to be endemic in regions of high pasture molybdenum (Mo) concentrations (91S); cattle appear to be more susceptible to Mo-induced Cu deficiency than sheep (89GB). There is increasing evidence in support of the hypothesis that thiomolybdates (TMs) are formed in the rumen. By microbial action, sulfates (often found in well-derived feed water) and other sulfur (S)-containing compounds can be reduced to sulfides, which combine with Mo in the feed (84SM) to

form TMs (See Section 1.5.3.1 for details). These, particularly TM4, then react with Cu(II) and render it unavailable (See Section 1.5.3.2 for details). The rapidity of the effect and the low levels of TM4 required to inhibit Cu metabolism makes this ion probably the most effective Cu antagonist yet discovered (81ME, 83MD, 84SM, 89GB). However, the chemical basis of the interaction between TMs and both dietary and systemic Cu remains unclear (86KM).

To alleviate the problems associated with Cu deficiency, Cu supplements are supplied to ruminants (98A). Administration of Cu in the form of chelates has been recommended as a remedy to Cu deficiency. There are conflicting reports however regarding their advantage over their inorganic counterparts for ruminants (96LH), especially in the presence of dietary Mo.

1.5.2.1 Formation of TMs in the Rumen

Although there is ample evidence to support the fact that any of the TMs can in theory be formed in the rumen as mentioned above, the question as to whether TM4 can be formed in *vivo* has been an issue of contention in the literature. In a variety of feed studies in cattle (82MK, 84HL, 85HW, 87WM) and sheep (82MK, 87WM), radioactive $^{99}MoO_4^{2-}$ was introduced into the rumen of these animals and maintained on a basic diet supplemented with elemental S at a level of 3g per day. In each case, a trichloroacetic acid-insoluble Mo fraction and protein bound ^{99}Mo-labeled TM2 and TM3 (but not TM4) were detected. In some early classical solution chemistry experiments, Clarke and Laurie (80CL) could not detect the presence of TM4 on mixing S^{2-} and MoO_4^{2-} at ratios < 10:1 under simulated but non-fermentative rumen conditions, at a Mo level of 1×10^{-4} **M**. This has led to the conclusion by some researchers that TM4 cannot be formed under normal conditions in the rumen (82M, 90M).

The characteristic absorption spectrum of TM4 has been detected by a variety of authors in rumen liquor incubated *in vitro* with Mo and S compounds providing

10 mg L^{-1} (~1 x 10^{-4} **M**) Mo and 20-50 mg L^{-1} (6.3 x 10^{-4} – 1.6 x 10^{-3} **M**) S (83EM, 87PW). The levels of Mo and S used in these studies, however, have been criticized as being above their normal levels (82M, 87PW). Using Mo and S concentrations which are closer to those normally pertaining in the rumen, and in a fermentative system, substantial conversions of MoO_4^{2-} to TM4 were observed (35, 30 and 25% at S:Mo ratios of 12, 7.2 and 3.6 respectively) (82BSb). Under dietary conditions purported to be similar to those encountered in field cases of Mo-induced Cu deficiency (6.2 mg Mo kg^{-1}, 6 mg Cu kg^{-1} and 4.3 g S kg^{-1} dry matter (DM)) TMs displaced from rumen, duodenal and ileal solid digesta after injecting ^{99}Mo-labelled MoO_4^{2-} were predominantly TM3 (41%) and TM4 (34%) (87PW). See Figure 1.5 for a scheme depicting the order of flow of digesta in the GI tract, the likely chambers of TM and Cu absorption, and showing typical pH values in the various chambers (66H, 82M, 87V, 87PW, 89GB, 90M, 91S). TM4 has also been detected in the liquid phase of bovine rumen fluid, spectrophotometrically, after the addition of MoO_4^{2-} to the diet to provide 100 mg/kg DM (83EM). At lower Mo levels TMs were not detected in the experiment.

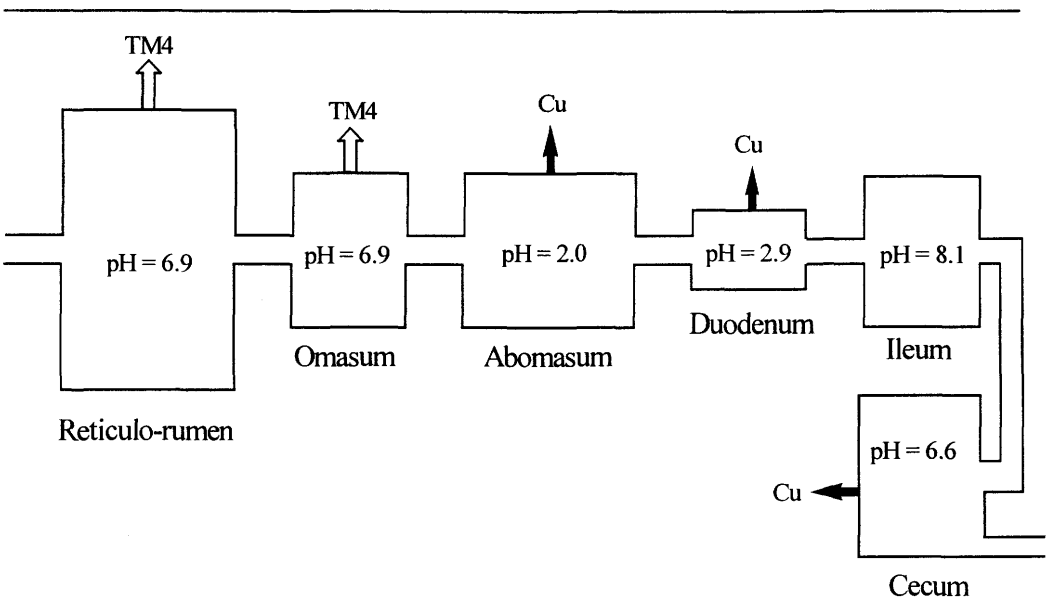

Figure 1.5: A sketch of the various chambers in the ruminant GI tract, indicating typical pH values of their fluid contents and the likely chambers for the absorption of TMs and Cu (indicated by arrows).

It should be noted at the outset that the inability to detect TM4 (or any other TM) spectrophotometrically in rumen fluids at normal dietary Mo levels does not necessarily mean that it is absent. High background absorbances may make such measurements difficult, as discussed in greater detail in Section 7.2.1.

1.5.2.2 The Effect of TMs on Cu Metabolism

Work to date in the field of feed studies, as presented in various reviews (86M, 87Ga, 89GB, 90M, 91S), seems to suggest that TMs exert their antagonistic role by rendering Cu unavailable for use in animals, both pre- and post- absorption to the blood stream by

1. Causing impaired absorption of Cu
2. Altering the distribution of Cu in tissues.

A series of classical solution chemistry studies (80CL, 82CL, 86LP, 87CL, 87CLa) to simulate the Cu-Mo-antagonism in ruminants suggest the formation of insoluble and probably polymeric Cu-TM complexes, which sequester Cu against any biological utilization. In line with the solution chemistry studies, preformed TM4 reduces the absorption of Cu when added to the diet of sheep. Furthermore, when preformed "Cu-TM3" and "Cu-TM4" are placed in the rumen, they are quantitatively recovered from the feces (91S). Of late however, an opinion has been held widely in the field of feed studies, that TMs associate with protozoa, bacteria, undigested feed particles etc in the solid phase of the rumen liquor to form a stable and more potent ligand (than the unreacted TM) that binds Cu to form a tripartite complex involving the solid phase and thus preventing the absorption of Cu (87Ga, 87PW, 89GB, 90M, 91S). By this idea, the solid digesta bound TMs are thought to be able to pass the abomasum without being degraded (87PW, 90M, 91S). Furthermore, this idea holds that TM is found in the liquid phase of the rumen fluid only when the solid phase has reached saturation, that is, it can bind no more the TM in the solid phase (87PW, 90M).

There is a general agreement in the literature, from both *in vitro* and feed studies, that tripartite albumin-Cu-TM complexes are formed (91S, 87WM, 87Ga, 89GB, 00L, 87CLa), although exactly how this binding occurs is not understood. TMs are usually found bound to albumin in two different forms, one of which is TCA soluble and also easily hydrolysed (82ML, 94ML) and the other which is TCA -insoluble and takes a long time before disappearing from the blood stream (83EM, 83ML, 94ML). It seems clear that the first form is an albumin bound TM, which later combines with Cu from various tissues to form the TCA-insoluble TM form. By this means, Cu is removed from various organs, especially the liver where it is known to be stored.

TM4 given intravenously to sheep has been reported to cause ceruloplasmin Cu to precipitate quantitatively as TCA-insoluble Cu (84SM), an indication of the systemic consequences of TM4. However, elsewhere, TM4 is said to be unable to inhibit the diamine oxidase activity of ceruloplasmin *in vivo* (81GM). TM2, TM3, and TM4 can all inhibit Cp oxidase activity in sheep and ovine plasma *in vitro*, although there is some contention whether such inhibition is reversible (86KM) or irreversible (84CBa).

To ascertain if TMs act as substrates for Cp (i.e. inhibit Cp activity by serving as electron donors), Kelleher and Mason (86KM) studied the effect of ovine Cp on the absorption spectra of both TM3 and TM4 in acetate buffer of pH 5.6. They observed that the characteristic spectral peaks of TM3 (392 nm) and TM4 (465 nm) decreased in magnitude faster in the presence of the ovine Cp. They speculated that Cp catalyzed the degradation of the TMs, by accepting electrons via a standard redox couple mechanism. However, it can equally well be speculated that this involves an interaction between Cu (derivable from Cp) and TMs, in either "free" or protein (Cp)-bound form. In any case, the interaction of TM with Cu(II) involves electron transfer (86LP). The electrode potential (E^{o}/V vs SHE) for the Cu(II)/Cu(I) couple is greatly increased in Cp (0.39 V) and some Cu proteins compared with water (0.16 V). Cu(I) is much softer than Cu(II), so S donors are bound more strongly by Cu(I) than by Cu(II), thereby making S ligands (e.g. TMs) important *in vivo* (86M). Even though the "redox couple" mechanism suggested by Keheller and Mason (86KM) appears to involve the Cu(II)/Cu(I) couple in

Cp, it is still uncertain whether the observed decline in Cp activity could simply be due to the ***removal*** of Cu from Cp to form Cu-TM and/or albumin-Cu-TM, or to the formation of a ***ternary*** complex that involves Cp, i.e. a Cp-Cu-TM complex.

1.6 THE AMINO ACID SEQUENCES OF SERUM ALBUMINS

Albumins consist of single polypeptide chains. BSA has 582 amino acid residues and contains 17 disulfide bridges and 1 free cysteine (Cys 34) (82BS). HSA also has 17 disulfide bridges and one free cysteine (Cys 34), but contains 585 residues (98CM, 99SKa).

BSA, HSA, and the rat serum albumin (RSA) have very similar sequences for the first four residues (amino acid with carboxlyate side chain, amino acid with nonpolar sidechain, His (position 3) and Lys (position 4)). CSA and pig serum albumin (PSA) on the other hand, have Tyr in position 3 (74DS, 97HS). These species lack the Cu(II) binding site, suggesting the unique role of His-3 in Cu(II) binding.

1.7 COPPER COMPLEXATION TO BOVINE SERUM ALBUMINS

One of the most prominent functions of albumin, apart from maintaining the pH and osmotic pressure of the plasma, is the transport of small molecules in the bloodstream, e.g. fatty acids, amino acids, bilirubin and ions (including metal ions), to their target organs (99SKa). Metal ions including Cu(II), Ni(II), Cd(II), Zn(II), Co(II), Hg(II) and Mn(II) have been shown to bind albumin at a variety of binding sites (97HS).

As mentioned above, strong Cu(II) binding to serum albumin occurs at the amino-terminal. This site has been proposed for the transport of Cu(II), based on the result of a series of investigations on Cu(II) binding to BSA in the laboratories of Peters and Gurd (67PB, 67SB, 68BS). The involvement of the amino nitrogen, the two peptide N atoms and the N-3 imidazole N in the binding of Cu(II) to BSA was proposed.

1.8 PEPTIDE MODELS OF ALBUMIN AND OTHER PROTEINS

1.8.1 Model Selection

A protein may bind metal ions irreversibly and essentially to enable it to perform its catalytic function, or it may bind these metal ions reversibly to transport them or store them in this complex form in living systems. The coordination of the former type of proteins, also known as metalloenzymes (Section 1.5.2.1 to 1.5.2.4), is unusual in the sense that they differ thermodynamically and kinetically from the more familiar low-molecular-weight (LMW) complexes (87L). The selection of LMW metalloenzyme models is therefore not a trivial issue, since a model may be very suitable as far as the coordination site is concern, but may have no bearing with the functional property of the enzyme.

However, in the case of proteins transporting metal ions via coordination, as in the case of albumin-Cu(II), it has been hypothesized that the metal ion dictates the coordination requirements and, hence, will have more normal properties of thermodynamic reversibility and kinetic lability (87L). Therefore, the requirement of considering the entire protein fold in the chemical model, as is the case for metalloenzymes, is less stringent in the case for Cu transporting proteins. Small model peptides have proven valuable in elucidating the structural features that contribute to the formation of such metallo-complexes (90CB).

1.8.2 Cu(II)-Peptide Systems as Models of Serum Albumins

The tripeptides Gly-Gly-His, Gly-Gly-Gly-N-methyl-amide, and Asp-Ala-His-N-methyl-amide have been used as models to mimic the Cu(II) transport site of HSA (74LK, 76CC, 76KL, 78IL, 80LS). Earlier studies with Asp-Ala-His-N-methylamide (78IL) and Gly-Gly-His and its N-methylamide derivatives as HSA models (74LK, 76CC, 78IL, 78KL) suggested the involvement (in neutral solution) of the α-amino N atom, two intervening peptide N atoms and the imidazole N atom, as also observed for

BSA-Cu coordination. The X-ray structure of (Gly-Gly-His-N-methylamide)-Cu complex showed a distorted square-planar structure involving these four N groups with one weak axial water coordination (76CC).

The above studies, involving visible and optical rotatory dispersion spectroscopy, calorimetry and EPR spectroscopy could not correctly pinpoint the involvement of the β-carboxylate side chain in the complex, although its involvement was later demonstrated clearly by the same research team employing ^{1}H and ^{13}C NMR, using Asp-Ala-His and the 24-residue peptide fragment from the NH_2-terminal of HSA as peptide models of HSA (80LS, 84LS). The complex species so formed as the main species for the tripeptide between pH 4 and 6 in aqueous solution was attributed to a penta-coordinated structure involving the four nitrogen donors in addition to the β-carboxylate (80LS). In the pH interval 6 to 10, the ^{13}C NMR study gave results consistent with the four nitrogen donor coordination earlier proposed for both BSA-Cu.

The apparent ambiguity concerning the role of the β-carboxylate in the HSA models studied earlier can clearly be attributed firstly to unsuitable selected models and secondly to the techniques used (mostly potentiometry, which does not provide structural details). The amino acid sequence of the peptides Gly-Gly-His, Gly-Gly-Gly-N-methyl-amide used as models for HSA are substantially different from the α-amino terminal sequence of HSA (Asp-Ala-His-Lys) and may lead to substantial differences in their coordination properties to Cu(II).

Only few studies modeling BSA have been conducted, all in the late 1960s (67PB, 67SB). By the comparison of the hydrogen ion titration, c.d. spectra and visible spectra of the Cu(II) complexes of BSA and the isolated 24-residue polypeptide chain from the peptic digestion of BSA or Asp-Thr-His-Lys, a binding coordination (4N) similar to that of HSA-Cu and BSA-Cu was implicated with no indication of the involvement of the β-carboxylate group. Systematic peptide model studies employing methods that would provide structural information (such as NMR) as studied for HSA above, are lacking for BSA. Despite the similarities in the amino acid sequence, HSA

models cannot effectively model the activity of BSA, since "minor" changes such as replacing Ala with Thr could lead to substantial differences in coordination ability. Complexation studies between peptide models of BSA and Cu(II) are still needed to ascertain the role (if any) of the β-carboxylate in the coordination of Cu(II) to BSA.

Gly-Gly-Tyr-N-methyl amide has also been used as a model for CSA; the complexing strength of this peptide was found to be less than that of the Cu(II) binding peptide models of HSA (84MR), consistent with the Cu(II) binding of CSA versus BSA or HSA (see Section 1.7 above) The presence of His seems imperative for the strong binding of albumin to Cu(II) and thereby its role in transporting Cu(II) in the blood. The next section explores this in detail.

1.9 THE CHEMICAL SIGNIFICANCE OF HISTIDINE IN BIOLOGICAL SYSTEMS

The side chain of His is one of the strongest metal-binding sites in proteins. The His residue is found in the active sites of several metal containing enzymes, e.g. hemoglobin, or metal transport proteins, e.g. HSA and BSA (97TH). In zinc enzymes, Zn(II) is located in an composed of His residues in the polypeptide chain. For example, in carboxypeptidase A, Zn(II) coordinates to two imidazole N atoms from His residues, two O atoms from glutamate and an H_2O molecule. In carbonic anhydrase C, Zn(II) is firmly bound with three imidazole Ns from His residues (97UH).

The imidazole ring has two coordination sites: the pyrrole nitrogen N-1 (or N^{δ}) which only ionizes at high pH values (> 13), and the pyridine nitrogen N-3 (N^{ε}) whose protonation occurs in the physiologically relevant pH of 6 to 7 (87L, 97S, 98A) as shown in the diagram below. Complexation involving the imidazole ring of His invariably involves the N-3 nitrogen atom. However, at higher pH values, N-1 can undergo deprotonation to become an alternative donor atom. A tautomeric equilibrium exists in His, resulting from placing the hydrogen (see the middle structure in Figure 1.6 below) on either of the two ring nitrogen atoms of the imidazole ring (98A).

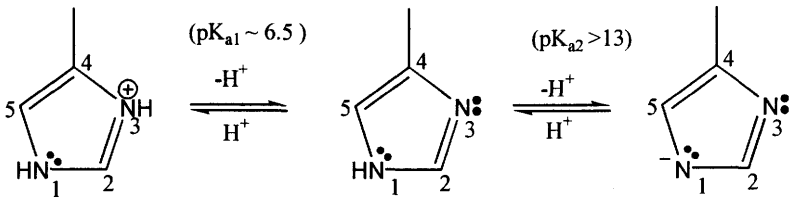

Figure 1.6: Tautomeric equilibrim in the imidazole ring

Comparison of the donor properties of terminal amino and imidazole N, in peptides like Ala-Gly-Gly-His indicate that the primary anchoring site for the metal iss the N-3 of the imidazole ring of His (97TH). For peptide chains not containing His residue, however, the first anchoring site for metal ions such as Cu(II), Ni(II), Pd(II) and Pt (II) is the amino N (82SM). Thus, the presence of a His residue in the peptide sequence alters coordination behavior dramatically. In general, more stable complexes are formed (95BK, 90PP).

Apart from being good models for the study of the interactions of Cu(II) with proteins (Section 1.8.2), small His-containing peptides, e.g. Gly-His-Lys, are known to have some specific biological activities such as altering the growth rate and survival of cultured hepatoma cells and hypotocytes (80PF). These activities are enhanced when they are complexed to Cu(II) and other transition metals (83MW). Structure–function studies have revealed that several tripeptides with a His-Lys linkage are nearly as active as Gly-His-Lys (80PF). It has been shown that Gly-His-Lys stimulates collagen synthesis and hence serve as an activator for wound repair (93MB).(Gly-Gly-His)-Cu(II) complex has also been reported to have anti-tumor activity (96HN). A (Gly-Gly-His)-Cu(II)/Ascorbate system was able to kill Ehrlick ascites tumor cells *in vitro* (97HS). These roles can be attributed primarily to the His residue. The metallopeptide-derived anti-tumor agent bleomycin contains a His moiety (01NK).

Complexes of His-containing peptides may also be involved in the exchange and transport mechanism of trace Cu ions in animals (80PF). Due to the presence of an imidazole ring, His-containing peptides exhibit metal binding and DNA binding

activities that differ from peptides containing other amino acids (97HS). The amino terminal Cu(II) and Ni(II)-binding (ATCUN) motif with the structural features of a free NH_2 terminus, a His at the third position and two intervening peptide nitrogen atoms has been hypothesized to cleave DNA or proteins by the production of hydroxyl radicals. The hydroxyl radicals ($^{\cdot}OH$) would then react with the DNA backbone to cleave the DNA strand (83C, 96HN, 97HS).

1.10 Cu(II) COMPLEXATION STUDIES OF HISTIDINE-CONTAINING PEPTIDES

In Section 1.8.2, Cu(II) complexes with serum albumins were discussed which inevitably involved His-containing peptides. The scope was limited to His-containing peptides whose structures model only those of various serum albumins- specifically His-containing peptides with the His positioned as the third amino acid from the NH_2-terminal of the peptide. In this section are discussed the factors affecting Cu(II) complexation to His-containing peptides in general, and the characteristics of the resulting products.

Complexation between His-containing peptides and metal ions in general depend on several factors, including the nature of the metal ions, the metal ion to ligand ratio and especially the location of the His residue in the amino sequence (00VS). Particularly with reference to Cu(II) complexation, the latter factor has been observed to be critical with regard to the type and structure of complex(es) formed, its (their) stability in solution and the speciation of these complexes (00BC, 91DZ).

It is widely accepted that the interaction of Cu(II) with equimolar N-terminal His-containing dipeptides, above pH ~6, is characterized by the formation of a dimeric species $[Cu_2H_{-2}L_2]$, i.e. an NH_2 (amino N), N^- (deprotonated amide N), O^- (carboxylate O) coordination (as for Gly-Gly) with the fourth Cu(II) binding site occupied by the imidazolyl side chain of another unit, as shown in Figure 1.7a (90B).

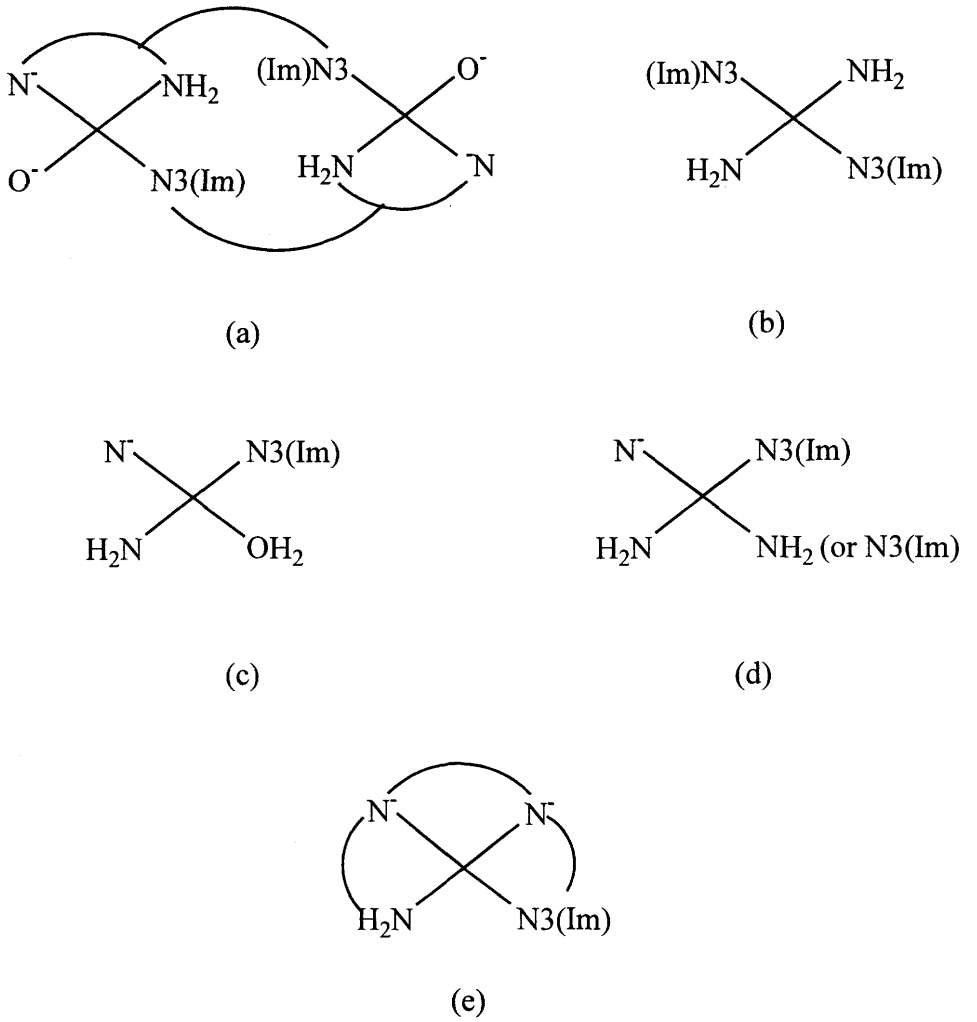

Figure 1.7: Coordination modes of complexes of Cu(II) and His-containing peptides. Details of the individual systems are described in the text.

In the presence of excess dipeptide, however, the deprotonation of the peptide linkage is suppressed and stable bis complexes with 4N-coordination are formed (82SF), as in Figure 1.7b (90B). The bis complex and the binuclear complex formation have been reported for His-Gly, His-Phe, His-Tyr, His-Met, His-Ala, His-Val, and His-Lys and are cited in a manuscript by Burger (90B). There are a few instances where other coordination has been proposed. For instance, glycine-like coordination (without the involvement of the imidazole ring) was proposed on the basis of EPR studies for the Cu(II)-Val-His system (84HV). The existence of monomeric-dimeric equilibrium has also been reported for the Cu(II) complexes with dipeptides His-X having a bulky non-coordinating side chain on the amino acid (X) in the C-terminal position (87RK).

Insertion of His in the second position of a peptide chain results in enhanced metal binding capability of the ligand via NH_2, N^-, and N(Im) coordination (90B, 00VS) as shown in Figure 1.7c. This structure, originally deduced from potentiometric titrations, is consistent with the crystal structure of the Cu(II) complex of Gly-His at pH 6.5 (67BF). The species has one "free" coordination site, which makes the binding of another X-His possible. Binding in this case is done monodentately via the terminal amino or imidazole N-3 moieties (90B) as shown in Figure 1.7d. The same type of coordination is observed for different His-containing dipeptides with His at the C-terminal; Lys-His, Ala-His, Gly-His (85RR).

The structure for the Cu(II) complex of β-Ala-His, a naturally occurring peptide known as carnosine is, however, different. The crystal structure of the solid obtained at pH 10-11 (65FS) indicates the formation of a dimer as in Figure 1.7a, but contrary results have been reported from solution equilibrium studies for this system (90B). The predominance of the same dimer species in solution has been shown by employing various techniques including visible spectroscopy, calorimetry, NMR-relaxation and EPR data (82SM, 90B).

For His-containing tripeptides with the His residue at the third position from the α-amino terminal, the most stable species formed in solution involves the coordination of four donor N atoms, belonging those of the two dissociated peptide groups and of the N-terminal amino groups and the N-3 imidazole nitrogen (Figure 1.7e). The Cu(II) complex of Gly-Gly-His is an example; this is the most widely studied, since it serves as a model for HSA (Section 1.8.2). The crystal structure of the Cu(II) complex of Gly-Gly-His-N-methylamide shows the expected quadridentate chelation (76CC), as in Figure 1.7e. The C-terminal carboxylate group was not thought to take part in the coordination, since adding amino acid to the C-terminal position of these tripeptides, as in Gly-Gly-His-Ala, did not change the coordination properties (00BC).

The tripeptide Asp-Ala-His N-methylamide has also been well studied as an HSA model, as discussed in Section 1.8.2. A pentacoordinated structure involving the

four nitrogen atoms (1 NH_2, 2 N^-, and imidazole N-3) and the β-carboxylate has been proposed (80LS).

The Cu(II) complex of Gly-His-Gly (His at position 2) (81LS, 84FS, 00BC) show the same binding mode as reported for Gly-His (82FS), shown in Figure 1.7c. The structure was confirmed in an X-ray crystallographic study (72OS). The crystal structure of the Cu(II) complex with Gly-His-Lys has also been solved (80PF) and has the same coordination mode as shown in Figure 1.7c. At higher pH values however, the involvement of the C-terminal Gly for the tripeptide Gly-His-Gly as well as the formation of polymeric species, with four N donors coordinated to each Cu (II) atom and bridging imidazolate groups, have both been hypothesized (91DZ).

Only a few studies have been performed for tripeptides with the His residue at the α-amino terminal. Cu(II) complexes of His-Gly-Gly were studied by Aiba et al. (74AY) and Demaret et al. (83DE). As in the case of the dipeptide His-Gly, the formation of a dimeric species (Figure 1.7a) or bis complex (Figure 1.7b) was reported in neutral solution. The dimer is decomposed in alkaline solution, and the deprotonation of the second amide group was presumed, with triglycine-like coordination (90B).

From the above results, it seems quite clear that the position of the His group is important in predicting the coordination mode to Cu(II) of small peptides, at least in neutral solution. Findings can be summarized as follows. Di-, tri-, and tetra-peptides with His residue at the α-amino terminal (e.g. His-Gly-X-Y) are likely to exhibit the coordination modes in either Figure 1.7a or b in the absence of other side-chain donor groups. When the His residue is inserted in the second position (e.g. Gly-His-X-Y), the coordination modes in Figure 1.7c or d will be exhibited. The preference of one particular coordination over the other for each of the two different His positions, will be dictated by the ligand to Cu(II) ratio or steric factors. The coordination mode for peptide-Cu(II) complexes with His at the third position seems to be more predictable at moderately high pH that permits the deprotonation of the peptide NH and the

α-ammonium proton. Generally, at pH > 9, there seems to be unequivocal agreement in literature for the coordination mode shown in Figure1.7e. However, for such peptides with Asp at the α-amino terminal, the involvement of the β-carboxylate group at lower pH values (< 7) has been found. The insertion of the His residue in the position 2 or 3 in the peptide chain hinders the binding of the amino acid residue following His (90B).

To understand the role of His in more complicated peptides (i.e. oligopeptides or peptides with multiple His residues), the anchoring capability of the imidazoyl moiety should be considered (90B). In spite of the stability of Cu-N^- bonds, coordination of peptides to Cu(II) cannot be initiated through such interactions. Presumably, this is because of the extremely high pK_a, i.e. > 14 of amide hydrogen (NH) which does not permit deprotonation in solutions at moderate pH values for the nitrogen of the amide group to act as Lewis base to coordinate Cu(II). Simply amides (-C=ONH-), for example methanamide ($H(CO)NH_2$) and N-methylacetamide ($CH_3(CO)NHCH_3$) in aqueous solutions of moderate pH, form adducts with metal ions (e.g. Cu(II)) at the O of the amide, but substitution of an amide H does not occur (82SM). It seems that this weak coordinating capabilities of the amide group point to the necessity for chelate ring formation to bring out its full metal ion binding capabilities. A metal ion needs a primarily coordinating site or anchor in order to coordinate to the amide N^- and displace the hydrogen (82SM). By providing an anchor for the metal ion, it permits attainment of pH regions where the binding of a metal ion causes the deprotonation of the amide nitrogen.

For peptides with no His residue, the first anchor site is the terminal amino-nitrogen which forms a Cu-NH_2 bond at or above pH 5 (90PP). This is then followed by Cu(II) attacking the peptide N of the neighboring peptide linkage causing the simultaneous displacement of H^+ (i.e. and SN_2 process), leading to the formation of Cu-N^-. This is repeated until three successive Cu-N^- bonds have been made to form a square planar complex with 4N coordination. With insertion of a Pro residue, the situation changes since it contains a secondary N, which is incapable of forming a

Cu-N^- bond. This "break-point" often leads to the formation of macrochelate rings or to the bonding of amino acid side-chain donor centers such as Lys ε-NH_2 or Tyr phenolate oxygen (90PP). In peptide sequences containing both a terminal amino N and His residue, the N-3 of the imidazole ring of the His residue has been found to be the primary anchoring site (90PP).

Cu(II) complexes containing two or more His residues at different positions have also been studied. Complexes with His residues at the first and second positions i.e. His-His (87LP) and His-His-Gly (87UI) have been studied, and both exhibit the same dimeric complexation, with each Cu(II) center involving 2 imidazole Ns (1 each from the two peptides), a deprotonated amide N, and a terminal N (90B). The Cu(II) complexes of the peptides with two His residues at the first and third positions exhibit the same coordination mode as those with only one His residue at the third position (Figure 1.7e) (87UI).

1.11 COMPLEX FORMATION CONSTANTS

The term complex formation constant is a special name for the equilibrium constant of a metal complex formation reaction in solution (usually, but not necessarily aqueous). The equation may be written generally as

$$aM + bL + cH + \ldots = M_aL_bH_c\ldots \qquad \textbf{(1.10)}$$

giving the generalized stability constant

$$K_{a,b,c} = [M_aL_bH_c\ldots]/[M]^a[L]^b[H]^c \ldots \qquad \textbf{(1.11)}$$

where M = a metal ion species; L = a ligand; H = hydrogen ions; a, b, c, are the stochiometric coefficients of the reactants; electrical charges are omitted for clarity of presentation. A widely adopted convention is that c may be positive or negative; a negative value implies the presence of a hydroxide ligand (95L).

When a = 1 and c = 0, reaction 1.10 refers to the formation of mononuclear binary complexes, ML_1, ML_2, ... When a = 1 and c > 0, the complexes formed are protonated species MLH, MLH_2, ML_2H, ... For c < 0, the hydroxo complexes MLOH, $ML(OH)_2$, etc. and the hydroxo metal species M(OH), $M(OH)_2$ corresponding to b = 0 are formed. Oligonuclear and polynuclear complexes are catered for when a > 1.

When a = 0 (i.e. in the absence of metal ion), the reaction 1.10 constitutes a protonation equilibrium and the constant $K_{a,b,c}$ in Equation 1.11 is appropriately called protonation constant. Traditionally, the reciprocal of this value, which represents the reversed reaction in 1.10 when a = 0, is what is normally reported in literature and referred to as the acid dissociation constant (K_a).

When a given metal species M interacts with a given ligand L, in general, several complex formation reactions take place concurrently, corresponding to several sets of values of the stoichiometric coefficients, a, b, and c (95L).

For systems containing up to two kinds of metal ions (M^I and M^{II}) and two kinds of ligands (L and L^{II}) as an example, the general complex may be written as ($M^I_{a1}M^{II}_{a2}L^I_{b1}L^{II}_{b2}H_c$) and the stability constant given in Equation 1.11 will be modified as

$$K_{a1,a2,b1,b2,c} = [M^I_{a1}M^{II}_{a2}L^I_{b1}L^{II}_{b2}H_c]/[M^I]^{a1}][M^{II}]^{a2}][L^I]^{b1}][L^{II}]^{b2}[H]^c \qquad \textbf{(1.12)}$$

Thus, more complicated species including mixed ligand complexes $M^IL^IL^{II}$ ($K_{1,0,1,1,0}$), protonated complexes $M^IL^I_2H$ ($K_{1,0,2,0,1}$), polymeric complexes $M_2^IL_2^I(OH)_2$ ($K_{2,0,2,0,-2}$), mixed metal complexes $M^IM^{II}L^I$ ($K_{1,1,1,0,0}$), or even complexes containing two metals and two ligands $M^IM^{II}L^IL^{II}$ ($K_{1,1,1,1,0}$) can be formed (85PS). The complexity of such equilibrium systems has made the use of computer programs necessary for the computation of stability constants.

1.11.1 Types of Formation Constants

Formation constants can be classified in terms of the ***details*** regarding the various stages of equilibration involved in the metal-ligand interactions (i.e. for instance whether they define interactions with respect to a whole molecule or only one part of it (i.e. microscopic or macroscopic constants) or by whether they are defined in terms of activities or concentrations (Section 1.11.1.1).

1.11.1.1 Thermodynamic, Concentration and Mixed Formation Constants

A formation constants expressed in terms of activities is referred to as a ***thermodynamic*** equilibrium constant (K), and is defined as

$$K = a_{MaLbHc}/a_M{}^a.a_L{}^b.a_H{}^c$$

$$= M_aL_bH_c]/[M]^a[L]^b[H]^c.\ \gamma_{MaLbHc}/\gamma_M{}^a.\gamma_L{}^b.\gamma_H{}^c = K_c.K_\gamma \qquad \textbf{(1.13)}$$

where a, γ, and c refer to activity, activity coefficient and concentration respectively.

Indeed, formation constants should strictly be defined in terms of activities. However, since it is often not practicable to measure the activities of all the reacting species present in a given solution and in fact, it is the concentration of species that are normally measured, the custom has been to measure and report formation constants in terms of concentration. The formation constant defined in Equation 1.11 (in terms of concentrations) is called the ***concentration*** equilibrium constant (K_c). Concentration equilibrium constants are in actual sense not true constants since they depend on factors such as ionic strength.

It is a fundamental thermodynamic law that

$$\Delta G^o = -\ RT\ In\ K = RT\ In\ K_c.K_\gamma \qquad \textbf{(1.14)}$$

ΔG^{o} is the change in free energy per mole, accompanying the conversion of reactants to products when all substances are in their standard states. Evidently, when all the substances are in the reference states, that is the state of the system in which the activity coefficient of each substance is unity, K (thermodynamic) = K_c (concentration). The activity coefficient is an empirical measure of non-ideal behavior as a consequence of inter-particle interactions. Thus in order to obtain the true constant (K), there is the need to know $K\gamma$ (Equation 1.13 and 1.14) or create a condition such that the contribution from the activity coefficients is negligible (87C).

Firstly, the activity coefficients and hence $K\gamma$ can be measured or estimated theoretically with the Debye-Hückel equation or with empirical extensions of it, such as the Davies equation (62D).

$$\log \gamma_{\pm} = - 2Az_Az_B (\sqrt{I}/(1+\sqrt{I}) - 0.2I) \qquad \textbf{(1.15)}$$

where A is a constant with a value of 0.509 at 25° C, z_A and z_B are the charges of the two counter ions and I is the ionic strength of the solution.

An alternative method is to measure K_c as a function of the ionic strength of the experimental solutions, and find K by extrapolating to infinitely dilute solution (i.e. an ionic strength of 0). The difficulty with this approach is that there is seldom a theoretical basis for the extrapolation, though in aqueous solutions at very low ionic strengths the square root of the ionic strength is known to be an appropriate extrapolation variable.

A third approach is to define the experimental solvent as the reference state (i.e. activity coefficients are unity). Experimentally, the metal-ligand complex formation reaction is carried out using a relatively high and constant concentration of supposedly inert background electrolyte as solvent. By this means, the activity coefficient of ionic species in solution is held constant throughout the experiment to find K_c. Since the solvent is the reference state, $K_\gamma = 1$ by definition, and $K = K_c$.

(Of course, the activity coefficients in an infinitely dilute solution may be far from unity when referred to this reference state.)

So far, the discussion has dwelt on two types of formation constants; the thermodynamic and the concentration formation constants. There is yet another formation constant, the ***mixed*** activity-concentration constant, which refers to a formation constant equilibrium expression which is defined in terms of a "mixture" of activities and concentration.. For example, the stepwise mixed dissociation constants K_{a1} and K_{a2} of a dibasic ligand L are defined as $K_{a2} = [L].a_{H^+}/[HL]$ and $K_{a1} = [HL].(a_{H^+})/[H_2L]$.

Why are mixed constants formation constants used? It is worthy of note, that in measuring pH, it is (to a good approximation) the activity of H^+ which is actually measured and not $[H^+]$. ($pH \sim -\log a_{H^+}$). As also stated earlier, other species are normally measured in terms of concentrations and not activities. Since we are unable to measure individual activities, the concept of pH is open to interpretation right from its definition (95H). Since $pH = -\log a_{H^+}$, a pH of 0 corresponds to a_{H^+} of 1 **M** and a solution with a_{H^+} of 10^{-14} **M** would have a pH 14. There are of course deviations from this ideal scale due to ionic strength of solution and various other factors affecting the activity and therefore different pH scales arise. These different pH scales arise mostly from differing approaches to address or eliminate junction potentials that arise when two different solutions are in contact. The most widely accepted scale is that known as the NBS (National Bureau of Standards) based on the Bates-Guggenheim convention for assigning approximate hydrogen activities, and thus values very close to true pH values based on activity, to a series of carefully prepared standard solutions. Calibrations of a glass electrode with these solutions afford pH values essentially the same as the true one, and hence true hydrogen activities.

1.11.2 Methods for the Determination of Formation Constants

A variety of techniques has been developed for carrying out the measurement of data to calculate formation constants; these techniques have been described, in detail, in several publications (61RR, 87C, 95L, 95LW). Amongst the techniques in current use are potentiometry, spectrophotometry, nuclear magnetic resonance (NMR), polarography and associated methods, ion exchange, conductance measurements, solvent extraction methods and solubility measurements. In this section, emphasis is laid on the advantages and the disadvantages of the first four listed methods above, which are the most commonly used.

Analytical methods that are based on upon potential (E) measurements are termed potentiometric methods or potentiometry. Potentiometry is the most widely used method for the determination of formation constants. It may be classified into two divisions, namely glass electrode-based potentiometry for determining hydrogen ions (pH-metry) and potentiometry involving other ion-selective electrodes.

The pH-metric method alone accounts for over 90 % of reported formation constant data (95L). The method is sensitive, precise and reliable. It is, however, prone to many possible systematic errors (92MM) and therefore the quality of the formation constants derived from such measurements depends on the control of these errors. Errors may result from variations in liquid junction potentials, ionic strength variations (leading to variations in activity coefficients), and improper calibration of the electrode(s). The pH-metric method cannot be used in certain situations, for example, when the pH is less than 2 or exceeds 12 or when the concentrations of the metal or the ligand is small due to low solubility.

A major limitation of pH-metry, is that it cannot supply site-specific information, and therefore cannot be used to determine microconstants unless it is combined with other methods.

Perhaps the greatest potential problem with pH-metry is that in the absence of any structural information, it is easy to assume an incorrect equilibrium "model" for the calculation of the formation constants from the data. For instance, in a previous study in this group, the inclusion or the neglect of the diprotonated species MYH_2^- in the K-EDTA system resulted in significantly different reported formation constants. The log K_f value obtained for the K-EDTA (i.e. $K\text{-}Y^{3-}$) complex in the case where the deprotonated species was added was 1.60 as compared to 0.57 when it was neglected (93CR).

The spectrophotometric method is probably the second most popular. A spectrophotometric method is a molecular absorption spectroscopic methods based usually upon the absorption of UV/visible light. The underlying principle involved in this technique is based on Beer's Law (Equation 1.9) which relates the absorbance, A, at a given wavelength to the concentration of species. It is often used as a complement to the pH-metric method. Precision is dependent on that in the individual absorbance measurements; for modern instruments, this is usually comparable to the potentiometric method (95LW). It is a sensitive technique, permitting the measurements of concentrations less than 10^{-5} **M** – an advantage where limited solubility makes it difficult to obtain reliable potentiometric data. It also provides structural information such as the coordination modes around metal centers. There are some limitations to spectrophotometric methods, in that not all ligands absorb light in the UV/visible region of the electromagnetic spectrum. Further more, the absorptivity coefficient (ε) values some of the species formed may be too small to make significant contributions to the absorbance of the solution even when the concentration is substantial. Although spectrophotometric method and as that matter other spectroscopic methods can be used in the determination of microconstants, they are limited in cases when:

1. The basicities of the functional groups are very different and the contribution of the minor protonation isomer(s) to the spectroscopic signal may be negligible.
2. The close vicinity or similar spectroscopic characters of the protonation states of one (or some) of the proton-binding sites may not always permit selective monitoring by spectroscopic methods.

3. The molecules are too complicated for spectral resolution.

Polarography and related electrochemical methods can also provide useful data, which are complementary to pH-metric data. The principle involved is to measure the shift in half-wave potential of the metal ion under investigation upon stepwise addition of the ligand. It has the advantage of providing direct evidence for the maximum number of ligand molecules that can be bound by a given metal. Further, polarographic measurements can be applied to confirming a chemical model postulated on the basis of pH-metric measurements. The errors in the determination of formation constants by the polarographic approach are however, appreciably higher than the other methods already discussed (95L). One contributing factor is the possibility of adsorption of the ligand and/or the complexes at the surface of the mercury drop (95L). A general disadvantage is that experimental $\Delta E_{1/2}$ values are often small and difficult to measure accurately. Another frequently encountered disadvantage is that the polarograms obtained may be irreversible and therefore difficult to interpret.

Nuclear magnetic resonance spectroscopy (NMR) can also be used in metal-ligand equilibrium studies, not only to determine formation constants but also to provide information on the structures of the complexes formed, including the determination of micro formation constants.

NMR is rarely used in conjunction with Beer's Law, since the precise, accurate measurement of resonance integrals is difficult. However, other methods can yield data of acceptable quality; spin-lattice relation times, T_1 and chemical shifts have been used to determine constants (87C). The standard errors for T_1 determinations are normally about 5 – 10 % and therefore this method is often used for semi-quantitative binding strength studies (95LW). The chemical shift method (see 1.12.2 for more details) is more accurate but its accuracy depends heavily on the chemical shift range of the nucleus and the broadness of the resonance lines. The NMR method has an upper restriction of $\log \beta \leq 5$; competitive methods provide access to $\log \beta > 5$ (95LW). NMR techniques are generally less sensitive than potentiometric or spectrophotometric

methods, so a relatively large quantity of sample is required for the measurements of formation constants. Thus, although many different nuclei are potentially available for NMR, ^{1}H NMR chemical shift measurements has been preferred for the estimation of formation constants in biochemical systems in which only a few milligrams of material are available.

Some details about the principles of NMR of relevance to this thesis and how this tool is used to determine the binding constants or elucidate structural information are presented in the next section.

1.12 NMR FOR AQUEOUS COMPLEXATION CHEMISTRY STUDIES

NMR is a form of spectroscopy based on the absorption of radiofrequency electromagnetic radiation (~ 10^{8} Hz) by atomic nuclei placed on a strong magnetic field. In practice, there are three principal measurable parameters for a resonance (70RJ):

1. intensity, given by the area under the absorption curve, and directly proportional to the number of nuclei in a given chemical environment. As mentioned above, this is of limited utility, since response for a given concentration is heavily dependent on a variety of instrumental settings.
2. resonant frequency at the centre of the resonance, usually as a chemical shift.
3. linewidth, discussed in Section 1.12.2.

1.12.1 Solvent Suppression

An Analog to Digital converter (ADC) is used in an F.T. NMR spectrometer to convert the analog signal to digital form so that the Fourier transformation, and other digital processing, can be performed. The number of bits (typically 8, 12 or 16) being used by the digitizer imposes some limit to the dynamic range of the data and precision with which the signals can be represented. For example, using an 8-bit digitizer, the largest possible signal would be set to produce an output of 255 (2^{8}-1); the *smallest* signal that would be recognizable is then 1, or 0.4% of the largest signal. When the

dynamic range of signal intensity in the spectrum exceeds that of the digitizer, either overflow of large signals occurs, or the weakest signals are displayed (87SH). The quantity of the solvent present as compared to the solute (analyte), especially in dilute solutions, for NMR measurement can be very high in some cases and hence, the dynamic range problem is encountered.

For NMR measurements in aqueous solutions, for example, as applies to this thesis (Chapter 5 and 6), the concentration of hydrogen atoms is ~ 111**M** (i.e. twice that of water) as compared to usual solute concentrations of only few millimolar or even less. A dynamic range problem is therefore bound to occur, unless proper measures are taken to alleviate the problem. To obtain a good quality NMR data in the instance where the solvent (in this case H_2O) peak is a "nuisance", the need to suppress such solvent peaks become imperative. Numerous published experimental methods, collectively termed as solvent suppression techniques, have been devised to solve these problems (87BR). Most of these approaches are based either on selective saturation, relaxation or selective excitation techniques (87SH). Details of the mode of operation of such techniques are well-outlined elsewhere (87SH, 98A) and further detailed discussion of most are therefore intentionally omitted here.

Perhaps the most straightforward approach to solvent suppression is simply to saturate the solvent signal by strong irradiation with the decoupler, i.e., homonuclear decoupling. This approach is generally referred to as selective (pre)saturation. Another approach, selective relaxation, takes advantage of the fact that solvent molecules are generally smaller in size than the molecules of interest, and therefore their proton signals relax more slowly. The delay time of acquisition (t_D) in an inversion recovery sequence (π - t_D- $\pi/2$ – acquire) is set such that the solvent resonance is at an intensity null at the time of data collection. Resonances which have relaxed at different rates will have non-null responses.

The last general approach uses pulse sequences to selectively excite resonances of interest while not exciting any resonances at or near the resonant frequency of the

solvent. Such a method is the "binomial composite pulse" approach of solvent suppression, the principal method used in the work reported in this thesis. This consists of series of pulses, spaced and alternating the direction in which they tip the magnetization, and with amplitudes given by the binomial coefficients (e.g. 1$\underline{1}$, 1$\underline{2}$1, 1$\underline{3}$3$\underline{1}$, etc.). The 1$\underline{3}$3$\underline{1}$, pulse sequence (83H) has been found to be simple to implement and gives better results, giving solvent suppressions of more than 1000-fold (83H, 98A) and that was what was used in this study. Details about the actual pulse sequence, and how spacing of excitation notches relates to the delay used are well described by Attaelmannan (98A).

1.12.2 NMR Linewidth

Some rate processes which affect the NMR spectra, include interconversions between different molecular conformations, ligand exchange reactions in intermolecular complexes, spin-spin coupling with rapidly relaxing nuclei and electron exchange in paramagnetic systems.

The width of a resonance is ultimately determined by the rate of atomic motions. In general terms, the populations of nuclei in rapid motion give sharp absorption lines (half-width $\Delta\nu_{1/2} \sim 0.1$Hz), whereas populations of nuclei in slow motion such as diffusion of macromolecules, with periods of 10^{-8} sec, give much broader absorption lines ($\Delta\nu_{1/2}$ = 10 to 1000 Hz or more)(70RJ). Hence, inferences can be drawn about the mobility in space, including its exchange between two or more different environments, from line widths. These broadened peaks for large molecules are because they tumble slowly in solution and short T_2, which in turn leads to the broad peaks.

NMR can monitor the exchange between two environments (A) and (B) of the same nucleus whose chemical shifts are ν_A and ν_B (See Section 1.12.3). There are two extreme cases that can occur, referred to as fast and slow exchange. In the fast exchange limit (ν_e (frequency of exchange) >>> $|\nu_A - \nu_B|$), the spin is jumping very rapidly between the two environments compared with the difference in resonance frequencies

that it experiences on the NMR time scale. Therefore a single line at the average resonance position is observed. The influence of the exchange reaction on the linewidth, under fast exchange limit, is often dominant over that imposed by spin relaxation. The half-width $\Delta\nu_{1/2}$ is given approximately as $(\nu_A-\nu_B)^2/\nu_e$.

In the slow exchange limit, ($\nu_e <<< | \nu_A - \nu_B |$), i.e. on the NMR time scale the spin sees only one of the two environments A and B, and hence two separate resonances are seen in the positions ν_A and ν_B. In this case too, the half-width $\Delta\nu_{1/2}$ of the two resonances, is determined predominantly by the exchange process and is given as approximately equal to ν_e (76W).

Addition of paramagnetic substances also shortens T_1 values, as the unpaired electrons provide a more efficient means for NMR relaxations. This also leads to line broadening, as discussed in greater details in Sections 1.12.5 and 1.12.6.

Quadrupolar effects also cause line broadening of NMR signals and have been discussed in Section 1.3.4 for the ^{95}Mo nuclei.

1.12.3 Proton Complexation Studies

One of the unique properties of NMR is that it affords the opportunity to study systems in equilibrium without perturbing them, whereas most techniques displace the system from equilibrium (98A). As discussed in Section 1.12.2, for a ligand with an acid-base property, equilibrium exists between the two environments; the acid (A) and its conjugate base (B), whose chemical shifts are different (i.e. ν_A and ν_B, respectively). It is important to note that the chemical shift of the ligand is dependent on the state of ionization of the ligand. The exchange between these two environments may in principle be either fast or slow. For proton NMR typical resonance frequency differences would be of the order 10^2 Hz, corresponding to a lifetime of approximately 10^{-2} s. The slow exchange limit would require lifetimes longer than this and the fast exchange limit requiring much shorter time than that. Relatively few complex formation

systems will meet the requirement for very slow exchange on the NMR time scale, except in very tightly bound complexes (87C). Exchange of the acidic group between its acid and conjugate bases is generally fast on the NMR time scale (97RH), and thus the signals of the resonance are merged into one sharp peak. During pH-titration, one therefore observes only one spectrum, which corresponds to the weighted average of the species present in the solution (76W, 97RH). The observed chemical shift is given by:

$$\delta_{obs} = \Sigma\, \delta_i \alpha_I \qquad \textbf{(1.16)}$$

where δ_{obs} is the observed chemical shift and δ_i is the chemical shift of the individual species i and α_i is the fraction of species i. The fractions of the different species in solution are related to the acid dissociation constant (see Section 5.3). By using Equation 1.7 to minimize the residual between the observed chemical shift to the predicted values the chemical shift values of the individual species can be obtained.

1.12.4 Diamagnetic Metal ion-Ligand Systems

^{1}H NMR spectroscopy allows structural assignment of the relative chemical shifts to complex structures and the method, therefore, is a powerful tool for the determination of complex structures when the metal ion is diamagnetic (84RRa). Zn complexes have been well studied with NMR and yield some general rules for the interpretation of such spectra (84RRa):

1. The replacement of a proton by Zn(II) leads to a sharp upfield for protons near the center of replacement.
2. The total loss of a proton from aliphatic nitrogen will cause a larger upfield shift than its replacement by Zn(II), so that a general complex $M_aH_bL_c$ will display a downfield shift for protons near the complex binding site, compared to the pure species, $M_0H_bL_c$.
3. The extent of the shift depends on the number of bonds between proton and complex binding site.

1.12.5 Paramagnetic Metal Ion-Ligand System

NMR spectroscopic investigations of a wide variety of paramagnetic transition or rare earth metal complexes and metalloproteins have been reported over the years, yet many chemists are still convinced that it is impossible to obtain NMR spectra of paramagnetic compounds (97W).

NMR spectra of paramagnetic complexes are usually very sensitive to molecular structure and to the molecular orbital into which the unpaired electron is delocalized. Detailed information about molecular shape and conformation and intimate details about the nature of the molecular orbital(s) of the ligands that interact with the unpaired electron(s) of the metal are obtained. One or more unpaired electrons on a metal center cause the protons (or ^{13}C nuclei) that are close to the metal through bonds and/or through space to experience (70IB, 80LS, 97W); 1) a much wider range of chemical shifts than are typically observed for diamagnetic compounds and 2) linewidths that vary strongly with distance between the metal and the nucleus of interest.

Due to the lack of sensitivity arising from both low concentration and extreme line broadening, signals from the ligands are usually barely observable, if at all, in solutions with a metal to ligand ratio equal to unity (96GH). Indirect information upon complexation can however be obtained by observing systems where the free ligand is in excess, provided that there is fast chemical exchange between the free and bound forms of the ligand. This approach of using excess ligands has faced criticism on the grounds that, first, simultaneous breaking of metal-ligand bonds would be required to permit chemical exchange between the free and the bound ligand and hence even if such chemical exchange exists, it would be slow on the NMR time scale. However, multi-dentate ligands can displace each other without the metal ion being fully dissociated at any time. In this case, ligand exchange would involve the fast reversible release of one end of a molecule in the complex (96GH). Secondly, the use of excessive (10^3-fold peptide excess) has been criticized on the grounds that it may produce higher order complexes absent in more nearly stoichiometric ratios (82SM). Such excessively high

ratios are not in fact recommended, since under even a fast exchange regime, the contribution of the complex to the observed chemical shift (i.e. exchange-averaged) would be negligible. Furthermore, the ratio of albumin (~ 0.63 m**M** (94ST), the most abundant plasma protein to available Cu (~ 17μ**M** (92BB) in blood is approximately only 40. A free ligand to Cu(II) ratio of 50 (96GH) has been used in studies, and was shown to involve fast exchange in the pH range < 8.

1.12.6 Cu(II) Complexation Studies

Cu(II), like any other paramagnetic metal ion, causes the alterations of the chemical shifts and linewidths of the nuclear resonances of the ligand it binds to, as discussed in Section 1.12.5. However, the extent to which paramagnetic ions affect the chemical shifts and linewidths of bound ligand resonances depends on the properties of that particular metal ion. For instance, although Co(II) and Cu(II) are both paramagnetic ions, the former having S = 3/2 and possessing a short electron spin-lattice relaxation time of ~ 10^{-12} sec is an example of a metal whose principal effect is to cause large contact shifts with relatively little broadening, whereas, Cu(II) with S = 1/2 but with a much longer electron spin relaxation time (~10^{-9} to 10^{-8} sec), gives rise primarily to line broadening (90BB, 80LS).

Perhaps the greatest drawback in using NMR to study Cu(II) complexes is its limitation in obtaining reliable formation constants (90TC). This could be attributed to 1) the lack of sensitivity of NMR spectroscopy, hence often precluding measurements of large equilibrium constants (see Section 1.11 above), and 2) the difficulties in measuring chemical shifts accurately, due to linebroadening (85BP).

1.13 SCOPE OF THE PRESENT STUDY

Understanding of how TMs affect Cu deficiency in ruminants is still incomplete, as demonstrated by conflicting opinions in the literature in this field. Many of these opinions are based on feed studies. The digestive system of ruminants, where the Cu-

TM interactions are of considerable biological importance, is an extremely complex aqueous solution, with a large number of competing ligands. A good understanding of the mechanism by which TMs render Cu unavailable requires systematic aqueous solution chemistry studies of the binding of the individual TMs with Cu(II) in both the presence and absence of ligands of biological significance. Few attempts have been made to understand the chemistry of Cu-(S)-Mo-S interactions under conditions that mimic biofluids in ruminants. Understanding is further hampered by the question of which specific TM or TMs is/are prevalent in the rumen and elsewhere in the digestive tract. In part, these problems can be ascribed to the lack of availability of synthesized TMs of known purity, since previous approaches in the characterization of TMs were quite ambiguous or not rigorous enough.

The main objective of this study was to determine the chemical mechanism by which thiomolybdates render Cu(II) unavailable for utilization in ruminants, particularly cattle.

To achieve this, TMs of high purity will be synthesized and methods for the rigorous analysis of the purity will be demonstrated (Chapter 2). This will make it possible to perform meaningful studies of the solution chemistry of the individual TMs, and their interactions with Cu(II) ions in simple aqueous solution, as a necessary step in understanding the detailed mechanism by which Mo compounds effect ruminant deficiency (Chapter 3). Since TMs affect also the transport of Cu(II) by serum albumins, pure peptide models will be synthesized (Chapter 4) and utilized to study in details the acid-base properties, their complexation with Cu(II) (Chapter 5) and how these systems are affected by TMs (Chapter 6). Finally, the biological implications of the findings in this study will be presented, based on available information in the animal science literature (Chapter 7). It is hoped that this study will help resolve the many apparent contradictions in this field, and contribute to developing better solutions to Cu deficiency in ruminants, notably cattle.

2. SYNTHESIS, CHARACTERIZATION AND STABILITY IN AQUEOUS SOLUTIONS OF MONO-, DI-, TRI- AND TETRATHIOMOLYBDATE

2.1 INTRODUCTION

Thiomolybdates (TMs) are known to be formed in ruminants (77U, 84SM, 91S). Microbial activity in the rumen can produce sulfides by the reduction of sulfates and from the degradation of sulfur-containing amino acids (84SM). Based on numerous feed studies (Section 1.5.2), it has been concluded that the TMs are formed from ingested MoO_4^{2-} and sulfides (84SM, 91S).

It might therefore be expected that *in vitro* synthesis of the TM ions in solution from MoO_4^{2-} and water soluble sulfides would pose little difficulty, especially in basic media, where most of the TMs are known to be stable (22M, 87WM). However, this is not the case. Attempts made initially in this study to prepare TMs from Na_2S under basic conditions proved futile.

A variety of workers have reported preparation of one or more of the TMs, as outlined in Section 1.2.1, but none has reported preparation of samples of all four from a single synthetic route. The literature also contains conflicting data about the properties of the synthesized materials. The nucleophile responsible for the formation of TMs from molybdate has also been an issue of contention in the literature (69AR, 81MD, 80HS); is it H_2S, HS^- or S^{2-}?

The preparation of TM1 (MoO_3S^{2-}) has been said to be difficult (81MD, 80CL, 80HS) and various workers have attempted in vain to produce salts of this anion (81MD). Although the formation of TMs on passing H_2S into aqueous ammoniacal solution (22M, 68MD, 69AR, 81MD, 80CL, 80HS, 83MF, 00L) appears to be the most established approach, it has not proven suitable for the formation of TM1 due to the rapid conversion of TM1 to TM2 ($MoO_2S_2^{2-}$) (80CL). The presence of this anion has therefore been mainly inferred from analysis of aqueous reaction mixtures containing low S:Mo ratios (80CL, 80HS).

A simple, robust synthesis of all the TMs by a single synthetic pathway is still lacking. So too is a detailed characterization of the products to ascertain their purity. In particular, as for any reaction scheme based on sequential replacement, it is highly probable that any TM prepared thus is contaminated with one or more of the others. If the properties of the individual TMs are to be explored, knowing the degree of this cross-contamination is obviously crucial.

In this chapter are described a synthesis of all four TMs in pure form and the unambiguous characterization of the purity of these materials. The formation of the TMs under conditions that mimic those in the rumen has also been investigated.

2.2 EXPERIMENTAL

2.2.1 Sources of Chemicals

All chemicals used were reagent grade and were used without further purification unless stated below. Sodium molybdate ($Na_2MoO_4.2H_2O$) was obtained from Baker Chemical Company (Phillipsburg, USA). Ammonium sulfide solution (21.8% $(NH_4)_2S$), potassium dihydrogen phosphate (KH_2PO_4), disodium hydrogen phosphate (Na_2HPO_4) and starch were obtained from Fisher Scientific Company (Fair Lawn, USA). Potassium iodate (KIO_3), sodium thiosulfate pentahydrate

($Na_2S_2O_3.5H_2O$), iodine (I_2) crystals, potassium iodide (KI), cesium chloride (CsCl), concentrated aqueous ammonia solution (28-30% NH_3) and anhydrous diethylether (99%) were obtained from BDH (Toronto, Canada). Sephadex G-25 and G-50 were both products of Sigma Chemical Company (St. Louis, USA). For studies of TM purification by passage through a column of Sephadex, Millipore water (resistivity 18.2 $M.\Omega.cm^{-1}$) obtained from a Milli-Q water system was used as eluent. Water used in all other studies was de-ionized and distilled, obtained by the passage of a reversed osmosis tap water source through a Corning Mega-Pure^{TM} system (MP-6A) containing a high capacity deionizer cartridge, an organic removal cartridge and a distiller in succession.

2.2.2 Preparation of Solutions

All solutions were prepared using the de-ionized and distilled water described in Section 2.2.1. Potassium iodide solution (~ 0.60 **M**) was prepared by dissolving 20 g KI in water and diluting to volume in a 200 mL volumetric flask. Starch indicator solution was prepared by first adding little cold water into a beaker containing 0.5 g soluble starch and stirring to make a smooth paste. This was then poured into 100 mL boiling water, and the solution stirred constantly for about 1 min, then allowed to cool before use. A dilute solution of H_2SO_4 (~ 6 **M**) was prepared by adding 50 mL of concentrated H_2SO_4 (98 %) to 150 mL water with gentle swirling. The stopper was inserted and the flask well shaken. Standard 0.0210 **M** KIO_3 solution was prepared by dissolving in water 2.2470 g of KIO_3, which had been weighed from a KIO_3 sample (~ 3 g) dried at 120°C overnight, and diluting to volume in a 500 mL flask. Approximately 0.125 **M** $Na_2S_2O_3$ solution was made by dissolving 15.6047 g of $Na_2S_2O_3.5H_2O$ in 500 mL of freshly boiled and cooled water. 3 drops of $CHCl_3$ was added to stabilize the solution. The solution was stored in a dark bottle, allowed to stand for at least two days, and standardized against KIO_3 (Section 2.2.3.1) before use. Approximately 3 **M** KI aqueous solution, prepared by dissolving 25 g of KI in about 50 mL of water was used to dissolve I_2. Approximately 0.0625 **M** I_2 was prepared, by first transferring by pipette 10 mL of the 3 **M** KI into a 200 mL glass volumetric flask. 3.18 g of I_2 was weighed into a

small beaker and transferred by means of a small dry glass funnel to the 200 mL flask. This flask was stoppered, shaken until dissolution of the I_2 by KI was complete, and diluted to 200 mL. The iodine in the solution was then standardized against $Na_2S_2O_3$ (Section 2.2.3.2).

A buffer solution of pH 7.0 (see Section 2.2.11) was used as a solvent to dilute 0.68 mL of the ammonium sulfide solution (21.8%) to 250 mL, to prepare a stock ammonium sulfide solution of approximate concentration 8.0×10^{-3} **M**. Upon preparation, the solution formed slight pale yellow precipitate, probably elemental sulfur. This was filtered off and the supernatant standardized by the iodometric method (73H) as outlined in Section 2.2.3 to determine the actual S^{2-} concentration present.

2.2.3 Standardization of Solutions

Due to the possible loss of S^{2-} from aqueous solutions in form of gaseous H_2S, standardization of S^{2-} to determine the exact concentration of S^{2-} in the aqueous solution is therefore a necessity for any meaningful quantitative studies. S^{2-} standardization is even more required in this situation (Section 2.2.2 above) where in the preparation of the solution some of the S^{2-}, reacted with the buffer solution to form elemental sulfur.

S^{2-} is oxidized by I_2 as shown in the reaction below (Equation 2.1).

$$I_2 + S^{2-} \rightarrow 2I^- + S_{(s)} \qquad \textbf{(2.1)}$$

When an S^{2-} solution is added to an excess solution of I_2, as is the case here, the amount of I_2 consumed can be determined by titration with thiosulfate ($S_2O_3^{2-}$) solution. The reaction is

$$I_2 + 2S_2O_3^{2-} \rightarrow 2I^- + S_4O_6^{2-} \qquad \textbf{(2.2)}$$

The common form of $S_2O_3^{2-}$, $Na_2S_2O_3.5H_2O$ that was used in this study is not pure enough to be a primary standard. Instead, $S_2O_3^{2-}$ solution is usually standardized by reaction with a fresh solution of I_2 prepared from KIO_3 (a primary standard) plus KI as shown by the reaction in Equation 2.3.

$$IO_3^- + 5I^- + 6H^+ = 3I_2 + 2H_2O \qquad \textbf{(2.3)}$$

2.2.3.1 Standardization of S^{2-} Solutions

About 100 mL of water and 10 mL of diluted H_2SO_4 were measured into a 250 mL Erlenmeyer flask. 20 mL of 0.0625 **M** I_2 solution was pipetted into the acid solution. 10 mL of the S^{2-} sample solution (Section 2.2.2) was added immediately and quickly stoppered. The flask was shaken vigorously to complete the reaction of the S^{2-} with I_2 as shown in Equation 2.1. Excess I_2 was titrated with standardized 0.125 **M** $Na_2S_2O_3$ solution (Section 2.2.3.3 below) until the solution become pale yellow. 2 to 3 drops of the starch indicator was then added and titrated until the blue color just disappeared (Equation 2.2). The difference in the titer values obtained from Section 2.2.3.2 and the one in this section represents the volume of the $S_2O_3^{2-}$ that would have reacted with I_2 in Equation 2.2, if that quantity of I_2 had not been consumed by S^{2-} in the reaction in Equation 2.1. The concentration of the S^{2-} (Section 2.2.11) can hence be obtained from the stoichiometric relationships in the two equations.

2.2.3.2 Standardization of 0.0625 M I_2 Solution

20 mL of I_2 solution (Section 2.2.2) was pipetted into 250 mL conical flask. 100 mL of water was added, and the solution titrated with the standardized 0.125 **M** $Na_2S_2O_3$ solution (Section 2.2.3.3 below) until the solution become pale yellow. 2 to 3 drops of the starch indicator was then added and titrated until the blue color just disappeared (Equation 2.2).

2.2.3.3 Standardization of 0.125 M $Na_2S_2O_3$ Solution

5 mL of KI solution (Section 2.2.2) was pipetted into 250 mL conical flask. 100 mL of water was measured with a measuring cylinder into the flask. 20 mL of 0.0210 **M** KIO_3 solution was pipetted into the content of the flask. The mixture was acidified with 10 mL of dilute H_2SO_4 causing the reaction in Equation 2.3 to occur quantitatively. The liberated I_2 was then titrated with the 0.125 **M** $Na_2S_2O_3$ solution to obtain a pale yellow color. 2 to 3 drops of the starch indicator was then added, and the titration continued until the blue color just disappeared (Equation 2.2).

2.2.4 Instrumental Measurements

The UV/visible spectra of aqueous solutions were recorded at room temperature on a Perkin-Elmer Lambda 4B spectrophotometer equipped with tungsten bromide and deuterium lamps and with a microcomputer controlled via a keypad. Before taking the spectra of any sample, the appropriate parameters (i.e., scan speed, ordinate mode, e.g. absorbance or transmission modes, etc.), were set and background corrections were performed. The scan speed was typically 300 nm min^{-1} and the wavelength range was typically 230 nm to 500 nm.

Background corrections were performed as follows. Two 1 cm light path quartz cuvettes were filled with the appropriate solvent, making sure that there were no bubbles adhering to the inner surface. The background correction scan was then done by pressing the Background Correction key and then the RUN key to perform. To perform a sample run, approximately 3.5 mL of both the reference solution and the sample solutions were pipetted into quartz cuvettes and placed in their respective sample cells, before pressing the RUN key on the keypad. The "SCAN" software and the wavelength programming (WPLG) software of the spectrophotometer permit the spectral scanning and the measurement of absorbance at up to 6 discrete wavelengths, respectively. The

spectral data so obtained were displayed on the spectrometer monitor and printed out from an Epson FX-85 dot matrix printer for analysis.

Elemental analyses for C, H and N were performed by Ken Thoms (Department of Chemistry Department, University of Saskatchewan), using a Perkin Elmer 2400 elemental analyzer. The ICP analyses for Mo and Na were conducted by the geochemical and analytical laboratories, respectively, of the Saskatchewan Research Council using a Jarell Ash Plasma Emission Spectrometer (super-trace with axial touch). Data analyses were performed using Microsoft Excel. The electrospray mass spectroscopy analyses (ESMS) were conducted by the Plant Technology Institute of the National Research Council of Canada (NRC-CNRC), Saskatoon, using Micromass-Quattro-LC with Zspray source in the negative-ion mode. The ^{95}Mo NMR spectra were collected on a Bruker AMX 300 spectrometer at a frequency of 19.58 MHz using a broadband multinuclear probe.

2.2.5 Syntheses

2.2.5.1 $(NH_4)_2MoS_4$

$Na_2MoO_4.2H_2O$ (1.0 g, 4.13 mmol) was dissolved in water (2 mL). 15 mL of ammonium sulfide solution (21.8%) was added to the solution, which was stoppered and shaken. The reaction mixture (ca. pH 10) was then left to stand at ambient temperature. An orange solution formed and quickly turned dark red. Red crystals of $(NH_4)_2MoS_4$ formed after less than 45 min. To ensure completeness of the reaction (and hence freedom from partially reacted species, i.e., the other TMs), the reaction was left for approximately 3 hr. Then cold 1:1 ethanol/ether mixture (ca. 10 mL) was added to the solution, and it was kept in an ice-bath for about 30 min to increase the yield of the product to 0.85 g, i.e., approximately 79% yield. The crystals (dark red with a green shimmer) were filtered and washed initially with about 10 - 15 mL of cold water. This led to the dissolution of some of the crystals. Further washing with about 10 mL of 1:1

ethanol/water and 10 mL of diethyl ether in succession, re-precipitated the dissolved solid. This "new" precipitate was filtered and subsequently washed with about 10 mL ethanol/diethyl ether (1:1) mixture, and finally 10 mL diethyl ether three times to obtain, in this case, a clear red scaly crystal of TM4 (approximately 22 % yield). Hence, two solid crystals of different purities of TM4 (see Sections 2.3.3) were isolated; the dark red with a green shimmer and the clear red scaly products. Both products were separately dried *in vacuo*, kept under N_2, sealed and stored in the refrigerator.

2.2.5.2 $(Cs)_2MoOS_3$

$Na_2MoO_4.2H_2O$ (0.5 g, 2.07 mmol) was added to 1 mL water and 1 mL NH_3 (28 – 30%) to dissolve. The solution was placed in an ice bath to reduce the temperature to 5 °C or less. 5 mL of cold $(NH_4)_2S$ solution (~21.8%) was added to the solution, stoppered, shaken and placed in an ice-bath for 7 min. A solution of CsCl (1.4 g, 8.32 mmol in 2 mL water), to correspond to an Mo:Cs mole ratio of about 1:4 (as employed by Harmer and Syke (80HS) in an earlier synthesis of Cs_2TM3 but with a different synthetic approach) was quickly added to the reaction mixture. A fine orange precipitate immediately formed, yielding after filtration an orange to red solid product $(Cs)_2MoOS_3$ contaminated with salt(s) of MoS_4^{2-} as evidenced from the analysis of the product (Section 2.3.3). The impure product (0.69 g, an approximate yield of 71%) was washed with about 10 - 15 mL cold water, twice with 10 mL ethanol and finally twice with 10 mL diethyl ether. As in the case of $(NH_4)_2MoS_4$, water dissolved part of the product and in the presence of the non-polar solvent (ether) caused the re-precipitation (in the mother liquor) of some orange solid with reduced redness and of higher purity (see Section 2.3.3). This product was then filtered and washed three times with 10 mL diethyl ether. It was dried and stored as in Section 2.2.5.1.

2.2.5.3 $(NH_4)_2MoO_2S_2.2H_2O$

$Na_2MoO_4.2H_2O$ (1.0 g, 4.13 mmol) was dissolved in a solution of 1.2 mL water

and 5 mL aqueous ammonia (28 - 30%) and placed in an ice-bath to reduce the temperature to 5 °C. 4.8 mL of $(NH_4)_2S$ solution, (~21.8%) previously cooled to the same temperature, was added. The reaction mixture (ca. pH 11.6) was placed in an ice-bath for 10 min, after which 20 mL of cold 1:1 ethanol/ether mixture followed by 20 mL ether and 12mL ethanol were added in that sequence. The mixture was left to stand for an additional 15 - 20 min. Yellow crystals separated out. These crystals were air sensitive and easily darkened. The product was therefore filtered and washed with two 10 mL portions of ethanol followed by the same amount of ether, under an inert atmosphere. They were dried, and stored as in Section 2.2.5.1.

2.2.5.4. $(Cs)_2MoO_3S.1/2H_2O$

$Na_2MoO_4.2H_2O$ (1.0 g, 4.13 mmol) was dissolved in a solution of water (1.2 mL) and 8 mL aqueous ammonia (28 – 30%) and placed in an ice-bath to reduce the temperature to ca. 5°C. 2 mL of $(NH_4)_2S$ solution, (~21.8%) previously cooled to about the same temperature, was added. The reaction mixture (ca. pH 13) was allowed to stand for 10 minutes and CsCl solution (2.8 g, 16.63 mmol in 2 mL water) quickly added. The resulting mixture was transferred into previously cooled solvent mixture (15 mL ether and 5 mL ethanol), shaken and left for 15 min to crystallize. Yellow crystals of weight 1.39 g (approximately 75% yield) were formed. These were washed 3 times each with 10 mL ethanol followed by twice washing with 10 mL ether to obtain purer light yellow crystals of $(Cs)_2MoO_3S.1/2H_2O$. Drying and storage was as in Section 2.2.5.1.

Because the conditions for the preparation of the different TMs differ only slightly, contamination of a given product with a small amount of one or more of the others is a real possibility. This issue is examined below. The products prepared above will be referred to as "TM4", "TM3", "TM2" and "TM1" respectively, but this indicates only the identity of the most prevalent compound in each case.

2.2.6 UV/visible Spectral Analysis

Aqueous stock solutions of "TM4" and of "TM3" at concentrations of about 8.0×10^{-5} **M** were prepared. These two stock solutions were then mixed in varying mole ratios, of approximately 1:0, 2:1, 7:3, 1:1, 3:7, 1:2 and 0:1, by measuring the appropriate volumes of each of the solutions with graduated pipettes. These initial estimates of mole ratios were determined from the number of moles of each of TM3 and TM4 in the mixture, which was calculated as a product of the added volume (with the graduated pipettes) of the relevant stock TM solution in the mixture and the concentration of that stock TM solution, based on the initial assumption of 100% purity. The UV/visible spectrum of each solution was taken and the absorption measured at wavelengths of 250, 300, 350, 400, 450, and 500 nm. Similar data were collected for "TM3" and "TM2" and "TM2" and "TM1" mixtures.

The computer analysis of these data to derive that for individual pure TMs, and the estimation of purity of the synthesized materials, is described in Section 2.3.3.

2.2.7 Thiomolybdate Purification with Sephadex

Concentrated solutions of "TM4", "TM3", "TM2" and "TM1" were each passed through a glass small column (20 cm long x 1 cm diameter) containing Sephadex G-25 (88WM), using water as the eluent. Since all the TMs are colored, the different bands could be readily visualized and the eluant collected accordingly. The purity of the various fractions or separations was monitored spectrally (see Section 2.3.3.). The purest TM fractions on passage through the Sephadex G-25 were collected and vacuum evaporated to dryness using a rotary evaporator.

2.2.8 ^{95}Mo NMR Spectroscopy

Sample concentrations were approximately 0.1 **M** in D_2O for samples containing

"TM1" and "TM2". For the other TMs, saturated solutions in D_2O were prepared and filtered. All samples were prepared immediately before spectral acquisition. 10 mm tubes were used. Chemical shifts were measured and are quoted against external 0.1 **M** Na_2MoO_4 in D_2O as a reference, positive shifts to high frequency. Spectral width was 7.1 kHz, or 3648 ppm; 16K data points were collected. Total acquisition time for a spectrum was between 5 and 20 min.

2.2.9 Determination of Water content of "TM2" by ^{1}H NMR

The standard additions method was used. Approximately 0.015 g of "TM2" was accurately weighed directly into a 5mm NMR tube. About 1.2 mL of deuterated DMSO was added, and the ^{1}H-NMR spectrum of the solution collected. 2.0 μL of Millipore water was then added to the solution and the spectrum collected again. A "blank" spectrum for the deuterated DMSO was also taken. The water peak integral in each case was normalized to the residual DMSO peak. The increase in integral due to the added water was used to calculate the water content of "TM2". The experiment was repeated several times, vacuum drying the sample between experiments, until a constant value was obtained to ensure that all surface water was removed.

2.2.10 Electrospray Mass Spectrometry (ESMS)

Samples for ESMS analysis were prepared by dissolving the relevant "TM" in 10% aqueous methanol to give concentrations of 100, 70, 120 and 260 μg mL^{-1} for "TM1", "TM2", "TM3" and "TM4" samples respectively. The samples were injected into the mass spectrometer source (85 ^{0}C) in the flow of solvent (10% methanol) at a rate of 0.02 mL min^{-1}. The capillary voltage and the cone voltage were respectively 4.09 kV and 20 V. The desolvation temperature was 350 ^{0}C.

2.2.11 Thiomolybdate Formation under Rumen-like Conditions

A buffer solution of pH 7.0 and ionic strength 0.2 **M** was prepared by dissolving 2.3557 g KH_2PO_4 and 3.9248 g Na_2HPO_4 in water and diluting to volume in a 500 mL volumetric flask (94C). This buffer solution was used in the preparation of a stock sodium molybdate (Na_2MoO_4) solution, 5.0×10^{-3} **M,** and a stock ammonium sulfide solution, 8.0×10^{-3} **M** (Section 2.2.2). The $(NH_4)_2S$ solution thus obtained was added to the Na_2MoO_4 solution to give a reaction mixture with an overall molybdenum concentration of 1×10^{-4} **M** (80CL) and a S^{2-}:Mo ratio of 22:1 in one instance. In a second instance a reaction mixture of overall molybdenum concentration of 2.5×10^{-4} **M** and a S^{2-}: Mo ratio of 5.5:1 was made. In each case, the reaction mixture was thermostatted at 38 ± 1 °C using a water bath equipped with a Haake D1 circulator. Formation of the various TMs was monitored over time by analysis of UV/visible spectrophotometric data using methods described in Sections 2.2.6 and 2.3.3. Spectra were acquired immediately after aliquots were taken from the reaction vessel.

2.3 RESULTS AND DISCUSSION

2.3.1 Synthetic Methods

The sequential replacement of O^{2-} by S^{2-} was favored by a somewhat lower pH, longer reaction times, higher S : Mo ratios and higher temperatures. This agrees with the findings of Clarke et al. (80CL). $(NH_4)_2MoS_4$ was the easiest TM to prepare, since prolonged reaction time could not form any TM of higher S content, but rather only improve on the yield as well as the purity of the product. As noted by Laurie et al. (84LP), heating to 60°C, as previously suggested (83MF) is not necessary. The pH used is well above the low values, which could cause the formation of the insoluble MoS_3 (73DM), commonly found as an impurity in commercial TM4 (84LP):

$$MoS_4^{2-} + H^+ \leftrightarrow HMoS_4^- \rightarrow MoS_3 + SH^-$$

In the case of the other TMs, careful manipulation of conditions is required to obtain products of acceptable purity. Nonaqueous solvents were required to induce the formation of the crystals. It was not possible to crystallize TM1 and TM3 as ammonium salts. Solid salts were therefore obtained by adding CsCl solution to form the less soluble cesium salts. The only hitherto reported pure salt of the TM1 anion, the potassium salt (80MB), could only be isolated in methanol at -15 ^{o}C for 24 hours and with a yield of only 10% (80MB).

2.3.2 Mechanism of Reaction

The successful use of ammonium sulfide in these syntheses is consistent with the idea that HS^- is the nucleophile (80HS), not S^{2-} (84SM, 91S) or H_2S (81MD, 69AR). The first and second acid dissociation constants of H_2S are 1.6×10^{-7} and 4.0×10^{-13} respectively (79WL). Thus, whether sulfur is originally added as H_2S, HS^- or S^{2-}, in aqueous solutions at neutral to moderately alkaline pH values HS^- is the most prevalent species of the three. In fact, all syntheses reported appear to buffer the pH in this range. Interestingly, in one of the earliest studies, 'freshly prepared NaSH' was reported to have been used in the preparation of the sodium salt of TM1 (22M).

2.3.3 UV/visible Spectra

All the TMs have strong and characteristic UV/visible absorption spectra. The spectra obtained for the synthesized materials agreed reasonably well in overall appearance with those published in the literature (22M, 68MD, 69AR, 81MD, 80CL, 80HS, 83MF, 84LP, 00L). However, details (exact λ_{max} values and molar absorptivities) show a lack of consistency between the various studies, including this one. (See Table 2.1.) This is especially pronounced for "TM3" and "TM2". These discrepancies can be ascribed to the considerable variations between studies in the purities of the synthesized materials, and in particular to the degree of cross-contamination.

Table 2.1: Wavelengths for UV/visible absorption maxima, λ_{max} (nm), and (in parentheses) molar absorptivities, ε (x 10^{-4}, in $Lmol^{-1}cm^{-1}$), for synthesized TMs in H_2O

Anion	Present Work	Present Work[a]	(80CL)	(68MD, 81MD, 79WL)	(83MF)
"TM4"	468 [1.17]	468 [1.16]	470[1.18]	467[1.30]	467[1.19]
	316 [1.59]	317 [1.56]	318[1.66]	317[1.70]	316[1.68]
	241[2.31]	241 [2.27]	-	242[-]	241[2.47]
"TM3"	461[0.21]	[b] -	465[0.14]	465[0.23]	457[0.20]
	396[0.90]	396 [0.87]	398[0.81]	392[0.87]	395[0.91]
[c] Ratio	4.3	4.1	5.8	3.8	4.6
	312[0.78]	311 [0.72]	315[0.84]	313[0.66]	308[0.73]
"TM2"	395[0.32]	394 [0.40][d]	394[0.29]	394[0.30]	393[0.31]
	322[0.68]	322 [0.85][d]	322[0.64]	318[0.60]	320[0.74]
	287[0.41]	286 [0.46][d]	288[0.39]	288[-]	-
"TM1"	-	-	392[-][d]	394[-][d]	-
	290[0.70]	-	288[-][d]	288[-][d]	[e]292[0.74][d]

[a] after Sephadex treatment, as discussed in section 2.2.7.
[b] a shoulder at 461 nm with ε of 0.21 x10^{-4} dm^3 mol^{-1} cm^{-1}.
[c] ratio of ε values at ~ 396 nm and at ~ 461 nm.
[d] values inferred from solutions at low S : Mo ratios. See text for details.
[e] values are from 80HS.

The actual amount of TM3 and TM4 in the synthesized materials "TM3" and "TM4", and the expected absorptivities of pure TM4 and TM3 at several wavelengths, were calculated using a non-linear least squares approach to optimize the "fit" of the acquired UV/visible spectral data to a Beer's Law model:

$$A_{calc}(\lambda) = \alpha_{TM4}A_{TM4}(\lambda) + \alpha_{TM3}A_{TM3}(\lambda)$$

where $A_{TM4}(\lambda)$ and $A_{TM3}(\lambda)$ are the individual absorbances at the wavelength λ for TM3 and TM4 respectively, and α_{TM4} and α_{TM3} their mole fractions in the sample. The α values are a function of the relative amounts of "TM3" and "TM4" mixed together (which is known), and the actual mole fraction of each pure substance in the two synthesized materials (which is determined by the fit). Absorbance measurements for 7 samples at each of 6 wavelengths were used to derive values for 14 parameters (A_{TM4} and A_{TM3} values at the 6 wavelengths, and the mole fraction of each pure substance in each of the two synthesized materials). Similar models were used for the analysis of data obtained for "TM3" and "TM2" and "TM2 and TM1" mixtures.

Once this initial analysis had been completed, the modeling was extended to allow for the presence of other impurities, for instance, to allow for the possibility that "TM3" might also contain TM2 and even some TM1. Similarly, the possibility of the presence of unreacted molybdate anion (TM0) was also accounted for in the model, using absorbance values measured for pure $Na_2MoO_4.2H_2O$.

The selection of the best fit was based on achieving a minimum for the residual factor R,

$$R = \Sigma_\lambda [A_{exp}(\lambda)-A_{calc}(\lambda)]^2$$

where $[A_{exp}(\lambda)-A_{calc}(\lambda)]$ represents the difference between experimental and calculated absorbance values at the chosen wavelength, and the summation is over all measured wavelengths. The minimization of R was accomplished using the "goal seek" function in Microsoft Excel®. The parameters were varied in a "building block" fashion (one at a time). The standard deviation of A_{calc} values from A_{exp} values, S, was determined by Equation 2.4 for data collected at N wavelengths:

$$S = \sqrt{\{R/(N-1)\}} \qquad \textbf{(2.4)}$$

The final quality of the fit of experimental and calculated UV/visible absorbances was excellent; S was typically 0.005 or less. The best fit of the calculated to the experimental UV/visible data for the ("TM4" and "TM3"), ("TM3" and"TM2") and ("TM2 and TM1") mixtures were achieved with S of 0.002, 0.005 and 0.003, respectively. Table 2.2 gives the observed and the calculated absorbances of 50:50 mixtures of two TMs to further illustrate the goodness of the fits.

Table 2.2: The observed and (in parentheses) calculated absorbances at wavelengths of 250 nm, 300 nm, 350 nm, 400 nm, 450 nm and 500 nm for 50:50 mixtures of ("TM4" and "TM3"), ("TM3" and "TM2") and ("TM2 and TM1").

Mixture	250 nm	300 nm	350 nm	400 nm	450 nm	500 nm
"TM4" and "TM3"	0.8534 (0.8586)	0.4468 (0.4447)	0.1710 (0.1714)	0.3692 (0.3674)	0.4041 (0.3991)	0.1370 (0.1369)
"TM3" and "TM2"	0.3837 (0.3855)	0.3637 (0.3572)	0.1808 (0.1801)	0.4356 (0.4324)	0.0844 (0.0841)	0.0344 (0.0339)
"TM2" and "TM1"	0.2474 (0.2494)	0.4052 (0.4109)	0.1581 (0.1614)	0.1473 (0.1484)	0.0134 (0.0156)	0.0004 (0.0028)

The calculated molar absorptivites, which the model yields for the pure thiomolybdates, are shown in Table 2.3.

As indicated in Section 2.2.5.1, two products were obtained for "TM4", a red crystal with green shimmer and a shiny red crystal formed in the filtrate after washing the former. Their aqueous solutions were both red in color when concentrated ($\geq 10^{-3}$ **M**) and orange when dilute ($\leq 10^{-4}$ **M**). The analysis above showed that the shiny red crystals were of higher purity (with molar composition of 99.3% TM4 and 0.7% TM3) than the other product, which had a percentage TM4 purity of 97.3 %. (Purity figures are precise to within ~ 0.1%). Therefore, only the former was used for subsequent studies

Table 2.3: Calculated molar absorptivities, ε ($x10^{-4}$, in $L\,mol^{-1}\,cm^{-1}$) for pure TMs in aqueous solution at different wavelengths. Standard deviations are given in parentheses underneath.

Anion	250 nm	300 nm	350 nm	400 nm	450 nm	500 nm
TM4	1.307	0.464	0.262	0.027	0.707	0.212
	(0.003)	(0.001)	(0.001)	(0.003)	(0.001)	(0.001)
TM3	0.584	0.529	0.121	0.810	0.185	0.092
	(0.004)	(0.002)	(0.002)	(0.007)	(0.002)	(0.001)
TM2	0.374	0.351	0.309	0.313	0.028	0.006
	(0.004)	(0.004)	(0.004)	(0.007)	(0.002)	(0.002)
TM1	0.170	0.598	0.038	0.004	0.001	0.000
	(0.003)	(0.005)	(0.005)	(0.003)	(0.002)	(0.002)
TM0[f]	0.130	0.005	0.004	0.003	0.003	0.003

[f] Values obtained from the directly measured spectra of $Na_2MoO_4.2H_2O$

with "TM4". Previous workers have described the colors of the salts of TM4 differently (22M, 80HS, 79WL, 82CL) even when the associated cations are the same. This can now be ascribed to differences in purity. This also explains other inconsistencies in the literature. For instance Weber et al. described their synthesized potassium -"TM4" as consisting of 'orange crystals', and determined the relative proportions of TM4, TM3 and TM2 in aqueous solution as 67, 26, and 6 % respectively within 2 min of dissolution (79WL). This they attributed to rapid and considerable hydrolysis of the salt. In fact, TM4 has been observed by other workers (82CL) and confirmed in these studies (Section 2.3.8) to be stable in simple aqueous solutions over a period of at least 3 hours. The percentage values reported almost certainly simply reflect the composition of the material that was synthesized.

The "TM3" obtained in this work was an amorphous orange solid, orange in concentrated solutions and yellow in dilute solutions. The spectral analysis gives the actual composition as 99.10% TM3, 0.88% TM4 and 0.02% TM2. Amongst the TMs, most difficulty was experienced in defining the appropriate conditions for TM3 formation in a pure state. This has been previously recognized. McDonald et al. (83MF) reported that the presence of TM4 in "TM3" salts could be inferred by comparing the ratio of the intensity of the peaks at 395 and 457 nm (as observed by their group) to an 'expected' ratio of 4.6. A lower value for this ratio was said to be an indication of contamination by TM4 (83MF). The ratios obtained by different research groups for "TM3" products are shown in Table 2.1. In the present study the ratio for "TM3" is 4.3. The ratio for the Sephadex G-25 purified "TM3" (see Section 2.3.7) is also 4.1. It is unclear as to how the "optimum" value of 4.6 in the previous study was determined; this may simply be the ratio for their synthesized material. Higher ratios do **not** necessarily indicate higher purity of the TM3; contamination by TM2 will also increase this ratio.

The crystalline "TM3" products obtained by Müller et al. (68MD) and described as orange to red probably contained significant amounts of TM4 (83MF). An early "TM3" product obtained in the present study was a similar color, and the spectral analysis indicated significant TM4 contamination. Several of the other "TM3" salts reported in the literature are similarly suspect (87WM, 22M, 68MD, 69AR, 81MD, 80CL, 82ML).

Probably because of the sensitivity of the synthesized "TM2" product to air (Section 2.2.5.3), it was the most difficult amongst the TMs to obtain in pure form, and also the most difficult to characterize unambiguously. The purest form obtained, as indicated by the spectral analysis, was 95.3% TM2 and 4.6% TM1 and 0.1% TM0. It was noted that the disappearance of the characteristic peak at wavelength 287 or 288 nm for "TM2", as previously observed (79WL), could be used as a qualitative indication of contamination, usually by TM3.

The synthesized "TM1" was found by spectral analysis to be 98.3% TM1, 1.1% TM0 and 0.6 % TM2. Spectra previously inferred for TM1 from solutions containing low S:Mo ratios (80CL, 81MD, 80HS) indicated absorption peaks at 288 nm and at approximately 393 nm (Table 2.1). It is probable that the latter absorption is due to contamination by TM2.

2.3.4 ^{95} Mo NMR Spectroscopy

The ^{95}Mo NMR spectra of five TM samples are shown in Figure 2.1. The chemical shifts observed at 0, 497, 1067, 1654 and 2261 ppm for TM0, TM1, TM2, TM3 and TM4 respectively, are in good agreement with values reported in the literature (77LN, 77LNa, 84GH, 90NS, 96TS). The spectra were collected with a comparatively long interpulse delay so that integrals can be used as a trustworthy estimate of relative amounts of each TM in a given sample. For instance, Figure 2.1 (E) is a spectrum of an impure "TM1", clearly indicating gross contamination by both TM2 and TM0. Table 2.4 also compares the calculated purity levels of the "TM" samples in Figure 2.1, measured by ^{95}Mo NMR and by UV/visible spectral analysis. The two methods are in good agreement, with somewhat higher precision for the UV/visible results. The lower precision in the NMR case is due to the finite noise in the spectra that can be collected in a reasonable time.

2.3.5 ESMS

Attempts to assess TM purity with Fast Atomic Bombardment (FAB) mass spectrometry proved unsuccessful, due to the large degree of fragmentation. The gentler technique of ESMS was somewhat more successful for the detection of the TM species in CH_3OH/H_2O solution. Unfortunately however, the conditions used still resulted in some degree of fragmentation; the heating at the jet source (85°C), and the extremely high temperature (350^{0}C) for the desolvation, caused the TMs to hydrolyze or deteriorate generally into their respective lower forms.

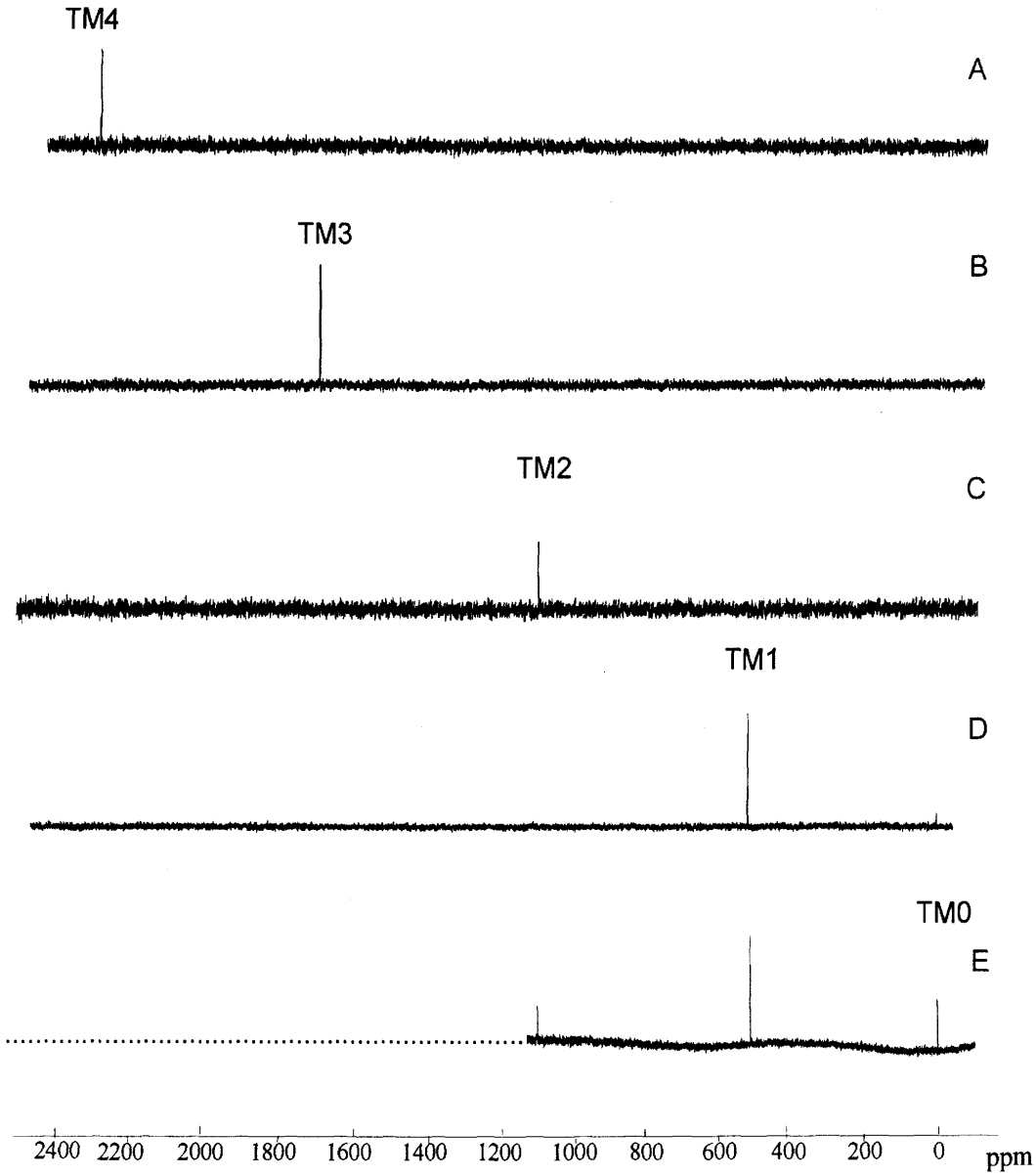

Figure 2.1: ^{95}Mo NMR spectra for (thio)molybdate solutions in D_2O. (A) Sephadex treated TM4 (see Section 2.2.5), (B) Sephadex treated TM3, (C) "TM2", (D) "TM1" (E) an early, impure "TM1" sample.

Table 2.4: Comparison of TM levels in "TM" samples measured by analysis of UV/visible spectra and by ^{95} Mo NMR spectra of their aqueous solutions. The letters (A) through (E) refer to Figure 2.1

Samples	Method	% levels of TMs				
		TM0	TM1	TM2	TM3	TM4
"TM4"	UV	0	0	0	0.3	99.7
(A)	NMR	0	0	0	0	100
"TM3"	UV	0	0	0	99.3	0.7
(B)	NMR	0	0	0	100	0
"TM2"	UV	0.1	4.6	95.3	0	0
(C)	NMR	0	7	93	0	0
"TM1"	UV	1.1	98.3	0.6	0	0
(D)	NMR	4	96	0	0	0
"TM1"	UV	18.5	64.4	17.1	0	0
(E)	NMR	20	63	17	0	0

The Electrospray mass spectra obtained for "TM1" "TM2", TM3 and "TM4" samples dissolved in 10% methanol showed peaks in the region 155-166 (m/z) attributable to $HMoO_4^-$, 172-183 to $HMoSO_3^-$, 189-199 to $HMoS_2O_2^-$, 204-213 to $HMoS_3O^-$ and 220-231 (m/z) to $HMoS_4^-$ respectively. In all cases the observed isotopic mass distribution agreed with the calculated pattern.

By summing peak integrals, it is possible to obtain the percent composition of samples, with the following results (Table 2.5). Generally the values obtained for impurity levels by ESMS are higher than those observed by UV/visible spectroscopy.

Table 2.5: Comparison of percentage TM levels in synthesized "TM" products measured by analysis of UV/visible spectra and ESMS spectra.

Samples	Method	% levels of TMs				
		TM0	TM1	TM2	TM3	TM4
"TM4"	UV	0.0	0.0	0.0	0.7	99.3
	ESMS	17.2	18.8	10.6	7.2	46.1
"TM3"	UV	0.00	0.00	0.02	99.10	0.88
	ESMS	30.3	22.9	6.8	37.1	3.0
"TM2"	UV	0.1	4.6	95.3	0.0	0.0
	ESMS	31.2	30.9	30.9	5.7	1.3
"TM1"	UV	1.1	98.3	0.6	0.0	0.0
	ESMS	31.1	62.4	4.3	1.4	0.8

The electrospray technique obviously results in significant loss of S from the predominant TM in each case. It also appears probable that free "sulfide" released by fragmentation also reacts with lower TMs (which are less stable - see below) to give increased amounts of higher TMs. Relatively, there is better agreement between the two techniques when more intrinsically stable samples are analyzed. However, it is concluded that ESMS is not a trustworthy method of assessing "TM" purity.

2.3.6 Elemental Analyses

See Table 2.6 for the results of the Mo, N, H, and Na analyses of "TM1", "TM2", "TM3" and "TM4" salts.

Table 2.6: Elemental Analysis of the Thiomolybdate Salts (%). Values in parentheses represent calculation of Mo based on analyses of measured UV/visible spectra.

Compound		Mo	N	H	Na
$(NH_4)_2MoS_4$	Exp.	37.1 ± 1.1	10.5 ± 0.3	3.0 ± 0.3	0.13
("TM4")	Calc.	36.9 (36.9)	10.8	3.1	-
$(Cs)_2MoOS_3$	Exp	20.7 ± 1.1	0.0 ± 0.3	0.1 ± 0.3	0.16
("TM3")	Calc.	20.3 (20.3)	0.0	0.0	-
$(NH_4)_2MoO_2S_2.2H_2O$[g]	Exp.	36.8 ± 1.1	10.4 ± 0.3	3.4 ± 0.3	0.15
("TM2")	Calc.	36.3 (36.5)	10.6	4.5	-
$(Cs)_2MoO_3S.1/2H_2O$[h]	Exp.	20.8 ± 1.1	0.5 ± 0.3	0.4 ± 0.3	0.10
("TM1")	Calc.	21.3 (21.3)	-	0.2	-

[g] The water content was found by ^1H NMR.
[h] The water of crystallization in this compound was found by X-ray spectroscopy

Satisfactory elemental analysis is a necessary but not sufficient condition for establishing purity. It should be recognized that an equimolar blend of TM1 and TM3 would have an identical analysis to pure TM2! For N, H, and Mo, good agreement between found and calculated values for "TM4", "TM3" and "TM1" were obtained. Crystallographic study of the "TM4" salts indicates the absence of water of crystallization (01T). The TM1 calculation includes 0.5 H_2O of crystallization as detected by x-ray crystallographic study of the same "TM1" salt (01T). The TM2 calculation includes 2 waters of crystallization, as determined by ^1H NMR

(Section 2.2.9). The amorphous nature of both "TM3" and "TM2" prepared by the method in Sections 2.2.5.2 and 2.2.5.3 did not permit crystallographic studies of these salts. However, modification of these methods (01T) to yield crystals of "TM2" and "TM3" indicate the absence of water of crystallization in both salts. Perhaps the structure for the amorphous TM2 is different from the crystallized TM2 product.

2.3.7 Purification of Thiomolybdates using Sephadex G-25

The purification of synthesized TMs using preparative column chromatography on Sephadex G-25 has been previously recommended by Zumft (78Z). The purities of the fractions collected were assessed by Mo analysis, and (82ML, 89GL) by matching with any of the UV/visible spectra available in the literature, notably references (68MD, 69AR, 80CL, 81MD). These fractions were then assumed to be pure. Since it is now possible unambiguously to assess the purity of "TM" materials before and after Sephadex treatment, the efficacy of this approach to purification can be re-examined.

When passed through a column of Sephadex G-25, the (thio)molybdates are retained in the order, TM4 > TM3 > TM2 > TM1 > TM0. Figure 2.2 gives the UV/visible spectra of the various Sephadex G-25 treated "TMs" in their pure states. The UV/visible spectra of the eluted fractions were analyzed as before. Sephadex- treated "TM4" in solution was of 100% purity (with only an indication of 0.0002% TM3), compared with 99.3% before treatment. After Sephadex treatment the solution of "TM3" was 99.92 % pure, with only 0.08% contamination from TM4. The Sephadex-treated "TM2" solution consisted of 99.97% TM2 and 0.03 % TM3. By contrast, Sephadex treatment actually impaired the purity of "TM1" solutions; the purest fraction obtained was only 45.5% TM1, 22.7% TM2 and 31.8 % TM0 (see stability discussions below in Section 2.3.8).

Zumft's (78Z) recommendation of using Sephadex G-25 for purifying thiomolybdates appears sound, with the obvious exception of TM1.

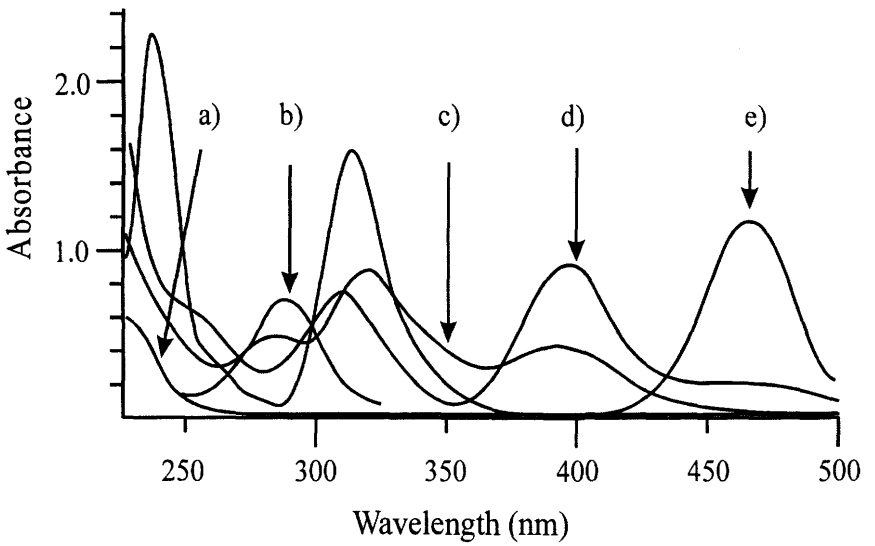

Figure 2.2: UV/visible spectra of molybdate and the thiomolybdates.
(a) TM0, (b) TM1, (c) TM2, (d) TM3, (e) TM4. The TM1 spectrum is calculated from fit results (see Section 2.3.3); others are real spectra of Sephadex-purified samples.

2.3.8 Stability of the Thiomolybdates

It is generally recognized that the lower TMs are less stable. This was confirmed. Although a TM2 solution of quite acceptable purity could be obtained (see above), it was not possible to isolate a solid product at this level of purity. Vacuum evaporation at room temperature gave a material containing 77.1% TM2, 1.4% TM1 and 21.5% TM0. The situation was even worse for TM1. As noted, purity was actually decreased by Sephadex treatment. It worsened even further after vacuum evaporation to obtain solid, to 20.1% TM1, 6.1% was TM2 and 73.8% of the more stable TM0.

These analyses are consistent with a combination of two processes; a loss of S from TM1 to give TM0, and an S atom transfer resulting in the reaction of TM1 to TM2 and TM0. This was confirmed by monitoring both the UV/visible and ^{95}Mo NMR spectra of TM1 and TM2 solutions over time. Although detailed kinetic studies were not conducted, preliminary studies indicated the appearance of the peak at 394 nm, diagnostic of TM2, about 1 hr after the preparation of the TM1 solution (see Figure 2.3). The actual absorbances of the two peaks have been plotted in Figure 2.4.

There was a general decrease of the absorbance of the peak at 290 nm with a concomitant increase in absorbance for the peak at 394 nm up to about 4 hr (see both Figures 2.3 (a to e) and 2.4. At 22 hr after the preparation of the aqueous solution of TM1 (see Figure 2.3f), both peaks were enhanced, possibly as a result of a reaction between released sulfides (from TM1 deterioration) with MoO_4^{2-} and TM1 to form TM1 and TM2 respectively. Over longer periods however, especially in an open container, the peaks at both 290 and 394 nm disappeared completely, and a spectrum similar to that of MoO_4^{2-} was observed. Presumably this is because any S^{2-} formed is in acid-base equilibrium with a small amount of H_2S, which can be irretrievably lost by evaporation, and thus "pull" the system towards complete reaction. A TM2 solution, which shows mainly a single ^{95}Mo resonance at a chemical shift of 1067 ppm (Figure 2.1 C) when acquired within 5 min, shows an additional resonance at a chemical shift of 497 ppm (TM1) after 15 min, and three additional resonances at chemical shifts of 497 ppm (TM1), 1654 ppm (TM3) and 2261 ppm (TM4) 45 minutes (or longer).

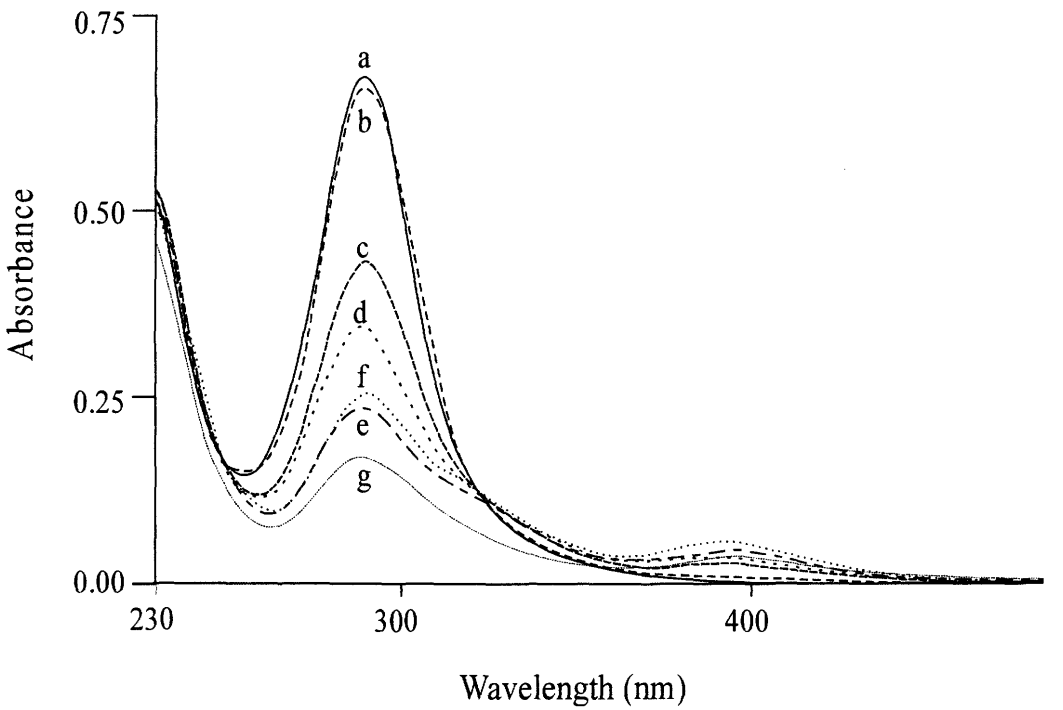

Figure 2.3: The UV/visible spectra of a 1 x 10^{-4} **M** aqueous solution of TM1 (a) 3 min, (b) 6 min, (c) 50 min, (d) 1hr 10min, (e) 3hr 30min, (f) 22hr, (g) 3 days after solution preparation.

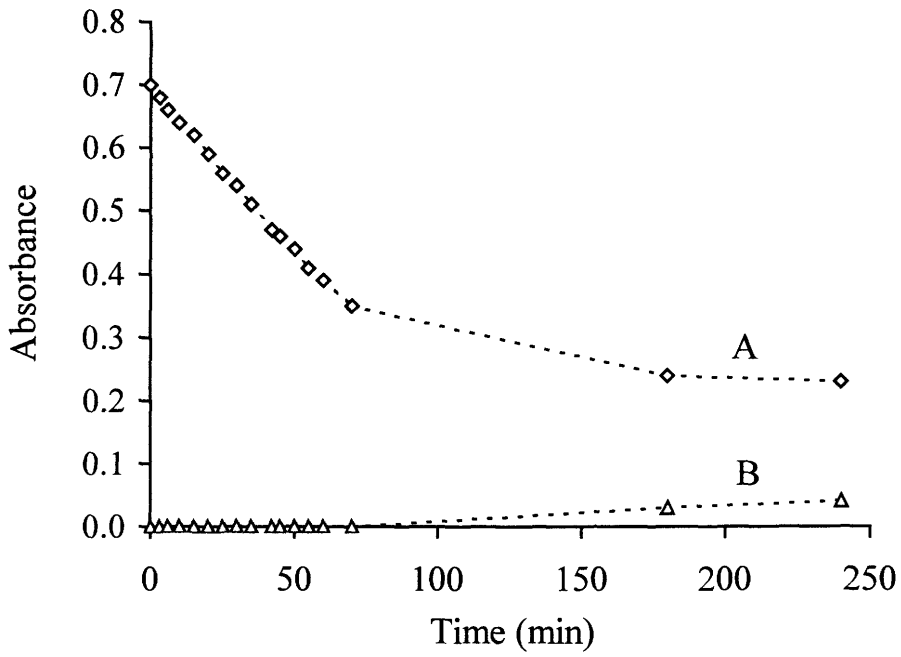

Figure 2.4: The absorbance of a 1 x 10^{-4} **M** TM1 aqueous solution as a function of time at wavelengths of (A) 290 nm, (B) 394 nm.

Sephadex treated TM4 and TM3 (Figure 2.1 A and B) showed single signals only, at chemical shifts of 2261 and 1654 ppm respectively, even when allowed to run for longer periods (50 min or even more) to assess the stability of these samples. This obviously is an indication that these do not contain the other TMs even after these prolonged lengths of time. Another experiment (not shown) run under similar conditions for a synthesized "TM3" sample suspected (based on the UV/visible spectra) to be cross-contaminated by other TMs, shows the presence of TM2. Observations in the literature of significant levels of contaminating TMs in solutions shortly after sample dissolution are in the main simply due to contamination in the synthesized material especially for the more stable TMs (TM3 and TM4).

2.3.9 Thiomolybdate Formation under Rumen-like Conditions

Figure 2.5 shows the levels of the various TMs at various times after mixing Na_2MoO_4 and $(NH_4)_2S$ with a S:Mo ratio of 22:1, under conditions which mimic those

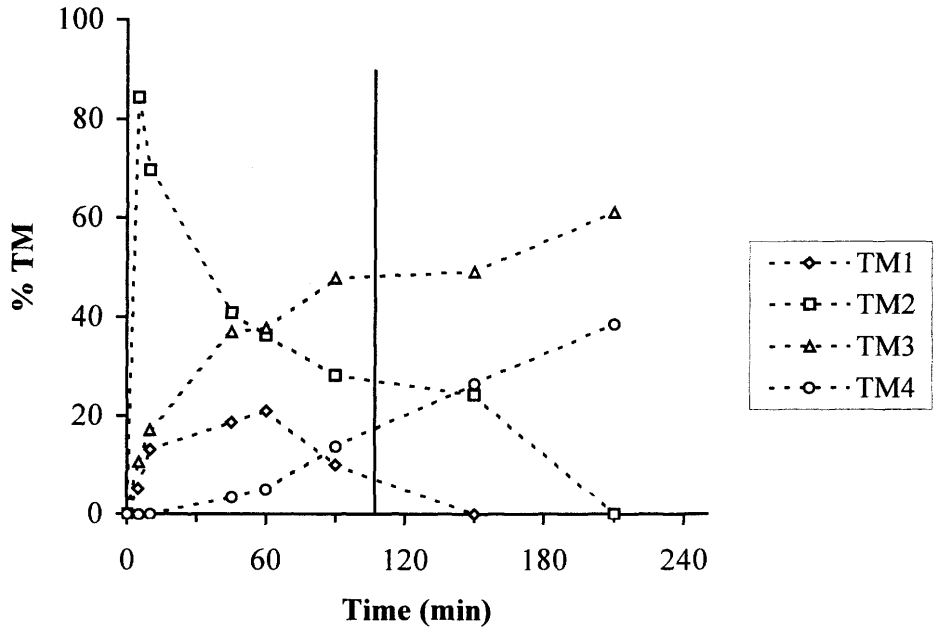

Figure 2.5: TMs as a fraction of total Mo present at different times after mixing Na_2MoO_4 in solution with ammonium sulfide solution to give an S:Mo ratio of 22:1, pH 7.0, ionic strength 0.2 **M**, and a temperature of 38°C. Initial concentration of molybdate in the mixture was 1x 10^{-4} **M**. The vertical line represents the mean residence time of S^{2-} in the rumen.

in rumen fluid, i.e., pH = 7, ionic strength 0.2 **M** and a temperature of 38°C (Section 1.5.3.1).

Within 5 min about 85% of the TM formed is TM2, in agreement with an earlier observation that TM2 is rapidly formed for S:Mo > 10:1 (80CL). There is then a steady decline of TM2 (slowing down only between 60 to 90 min), with a concomitant increase in TM3. A substantial amount (35%) of TM3 is formed within 30 min of reaction. The graphs for the levels of TM2 and TM3 are almost symmetrical, and the two stay almost constant between 90 to 150 min, suggesting that TM3 is formed from TM2. The mean residence time of sulfide in the rumen of sheep, reported (76GN) to be 107 min, falls within the time period where the percentages of TM2 and TM3 are almost constant, at ~28 % and ~ 48% respectively. Formation of TM4 is slow but noticeable within 30 min. TM4 then increases steadily, constituting about 18% at the mean sulfide residence time

and 30% after 3 hr. TM1 formation is gradual under the conditions employed in this study, up to about 60 min, then its level begins to decline. No unreacted molybdate was found beyond 5 min.

With the increase in the Mo concentration to 2.5 x 10^{-4} **M** and a variation of S^{2-} concentration to give a Mo:S ratio of 5.5:1, the formation pattern of the TMs changed markedly (Figure 2.6). TM1 and TM2 were formed rapidly to ca. the same extent (50%) within 5 min. TM2 then declined gradually to ~ 20% within 3 hr, with a concomitant increase in the TM0 level. The graphs for these two levels were also almost symmetrical. There was also little variation in the TM1 level between 5 min and 180 min. TM3 and TM4 were formed, but only gradually. Their levels never exceeded 5% over 180 min.

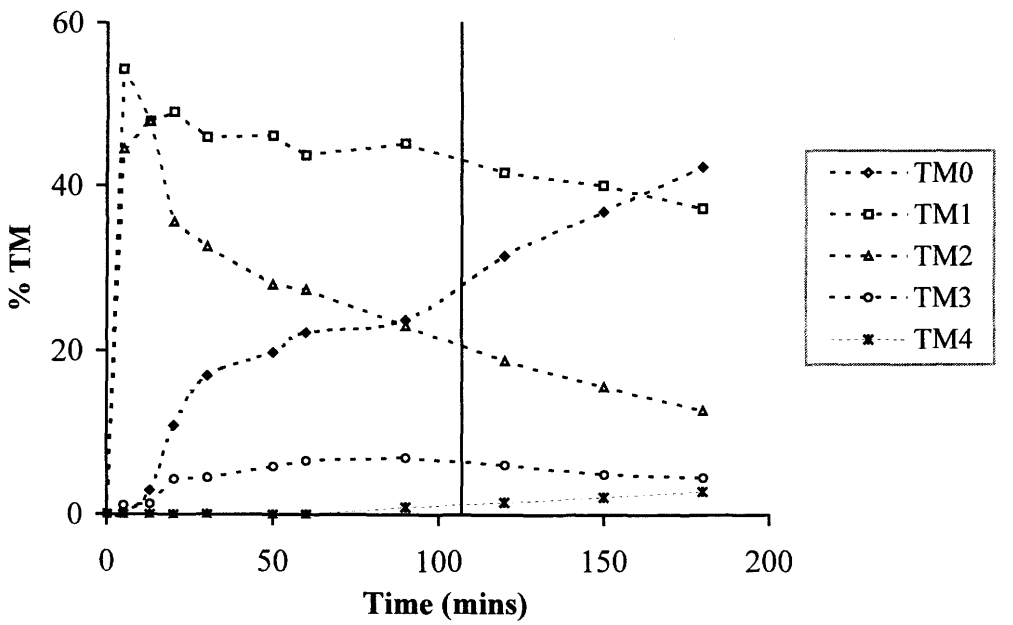

Figure 2.6: TMs as a fraction of total Mo present at different times after mixing Na_2MoO_4 in solution with ammonium sulfide solution to give an S:Mo ratio of 5.5:1, pH 7.0, ionic strength 0.2 **M**, and a temperature of 38°C. Initial concentration of molybdate in the mixture was 2.5 x 10^{-4} **M**. The vertical line represents the mean residence time of S^{2-} in the rumen

2.4 CONCLUSIONS

This chapter outlines facile synthetic methods for preparing pure samples of all four TMs, and methods for unambiguously determining their degree of cross-contamination. This should serve as the groundwork for definitive studies of the solution stability and *in vivo* reactivity of these important species, and help to remove the current ambiguities in our understanding of their properties. Employing conditions that mimic that in the rumen, the levels of TMs have been determined as a function of time. Under these conditions, the formation of each TM is possible, but the "higher" TMs (TM4 and TM3) are more likely to form at later times than the "lower" ones (TM2 and TM1) due to the inherent instability of the latter forms.

3. UV/VISIBLE SPECTROPHOTOMETRIC STUDIES OF INTERACTIONS BETWEEN Cu(II), THE THIOMOLYBDATES AND OTHER LIGANDS

3.1 INTRODUCTION

In Section 1.5.2 the ways in which TMs may be implicated in secondary Cu deficiency, and attempts to remedy the situation by the administration of Cu in a complexed form, were discussed.

The digestive system of ruminants, in which interactions involving Cu, TMs and other ligands take place, is obviously a complex aqueous system with innumerable ligands. A good understanding of the mechanism by which TMs in general, and TM4 in particular, render Cu unavailable, requires systematic aqueous solution chemistry studies of the binding of the individual TMs with Cu(II) in both the presence and absence of other ligands of biological significance. Few attempts have been made to understand the chemistry of Cu-(S)-Mo-S interactions under conditions that mimic the biofluids in the digestive system of ruminants (84SM, 86LP, 87WM, 80CL, 82CL, 87CLa). Understanding is further hampered by the question of which specific TM or TMs is/are prevalent in the rumen and elsewhere in the digestive tract.

In part, these problems can be ascribed to the previous lack of availability of synthesized TMs of known purity. In Chapter 2, the synthesis of the four TMs, TM1, TM2, TM3 and TM4 in aqueous-soluble form, and precise determination of the levels of mutual cross-contamination was discussed. It was shown that several conflicting observations in the literature regarding the properties and stability of the TMs could be ascribed to the varying purities of the materials prepared by different authors. Studies of

TM formation under rumen-like conditions suggest that any of the four TMs can be formed in the rumen depending on the level of S. However, it was concluded in Chapter 2 that TM3 and TM4 are more likely to be prevalent in the rumen due to their higher relative stabilities over TM1 and TM2.

It is therefore now possible to perform meaningful solution chemistry studies of the interactions of the individual TMs with Cu(II) ions in simple aqueous solutions, as a necessary first step in understanding the detailed mechanisms by which Mo compounds effect ruminant Cu deficiency. These studies form the subject of this Chapter.

3.2 EXPERIMENTAL

3.2.1 Sources of Chemicals

All chemicals used were reagent grade and were used without further purification unless stated below. Potassium dihydrogen phosphate (KH_2PO_4), copper sulfate pentahydrate ($CuSO_4.5H_2O$), and disodium ethylenediaminetetraacetate (EDTA, disodium salt) were obtained from the Fisher Scientific Company (Fair Lawn, USA). Potassium hydrogen phthalate (KHP) and L-Histidine hydrochloride were obtained from BDH Chemicals Ltd. (Poole, England). Sodium sulfide ($Na_2S.9H_2O$), potassium nitrate (KNO_3), sodium hydroxide (NaOH), hydrochloric acid (HCl) and nitric acid (HNO_3) were obtained from BDH Chemicals Ltd. (Toronto, Canada). Sodium chloride (NaCl) was obtained from Amachem, American Scientific and Chemical (Portland, USA). Anhydrous sodium sulfate (Na_2SO_4) was obtained from J. T. Baker Chemical Co. (Phillipsburg, USA). The TM salts $(NH_4)_2MoS_4$, Cs_2MoOS_3, $(NH_4)_2MoO_2S_2$ and Cs_2MoO_3S were synthesized and characterized as described in Section 2.2.5.

Bovine Serum Albumin (BSA-A7906) was obtained from the Sigma Chemical Company (St. Louis, USA). Albumin solution concentrations were estimated from the measured absorbance at 278.5 nm and an $A_{1\ cm}^{1\%} = 6.61$ (87WM). Other chemicals were obtained as detailed in Section 2.2.1.

3.2.2 Preparation of Solutions

Except otherwise stated, all solutions were prepared using distilled and deionized water, prepared as described in Section 2.2.1.

A stock 1.00×10^{-1} **M** EDTA solution was made by dissolving in water 37.2260 g of the disodium salt of EDTA, weighed from about 40 g of the salt previously dried overnight at ~ 110 ^{O}C, and diluting to volume in a 1 L volumetric flask. From this stock solution, 100 mL was pipetted into another 1 L volumetric flask and diluted to volume to make a 1.00×10^{-2} **M** EDTA solution. Further serial dilutions were made to prepare 1.00×10^{-3}, 1.00×10^{-4} and 1.00×10^{-5} **M** solutions of EDTA.

A stock Histidine (His) solution of concentration 1.00×10^{-1} **M** was prepared by dissolving 0.5241 g of L-Histidine Hydrochloride in water and diluting to volume in a 25 mL volumetric flask. 1.00×10^{-2}, 1.00×10^{-3}, 1.00×10^{-4} and 1.00×10^{-5} **M** solutions of His were made by serial dilutions of this stock solution.

A stock Na_2S solution was obtained by dissolving about 6.5 g of $Na_2S.9H_2O$ in water and diluting to volume in a 250 mL volumetric flask. This solution was standardized by the iodometric method outlined in Section 2.2.3.3 to obtain an exact concentration of 8.78×10^{-2} **M**. Appropriate dilutions of this stock solution were made for studying the effects of sulfide concentrations on Cu-TM interaction.

A stock solution of 1.00×10^{-2} **M** copper(II) sulfate was made by dissolving 6.2400 g $CuSO_4.5H_2O$ in water and diluting to volume in a 250 ml volumetric flask. 1.00×10^{-1} **M** stock solutions of the other salts (KNO_3, NaCl, NaOH, Na_2SO_4, KH_2PO_4 and Potassium Hydrogen Phthalate, KHP) were made by dissolving the appropriate mass in water and diluting to volume in a 100 mL volumetric flask. Solutions of lower concentrations were made by appropriate dilutions of the stock solutions as required.

Freshly prepared 1.00×10^{-4} **M** TM1, TM2, TM3 and TM4 solutions were made by dissolving 0.00226 g, 0.00132 g, 0.00237 g, and 0.00130 g of $(Cs)_2MoO_3S.1/2H_2O$, $(NH_2)_2MoO_2S_s.2H_2O$, $(Cs)_2MoOS_3$ and $(NH_2)_2MoS_4$ respectively in water and diluting each to volume in a 50 mL volumetric flask Such solutions were used to study the stoichiometry of the interactions between Cu(II) and the TMs (Section 3.2.4.1). The 2.00×10^{-3} **M** solutions used in the more quantitative studies of Section 3.2.4.1 were prepared in a similar manner. A third set of stock TM solutions (2.12×10^{-3} **M**) were also prepared similarly, but in 5 mL volumetric flasks to study the effects of pH (Section 3.2.4.2) and other ligands (Sections 3.2.5 and 3.2.6) on the Cu(II)-TM reaction system.

Various pH buffer solutions (1.89, 3.00, 3.97, 4.95, 5.92 and 6.98) were prepared. Some were prepared by mixing various stock solutions of the salts NaCl, KH_2PO_4 or KHP, and the acid HCl or the base NaOH, as outlined in (88W).

For experiments involving BSA "mixed" phosphate buffers, which are claimed to be of more physiological relevance by Christian (94C) because biological systems usually contain phosphates, were used. ("Mixed" refers to the cations in the salts used to prepare the buffers.) These buffers were prepared from various mixtures of the phosphate salts Na_2HPO_4 and KH_2PO_4, and of H_3PO_4 as detailed in (94C).

3.2.3 Instrumental Measurements

UV/visible measurements and C, H, and N analyses were performed as described in Section 2.2.4. The pH measurements were made with an Acc-pHast standard combination glass body pH electrode (Fischer Catalogue No. 13-620-296) and an Accumet pH meter. The electrode was calibrated by standard U.S. National Institute of Standards and Technology (N.I.S.T.) approved methods, using a set of primary standard solutions whose pH values have been accurately established by the N.I.S.T. (73B). The primary standard solutions are not stable and were therefore used to

standardize a set of standard commercial buffers, which are more stable (98A). The standardized buffers were used for routine calibration.

3.2.4 Interactions of Aqueous Cu(II) with TMs

3.2.4.1 Stoichiometry

Two such studies were performed. The first, reported in Section 3.3.1.1 to Section 3.3.1.3, involved the mixing of 2.00 x 10^{-4} **M** Cu(II) and 1.00 x 10^{-4} **M** TM in various proportions (i.e. Cu(II):TM mole ratios of 0:1, 0.50:1, 0.67:1, 0.80:1, 1.00:1, 1.33:1, 1.50:1 and 2.00:1). The UV/visible spectra were all taken immediately after sample preparations.

For the second study, reported in Section 3.3.1.4, 5.0 mL of a freshly prepared 2.00 x 10^{-4} **M** solution of a TM was pipetted into each of eight 10 mL volumetric glass flasks. Different amounts of the stock aqueous Cu(II) solution (1.00 x 10^{-2} **M**) or a diluted solution (2.00 x 10^{-4} **M**) were pipetted into the flasks, water added to volume, and the flasks stoppered and shaken. This gave solutions with Cu(II):TM mole ratios of approximately 0:1, 1:50, 1:10, 1:5, 1:2, 1:1, 1.5:1 and 3:1. These initial estimates of mole ratios were determined by calculating from the accurate volumes of each stock solution used. The UV/visible spectrum of each solution was taken and the absorption measured at wavelengths of 250 nm, 300 nm, 350 nm, 400 nm, 450 nm and 500 nm in a similar fashion to that described in Section 2.2.6. The data were collected immediately after sample preparations.

3.2.4.2 Effect of pH on Cu(II) Interaction with TMs in Aqueous Solutions

Mixing of aqueous Cu(II) and TM solutions was performed both in buffered and non-buffered solutions at 25° C as follows.

For the studies in buffered solutions, reported in Section 3.3.1.1 for TM4, Section 3.3.1.2 for TM3 and Section 3.3.1.3 for TM2, 0.11 mL of the 0.01 **M** stock Cu(II) solution was pipetted into each of six 50 mL Erlenmeyer flasks. 10 mL of each of the buffer solutions of pH 2, 3, 4, 5, 6, and 7, was added by pipette. 0.5 mL of 2.12×10^{-3} **M** TM solution was also added by pipette, to give approximately equimolar reactant concentrations of 1×10^{-4} **M**. The UV/visible spectrum over the wavelength range 230 to 500 nm was taken for each solution within 20 min. No difference was observed between aerobic and anaerobic conditions in this particular study, as also observed by Clarke and Laurie (82CL), and therefore no special precautions were taken to exclude air.

Similar procedures were followed for the studies in unbuffered solutions, reported in Section 3.3.1.1 for TM4, Section 3.3.1.2 for TM3, and Section 3.3.1.3 for TM2, except for the replacement of the buffer solutions with 1×10^{-2} **M** HNO_3, 1×10^{-3} **M** HNO_3, H_2O, 1×10^{-4} **M** NaOH, 2×10^{-4} **M** NaOH, and 1×10^{-3} **M** NaOH to obtain solutions of different pH values. For instance, in the case of TM4, pH values of 2.05, 3.06, 4.29, 5.49, 6.30* and 10.55 were obtained. It is important to note that the order of mixing was the same as in the case of the buffer solutions with the exception of the Cu(II) and TM4 mixture whose pH was adjusted with 2×10^{-4} **M** NaOH, where the order of mixing was changed as marked asterisk above.

3.2.5 Effect of Ionic Strength on the Interaction of Cu(II) with TMs in Aqueous Solutions

Aqueous solution mixtures of Cu(II) and the various TMs were prepared at different ionic strengths, at ambient temperature, as follows. 0.11 mL of the 1×10^{-2} **M** stock Cu(II) solution was pipetted into different 50 mL Erlenmeyer flasks. 10 mL of an electrolyte solution of specified concentration was pipetted into each flask. 0.5 mL of 2.12×10^{-3} **M** TM solution was added by pipette to give, on dilution to the mark, approximately equimolar reactant concentrations of 1×10^{-4} **M**.

The electrolyte solutions used were either the same electrolyte but with varying concentrations of 0.01, 0.02, 0.05, 0.1, 0.15 and 0.2 **M** as studied for NaCl, or were of the same concentration but for various electrolytes (i.e. NaCl, KHP, KH_2PO_4, Na_2SO_4, KNO_3, HNO_3 and HCl). Solutions were observed for approximately 5 days for the formation of precipitates as reported in Section 3.3.1.2. The UV/visible spectrum of each solution in the wavelength range 230 to 500 nm was also monitored with the course of time, unless precipitation caused serious background absorption.

3.2.6 Cu(II) interactions with TM in Aqueous Solutions in the presence of some Low Molecular Mass Ligands

The low molecular mass ligands used in the studies were EDTA, L-Histidine and the sulfide ion.

3.2.6.1 Effect of EDTA on Cu(II) Interaction with the TMs

The effect of EDTA on the interaction of Cu(II) with TM solutions was studied in two main ways. In the first case, reported in Section 3.3.1.6 for TM4, Section 3.3.1.7 for TM3, and Section 3.3.1.8 for TM2, Cu(II) and EDTA were mixed in various quantities in 50 mL Erlenmeyer flasks at ambient temperature as outlined in Table 3.1. 0.5 mL of 2.12×10^{-3} **M** TM was then immediately pipetted into the flask, which was stoppered, shaken and allowed to stand. Aliquots of each sample were withdrawn with pipettes into quartz cuvettes for UV/visible measurements. Spectra were taken at different times, one at most 5 min after adding the TM and another at least 1 hr after adding the TMs. The actual times are specified in Section 3.3.1.3, where the results are discussed.

In the second experiment to study the effect of EDTA on Cu(II) and TM interactions, also reported in Section 3.3.1.6 for TM4, Section 3.3.1.7 for TM3, and Section 3.3.1.8 for TM2, EDTA was added in different quantities (i.e., 0, 10^{-5} , 10^{-4}, 10^{-3}, 10^{-2}, 10^{-1} **M**) to a reacting mixture of Cu(II) and TM at a ratio of 1:1 and a concentration of 1×10^{-4} **M**.

Table 3.1: Constituents of solutions containing EDTA, Cu(II) and TMs for the studies of Section 3.3.1.3. The values in the tables represent the volumes in ml for the concentrations (**M**) given in parentheses.

Sample	EDTA or H_2O	Cu(II) or H_2O	TM	[a]Mole ratio	Ionic strength
a	10.00 (H_2O)	0.110(10^{-2} **M**)	0.50 (2.12x10^{-3} **M**)	0:1:1	4.0 x 10^{-4} **M**
b	10.00 (10^{-5} **M**)	0.110(10^{-2} **M**)	0.50 (2.12x10^{-3} **M**)	0.1:1:1	4.2 x 10^{-4} **M**
c	10.00 (10^{-4} **M**)	0.110(10^{-2} **M**)	0.50 (2.12x10^{-3} **M**)	1:1:1	5.9 x 10^{-4} **M**
d	10.00 (10^{-3}**M**)	0.110(10^{-2} **M**)	0.50 (2.12x10^{-3} **M**)	10:1:1	9.0 x 10^{-3} **M**
e	10.00 (10^{-2}**M**)	0.110(10^{-2} **M**)	0.50 (2.12x10^{-3} **M**)	10^2:1:1	9.4 x 10^{-2} **M**
f	10.00 (10^{-1} **M**)	0.110(10^{-1} **M**)	0.50 (2.12x10^{-3} **M**)	10^3:1:1	9.4 x 10^{-1} **M**
g	10.00 (H_2O)	0.110(H_2O)	0.50 (2.12x10^{-3} **M**)	0:1:1	-

a. EDTA:Cu(II):TM

3.2.6.2 Effect of S^{2-} on Cu(II) Interactions with the TM4 and TM3.

For the TM4 experiments, three S^{2-} aqueous solutions of concentrations 8.78×10^{-3} **M**, 8.78×10^{-4} **M** and 8.78×10^{-5} **M** were prepared by the dilution of stock S^{2-} solution. 10.00 mL of the stock S^{2-} solution, the three diluted S^{2-} solutions and water were pipetted separately into five 50 mL Erlenmeyer flasks at ambient temperature. 0.500 mL of stock TM4 solution (2.12×10^{-3} **M**) was added to the content of each flask. 0.110 mL of 1.00×10^{-2} **M** aqueous $CuSO_4$ solution was added to each of the flasks, and the mixture shaken. This yielded different mixtures, each containing 1×10^{-4} **M** Cu(II) and 1×10^{-4} **M** TM and one of the following S^{2-} concentrations; 8.3×10^{-2} **M**, 8.3×10^{-3} **M**, 8.3×10^{-4} **M**, 8.3×10^{-5} **M** and zero. Aliquots of each mixture were taken for spectral data collection 5 min and 1hr after adding the Cu(II) solution. Solutions for TM3 studies were prepared in an identical manner.

3.2.6.3 Effect of L-His on Cu(II) Interaction with TM4

The same procedure described in Section 3.2.6.1 for studies involving EDTA was also used for those involving L-His. Reaction concentrations were as in Table 3.5 with the obvious exception of replacing EDTA with L-His and the modification of the ionic strengths in the reaction mixtures due to charge differences between the two ligands. This study was conducted only for TM4, and not the other TMs.

3.2.7 Interactions between Bovine Serum Albumin (BSA), Cu(II) and TMs

3.2.7.1 BSA Binding to TM

To investigate the interaction between BSA and the TMs, 0.0663 g of BSA was first weighed and transferred quantitatively into a 10.00 mL volumetric flask. Water or the buffer was added, just enough to leave at least 2.00 mL space in the flask. A small magnetic stirring bar was put into the flask, and the contents stirred continuously till the BSA dissolved, to yield a viscous solution. 0.500 mL of 2.00×10^{-3} **M** TM was added,

and the solution stirred magnetically. The stirring bar was then removed with a Teflon coated magnet, and washed carefully with water or the buffer from a washed bottle into the flask. The flask was filled to volume, to give a final reactant concentration of 1.00×10^{-4} **M** for BSA and TM.

Spectral scans were carried out at room temperature as outlined in Section 2.2.4 using the solvent (i.e. water or the particular buffer solution) used in the preparation of the BSA and TM reaction mixture as the reference solution. For the collection of the difference spectral data, 0.500 mL of the same stock solution of TM (i.e. 2.00×10^{-3} **M**) diluted to the mark of a 10.00 mL volumetric flask and prepared at about the same time as the reaction mixture of BSA and TM was used as the reference solution.

3.2.7.2 Ternary Complexation between BSA, Cu(II) and TMs

These studies were performed in three ways:

1. Mixing Cu(II) and the TMs first, followed by BSA addition. Studies are reported in Section 3.3.3.
2. Mixing TM and BSA first, in (phosphate) buffered solution of pH 7.0 (see Table 2.2), followed by the addition of aqueous Cu(II) solution. Studies are reported in Section 3.3.3.2 for TM3.
3. Mixing Cu(II) and BSA first, in both (phosphate) buffered solutions (pH 6.0, 7.0, and 8.0) and non-buffered solutions, followed by the addition of TM. Studies are reported in Section 3.3.3.1 for TM4, Section 3.3.3.2 for TM3 and Section 3.3.3.3 for TM2 and TM1.

In the first procedure, 0.100 mL of 1×10^{-2} **M** Cu(II) solution was mixed with 0.500 mL of 2.00×10^{-3} **M** TM by shaking in a 10 mL volumetric flask and allowed to stand for 5 min. 9.6 mL of fresh BSA solution (~ 1.04×10^{-4} **M**), prepared as above in a buffer solution of pH 7, was added, and the mixture shaken to give a solution with a concentration of 1.00×10^{-4} **M** for BSA, Cu(II), and TM.

In the second procedure, 0.0663 g of BSA was dissolved in a phosphate buffer of pH 7 as described in Section 3.2.7.1. 0.500 mL of 2.00 x 10^{-3} **M** TM solution was pipetted into the content of the 10.00 mL volumetric flask to obtain a 1:1 BSA:TM reaction mixture. Different volumes of 1x 10^{-2} **M** Cu(II) solution were added by pipette, then the flask was filled to volume with phosphate buffer of pH 7 to obtain different ratios of BSA:Cu(II):TM reaction mixtures as reported in Section 3.3.2.2a.

In the third procedure, 0.0663 g of BSA was dissolved as described in Section 3.2.7.1. 0.100 mL of 1x 10^{-2} **M** Cu(II) solution was pipetted into the flask, and the contents stirred magnetically for about 5 min to form a pale purple solution. 0.500 mL of 2.00 x 10^{-3} **M** TM was then added, and the solution stirred magnetically, to form an orange solution. The stirring rod was then removed with a Teflon coated magnet and washed carefully with water or the buffer from a wash bottle into the flask. The flask was filled to volume to give a solution with a concentration of 1.00 x 10^{-4} **M** for BSA, Cu(II) and TM.

Spectral scans were carried out at room temperature as outlined in Section 2.2.4 and above for BSA and TM mixtures. For the collection of the difference spectral data for 1:1:1 BSA:Cu(II):TM vs Cu(II):TM, a mixture of 0.50 mL of the stock TM solution (i.e. 2.00 x 10^{-3} **M**) and 0.10 mL of the stock 1.00 x 10^{-1} **M** Cu(II) solution, diluted to the mark of a 10 mL volumetric flask with the particular solvent used in the preparation of the 1:1:1 BSA:Cu(II):TM reaction mixture, was used as the reference solution.

3.2.7.3 Effect of EDTA on BSA, Cu(II) and TM3 Interactions

This study was also performed in two ways, using water as the solvent in the preparation of the reaction mixtures (see Section 3.3.2.3) or using pH 7.0 phosphate buffer. A 1:1:1 BSA:Cu(II):TM3 reaction mixture was prepared similarly to that described in Section 3.2.7.2 except for the addition of EDTA at various concentrations between 0 and 5.0 x 10^{-3} **M**.

3.3 RESULTS AND DISCUSSION

3.3.1 Cu(II) Interactions with TMs in Aqueous Solutions

3.3.1.1 Stoichiometry and pH Effects: TM4

Figure 3.1 and Table 3.2 give the results of the observed absorbance as increasing amounts of Cu(II) were added to non-buffered TM4 solutions, as detailed in Table 3.3 and Section 3.2.4.1.

In Table 3.2, the predicted (pred) absorbance is also included for comparison. It was assumed in calculating this that there was no reaction between Cu(II) and TM4, and therefore that only dilution due to the added Cu(II) solution would affect the absorbance. For example, for the Cu(II):TM reaction mixture of ratio 0.50:1, 1 mL of Cu(II) aqueous solution (2×10^{-4} **M**) was added to 4 mL of TM aqueous solution (1×10^{-4} **M**), so the predicted absorbance for the TM4 peak is 2.27 divided by 1.25 (i.e., 5 over 4) which gives the predicted absorbance of 1.82 as in Table 3.2. Note that the absorbance of the TM4 (1×10^{-4} **M**) peak at 241 nm prior to adding any Cu(II) was 2.27. The differences between measured and predicted absorbance of each of the three peaks (Table 3.2) can be attributed to the removal of TM from the solution, and possibly absorbance due to new species formed from the interaction between Cu(II) and TM4.

As increasing amounts of Cu(II) were added to the TM4 solutions the observed characteristic TM4 peaks absorbing at 468 nm, 316 nm and 241 nm (see Table 2.1) decreased gradually in intensity, with the major changes occurring up to a stoichiometry of 1:1, as shown in Figure 3.1. At Cu(II):TM4 stoichiometries from 1:1 up to 2:1, a new, broad peak emerged at ~ 285 nm (Figure 3.1 and Table 3.2). As noticed in Section 1.2.6.2 (see also Table 1.4), the interaction of Cu(II) compounds with TM4 causes a shift of the 241 nm peak of TM4 to longer wavelength. This shift in

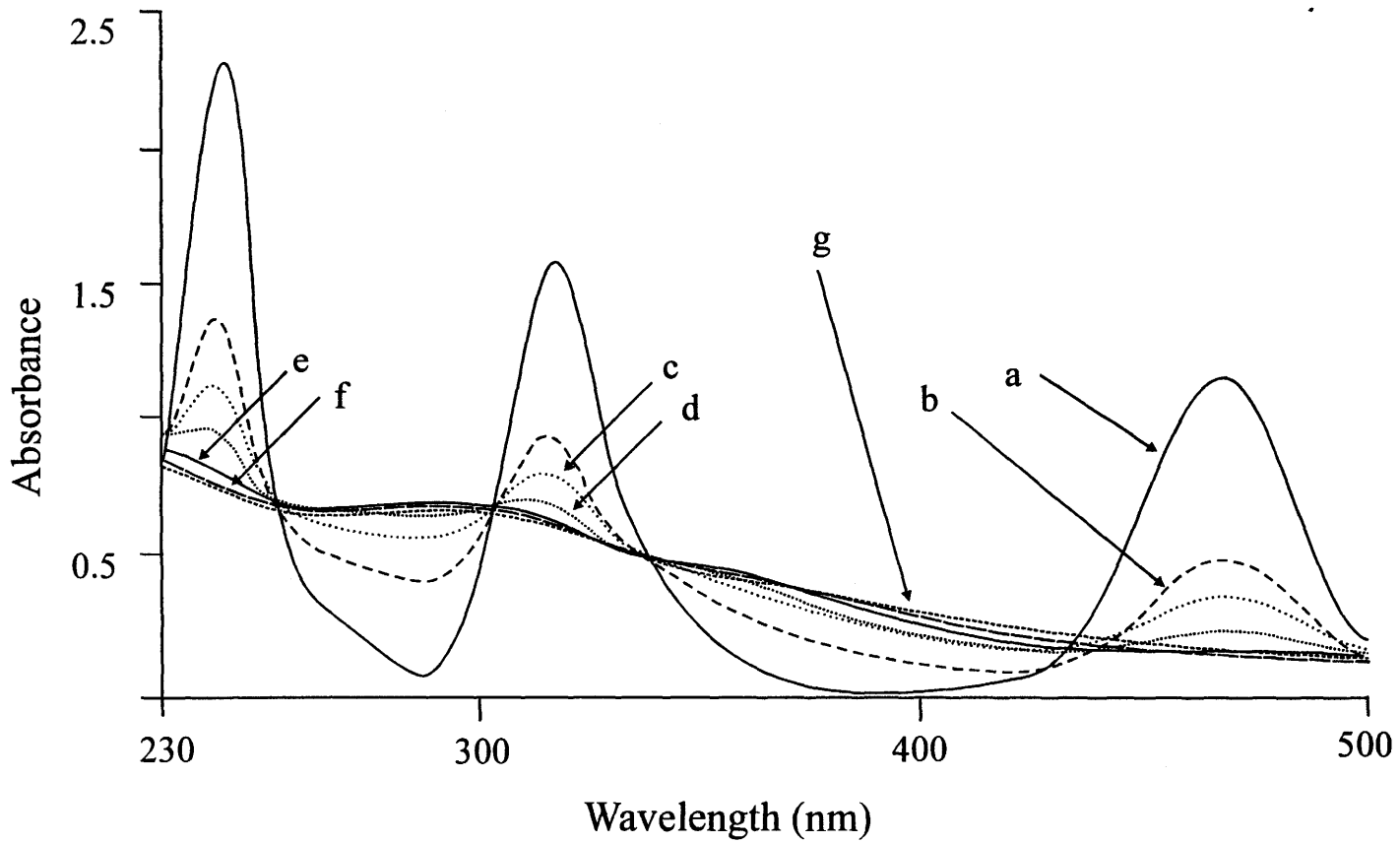

Figure 3.1: UV/visible spectra of TM4 as different amounts of Cu(II) are added to TM4 solutions as detailed in Table 2.3 to obtain a Cu(II): TM4 mole ratio of (a) 0:1 (i.e. 10^{-4} **M** TM4 alone), (b) 0.50:1, (c) 0.67:1, (d) 0.80:1, (e) 1.00:1 , (f) 1.33:1, (g) 1.50:1.

Table 3.2: Observed (obs) and predicted (pred) absorbances for the TM4 peaks on mixing different proportions of Cu(II) and TM4 aqueous solution.

Cu(II):TM4 ratio	Obs. at ~ 241 nm	[b]Pred. at ~ 241 nm	Obs. at ~ 317 nm	Pred. at ~ 317 nm	Obs. at ~ 468 nm	Pred. at ~ 468 nm	"new peak" at λ_{max} ~ 285 nm
0:1	2.2700	2.2700	1.5600	1.5600	1.1600	1.1600	-
0.50:1	1.3454	1.8160	0.9491	1. 2480	0.5350	0.9360	-
0.67:1	1.1188	1.7025	0.8150	1. 1700	0.3846	0.8700	-
0.80:1	0.9374	1.6214	0.7037	1.1143	0.2635	0.8286	-
1.00:1	[c]-	1.5133	-	1.0400	-	0.7733	0.7129
1.33:1	-	1.3620	-	0.9360	-	0.6960	0.7109
1.50:1	-	1.2971	-	0.8914	-	0.6629	0.6806
2.00:1	-	1.1350	-	0.7800	-	0.5800	0.6123

b. The predicted (pred.) absorbance based on the assumption that there is no reaction between Cu(II) and TM4 (see text for more details).

c. All dashed lines indicate that no peak maximum was observed at that wavelength.

wavelength indicates strong Cu-TM4 interactions due to charge transfer (92ST), which invariably leads to the formation of Cu-(S)-Mo-S clusters. Thus, peaks observed at 284 nm, 285 nm and 262 nm for Cu-(S)-Mo-S cluster anions; $[PhSCuS_2MoS_2CuSPh]^{2-}$, $[CCuS_2MoS_2CuC(phen)]^{2-}$, $[(bipy)CCuS_2MoS_2CuC(phen)]^{2-}$ respectively, have been assigned to the shift of the 241 nm TM4 peak to the longer wavelengths (see Section 1.2.6.2), after the reaction of the corresponding copper compounds with TM4.

The degree of completeness of this reaction was found to be pH dependent as can be seen in Figure 3.2. At pH 8, the characteristic TM4 band at ~ 317 nm was still evident for the 1:1 stoichiometric mixture, but the intensity was reduced as compared to TM4 alone of the same concentration (1 x 10^{-4} **M**) in the 1:1 Cu(II):TM4 reaction mixture prior to any reaction. The peak at 468 nm could, however, be barely recognized. In pH 7.0 buffer solution, the characteristic TM4 bands at ~ 317 and 468 nm were both still evident for the 1:1 stoichiometric mixture (Figure 3.2) but once again, with lower absorbances than for TM4 alone.

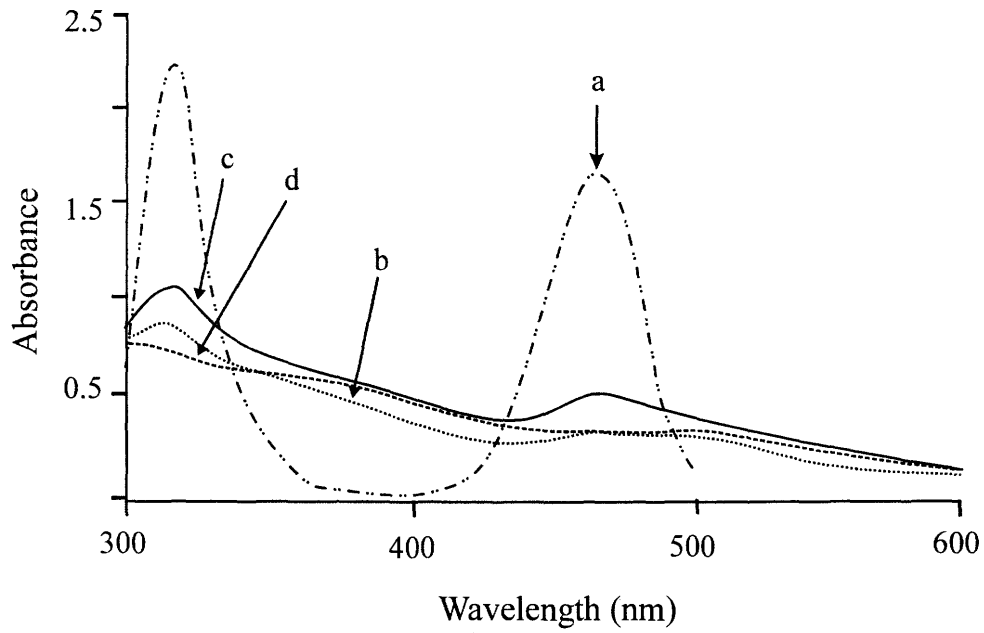

Figure 3.2: UV/visible spectra of (a) 10^{-4} **M** TM4 (pH ~ 7) and 1:1 Cu(II):TM4 (1 x 10^{-4} **M**) at a pH of (b) 8.0, (c) 7.0, (d) 6.0.

It should be noted that TMs are known to be **more** stable in aqueous solutions under basic conditions (22M, 87WM), so these lower absorbances are not due to TM degradation. The lack of observation of the formation of solid $Cu(OH)_2$ at these pH values is further evidence of interaction with the TM.

At pH 6.0 the peaks were more flattened and could barely be recognized ((d) of Figure 3.2). At pH ≤ 5 these peaks disappeared completely, and a new peak with a low absorbance emerged at ~ 285 nm, as was also observed for the 1:1 to 2:1 Cu(II):TM4 mixtures in water, where the resulting pH was 4.3 (Table 3.2 and Figure 3.1). Decreasing pH therefore seems to favor the completion of the reaction.

To ascertain whether the electrolytes used in the buffer preparations might be influencing the situation, similar studies were conducted in non-buffered solutions using HNO_3 to adjust the pH (see Section 3.2.4.2). The wavelength range was extended to cover lower wavelengths than 300 nm since the interference in these regions caused by KHP in the buffers is absent in this case. Figure 3.3 shows the spectra obtained. At pH values of 2.05, 3.06 and 4.29, the characteristic peaks of TM4 could not be observed (Figure 3.3) as was also the case for the buffered solutions of pH ≤ 5 discussed above. At pH 5.49 and 6.60, the characteristic peaks of TM4 could still be observed, although the intensities were reduced as compared to TM4 alone (Figure 3.3). The absorbance of the peaks at 317 and 468 nm in the solution of pH 6.60 was greater than that of pH 5.49.

The observation of the reduction in intensity of the 317 and 468 nm peaks of TM4 on adding equivalent amount of Cu(II) was also observed by Clarke and Laurie (82CL) in a buffer solution at pH 7.0; further studies (86LP) indicated that a 1.5:1 Cu(II):TM4 ratio was sufficient to ensure complete removal of the characteristic peaks at pH 7.4. They concluded that the stoichiometry in the Cu-Mo complex was 1.5:1. However, on the basis of the above experiments, it seems more likely that the excess half equivalent of TM4 at pH ~7 is only required to drive the reaction to completeness at a stoichiometry of 1:1. Recall that when the reaction is performed simply in water

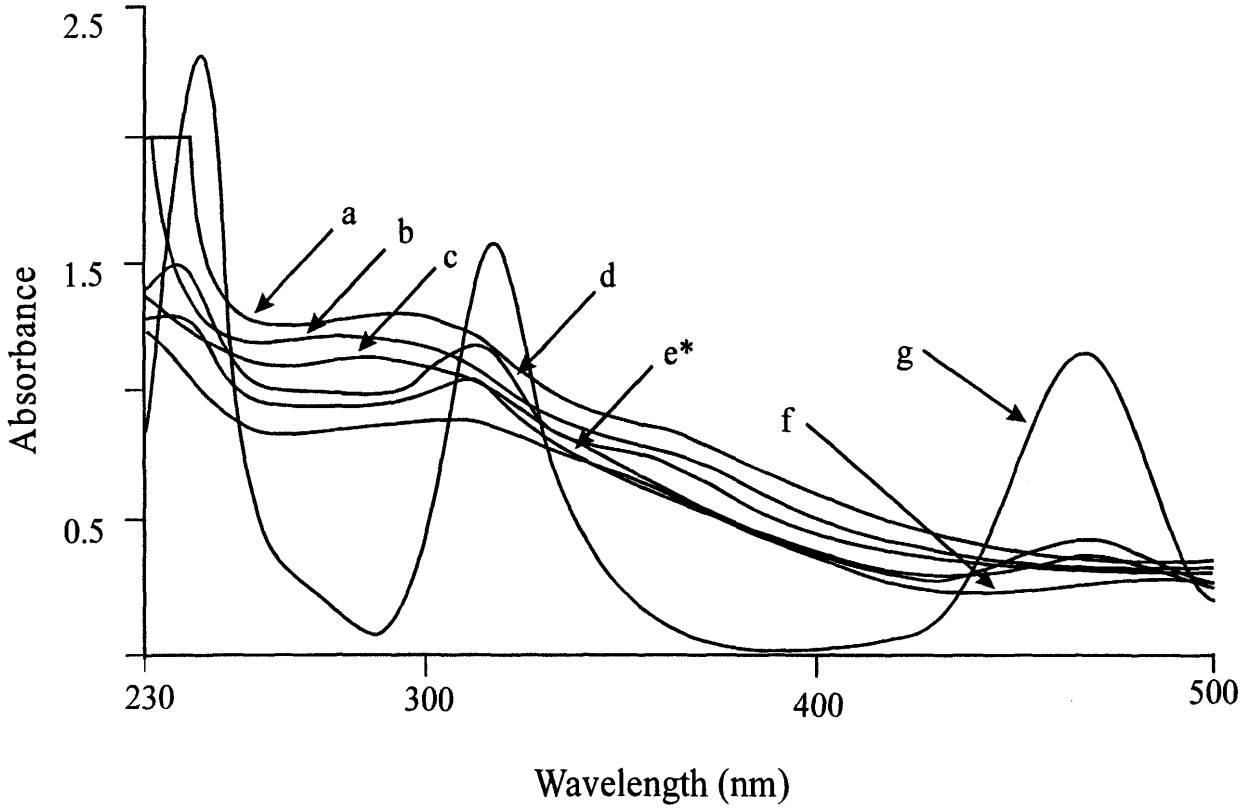

Figure 3.3: UV/visible spectra of 1:1 Cu(II):TM4 (1 x 10^{-4} **M**) in non-buffered solutions with pH values of (a) 2.05, (b) 3.06, (c) 4.29, (d) 5.49, (e*) 6.60 (the other of mixing the reactants was different from a to b and f), (f) 10.55, (g) TM4 alone (1 x 10^{-4} **M** at pH ~ 7) for comparison. See Table 3.4 and Section 3.2.4.2 of the text for experimental details.

the characteristic peaks at 317 nm and 468 nm is removed at 1:1 Cu(II):TM4 mole ratio and further addition of Cu(II) to up to a mole ratio of 2:1 results in no major change in the spectrum. This suggests a 1:1 stoichiometry for the interaction. Furthermore, it is clear from the pH experiment above, that pH influences the completeness of the reaction and at pH $\geq$ 5, the reaction is not complete. Excess Cu(II) would then be required to drive the reaction to completion.

3.3.1.2 Stoichiometry and pH Effects: TM3

Increasing Cu(II) concentration caused the decrease of the characteristic TM3 peaks at 311 nm , 396 nm and 461 nm (see Table 2.1 for spectral details). Results are given in Table 3.3. The 461 nm peak disappears first when ~0.5 equivalents of Cu(II) have been added. The increase in Cu(II) concentration also results in a decrease in absorbance in the other peaks. The 311 nm peak disappears completely at a 1:1 reaction ratio. The peak at 396 nm experiences a substantial decline in absorbance on adding ~0.5 equivalents Cu(II).

With a further increase in the Cu(II) concentration, up to a 1:1 Cu(II):TM3 reaction ratio, a new band appears at about 450 nm (Table 3.3). The reaction of Cu(II) with TM3 at a ratio of 1:1 has been found to lead to mutual reduction to Cu(I) and Mo(V) based on the EPR studies of the products (00L). It is therefore possible that the 450 nm peak originates from a lower wavelength shift of the 461 nm peak of TM3. This original wavelength band of TM3 has been assigned to $\pi(S) \rightarrow d$ (Mo) (or $a_2 \rightarrow e$) transition as discussed in Section 1.2.2. It seems, therefore, that the change of oxidation state of Mo from VI to V will cause an increase in the energy of the $a_2 \rightarrow e$ transition, assuming the coordination environment of the Mo is still tetrahedral in the complex formed from the reaction. Subsequent additions of Cu(II) give no major change in the spectrum up to a 2:1 Cu(II):TM3 ratio. This suggests that one equivalent of Cu(II) is sufficient to completely react with TM3. The approximate pH of the resulting solutions in the above study was ~ 4.1. The effect of pH on Cu(II) and TM3 reaction was also investigated in both buffered and non-buffered solutions, as outlined below.

Table 3.3: Observed (obs) and predicted (pred) absorbance for the TM3 peaks on mixing different proportions of Cu(II) and TM3 aqueous solutions (see Table 3.3).

Cu(II):TM3 ratio	Obs. at ~ 311 nm	[b]Pred. at ~ 311 nm	Obs. at ~ 396 nm	Pred. at ~ 396 nm	Obs. at ~ 461 nm	Pred. at ~ 461 nm	"new peak" at λ_{max} ~ 450 nm
0.00:1	0.7200	0.7200	0.8700	0.8700	0.2130	0.2100	-
0.50:1	0.5287	0.5760	0.2572	0.6960	-	0.168	-
0.67:1	0.5000	0.5400	0.1840	0.6525	-	0.1575	-
0.80:1	0.4724	0.5143	-	0.6214	-	0.1500	0.1751
1.00:1	-[c]	0.4800	-	0.5800	-	0.1400	0.1741
1.33:1	-	0.4320	-	0.5220	-	0.1260	-
1.50:1	-	0.4142	-	0.4971	-	0.1200	-
2.00:1	-	0.3600	-	0.435	-	0.105	-

b. The predicted (pred.) absorbance based on the assumption that there is no reaction between Cu(II) and TM4 (see text for more details).

c. All dashed lines indicate that no peak maximum was observed at that wavelength.

With 1:1 mixtures of Cu(II) and TM3 in buffer solutions, none of the three TM3 peaks at 311, 396 and 461 nm was discernable from pH 2 to7. In buffer solutions of pH 6.0 and 7.0, a new peak (almost a shoulder) at about 450 nm emerged just as observed also for the 1:1 Cu(II):TM3 reaction in water. Lower pH values, down to 2 did not yield a major change in the spectrum. However, in buffer solutions of pH 3.0 and 2.0, the peak at ~ 450 nm was not obvious, giving essentially a featureless spectrum. However the absorbance at the wavelength 450 nm was essentially the same at pH 2, 3 and 4.

When the pH was adjusted to 6.42 for a 1:1 Cu(II):TM3 reaction mixture in a non-buffer solution, only the new peak at ~ 450 nm was observed. Further decrease in pH to 4.85 for the interaction in non-buffer solution maintained this peak as the only main signal. As stated above, the 1:1 Cu(II):TM3 reaction mixture in water resulted in a pH of 4.1 and the peak at ~ 450 nm was still the only main peak. As also observed for the buffer solutions, decrease of pH down to 3 led to the complete disappearance of all peaks and further decrease to pH 2 led to no further change in the spectrum. Also, the absorbance at the wavelength 450 nm was essentially the same in the solutions of pH 2, 3 and 4.1. It appears, as also observed for TM4, that although only one equivalent of Cu(II) is required to completely react with TM3 as seems to be the case in lower pH ($\leq$ 3) solutions, in solutions of higher pH (e.g. under physiological conditions (pH ~ 7)), excess Cu(II) is required.

3.3.1.3 Stoichiometry and pH Effects: TM2 and TM1

In the case for TM2, the addition of half an equivalent of Cu(II) resulted in the disappearance of all the three characteristic TM2 peaks (i.e. at 286, 322, and 394 nm-see Table 2.1), with a concomitant appearance of a new peak at 307 nm (Figure 3.4). This new peak flattens leading to a shoulder on increasing the amount of Cu(II) added and disappears completely at 1:1 Cu:TM2 stoichiometry (pH ~4.1). The solution containing 1:1 Cu(II):TM2 gives a featureless spectrum between pH 3 and 4.5. Unlike TM3 and TM4, even at pH ~ 8 one equivalent of Cu(II) is sufficient to react completely with TM2 (Figure 3.5). It should be noted that the adjustment of pH towards extremely

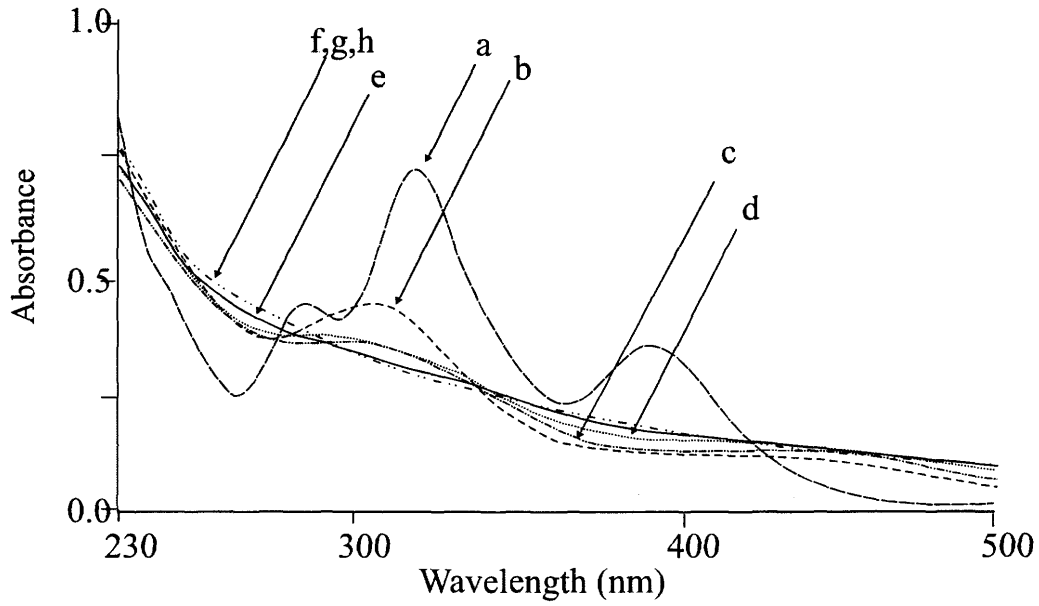

Figure 3.4: UV/visible spectra of TM2 as different amounts of Cu(II) are added to TM2 solutions as detailed in Table 2.3 to obtain Cu(II) and TM2 reaction mixtures of ratio (a) 0 (i.e. 10^{-4} **M** TM2 alone), (b) 0.50, (c) 0.67, (d) 0.80, (e) 1.00 , (f) 1.33 (g) 1.50, (h) 2.00.

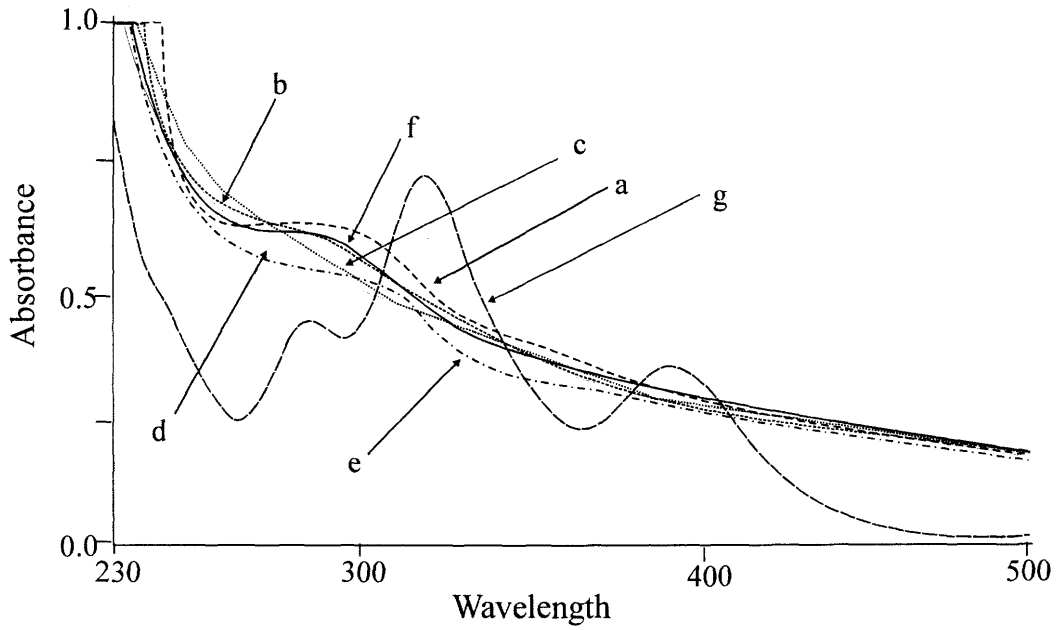

Figure 3.5: UV/visible spectra of 1:1 Cu(II):TM2 (1 x 10^{-4} **M**) in non-buffer solutions of different pH (a) 2.0, (b) 3.0, (c) 4.1, (d) 4.5, (e) 5.8, (f) 7.9, (g) TM2 alone (1 x 10^{-4} **M** at pH ~ 7) for comparison.

low pH and high pH by the mineral acids (e.g. HNO_3) or alkali (e.g. NaOH) used in this study led to some absorption at around 280 nm in both cases (Figure 3.5). Although the reaction in the acidic solutions may be attributed to the formation of a molybdenum sulfide (MoS_3 or MoS_2), it is uncertain what the product is in the basic solutions.

In the case of TM1, the addition of 2/3 of an equivalent of Cu(II) or more also led to the disappearance of the only peak at ~ 290 nm . Since TM1 easily hydrolyses, the effect of pH on the interaction was not studied.

3.3.1.4 Stoichiometry and pH Effects: Quantitative experiments

Although the solution chemistry results so far above seem to favor a Cu(II):TM stoichiometry of 1:1 for all the TMs, there are other views in the literature. For instance, typical values for the stoichiometry of the interaction between Cu(II) and TM4 in aqueous solution are in the range of 1 to 2 (00L, 84SM, 82CL, 86LP). To obtain more adequate data for the quantitative assessment of the stoichiometric relationship between Cu(II) and the TMs, a more comprehensive experiment was conducted to collect data at six different wavelengths for mixtures of Cu(II) and TM4, TM3 or TM2 at different mole ratios (Section 3.2.4.1). (Due to complications from the hydrolysis of the less stable TM1 it was excluded in this study.) Analyses of the data were based on Beer's Law. Assuming that a single "complex" results from the interaction:

$$A_{obs} = A_f + A_b = \{\varepsilon_f.\alpha_f + \varepsilon_b.\alpha_b\}\ C \qquad \textbf{(3.1)}$$

where A is absorbance, ε is molar absorptivity, α is mole fraction, obs refers to observed, b refers to a TM in the "bound" state, f to a TM in the "free" state, and C is concentration of TM in all forms. A cell path length of 1 cm is also assumed. Since all the TM are either free or bound, $\alpha_f + \alpha_b = 1$. Thus from Equation 3.1:

$$A_{obs} = \{\varepsilon_f (1 - \alpha_b) + \varepsilon_b.\alpha_b\}.\ C = \varepsilon_f.C - \{\varepsilon_f - \varepsilon_b\}.\alpha_b.C$$

Rearranging this,

$$\alpha_b = \{\varepsilon_f - A_{obs}/C\}/\{\varepsilon_f - \varepsilon_b\} \quad (3.2)$$

When $\alpha_b = 0$ (i.e. no added Cu(II)), $A_{obs} = \varepsilon_f.C$. On adding Cu(II) to less than the stoichiometric amount, and assuming that $\varepsilon_f > \varepsilon_b$, α_b rises and A_{obs} decreases. Assuming a complex with a large formation constant, α_b will be proportional to the mole ratio Cu(II):TM. For the stoichiometric amount of Cu(II) (and all higher amounts, assuming no other reaction), $\alpha_b = 1$ (i.e. all TM present are in bound form as Cu-TM) and $A_{obs} = \varepsilon_b . C$.

If the complexes involved here are of 1:1 stoichiometry, plots of α_b vs the Cu(II):TM mole ratio should be linear with a slope of 1 up to the mole ratio 1, and level thereafter. This was indeed observed for the interaction between Cu(II) and all three TMs studied, as can be seen for TM4 in Figures 3.6. Statistical analysis of this data is

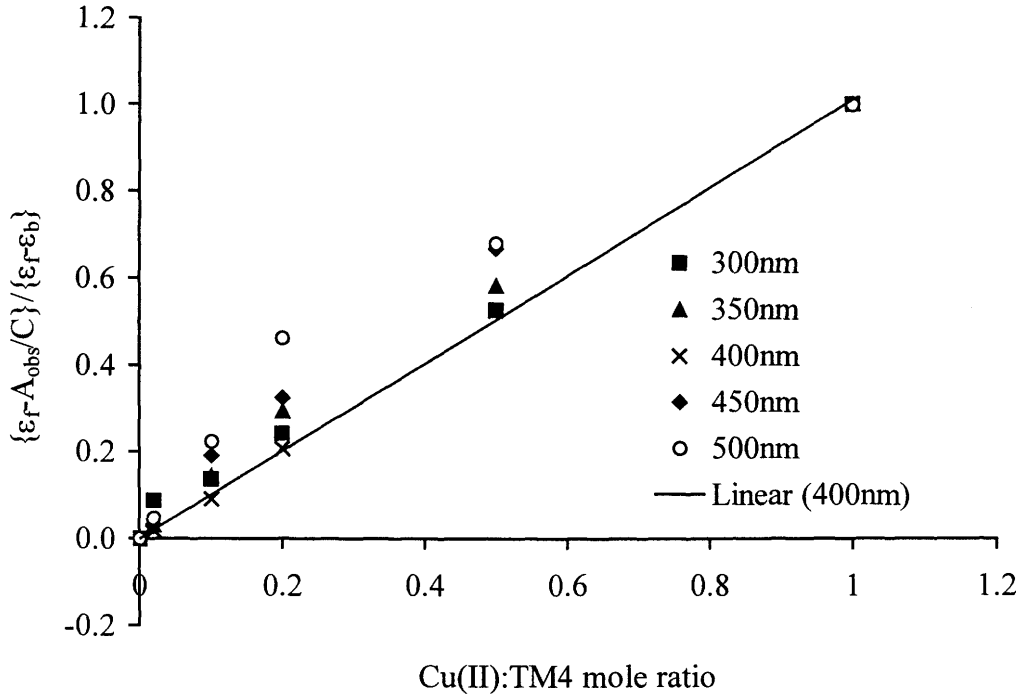

Figure 3.6: Graph of $\{\varepsilon_f - A_{obs}/C\}/\{\varepsilon_f - \varepsilon_b\}$ vs the Cu(II):TM4 mole ratio at different wavelengths. Linear (400 nm) represent the line of best fit for the data at 400nm.

summarized in Table 3.4. Curves yielding correlation coefficients (R^2) < 0.7 were ignored in the determination of the actual stoichiometry. Results confirm the 1:1 stoichiometry established above.

3.3.1.5 Solubility Studies

Although the mixtures of Cu(II) and TMs described in Section 3.2.4.1 appeared clear for approximately 10 min, and therefore permitted the solution chemistry studies discussed in Section 3.3.1.1 to Section 3.3.1.4, in most of these mixtures, especially those of higher ionic strength and lower pH, precipitation of fine red to brown solids occurred after standing for longer periods.

Variation of pH (Section 3.2.4.2) not only brought about changes in the spectrum (Sections 3.3.1.1 to 3.3.1.4) but also affected how fast the product(s) precipitated. Table 3.10 gives approximate times taken for mixtures of 1:1 mole ratio of Cu(II) and TM4 or TM3 to start precipitating, or the order in which solutions started forming precipitates in the cases where the actual times were not recorded. Obviously, precipitation is favored for both TMs by a lower pH. This pH effect is more pronounced for TM4 than TM3. Thus, for example, no precipitation was observed in a buffer solution of pH 7 for the case of TM3 after several days, although some precipitation occurred for that of TM4 within an hr.

The precipitation of the Cu-TM adducts could be as a result of polymerization, which, as discussed in Section 1.2.6, is thought to occur faster for the Cu-TM4 adduct than for the other TMs. Polymeric linear chains of Cu-(S)-Mo-S clusters that involve bridging S are formed in the TM4 case in aqueous solutions when there is no other ligand present in solution. The O atoms in the oxythiomolybdates (i.e., TM2 and TM3) presumably terminate such long chain polymerization as they are observed as terminal groups in Cu-(S)-Mo-S clusters, which are mostly cubane-like in shape.

Table 3.4: Statistical data obtained from the regression analysis of UV/visible absorbances at different wavelengths of solutions containing Cu(II) and TM4, TM3 or TM2. See Section 3.2.4.1 for details.

		Wavelength					
TM		250nm	300nm	350nm	400nm	450nm	500nm
TM4	slope	1.1 ± 0.1	1.02 ± 0.04	1.05 ± 0.5	1.01 ± 0 .01	1.09 ± 0.08	1.1 ± 0.1
(Trial 1)	R	0.898	0.988	0.980	0.999	0.946	0.870
TM4	slope	1.2 ± 0.1	0.97 ± 0.03	1.01 ± 0.02	0.98 ± 0.02	1.09 ± 0.07	1.04 ± 0.05
(Trial 2)	R	0.849	0.993	0.998	0.996	0.954	0.980
TM3	slope	1.01 ± 0.02	0.9 ± 0.1	1.1 ± 0.1	[d]-	0.8 ± 0.2	0.92 ± 0.08
(Trial 1)	R	0.996	0.923	0.881	-	0.812	0.947
TM3	slope	1.01± 0.02	0.9 ± 0.1	1.1 ± 0.1	-	0.8 ± 0.2	0.91 ± 0.08
(Trial 2)	R	0.998	0.898	0.864	-	0.780	0.949
TM2	slope	1.01 ± 0.03	0.94 ± 0.09	[d]-	-	1.1 ± 0.1	1.04 ± 0.07
(Trial 1)	R	0.995	0.919	-	-	0.918	0.954
TM2	slope	1.10 ± 0.02	0.9 ± 0.1	-	-	1.1 ± 0.1	1.06 ± 0.08
(Trial 2)	R	0.997	0.817	-	-	0.904	0.947

d. The regression coefficient (R^2) was less than 0.70.

Since the precipitation is favored by lowering pH, it is likely that the mechanism of such cluster formation depends somehow on protonation of the initial Cu-TM monomer, likely via any available terminal S atoms, before any bridging will occur. As mentioned in Section 3.3.1.4, the M-S or the M-O bonds in the TMs can be initially protonated. Protonation would reduce the M-S π character and hence promote intramolecular redox processes, which seem to be characteristic for the formation of polymeric species involving TMs as building blocks, as discussed in Sections 1.2.4 and Section 1.2.6. Although M-O can likewise be protonated (81MD), the S atom's enhanced ability over O to play the key role as a bridging ligand (00L), and also as a better coordinating (softer) ligand to Cu(I), should make the higher S containing TMs better building blocks for polymerization than the higher O containing TMs. Recall from Section 1.2.6 that Cu-(S)-Mo-S clusters have the Cu in the + 1 state.

Although 1:1 Cu(II):TM4 and Cu(II):TM3 reaction mixtures in unbuffered solutions (Table 3.5) were of pH 4.3 and 4.1 respectively, no precipitates were formed, even after some days. Since buffered solutions at these pH values did show precipitation (see above), this suggests factors in addition to pH also favor precipitation.

Table 3.5: Precipitation of Cu-TM products in different buffer solutions. The (+) sign indicates that precipitations occurred before the specified time (first row) after mixing the Cu(II) and the TM. The (-) sign indicates it had not precipitated by that time.

	Cu-TM4		Cu-TM3		
Buffer pH	1 hour	Ranking	5 hours	1 hour	5 days
2	+	1st	+	+	+
3	+	2nd	+	+	+
4	+	3rd	+	+	+
5	+	4th	+	-	+
6	+	5th	+	-	+
7	+	6th	+	-	-
H_2O[e]	-	7th	-	-	-

e. The pH of the resulting solution was 4.3 for Cu(II) and TM4 and 4.1 for Cu(II) and TM3 reaction mixtures.

It was hypothesized that this could be due to the higher ionic strength in the buffered solutions. A series of solutions were therefore prepared to study this possibility, as detailed in Table 3.6

Table 3.6 Precipitation of Cu-TM4 products in different electrolyte solutions. The (+) sign indicates that precipitations occurred before the specified time (first row) after mixing the Cu(II) and TM. The (-) sign indicates it had not precipitated by that time.

Electrolyte	Conc.	1 hour	3 hours	1 day	3days
H_2O		-	-	-	-
HNO_3	10^{-4} **M**	-	-	-	
	10^{-3} **M**	-	-	-	-
	10^{-2} **M**	+	+	+	+
HCl	10^{-3} **M**	-	-	-	
	10^{-2} **M**	-	+	+	+
NaCl	10^{-2}**M**	-	-	-	+
	10^{-1} **M**	+	+	+	+
KHP	10^{-2}**M**	-	-	-	-
	10^{-1} **M**	+	+	+	+
KH_2PO_4	10^{-2}**M**	_	_	-	-
	10^{-1} **M**	+	+	+	+

Increasing ionic strength (for all the electrolytes studied) favored the precipitation of the Cu-TM4 product. Precipitation of the Cu-TM4 complex did not occur in an unbuffered solution at pH 3 on standing for several hours. However, in the presence of various salts at a concentration of 0.1 **M**, precipitates formed in less than 1 hr at pH ~4. On the contrary, reaction mixtures of Cu(II) and TM3 in electrolyte solutions (i.e. KHP, NaCl, KH_2PO_4, KNO_3, and Na_2SO_4) of concentration 0.1 **M** of approximately the same pH, did not cause the precipitation of the Cu-TM3 adduct on standing for 1 hr. They all however precipitated on leaving them overnight (between 8 to 12 hr).

Since (see Table 3.6) the precipitation of the Cu-TM4 adduct occurred even in NaCl solution of 10^{-2} **M**, variation of concentrations of NaCl from 10^{-4} to 0.2 **M** at approximately the same pH were studied for reaction mixtures of Cu(II) and TM4, Cu(II) and TM3, and finally Cu(II) and TM2 (see Table 3.7). Results indicate clearly that increasing the NaCl concentration and therefore the ionic strength of the solution increases the rate of precipitation.

Table 3.7: Approximate (approx.) time taken for the precipitation of Cu-TM products in NaCl solutions of varying concentrations.

Concentration of NaCl	Approx. time for Cu-TM4 ppt.	Approx. time for Cu-TM3 ppt.	Approx. time for Cu-TM2 ppt.
0.20 **M**	10 min	[f] -	[f] -
0.15 **M**	20 min	45 min	1 hr
0.10 **M**	30 min	1 hr	2 hr
0.05 **M**	2 hr	18 hr	22 hr
0.02 **M**	48 hr	72 hr	[g] -
0.01 **M**	96 hr	[g] -	[g] -
0.001 **M**	[g] -	[g] -	[g] -

f. The reaction was not studied at the specified concentration
g. There was no obvious formation of precipitates.

No precipitation was observed for NaCl concentrations greater than 10^{-3} **M** on standing for 4 or more days. Results also confirm that the precipitation of the Cu-TM4 product is fastest, followed by Cu-TM3 and then Cu-TM2. Although ionic strength and pH effects were not systematically studied for the Cu-TM1 case, preliminary investigations showed that they also form an insoluble product at low pH and in high ionic strength solution, albeit slowly.

The UV/visible spectra obtained for 1:1 Cu(II):TM mixtures in the presence of electrolytes were essentially the same for high (0.1 **M**) and low ionic (0.01 **M**) strength

reactions, which suggests that the electrolyte ions are not part of the structure. Confirmation of this conclusion was derived from the C, H, and N analyses of the solid Cu-TM adducts when potassium hydrogen phthalate ($C_6H_4(COOH)COOK$) (an electrolyte containing substantial amount of C and H) was used as ionic strength adjustor. The C, H, N analyses of the solid Cu-TM adducts in the presence of this electrolyte gave insignificant levels of C and H.

Table 3.8 shows the maximum absorbance at about 280 nm for the 1:1 mixtures of Cu(II) and TM4 in the presence of various NaCl concentrations from 0 to 0.15 **M**. The table shows a gradual increase of the absorbance to ca. 1.22, at which point precipitation occurs and there is a gradual decline of the absorbance as the fine precipitates settle out of solution.

Table 3.8: Maximum absorbance (at ca. 280 nm) for 1:1 mixtures of Cu(II) and TM4 in the presence of various NaCl concentrations, collected 30 min after the reaction.

[NaCl] (**M**)	0	0.01	0.02	0.05	0.10	0.15	0.20
Abs	1.1692	1.1812	1.2204	1.1988	1.1859	1.1738	[i]

i. The fine precipitate settled from the solution and the supernatant after centrifugation gave only a background absorption with no peaks.

Table 3.9 also shows the maximum absorption peak at ca. 450 nm for 1:1 Cu(II):TM3 mixtures in the presence of various NaCl concentrations. As in the case for the TM4 there is a gradual increase of the absorbance to ca. 0.31, at which point precipitation begins to occur. The time it takes for the precipitation depends on the NaCl concentration.

Spectra obtained in the case of TM2 were all initially (i.e., within 2 min after reaction) the same and featureless as previously observed (Figure 3. 4(e)). However, the absorbance readings at the various wavelengths decreased with the passage of time for mixtures containing high NaCl concentration, due to precipitation of the Cu-TM2 adduct, as observed above in the case of both TM4 and TM3.

Table 3.9: Maximum absorbance (at ca. 450 nm) for 1:1 mixtures of Cu(II) and TM3 in the presence of various NaCl concentrations, collected 5 min and 1 hr after the reaction.

NaCl	Absorbance [5 min]	Absorbance [1hr]	Absorbance [2 days]
0 **M**	0.2567	0.2808	0.2747
1×10^{-4} **M**	0.2665	0.2901	0.2877
1×10^{-3} **M**	0.2666	0.2856	0.2934
1×10^{-2} **M**	0.2646	0.2824	0.2920
2×10^{-2} **M**	0.2753	0.2922	0.2918
5×10^{-2} **M**	0.2899	0.3075	-
1×10^{-1} **M**	0.2976	0.3098	-

The apparent decrease in solubility as ionic strength rises could be thermodynamic or kinetic in origin. Assuming for the sake of argument that the precipitated product of the interaction of Cu(II) and a TM is a simple 1:1 binary salt, its thermodynamic solubility product constant (K_{sp}) can be written in terms of the activities (a_i) in a saturated solution of Cu(II) and TMs as

$$K_{sp} = a_{cu(II)}.\, a_{TM}$$

$$= [TM][Cu(II)]\gamma_{\pm}^{2} \qquad \textbf{(3.3)}$$

where $\gamma_{\pm}$ is the mean activity coefficient and [Cu(II)] and [TM] are the molarities of Cu(II) and TM ion in the saturated solution. Estimators of mean activity coefficients, such as the Davies equation (Equation 3.4 below) (68G, 62D) which is suitable for the ionic strength range 0.01 to 0.5 **M** (73B, 70SM), predict a decrease in mean activity coefficients of divalent ions from near unity to ~ 0.5 over this range.

$$\log \gamma_{\pm} = -2Az_Az_B\,(\sqrt{I}/(1+\sqrt{I}) - 0.2I) \qquad \textbf{(3.4)}$$

Thus, from Equation 3.3, a rise in [Cu(II)] is expected, i.e. an **increase** in solubility with ionic strength. This is contrary to the trend observed.

The possibility that kinetic factors determine the observed behavior was also considered. Reactions between oppositely charged ions to form an insoluble salt are generally rapid, since the rate of reaction is governed by the diffusion of the ions towards each other and the activation energy for the combination is very small (61FP). Although precipitation as described above was only visible to the naked eye after ~ 10 min, the initial formation of adducts as seen by UV/visible spectroscopy was rapid. This confirms the suggestion earlier in the section that the process involved is one of aggregation or polymerization of adducts species (70BR) (see Section 1.2.6 for more details).

The rate constant for two species A and B reacting in a solution is given by:

$$k = k_o \gamma_A \gamma_{B/} \gamma_*$$

where k_o is the rate constant at infinite dilution in the given solvent, γ_A and γ_B are the activity coefficients of the two species, and γ_* is that for the activated complex. Again employing the Davies equation, a relationship between the rate constant and ionic strength can be established:

$$\log k = \log k_o + 2Az_Az_B (\sqrt{I}/(1+\sqrt{I}) - 0.2I) \qquad \textbf{(3.5)}$$

A theoretical plot of the relative rate (k/k_o) vs I (Figure 3.7) shows an increase in the rate of reaction as ionic strength increases. Observed variations in the precipitation times for the Cu-TM adducts due to ionic strength (Cl^- ions) (Table 3.7) are consistent with these theoretically predicted changes, as shown in Figure 3.7 for the TM4 case.

Attempts were also made to characterize the solid products isolated from mixtures of Cu(II) and TM4 at a mole ratio of 1:1. Due to the small quantities of solid, elemental analysis was limited to Cu and Mo. The Mo:Cu mole ratio was 1:1.08 ± 0.8. Results obtained thus far are all consistent with the 1:1 Cu(II):TM4 stoichiometry.

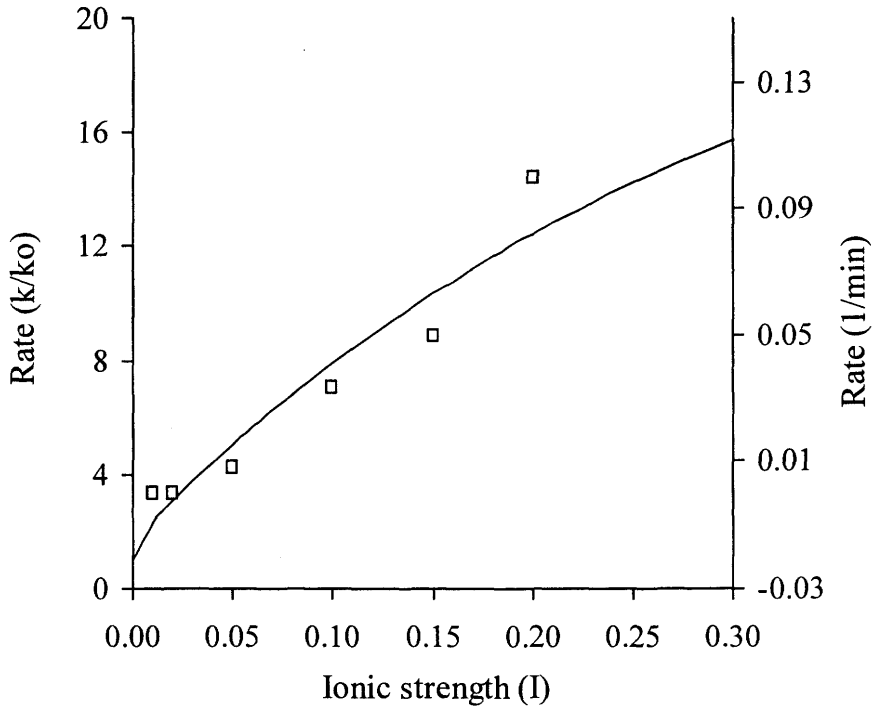

Figure 3.7: Relation between rate constant and ionic strength predicted based on the Davies equation as the solid line (left axis) and the rate of formation of Cu-TM4 adduct (calculated as simply the reciprocal of time in minutes) vs ionic strength as symbols (right axis).

This does not imply a simple binary salt; the previously characterized linear polymeric product, $(NH_4)_2CuMoS_4$, obtained in aqueous solution from the reaction between aqueous solution of Cu(II) and TM4 or CuS and TM4 is of the same stoichiometry (70BR).

Sulfur 1s NEXAFS spectra of the Cu-TM4, Cu-TM3, TM4 and TM3 obtained in this research were run by Dr. Urquhart (Department of Chemistry, University of Saskatchewan) and show the first peak of the latter three products to be at nearly the same energy, whereas that of Cu-TM4 is shifted to higher energy. This suggests that the sulfur atoms are more strongly involved in bonding to Cu in Cu-TM4 than in Cu-TM3. The Mo ($3p_{3/2}$) and ($3p_{1/2}$) NEXAFS spectra also run by Dr. Urquhart show the first peak of Cu-TM4 to be at slightly lower energy, suggesting an increase in the electron density at the Mo site of the complex. A dominant shoulder on the high-energy side was

also observed for the Cu-TM4 spectrum. Such shoulders are generally a characteristic of polymeric species. These results strongly suggest that the chemical or electronic structure in Cu-TM4 is different from that of Cu-TM3 and perhaps affirm the presumed linear polymerization of the Cu-TM4 adducts, which facilitates precipitation of the product from aqueous solutions as compared to the oxythiomolybdate adducts.

3.3.1.6 Effect of EDTA on the Interaction between Cu(II) and TM4

The effect of EDTA on the interaction of Cu(II) and TM4 was studied in two main ways. Firstly, fixed amounts of TM4 were added into EDTA and Cu(II) reaction mixtures of varying ratios as outlined in Table 3.1 (Section 3.2.6.1). The spectra obtained for the respective reactions mixtures, 1 hr after adding TM4, are shown in Figures 3.8. The presence of EDTA, up to an equivalent amount of Cu(II) and TM4 did not show the presence of any of the characteristic TM4 peaks at 468, 316, and 241 nm (Table 2.1). Instead, the weak peak at ca. 285 nm observed at Cu(II):TM4 stoichiometry of 1:1 up to 2:1 in the absence of any other ligand (Section 3.3.1.1) is what emerged in these reaction mixtures (Figure 3.8 a to c). This connotes that in the presence of EDTA up to an equivalent amount of TM4, a reaction can occur between Cu(II) and TM4 1hr after mixing the reactants. Since the Cu-TM4 product and EDTA or EDTA-Cu can absorb some radiation within the entire studied wavelength region (230 – 500 nm), the possibility that these absorptions overlap with absorptions from any unreacted TM4 exist, at least in wavelength regions where the absorption of the TM4 is weak and that of the others are strong. The inability to see the characteristic peak in itself does not therefore mean a complete reaction between Cu(II) and the TM4.

To evaluate quantitatively the amount of TM4 remaining after the reaction, and hence the amount that has reacted with the Cu(II), the absorbance contribution from all the other species present in solution should be subtracted. These assessments can however be done qualitatively, or semi-quantitatively, by measuring the reduction in intensity of a peak in a wavelength region where absorbance from other possible species in solution is negligible or small. In Section 3.3.1.1, it was obvious that the Cu-TM4

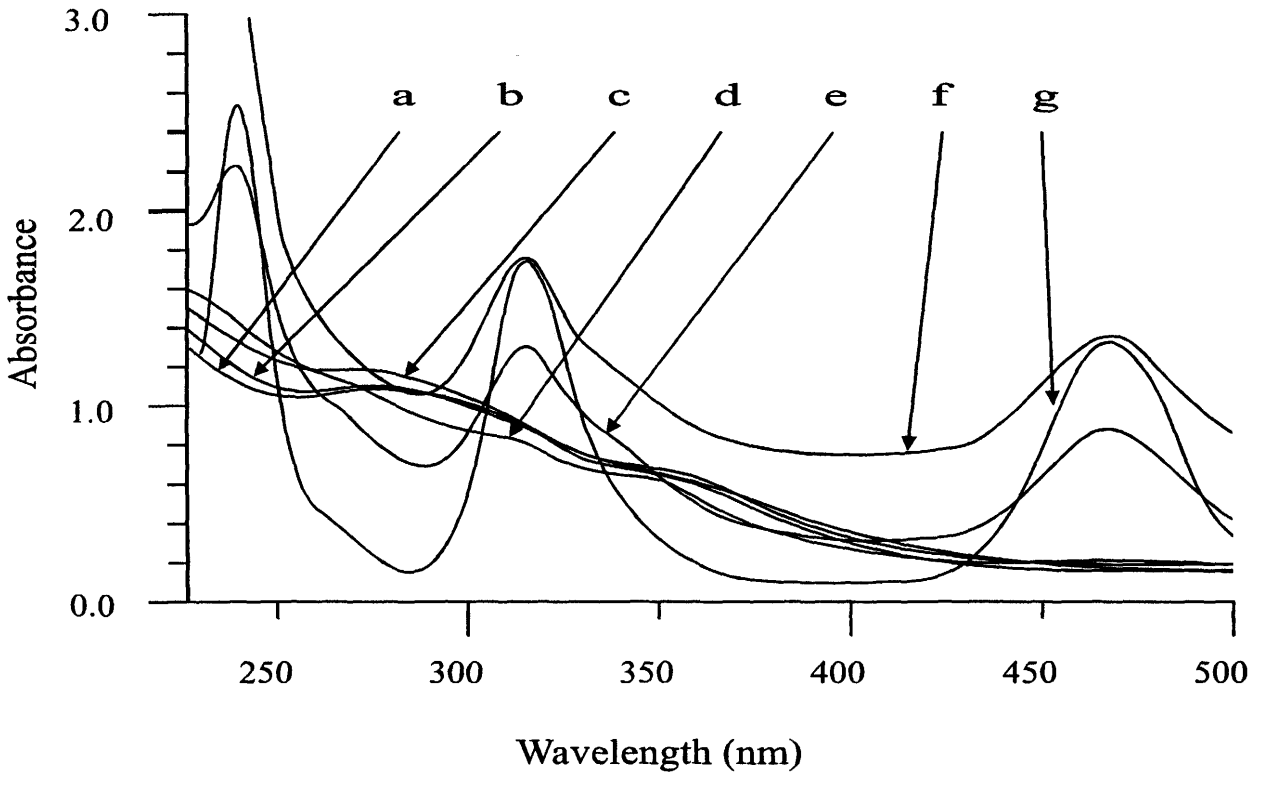

Figure 3.8: UV/visible spectra on adding TM4 (1 x 10^{-4} **M**) to (a) 10^{-4} **M** Cu(II) only, (b) a mixture of 10^{-5} **M** EDTA and 10^{-4} **M** Cu(II), (c) a mixture of 10^{-4} **M** EDTA and 10^{-4} **M** Cu(II), (d) a mixture of 10^{-3} **M** EDTA and 10^{-4} **M** Cu(II), (e) a mixture of 10^{-2} **M** EDTA and 10^{-4} **M** Cu(II), (f) a mixture of 10^{-1} **M** EDTA and 10^{-4} **M** Cu(II), (g) H_2O only. Reaction time is 1 hr.

products absorb more strongly down in the lower wavelength region (< 400nm). See Figure 3.1. Inspection of the Figure 3.11 also suggests significant contributions from EDTA (or EDTA-Cu) in the lower wavelength region (< 300 nm). Hence, the reduction in the intensity of the TM4 peak at 468 nm and to a lesser extent the one at 316 nm (but not the 214 nm peak) can be used qualitatively as a measure of TM4 that has reacted with Cu(II) in the presence of varying amounts of EDTA.

Comparison of the TM4 spectrum alone (Figure 3.8g) to that of the presence of 1 equivalent EDTA and Cu(II) (Figure 3.8c) suggest that the contribution of unreacted TM4 is small, if indeed any is present at all. Even up to a ten-fold excess of EDTA over Cu(II) and TM4, none of the three TM4 peaks was discernable (Figure 3.8d). In the presence of a hundred-fold excess of EDTA in the reaction mixture, unreacted TM4 was obviously present in the solution as evidenced by the presence of the characteristic TM4 peaks at 468, 316 nm (Figure 3.8e). However, their peak intensities reduced significantly on staying for 1 hr and 3.5 hr, as can be seen in Table 3.10.

Table 3.10: Percentage reduction of the intensities of the 316 and 468 nm peaks of TM4 in 10^{-4} **M** aqueous solution alone and in a 100:1:1 EDTA:Cu(II):TM4 mixture (TM4 concentration in the reaction mixture is 10^{-4} **M**) at different times of solution preparation.

	TM4 alone		100:1:1 EDTA:Cu:TM4	
Time	316 nm	468 nm	316 nm	468 nm
1 hr	0.8%	0.8%	24.2%	35%
3.5 hr	2.9%	1.6%	38.1%	56%

It is obvious from the Table 3.10 that the observed reductions in intensities cannot be attributed solely to hydrolysis. This peak reduction must primarily be due to binding with Cu(II). The lower values obtained for the peak at 316 nm as compared to that at 468 nm for solution containing 100:1:1 EDTA:Cu(II):TM4 reaction mixture (Table 3.10) should be expected, since the absorbance contribution from Cu-TM4 is greater at 316 nm than 468 nm (Figure 3.1 and Figure 3.8a).

On leaving the reaction mixtures of EDTA, Cu(II) and TM4 containing the compositions as specified in Figure 3.8 for longer periods, the reaction mixture containing EDTA of concentration 10^{-1} **M** and of ionic strength approximately 9.4×10^{-1} **M** (Table 3.1) formed precipitates within 9 hr.

These results suggest a competition from TM4 with EDTA for Cu(II) which is initially bound to the EDTA. TM4 seems to displace Cu(II) from the EDTA completely when EDTA and TM4 are present in comparable concentrations. However, when EDTA is in excessive amount over the TM4, the TM4 displaces the Cu(II) only partially and slowly with time. To investigate how the order of mixing would affect such competition for Cu(II), the second experiment discussed below was performed.

In the second procedure, EDTA was added in different amounts as specified in Table 3.1 to a 1:1 Cu(II):TM4 reaction mixture (10^{-4} **M**). The addition of EDTA gave spectral data the same as that for the 1:1 Cu(II):TM4 (Figure 3. 8a), the only exception being with cases where excessive (e.g. 10^{-1} **M**) EDTA was used, where the strong absorption by EDTA at wavelength < 300 nm is observed as can be seen with other reaction mixtures containing this high concentration of EDTA (see for example Figure 3.8f). It is concluded that once Cu(II) is bound to TM4 it cannot be stripped off by EDTA, even when it is present in 1000-fold excess.

3.3.1.7 Effect of EDTA on the Interaction between Cu(II) and TM3

As in the case of TM4, two main experiments were performed here.

The first involved adding fixed amounts of TM3 into reaction mixtures of Cu(II) and EDTA of varying ratios as outlined in Table 3.1 (Section 3.2.6.1). The spectra obtained for the respective reactions mixtures 2 min after adding TM3 are shown in Figure 3.9. At low concentrations of EDTA, up to an amount equivalent to the added TM3, the TM3 characteristic peaks could not be observed 2 min after the addition (Figure 3.9 a to c), an indication of almost complete reaction with Cu(II) in the reaction mixture, as in the case of TM4 (Section 3.3.1.6). As explained for the case of TM4 in

Section 3.3.1.6, reduction in the intensity of the most intense peak at 396 nm, where the absorbance from Cu-TM3 and EDTA (or EDTA-Cu) seem to be relatively smaller (Figure 3.9), can be used as a qualitative means to assess the interaction between Cu(II) and TM3 in the presence of varying amounts of EDTA as in Figure 3.9.

Increasing the EDTA concentration further to a ten-fold, a hundred-fold and a thousand-fold in excess prevented the complete reaction of TM3 with Cu(II) within 2 min as evidenced by the presence of TM3 characteristic peaks at 462 nm, 396 and 311 nm (see Figure 3.9 d, e, and f). Allowing the EDTA, Cu(II) and TM3 reaction mixtures to stand for 1 hr 20 min resulted in a spectra as shown in Figure 3.10. This prolonged period of time created the situation where the characteristic TM3 peaks could not be observed up to10-fold excess EDTA as shown in Figure 3.9 a to d. Excess EDTA of 100-fold or more at that time period of reaction, however, prevented Cu(II) from reacting completely to the added TM3 (Figure 3.9 e and f). Nevertheless, the peak intensities were substantially reduced.

Table 3.11 shows the percentage reduction in intensity of the TM3 peak at396 nm with reference to the intensity of that same peak in a freshly prepared TM3 (1.00 x 10^{-4} **M**) solution, as a qualitative measure of TM3 reacted with Cu(II). The table shows that, although initially excess EDTA prevents the reaction of TM3 with Cu(II), with the passage of time (e.g. at 1.5 hr), the TM3 is able to substantially displace Cu(II) from EDTA.

Table 3.11: Percentage (%) reduction of the intensities of the 396 nm peak of TM3 in 10^{-4} **M** aqueous solution alone and in a 10:1:1, 100:1:1, 1000:1:1 EDTA:Cu(II):TM3 reaction mixtures at different times after solution preparation. TM3 concentration in each reaction mixture is 10^{-4} **M**.

Time	TM3 alone	EDTA:Cu:TM3 10:1:1	EDTA:Cu:TM3 100:1:1	EDTA:Cu:TM3 1000:1:1
2 min	0	42.6	6.4	1.86
1.5 hr	12.5	-	57.0	57.0

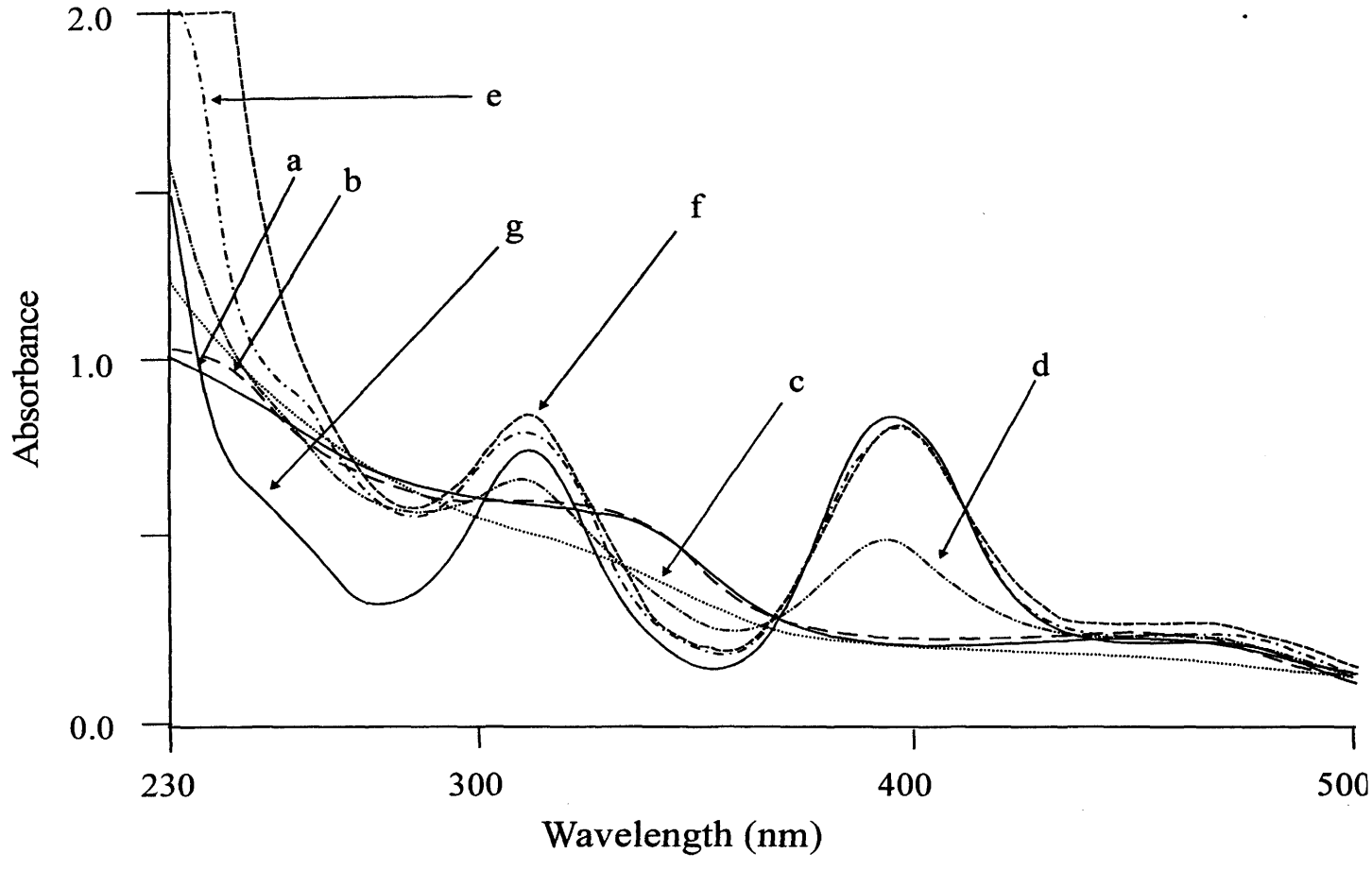

Figure 3.9: UV/visible spectra on adding TM3 (1 x 10^{-4} **M**) to a) 10^{-4} **M** Cu (II) only, (b) a mixture of 10^{-5} **M** EDTA and 10^{-4} **M** Cu(II), (c) a mixture of 10^{-4} **M** EDTA and 10^{-4} **M** Cu(II), (d) a mixture of 10^{-3} **M** EDTA and 10^{-4} **M** Cu(II), (e) a mixture of 10^{-2} **M** EDTA and 10^{-4} **M** Cu(II), (f) a mixture of 10^{-1} **M** EDTA and 10^{-4} **M** Cu(II), (g) H_2O only. Reaction time is 2 min.

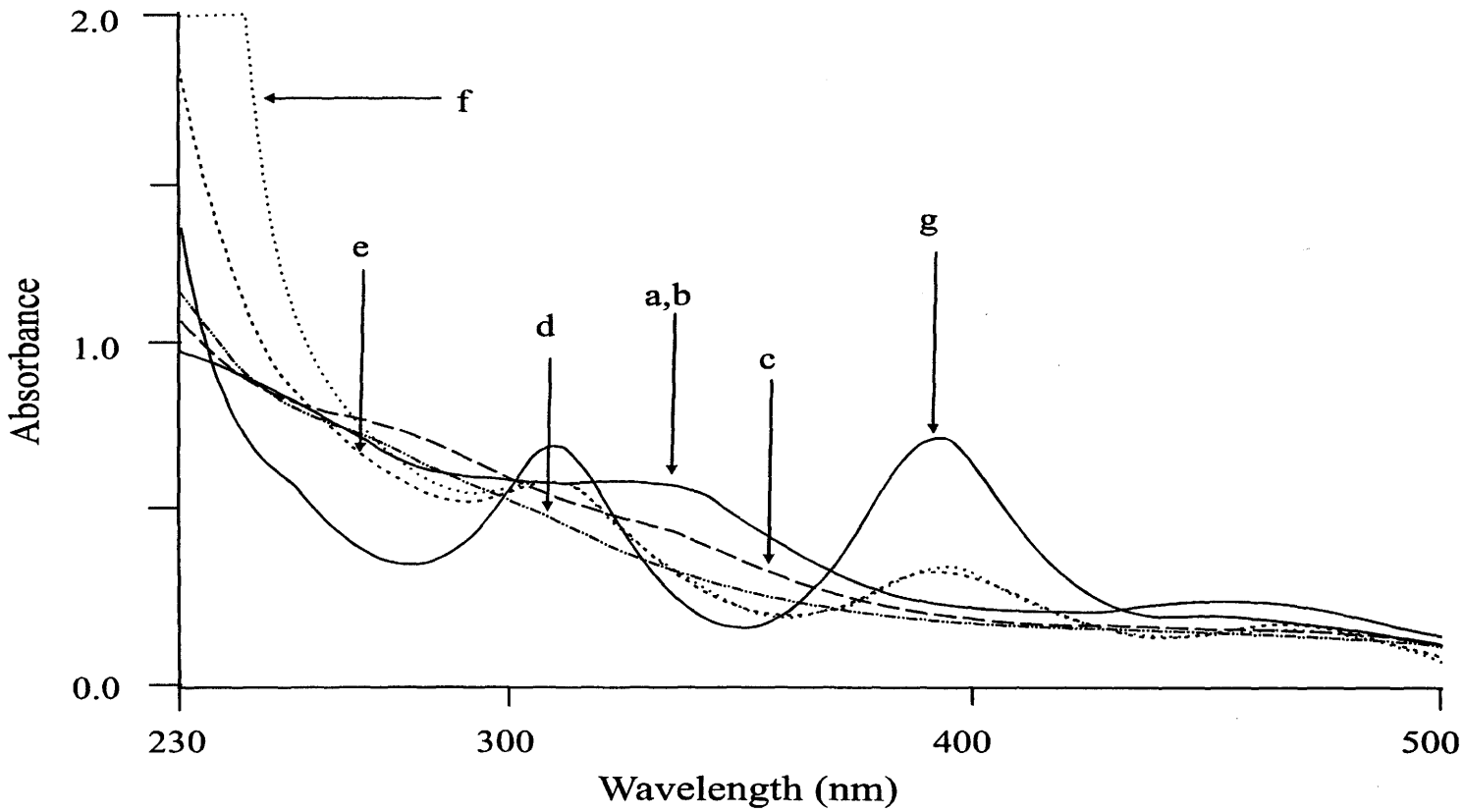

Figure 3.10: UV/visible spectra on adding TM3 (1 x 10^{-4} **M)** to a) 10^{-4} **M** Cu (II) only, (b) a mixture of 10^{-5} **M** EDTA and 10^{-4} **M** Cu(II), (c) a mixture of 10^{-4} **M** EDTA and 10^{-4} **M** Cu(II), (d) a mixture of 10^{-3} **M** EDTA and 10^{-4} **M** Cu(II), (e) a mixture of 10^{-2} **M** EDTA and 10^{-4} **M** Cu(II), (f) a mixture of 10^{-1} **M** EDTA and 10^{-4} **M** Cu(II), (g) H_2O only. Reaction time is 1 hr 20 min.

Although the reduction in intensity of the 396 nm peak due to hydrolysis of the TM3 after 1.5 hr is substantial, it is small as compared to the overall reduction in peak intensity in the presence of equivalent amount of Cu(II), even when a 1000-fold excess of EDTA is present. This suggests that the major factor accounting for the reduction in the intensity of the TM3 peaks is the interaction of TM3 with Cu(II), not hydrolysis. Thus, as in the case of TM4, there is a competition between TM3 and EDTA for Cu(II). On leaving the EDTA, Cu(II) and TM3 reaction mixtures for longer periods, the reaction mixture containing EDTA of concentration 10^{-1} **M** and of ionic strength approximately 9.4×10^{-1} **M** precipitated within 15 hr.

As in the case for TM4, a second experiment, to evaluate the influence of the order of mixing on the reaction, was also pursued. The addition of EDTA gave spectra data the same as that for the 1:1 Cu(II):TM3 (Figure 3. 9a and Figure 3.10a), the only exception being with cases where excessive (e.g. 10^{-1} **M**) EDTA was used, where the strong absorption from EDTA at wavelength < 300 nm is observed as before. (See Figures 3.9f and 3.10f). Thus, as in the case of TM4, once Cu(II) is bound to TM3 it cannot be stripped off by EDTA, even when present in 100-fold excess or more.

The marked difference in the results for the two different experiments discussed above led to a third experiment involving another different order of mixing the reactants Cu(II), TM3 and EDTA. In this third study, EDTA and TM3 of approximately the same concentration (1.00×10^{-4} **M**) were mixed first before adding Cu(II) of equivalent concentration. The UV/visible spectra were observed as a function of time (see Figure 3.11).

Two minutes after adding Cu(II), the peak at 396 nm had decreased by about 54 % and in 10 min, it had decreased by 69%. Beyond 25 min that characteristic peak had flattened out. The results from this experiment confirm those of the earlier two, that there is a competition between TM3 and EDTA for Cu(II), which is favored by TM3 as a function of time. In order words, both EDTA and TM3 initially, competitively bind Cu(II) to different degrees. For the Cu(II) bound initially to the EDTA, unreacted TM3

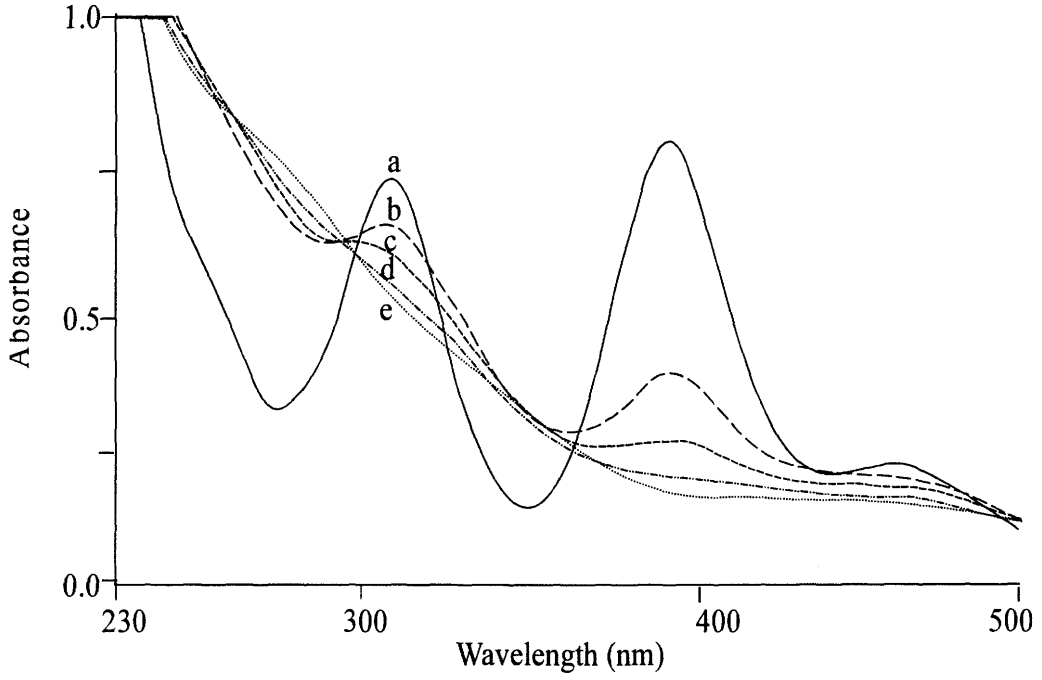

Figure 3.11: UV/visible spectra of (a) TM3 (1 x 10^{-4} **M**) and EDTA (1 x 10^{-3} **M**) mixture alone, and the spectra on adding Cu(II) (1 x 10^{-4} **M**) to the mixture in (a) above at the reaction times (b) 2 min, (c) 10 min, (d) 25 min, and (e) 1 hr.

forces it to "release" the Cu(II) in the course of time. Once, the TM3 binds the Cu(II), EDTA is incapable of getting it back. Thus, the competition between TM3 and EDTA for Cu(II) is kinetically favorable for the TM3 and this is also the case for the TM4.

3.3.1.8 Effect of EDTA on the Interaction between Cu(II) and TM2

As in the case of TM4, two experiments were performed.

The first involved the addition of fixed amount of TM2 to a mixture of Cu(II) and EDTA containing varying amounts of EDTA as outlined in Table 3.1. The spectra obtained for the respective reactions, 2 min after adding TM2, are shown in Figure 3.12. At low concentrations of EDTA up to an equivalent amount to the added TM2, the TM2 characteristic peaks could not be observed 2 min after the addition (Figure 3.12 a to c), an indication of almost complete reaction with Cu(II) in the reaction mixture as in the case of TM3 (Section 3.3.1.7).

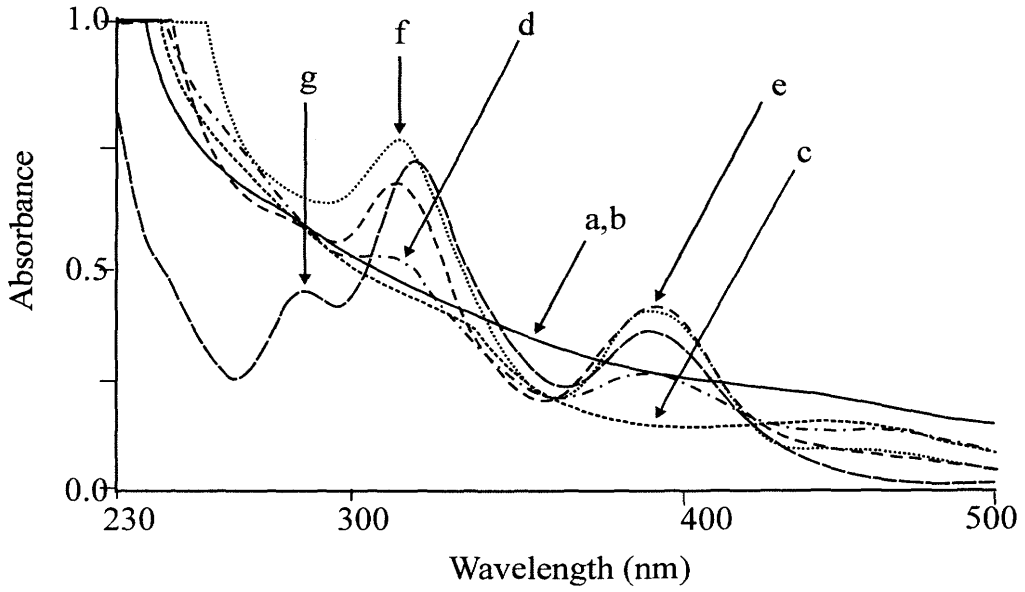

Figure 3.12: UV/visible spectra on adding TM2 (1 x 10^{-4} **M)** to a) 10^{-4} **M** Cu (II) only, (b) a mixture of 10^{-5} **M** EDTA and 10^{-4} **M** Cu(II), (c) a mixture of 10^{-4} **M** EDTA and 10^{-4} **M** Cu(II), (d) a mixture of 10^{-3} **M** EDTA and 10^{-4} **M** Cu(II), (e) a mixture of 10^{-2} **M** EDTA and 10^{-4} **M** Cu(II), (f) a mixture of 10^{-1} **M** EDTA and 10^{-4} **M** Cu(II), (g) H_2O only. Reaction time is 2 min.

With a 10-fold excess of EDTA in the reaction mixture, the characteristic peak at 394 nm was reduced in peak intensity about 33 % relative to a TM2 peak of the same reaction concentration (1 x 10^{-4} **M**) taken at the same time (Compare Figure 3.12 d to Figure 3.12 g). This cannot be attributed to hydrolysis. The characteristic TM2 peak at 322 nm could also be seen, but only as a shoulder due to the interference of the absorption from the likely formed Cu-TM2 complex in the mixture as explained in Section 3.3.1.6 for the case of TM4. When 100 fold or more excess EDTA are present in the reaction mixture, suppression of the TM2 characteristic peaks due to the interaction with Cu(II) is inhibited, suggesting that the Cu(II) is still bound to the EDTA, at least initially (Figure 3.12 e and f). The Cu(II),TM2 and EDTA reaction mixtures were allowed to proceed for 1 hr; the spectra obtained are shown in Figure 3.13. Generally, the TM2 peaks at 322 nm and 394 nm, which were discernable in the various Cu(II), TM2 and EDTA reaction mixtures, reduced more in intensity after 1 hr of reaction as compared to the 2 min spectra.

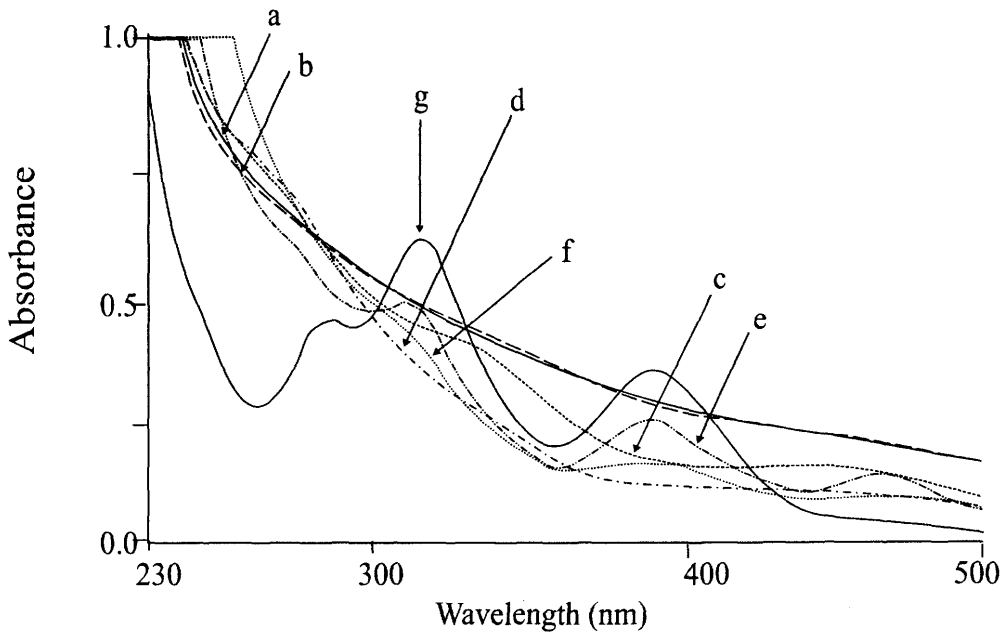

Figure 3.13: UV/visible spectra on adding TM2 (1 x 10^{-4} **M**) to a) 10^{-4} **M** Cu (II) only, (b) a mixture of 10^{-5} **M** EDTA and 10^{-4} **M** Cu(II), (c) a mixture of 10^{-4} **M** EDTA and 10^{-4} **M** Cu(II), (d) a mixture of 10^{-3} **M** EDTA and 10^{-4} **M** Cu(II), (e) a mixture of 10^{-2} **M** EDTA and 10^{-4} **M** Cu(II), (f) a mixture of 10^{-1} **M** EDTA and 10^{-4} **M** Cu(II), (g) H_2O only. Reaction time is 1 hr.

The spectrum for the 100:1:1 EDTA:Cu(II):TM2 reaction mixture after 1 hr showed an unexpected peak at 467 nm (Figure 3.13e), which is reminiscent of TM4. It is therefore tempting to suggest the formation of TM4 from the hydrolysis of TM2 as the EDTA concentration increases. However, no such peak was observed for the spectrum of TM2 alone at the same concentration and at the same time (Figure 3.13 g). Although hydrolysis of TM2 cannot be ignored completely in the competitive interaction between EDTA, Cu(II), and TM2, it cannot account by itself for the observation of this new peak. As also observed for both the TM3 and the TM4 cases, on allowing the reaction mixture containing equivalent amount of Cu(II) and TM2 in the presence of a thousand fold excess EDTA (10^{-1} **M**), precipitates formed within 20 hr.

The results obtained for the second experiments, where EDTA was added to Cu(II) and TM2, also suggest that EDTA is incapable of removing Cu(II) from any of the Cu-TM adduct once formed, as was the case for both TM3 and TM4.

3.3.1.9 Effect of S^{2-} on Cu(II) and TM4 Interactions

Figure 3.14 shows the UV/visible spectra taken 5 min and 1 hr after adding Cu(II) to the mixture of TM4 and varying amounts of S^{2-}. The addition of an equivalent amount of Cu(II) to TM4 in the absence of S^{2-} led to the suppression of the 468, 316, and 241 nm peaks of TM4, as already discussed (see Figure 3.1). However, addition of

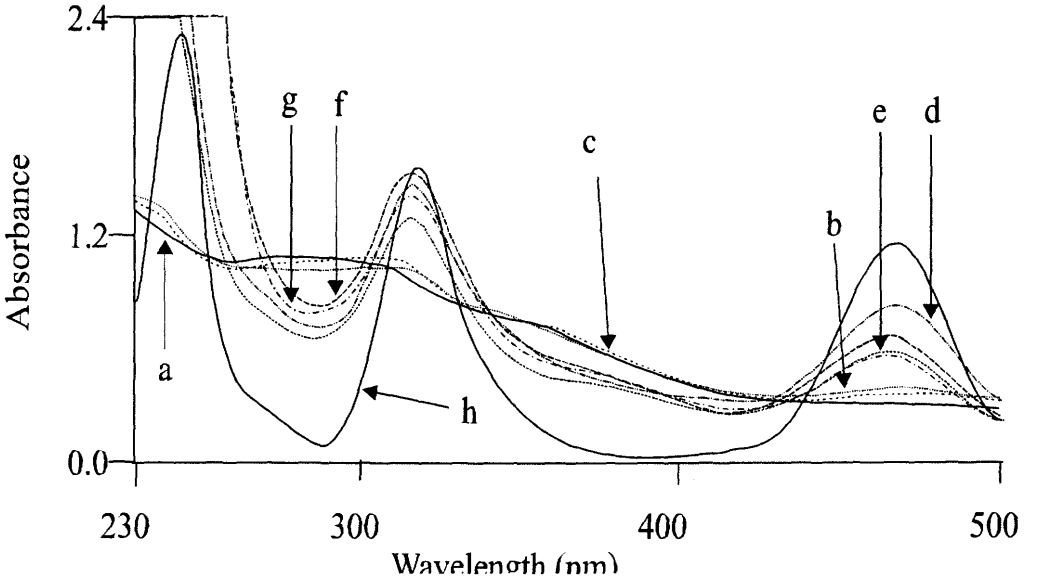

Figure 3.14: UV/visible spectra on adding Cu(II) (1 x 10^{-4} **M)** to (a) 10^{-4} **M** TM4 only, (b) a mixture of 8.3 x 10^{-5} **M** S^{2-} and 10^{-4} **M** TM4, reaction time = 5 mins; (c) a mixture of 8.3 x 10^{-5} **M** S^{2-} and 10^{-4} **M** TM4 , reaction time = 1hr; (d) a mixture of 8.3 x 10^{-4} **M** $S^{2-}$and 10^{-4} **M** TM4, reaction time = 5 min; (e) a mixture of 8.3 x 10^{-4} **M** S^{2-} and 10^{-4} **M** TM4, reaction time = 1hr; (f) a mixture of 8.3 x 10^{-3} **M** S^{2-} and 10^{-4} **M** TM3, reaction time = 5min; (g) a mixture of 8.3 x 10^{-3} **M** S^{2-} and 10^{-4} **M** TM4, reaction time = 1 hr; (h) 10^{-4} **M** TM4 alone.

S^{2-} to the reaction mixture with TM4 inhibited the complete reaction between Cu(II) and TM4 when observed 5 min after the addition of Cu(II). This is shown by the persistence of the 468 and 316 nm peaks in Figure 3.14 b, d, and f, and clearly demonstrates the competition from S^{2-} with TM4 for the Cu(II) ions to form CuS at the early stages of the reaction. As shown in Figure 3.14 a, b and d, increasing S^{2-} concentration up to ca an 8-fold excess increases the intensity of the 468 nm peak in

line with the argument that S^{2-} competes with TM4 and subsequently inhibits the complete reaction between TM4 and Cu(II). See also Table 3.12.

Table 3.12: Percentage (%) reduction of the intensity of the 468 nm peak of TM4 in 10^{-4} **M** aqueous solution alone and in a 0.8:1:1, 8:1:1, 80:1:1 S^{2-}:Cu(II):TM4 reaction mixtures at different times after solution preparation. TM4 concentration in each reaction mixture is 1.00×10^{-4} **M**.

Time	TM4 alone	S^{2-}:Cu:TM4 0.8:1:1	S^{2-}:Cu:TM4 8:1:1	S^{2-}:Cu:TM4 80:1:1
5 min	0	69.3	30.7	44.5
1 hr	0.8	73.1	50.9	52.7

Interestingly, however, S^{2-} in ca 80-fold excess causes more TM4 to disappear from the solution than in 8-fold excess. Thus, the presence of high excess of S^{2-} plays a synergistic role in the interaction between Cu(II) and TM4 whilst in comparable concentration with TM4 it seems to play an inhibitory role. This can be rationalized as follows. As shown in Table 3.12 and also from Figure 3.14, allowing the reaction to proceed for an hour causes a general decrease in the TM4 peaks as compared to the 5 min reaction time. These changes, although small, can nevertheless **not** be attributed to hydrolysis as can be deduced from Table 3.12 and also explained earlier in Section 3.3.1.6. The decrease should be due to further reaction of TM4 with Cu(II) compounds to form Cu-TM4. Freshly prepared insoluble CuS is reported to react with TM4 to form Cu-TM4 (70BR, 84SM). It is worthy of note that yields from the reaction of TM4 with CuS are poor as compared to reaction between aqueous Cu(II) solution and TM4 (70BR).

To confirm that the changes in the TM peak intensities are not due simply to pH changes as result of the varying S^{2-} concentration, 1.00×10^{-4} **M** Cu(II) was added to a pH 6 buffer solution containing 1.00×10^{-4} **M** TM4 in the presence or absence of 8.3×10^{-4} **M** S^{2-} and the spectra recorded 5 min after adding Cu(II) (see Figure 3.15).

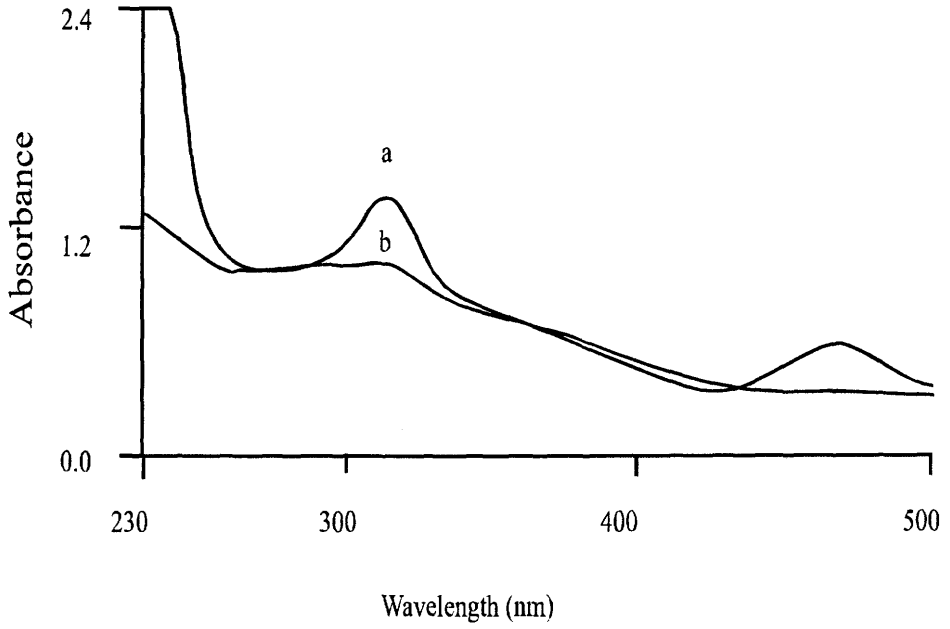

Figure 3.15: UV/visible spectra on adding Cu(II) (1 x 10^{-4} **M)** to (a) 10^{-4} **M** TM4 only in pH 6.0 buffer solution, (b) a mixture of 10^{-4} **M** TM4 and 8.3 x 10^{-4} **M** S^{2-} in pH 6.0 buffer solution. Reaction time = 5 min.

Although in both cases the reaction between Cu(II) and TM4 did not go to completion, it is obvious from the UV/visible spectra that more TM4 reacted in the absence of S^{2-} than in its presence. For example, whereas the peak at 468 nm can barely be seen in the absence of S^{2-}, it was very distinct in the presence of S^{2-} (Figure 3.15). The findings of this experiment confirm the one discussed above. When S^{2-} is present in a concentration of up to about 8-fold excess over TM4 it competes with the TM4 for any added Cu(II). The conclusion of earlier authors (82CL), that the interactions of Cu(II) with TMs do not depend on the S^{2-} level, appears to be incorrect.

The issue of the effect of S^{2-} on the Cu(II) and TM4 interaction was pursued further by looking at the effect of changing the order of mixing on the interaction. Figure 3.16 shows the UV/visible spectra obtained on changing the order of mixing of an approximately 8:1:1 S^{2-}:Cu(II):TM4 solution. Addition of the S^{2-} flattened out the TM4 peaks, as normally observed in the interaction of TM4 with excess Cu(II) in the absence of any other interfering species (Figure 3.1), suggesting that the excess S^{2-} could not prevent appreciably the reaction between TM4 and Cu(II).

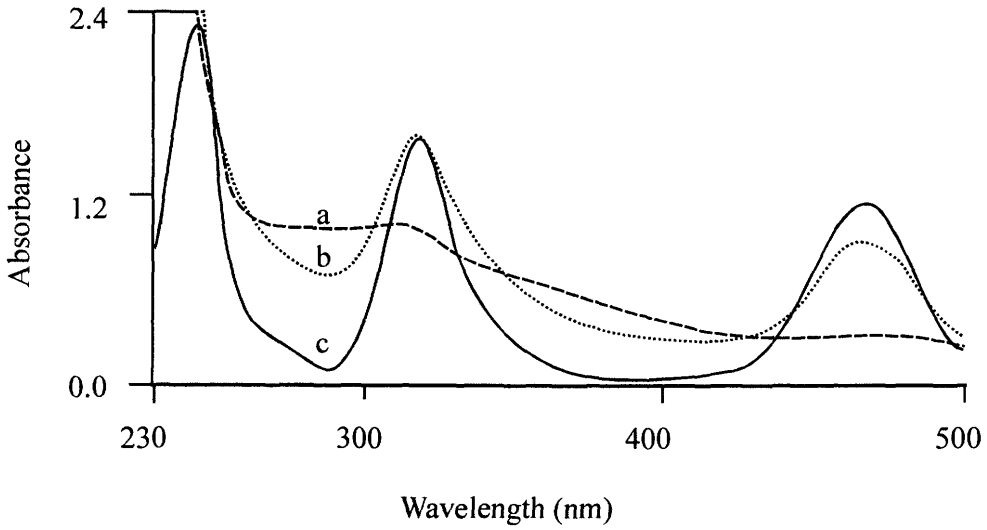

Figure 3.16: UV/visible spectra on adding (a) 8.3 x 10^{-4} **M** S^{2-} to a mixture of Cu(II) (1 x 10^{-4} **M**) and 1 x 10^{-4} **M** TM4 aqueous solution and (b) 1.0 x 10^{-4} **M** TM4 to a mixture of Cu(II) (1 x 10^{-4} **M**) and 1 x 10^{-4} **M** S^{2-} aqueous solution.

However, addition of TM4 to a solution containing an equivalent amount of Cu(II) and approximately 8-fold excess S^{2-} resulted in a spectrum which had the 468 nm peak of TM4 reducing in intensity only by 21.8%, which means the initial formation of CuS as expected prevented substantially the reaction between TM4 and Cu(II). As for EDTA, it seems once Cu(II) reacts with the TMs, S^{2-} cannot strip off the Cu(II) even with the excess of the ligand. Again, since the interaction depends on the order of adding reactants, it must be kinetically-based.

3.3.1.10 Effect of S^{2-} on the Interaction between Cu(II) and TM3

Figure 3.17 shows the UV/visible spectra taken 5 min after adding Cu(II) to the mixture of TM3 and varying amounts of S^{2-}. The addition of equivalent amount of Cu(II) to TM3 in the absence of S^{2-} led to the disappearance of the 461 and 396 nm peaks of TM3 and resulted in the expected spectrum as in Figure 3.1. However, increased amounts of S^{2-} in the reaction mixture with TM4 inhibited the reaction between Cu(II) and TM3 when observed 5 min after adding Cu(II), as observed for the case of TM4 above (Section 3.3.1.9).

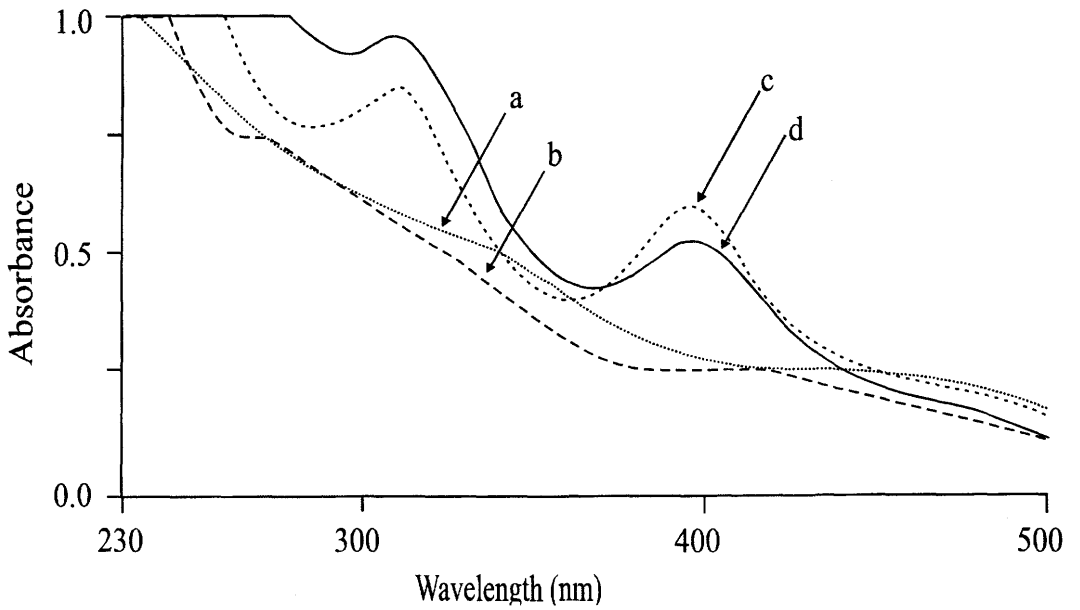

Figure 3.17: UV/visible spectra collected 5 min after adding Cu(II) (1 x 10^{-4} **M)** to (a) 10^{-4} **M** TM3 only, (b) a mixture of 10^{-4} **M** TM3 and 8.3 x 10^{-5} **M** S^{2-}, (c) a mixture of 10^{-4} **M** TM3 and 8.3 x 10^{-4} **M** S^{2-}, (d) a mixture of 10^{-4} **M** TM3 and 8.3 x 10^{-3} **M** S^{2-}.

This is shown by the presence of the 461 and 396 nm peaks in Figure 3.17 c, and d and clearly demonstrates the competition from S^{2-} with TM3, for the Cu(II) ions. As for TM4, increasing S^{2-} concentration competes with TM3 for Cu(II), but the trend is reversed for S^{2-} concentration in ca 80-fold excess over TM3. It is possible for S^{2-} concentration in such high excess that any unreacted TM3 can be converted to TM4 (see Chapter 2 for more details). The presence of TM4 in the resulting solution may eventually favor the reaction between the TMs (TM3 and TM4) and Cu(II) over the S^{2-} with Cu(II).

3.3.1.11 Effect of L-His on Cu(II) and TM4 Interactions

Unlike EDTA and S^{2-}, the UV/visible spectral taken on varying the concentration of L-His in a reaction mixture containing also Cu(II) and TM4 were essentially the same and similar to the 1:1 Cu(II):TM4 spectra in aqueous solution (Figure 3.1e). There is therefore no indication of any competition between L-His and TMs for Cu(II). Despite this similarities in the UV/visible spectra, incremental amounts

of L-His in the reaction mixture enhanced the precipitation of the Cu-TM adducts, probably due to increased ionic strength. It should, however, be noted that these observations do not preclude the possible involvement of L-His in ternary complexation. This issue is pursued further in Chapter 6.

3.3.2 TM Binding to BSA

3.3.2.1 TM4 Binding to BSA

The difference UV/visible spectra of a mixture of 1:1 BSA:TM4 vs TM4 (all at 1.00 x 10^{-4} **M)** in buffer solutions of different pH are shown in Figure 3.18. See Section 3.2.7.1. Binding between BSA and TM4 is indicated by a dip at around 317 and 468 nm, where TM4 absorbs. The intensity of the dip increases with a decrease in pH from 8 to 6. At pH 4.4, however, the spectrum obtained was almost the same as at pH 7.

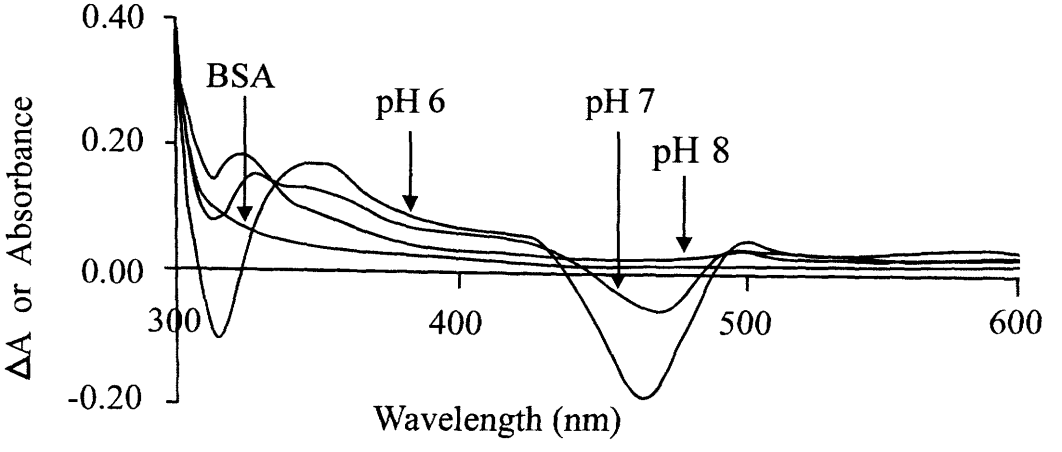

Figure 3.18: Difference spectra of 1:1 BSA:TM4 vs TM4 in different pH buffer solutions. See text for experimental details.

Although ca. 10^{-4} **M** TM4 alone in aqueous solution of pH 4.4 disintegrates, presumably via acid hydrolysis, to form precipitates within 48 hr, no such precipitates were observed when the 1:1 BSA: TM4 mixture was allowed to stand for 48 hr. BSA binding to TM4 seems to inhibit the hydrolysis of TM4. At pH ≤ 3, there was no evidence of binding. At such low pH values the TM4 is degraded to form brown precipitates,

presumably MoS_3 (86KM) or MoS_2 (80HS) even in the presence of BSA. Indeed the TMs hydrolyze more easily with decreasing pH. However, since both the BSA and TM4 mixture and TM4 were prepared in the same set of buffer solutions and measurements taken at the same time after mixing, the increased depth of the spectrum for TM4 at 317 and 468 nm from pH 8 to 6 cannot be attributed to hydrolysis at lower pH values. It rather indicates the strength of binding between BSA and TM4 at the lower pH values.

3.3.2.2 TM3 Binding to BSA

The difference UV/visible spectra of a 1:1 BSA:TM3 vs TM3 in buffer solutions of pH 6 and 7 are also shown in Figure 3.19.

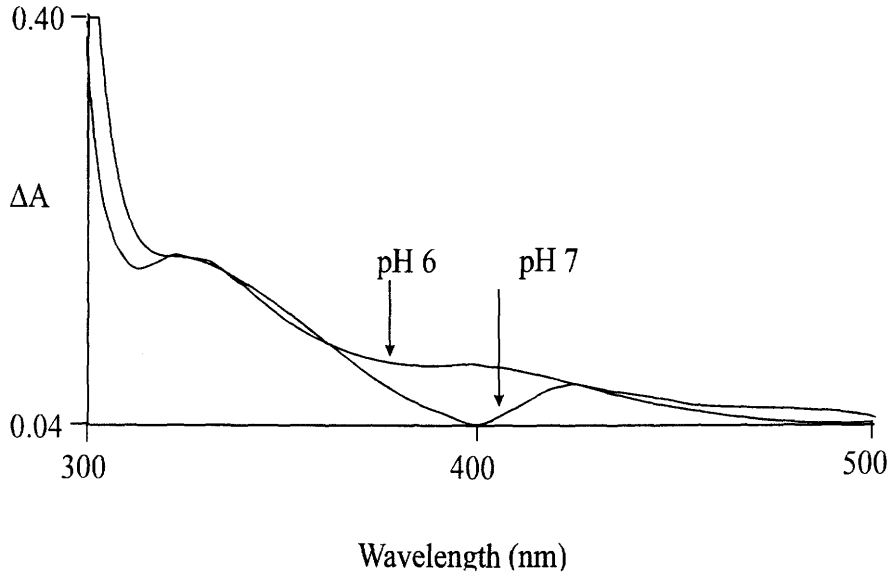

Figure 3.19: Difference spectra of 1:1 BSA:TM3 vs TM3 in buffer solutions of different pH values.

The experimental procedure was as described for the case of TM4 in Section 3.3.2.1. Similar dips as in the case of TM4 were observed in the 1:1 BSA:TM3 vs. TM3 difference spectrum at 311 and 396 nm in a buffer of pH 7. Two peaks emerge at 427 nm and 323 nm. Mason and Wood (87WM) reported similar peaks at 420 nm and 325 nm respectively in pH 7.4 when they performed similar difference spectra experiment

for a mixture of BSA and TM3 vs TM3. They observed the difference spectra to be affected by pH, since increasing the pH in their experiment to 9 and above caused the disappearance of the peak at 325 nm. The pH dependence was confirmed in this experiment since the binding between BSA and TM3 at lower pH values was not evident as demonstrated with the interaction in the buffer solution of pH 6 (Figure 3.19).

3.3.2.3 TM2 and TM1 Binding to BSA

The difference UV/visible spectra of a 1:1 BSA:TM2 vs TM2 in buffer solution of pH 8 and ionic strength 0.2 **M** is shown in Figure 3.20.

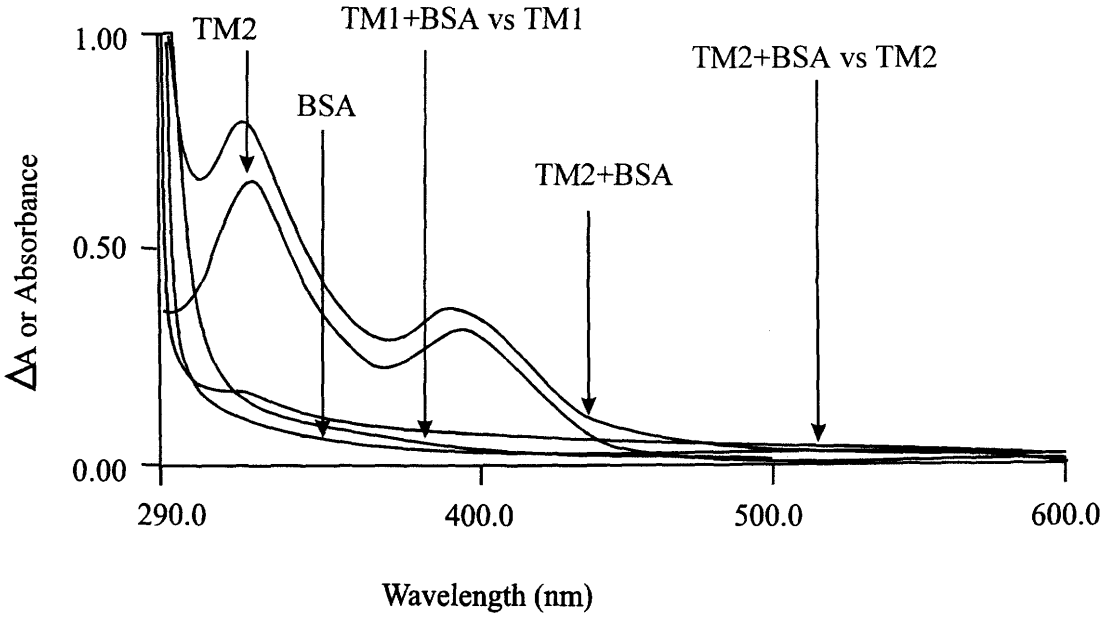

Figure 3.20: UV/visible spectra of 10^{-4} **M** 1:1 BSA:TM2, TM2 and BSA, and the difference spectra of 1:1 BSA:TM2 vs TM2 and 1:1 BSA:TM1 vs TM1 in buffer solutions of pH 8, ionic strength 0.2 **M**.

It is not obvious from this spectrum that there is any significant binding of TM2 to BSA, since the difference spectrum is almost similar to the spectrum of BSA alone (Figure 3.20). This applies also to TM1 and BSA interactions, as can be seen in Figure

3.20. Since these two TMs hydrolyze easily in lower pH solutions, they were not studied under those conditions.

3.3.3 Tripartite Interaction between BSA, Cu (II) and TMs

Preliminary studies indicated that whether Cu(II) is added first to BSA followed by the TMs, or TMs to BSA followed by Cu(II), a soluble product results in both cases. Woods and Mason (87WM) also observed likewise by using TM3. However, the prior mixing of Cu(II) and TM together in solutions of high ionic strength, as discussed earlier, forms a product that is insoluble, and the subsequent addition of BSA does not make it soluble.

3.3.3.1 Tripartite Interaction between BSA, Cu (II) and TM4

Figure 3.21 shows the difference spectra obtained for 1:1:1 BSA:Cu(II):TM4 vs 1:1 Cu(II):TM4 in buffer solutions of pH 6.0, 7.0 and 8.0. Experimental details are

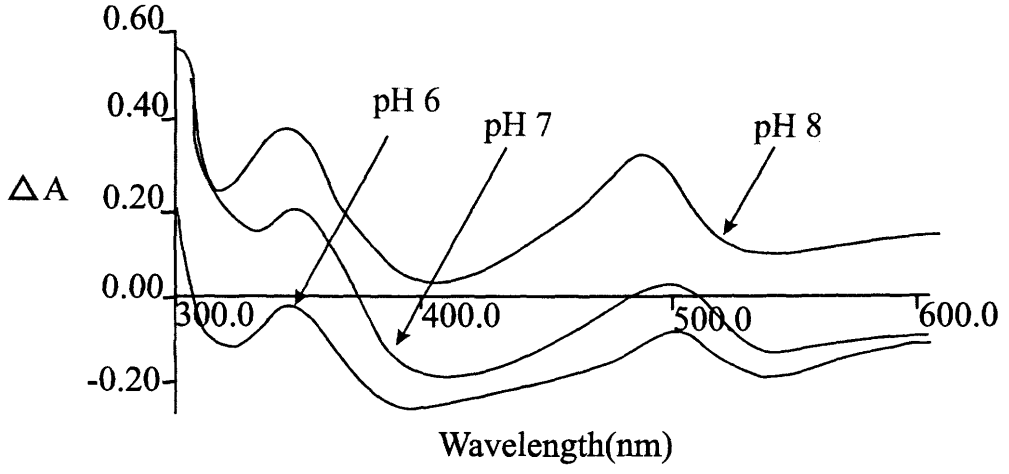

Figure 3.21: Difference spectra of 1:1:1 BSA:Cu(II):TM4 vs 1:1 Cu(II):TM4 in buffer solutions of different pH.

outlined in Section 3.2.7.2. It is obvious from the difference spectra that a mixture of BSA, Cu(II) and TM4 can interact (depending on the order of mixing as explained in the introductory part of the Section 3.3.3) to form a new product different from that

obtained from a reaction mixture of Cu(II) and TM4. In the absence of such 3-way binding, the spectrum should be the same as that of BSA (Figure 3.18 and 3.19).

As detailed in Section 3.2.7.2, each of the three reactants was of concentration 1.00×10^{-4} **M** in these studies. Furthermore, for each particular UV/visible difference spectrum of BSA:Cu(II):TM4 (1:1:1) vs Cu(II):TM4 (1:1), the same buffer solution was used to prepare the two different reaction mixtures. Hence, the contributions to the spectra from the buffer solutions are eliminated. The difference spectrum of 1:1:1 BSA:Cu(II):TM4 vs 1:1 Cu(II):TM4 shows peaks at ca. 340 and 490 nm in the pH 8 buffer solutions. These peaks are observed also at pH 7 but with reduced intensity. A decrease to pH 6 caused further reduction in intensity of these peaks. It is clear that pH has a substantial effect on this 3-way binding between BSA, Cu(II) and TM4.

The UV/visible spectra of the 1:1:1 BSA:Cu(II):TM4 in buffer solutions of 8.0, 7.0 and 6.0 are shown in Figure 3.22. For each of the three solutions two new broad peaks are observed; one around 490 -500 nm and the other at around 320 to 340 nm (almost a plateau). At pH 7.0, which is close to physiological pH (~ 7.4), the peaks were centered at 499 nm and 342 nm. The peak intensities decreased in the order pH 8 > pH7 > pH 6.

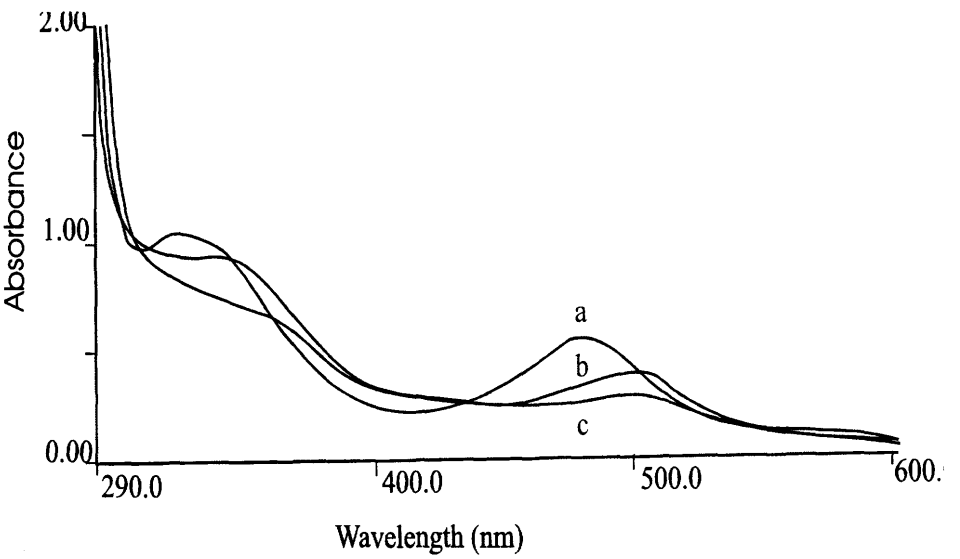

Figure 3.22: UV/visible spectra of 1:1:1 BSA:Cu(II):TM4 in buffer solutions of pH; (a) 8 (b) 7 and (c) 6.

These peaks, close to the characteristic λ_{max} = 468 nm and 316 nm of TM4 (Table 2.1), are likely to have resulted from red shifts of these TM4 peaks as a result of binding to BSA-Cu. Such red shifts of TM4 bands in the presence of Cu(II) have been identified in the literature and attributed to Cu-(S)-Mo-S core units (see Section 1.2.6).

The 3-way binding between BSA, Cu(II), and TM4 gives rise to soluble product(s) even at low pH and high ionic strength, in contrast to the binary interaction between Cu(II) and TM4, as discussed in Section 3.3.1.5. In fact a 1:1:1 BSA:Cu(II):TM4 at a reactant concentration of approximately 1 x 10^{-4} **M** can be kept for several weeks without forming any precipitates.

3.3.3.2 Tripartite Interaction between BSA, Cu(II) and TM3 or TM2

The difference spectrum of 1:1:1 BSA:Cu(II):TM3 vs 1:1 Cu(II):TM3 in a buffer solution of pH 7.0 and of ionic strength 0.2 **M** is shown in Figure 3.23a.

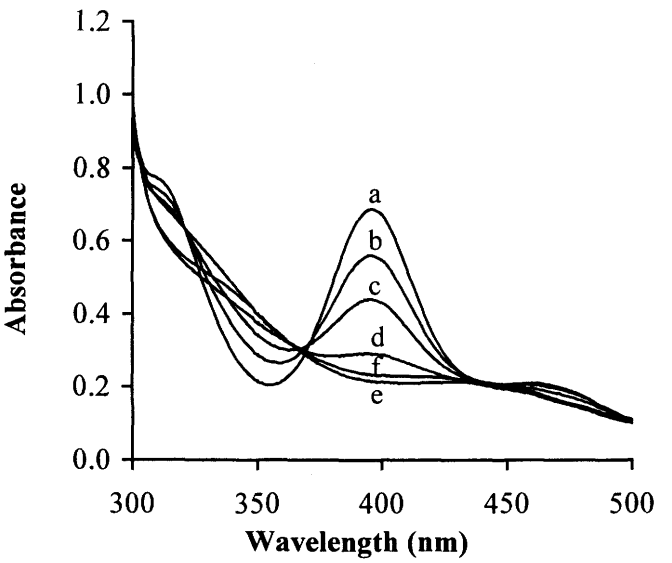

Figure 3.23: UV/visible spectra as different amounts of Cu(II) ions are added to a mixture of BSA andTM3 (1:1 at a concentration of 10^{-4} M). a) No Cu(II), b) 1:0.1:1 BSA:Cu:TM3, c) 1:0.2:1 , d) 1:0.4:1 e) 1:1:1 f) 1:2:1.

The spectrum displays a peak at 420 nm, as also observed by Wood and Mason (87WM) at pH 7.4. In addition, they observed a large peak at 335 nm, which was absent in this work; only a shoulder was observed in that region. The difference is probably due to additional absorption from unreacted TM3 at the slightly higher pH in their study.

Figure 3.24 shows the UV/visible spectra of a 1:1 mixture of BSA and TM3 with varying concentration of Cu(II). See Section 3.2.7.2 for the experimental details. The spectra suggest that an equivalent amount of Cu(II) is required for the complete reaction with a mixture of BSA and TM3. Excess Cu(II) did not result in any further significant changes in the spectrum (Figure 3.24).

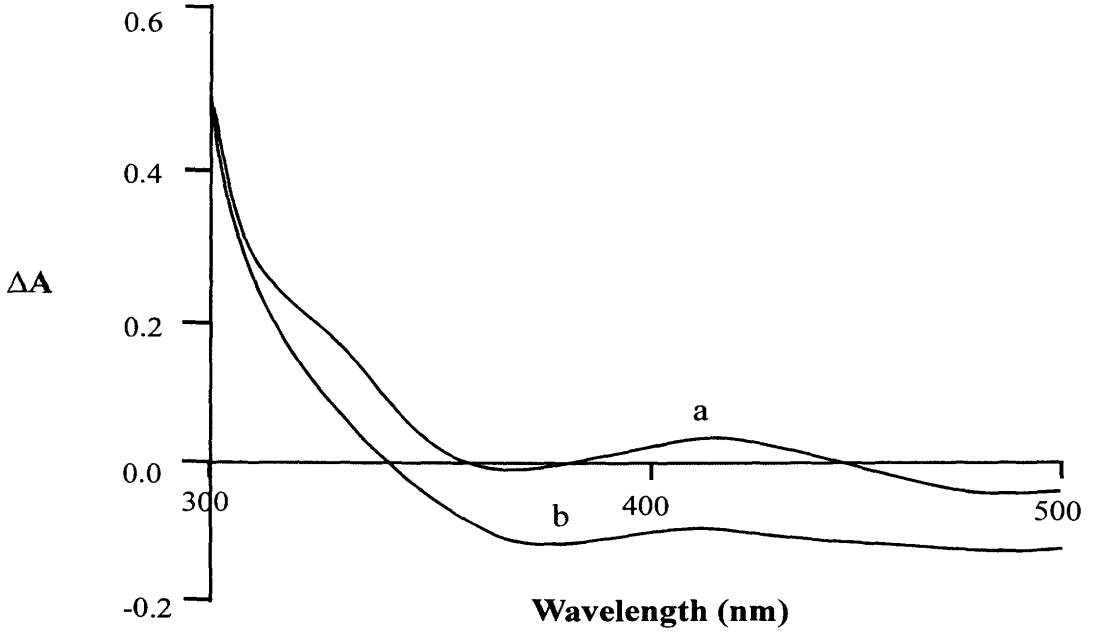

Figure 3.24: Difference spectra of (a) 1:1:1 BSA:Cu(II):TM3 vs 1:1 Cu(II):TM3 in pH 7.0 buffer solution (b) 1:1:1 BSA:Cu(II):TM3 vs 1:1 Cu(II):TM3 in pH 8.0 buffer solution.

For the case of TM2, the difference spectra of 1:1:1 BSA:Cu(II):TM2 vs 1:1 Cu(II):TM2 in a pH 8.0 buffer solution of the same ionic strength as above indicates a

new peak at 413 nm (Figure 3.24b). This peak is however weak as compared to what is observed for the case of TM3 at 420 nm.

The above suggests ternary complexation between BSA, Cu(II) and TMs. TMs absorbed into the blood stream of ruminants will result in the formation of such ternary complexes rather than the insoluble Cu-TM adduct.

This study does *not,* however, support the hypothesis of the binding of a "soluble Cu-TM complex" to albumin in the blood (95SO, 00OC) since the addition of BSA to a Cu-TM mixture did not prevent the formation of the insoluble Cu-TM adducts. Rather, the binding will be between TM and albumin-Cu(II) or between Cu(II) and TM-albumin, should the reaction observed for BSA in this study be applicable to albumins in general.

3.3.2.3 Effect of EDTA on the Tripartite Interaction between BSA, Cu(II) and TM3

The three way interaction between BSA, Cu(II), and TM3 has been claimed by Mason and Wood (87WM) to be reversible, whereas Suttle (91S) refers to it as irreversible. To ascertain the validity of either claim, incremental amounts of EDTA were added to reaction mixtures of 1:1:1 BSA:Cu(II):TM3 at a concentration of 1.00×10^{-4} **M** in water and in a pH 7 buffered solution. Figure 3.25 shows the effect of EDTA on the UV/visible spectra of 1:1:1 BSA:Cu(II):TM3 at concentration of 1×10^{-4} **M** in water. It appears that the addition of excess EDTA leads to the formation of another product that is not BSA-TM3, as might be expected from the stripping of Cu(II) from BSA-Cu-TM3. The conversion of BSA-Cu-TM3 to this product by EDTA is reversible. The identity of this product is not clear at present, an issue demanding further investigation. Interestingly, however, when the reaction was performed in a phosphate buffer solution of pH 7.0, the spectra for the same concentration range (i.e. 0 to 5.0×10^{-3} **M** EDTA) were all the same as also observed in Figure 3.25c, which is the spectrum of 1:1:1 BSA:Cu(II):TM3 reaction mixture in the absence of EDTA. This suggests that the phosphate buffer inhibits whatever reaction is occurring in water.

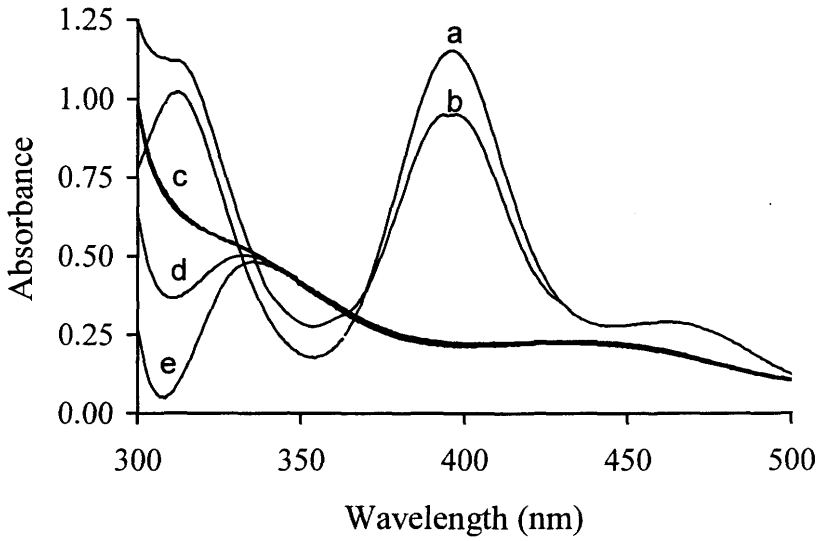

Figure 3.25: Effect of EDTA on the UV/visible spectra of mixtures of BSA, Cu(II), and TM3 in various proportions; (a) 10^{-4} **M** TM3 only, (b) 1:1 BSA:TM3 (10^{-4} **M**), (c) 1:1:1 BSA:Cu (II):TM3 (10^{-4} **M**), with or without 1 x 10^{-3} **M** EDTA. (d) as c but 2.5 x 10^{-3} **M** EDTA, (e) as c but 5.0 x 10^{-3} **M** EDTA.

3.4 CONCLUSIONS

Thiomolybdates (TMs) formed in the rumen are known to be involved in Cu deficiency in ruminants. The results in this study indicate a reaction between Cu(II) and all the four TMs with a stoichiometry 1:1 in aqueous solution. The study also indicates that the reaction is rapid leading to the formation of very stable complexes. Apart from the stability, they form precipitates in aqueous solutions with high ionic strength, comparable to that in the rumen and at low pH, matching that in the abomasum of ruminants. In terms of the rapidity and the quantity formed, the precipitation of Cu(II) by the TMs is in the decreasing order TM4 > TM3 > TM2 > TM1. The formation of insoluble "Cu-TMs" will certainly be one means of preventing the absorption of Cu *in vivo*. The results clearly demonstrate ternary complexation involving BSA, TMs and Cu(II). The solubilities of the ternary complexes ("BSA-Cu-TMs") and the binary complexes ("Cu-TMs") are different, although both appear very stable to hydrolysis and the influence of other ligands. This is an indication of another means of preventing the availability of "free" Cu(II) *in vivo*.

4. SYNTHESES AND CHARACTERIZATION OF HISTIDINE-CONTAINING PEPTIDES MODELLING THE N-TERMINUS OF BOVINE SERUM ALBUMIN

4.1 INTRODUCTION

4.1.1 Rationale for the Study

The amino acid sequences of the N-terminal regions of bovine (BSA), human (HSA) and rat serum albumin (RSA) are respectively Asp-Thr-His-Lys, Asp-Ala-His-Lys and Glu-Ala-His-Lys. In each case, the amino terminal region is known to provide a specific binding site for Cu(II) ions (67PB, 95HS), with His at the third position thought to be mainly responsible for the specificity. The important physiological implications of albumin-Cu(II) complexation for the transport of Cu(II) in blood (95B) make it of interest to investigate the structures and the stabilities of the complex species in solution. Furthermore, TMs are known to influence the binding of Cu(II) to BSA (87WM).

The use of small model peptides has proven valuable in elucidating the structural features that contribute to the formation of such metallocomplexes (67SB). Peptides containing His, especially in the third position, could serve as good structural models of albumin for Cu(II) complexation.

Small His-containing peptides such as Gly-His-Lys are also known to have some specific biological activities, such as altering the growth rate and survival of

cultured hepatoma cells and hypotocytes (83MW). These activities are enhanced when they are complexed to Cu(II) and other transition metals (83MW). It has also been shown that Gly-His-Lys stimulates collagen synthesis and hence serves as an activator for wound repair (93MB). Structure–function studies revealed that several tripeptides with a His-Lys linkage were nearly as active as Gly-His-Lys (80PF). It is noteworthy that the biological activity of the peptides containing His-Lys sequences is generally based on their function as carrier for Cu(II) ions (98BJ). They may also therefore be involved in the exchange and transport mechanism of trace Cu ions in animals (80PF).

For these reasons, the dipeptide His-Lys, the tripeptide Thr-His-Lys, and the tetrapeptide Asp-Thr-His-Lys were identified for study. This chapter describes the syntheses and characterization of His-Lys, Thr(Ac)-His-Lys , Thr-His-Lys and Asp-Thr(Ac)-His-Lys. Studies of interactions of these with Cu(II) and/or TMs will be described in Chapters 5 and 6.

4.1.2 Peptide Synthesis

A peptide is any compound produced by amide formation between the carbonyl function of a carboxy group of one amino acid (A) and an amino group of another (B). If the reaction were to be performed simply by reacting these 2 amino acids, four possible dipeptide products (A-A, B-B, A-B and B-A) could be formed. In addition, polycondensation products from all the four possible dipeptides would also result. An exclusive synthesis of one product, A-B for instance, therefore entails the protection of the amino group of one of the amino acids (A) (leaving the carboxy component "free") and also the protection of carboxy group of the other (B) (leaving the amino component "free"), followed by condensation (peptide-bond formation), and finally, the removal of the protecting groups. Other issues must also be addressed:

1. Possible side-reactions involving functionalities in some amino acid side-chains, necessitating further protection reactions.
2. The need to perform peptide synthesis without loss of stereochemical integrity at any of the chiral centers.

3. Ensuring the non-destruction of the peptide backbone and the avoidance of other side reactions during the final removal of all the protecting groups.
4. Ensuring the purity of the product by selecting appropriate reagents and/or solvents that would not themselves contribute to the formation of by-products, or make it difficult to separate by-products from the desired product.

Modern peptide synthesis employs the following approach. The amino group of the amino acid A, which will be the N-terminal residue of the peptide, is first protected. Then the carbonyl group is activated so that it is capable of coupling with a second amino acid B (which also preferably has the carboxy group protected). The coupling reaction is performed, and finally the two protecting groups are removed to produce the finished peptide AB (84BB, 91J).

The main challenge in this procedure lies in the selection of suitable protecting groups. To be efficient, a protection group should not introduce any problems of its own while in position; it must stay firmly at its post as long as it is needed and when the job is completed, it should be removable easily, under conditions that have no adverse effects on the rest of the structure being assembled.

4.1.2.1 α-Amino Protection

To protect the α-amino group, its nucleophilic reactivity must be suppressed by draining its electron density away into an appropriate substituent, or by concealing it using very bulky substituents to create steric hindrance (91J). Many different protecting groups that include benzylcarbonyl (Z), t-butoxycarbonyl (Boc), Dinitrophenyl (DNP) and fluorenylmethoxycarbonyl (Fmoc) have been proposed (91J, 84BB, 76BK). The structures of the Z and Boc protecting groups, the two groups actually used in the protection of the α-amino groups in this study, are given in Figure 4.1. Different approaches for removing these two groups are discussed below.

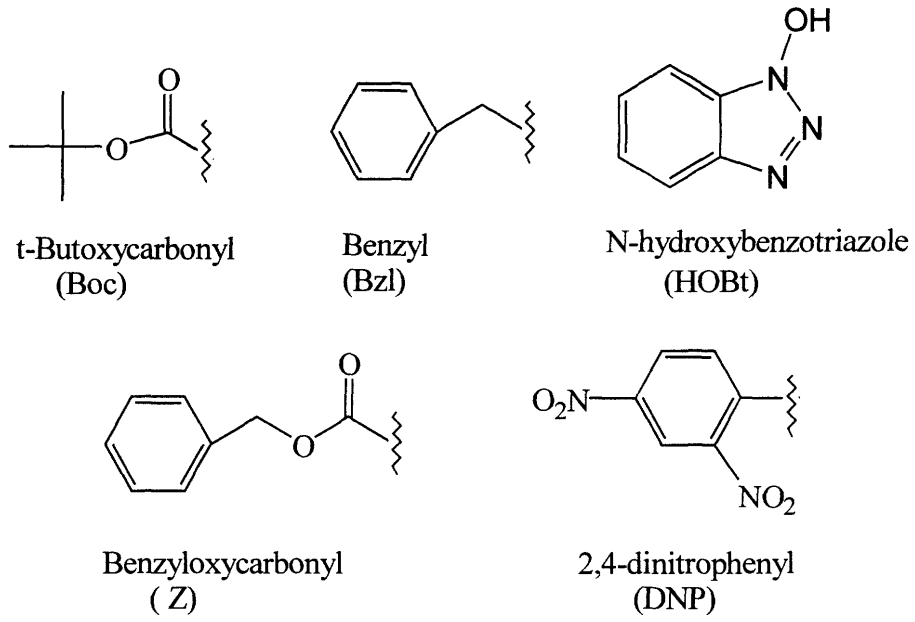

Figure 4.1: Structures of the Z (Benzyloxycarbonyl), Boc (t-Butoxycarbonyl), Bzl (benzyl) and DNP (2,4-dinitrophenyl) groups, and of HOBt (N-hydroxybenzotriazole).

Mildly basic and/or nucleophilic reagents - amines, hydrazine and dilute aqueous alkali - do not as a rule cleave Z from an amino group at ambient temperature. Mildly acidic conditions are also without effect. The classic cleavage conditions are HBr/AcOH (acetic acid) or catalytic hydrogenolysis i.e. using H_2/Pd(C)/AcOH (84BB). Cleavage by HBr/AcOH proceeds essentially by an S_N2 mechanism. It is very convenient to carry out, since most protected peptides are easily soluble in AcOH, especially in the presence of a high concentration of HBr, and the deprotected product may be precipitated as a hydrobromide on flooding with ether.

Increasing the acidity and/or polarity accelerates the cleavage; liquid HF and HBr/TFA (trifluoroacetic acid) both remove Z groups rapidly. With these powerful reagents, however, there is probably a more S_N1-like mechanism in operation, so side-reactions from "wandering electrophiles" (e.g. benzyl cations and their equivalents), which can attack the electron-rich side-chains of some amino acids (e.g. Trp, Tyr, Met) can become a serious problem.

The t- butoxycarbonyl (Boc) group is another commonly used protector of α-amino groups. The Boc group cannot be cleaved from an amino group under catalytic hydrogenolysis conditions (or by reducing agents generally), but removal is more labile to acids than for Z. Mineral acids attack Boc groups rapidly, and must be avoided in acidification and wash procedures to get rid of any excess base in the reaction system. Basic and nucleophilic reagents have no effect at all on the Boc group, even on prolonged exposure.

Boc removal is conveniently carried out using TFA as the deprotection reagent and DCM (dichloromethane) as the commonly used solvent, at ambient temperature and followed after about an hour by flooding with ether or evaporation.

4.1.2.2 α-Carboxy Protection

The usual means of carboxy group protection is esterification. Many different esters (e.g. methyl, ethyl, benzyl, and t-butyl esters) have been used (91B, 84BB).

Amino acids react easily with hot solutions of methanol or ethanol and HCl to give the corresponding ester hydrochlorides, which are usually stable crystalline materials. The corresponding free bases (distillable liquids in some cases) are obtainable by neutralizing the hydrochlorides. However, these free bases deteriorate rapidly at room temperature, so it is recommended that their generation from the hydrochlorides be done *in situ* when required, normally with a tertiary amine (84BB, 91J).

Methyl and ethyl esters provide good carboxy-protection. HBr/AcOH, TFA, catalytic hydrogenolysis conditions, thiols, or amines in organic solvents do not affect these esters at ambient temperature, so the selective removal of amino-protecting groups from peptide methyl or ethyl ester derivatives poses no difficulty. Problems are sometimes encountered at the dipeptide stage, because dipeptide methyl or ethyl ester free bases cyclize to diketopiperazines (DKPs) as shown in the reaction Scheme 4.1 below (91J).

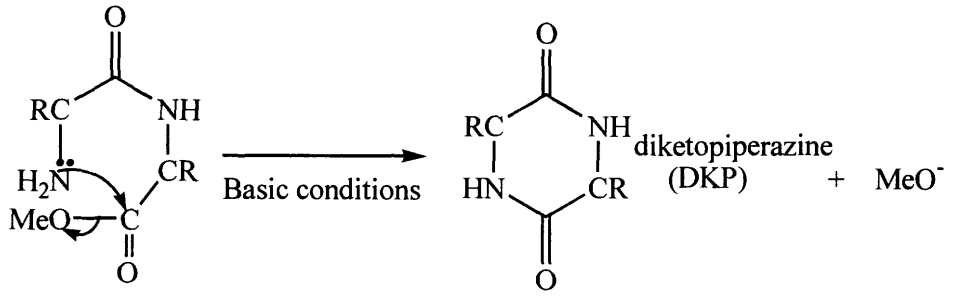

(4.1)

Methyl and ethyl esters are also quite stable, and their ultimate cleavage calls for harsh treatment. Saponification is sometimes satisfactory, but even under carefully controlled conditions, the alkali may cause racemization and other side-reactions such as hydantoin formation (see reaction Scheme 4.2).

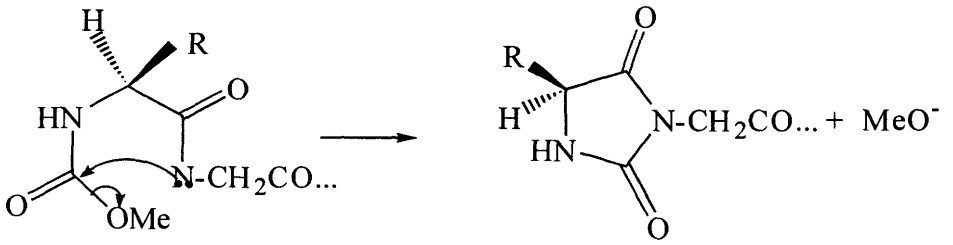

(4.2)

hydantoin

Benzyl esters have some advantages over the methyl and ethyl derivatives. The corresponding free bases are, like the amino acid methyl esters, unstable, and free base dipeptide benzyl esters are prone to DKP formation. Like the methyl and ethyl esters, benzyl esters are cleaved by saponification and by hydrazinolysis (84BB). However, HBr/AcOH, HF and catalytic hydrogenolysis also cleave benzyl esters. The most widely used of these is catalytic hydrogenolysis. The response of the benzyl esters to acidic media is similar to that of the Z group, with a slightly lower sensitivity. They therefore also suffer from side reactions due to the generation of electrophilic species as explained for the Z group above. The use of electrophile scavengers (e.g. anisole, cresol etc) is therefore recommended in reactions involving the removal of the Z and the benzyl groups (76BK).

4.1.2.3 Activation and Coupling

Ordinarily carboxylic acids simply form salts with amines at ambient temperature; the transformation of these salts into amides requires severe heating which is incompatible with presence of other functional groups. Many peptides are not thermally stable and hence would not form at all under such conditions. Efficient peptide bond formation requires "activation" of the carbonyl component of the α-NH_2 protected amino acid, by attaching a good leaving group, to enable efficient attack by the amino group of the other amino acid (91J). The activating reaction must be chosen carefully to achieve a very high coupling efficiency and at the same time avoid potential side reactions.

Carbodiimides have been some of the most popular activating reagents in peptide synthesis. Dicyclohexylcarbodiimide, DCC (Scheme 4.3), remains the most popular. DCC may be used to generate activated carboxy derivatives or as a direct *in situ* coupling reagent. In all cases, the primary activating event is addition of the carboxy group of the NH_2 protected amino acid ($R(C{=}O)O^-$) to the carbodiimide functionality to give an O-acylisourea (Scheme 4.3), which is a very reactive acylating agent and which is not isolable.

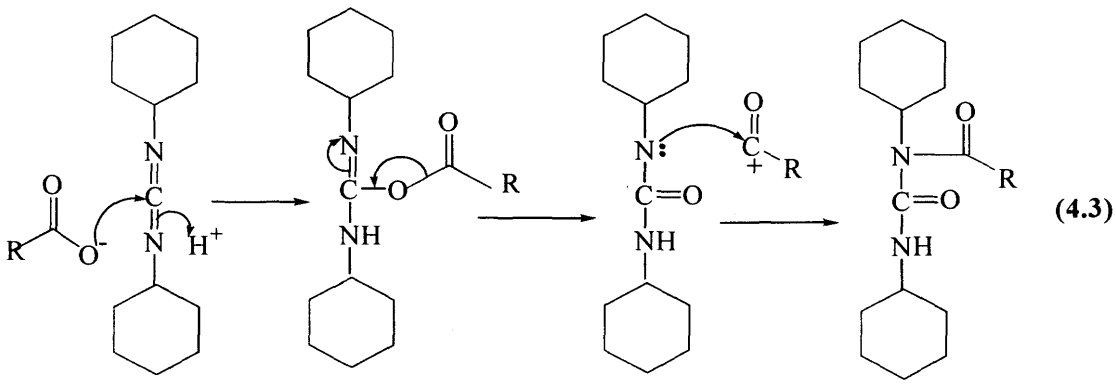

DCC O-acylisourea N-acylurea **(4.3)**

The formation of the O-acylisourea is very rapid; hence racemization, and side reactions leading to the formation of, for example, dicyclohexylurea can occur. Acyl-transfer

sometimes takes place to form the much less reactive N-acylurea (Scheme 4.3). This product does not only reduce the yield, but may also give rise to purification problems. This difficulty, and the danger of racemization, can both be greatly reduced by performing the coupling in the presence of a suitable secondary nucleophile, such as HOBt, which is able to react very rapidly with O-acylisourea before either side reactions or racemization emerge (Scheme 4.4).

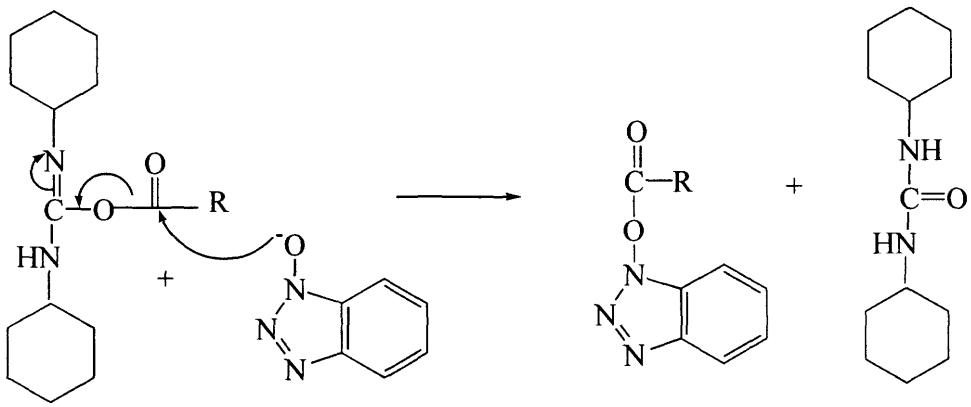

(4.4)

O-acylisourea (H)OBt HOBt active ester DCC

The HOBt active ester produced then couple with another amino acid whose carboxylate end is protected (R^1NH_2) to form the peptide (Scheme 4.5).

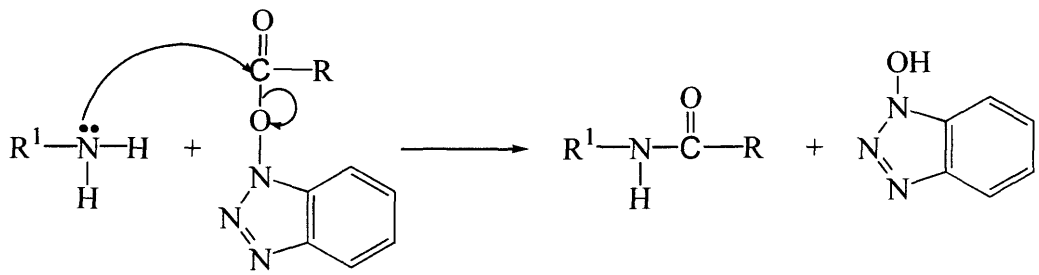

(4.5)

Other carbodiimides are available; notable is the water-soluble carbodiimide, 1-(3-dimethylaminopropyl)-3-ethyl-carbodiimide hydrochloride (EDC).

4.1.2.4. Side Group Protection

Since all four amino acids used in this study (aspartic acid (Asp), threonine (Thr), lysine (Lys) and histidine (His)) have side chain functional groups that can

interfere with the synthetic approaches discussed so far, these must also be protected. This section discusses the appropriate means of protecting these groups, and how the protection can be removed when desired.

The Asp β-carboxylate side chain functionality can be protected by a Z group (Figure 4.1). The Thr side chain OH functionality can be protected by adding on a benzyl group. The removal of the Z and benzyl protecting groups has already been discussed, in Sections 4.1.2.1 and 4.1.2.2 respectively.

Specific peptide bond formation with the α-amino group of Lys requires prior blocking of the side-chain ε-amino group. This group is more basic and nucleophilic, since there is an electron-withdrawing group next to the α-amino group. Also, the α-amino and α-carboxy- functionalities can form chelates with, say, Cu^{2+} (see and Chapter 5). These properties can be exploited to differentiate between the two amino groups. The principal ε-protecting groups are Boc and Z. Their removal is discussed in Section 4.1.2.1.

The basic and nucleophilic imidazole side-chain creates serious difficulties for the incorporation of His residue(s) without protection. Racemization occurs in carboxy-activated derivatives through pathways involving heterocyclic nitrogen, to a degree that makes the preservation of chiral integrity a more serious problem during peptide synthesis with His than with any other amino acid. Side-chain attack by DCC has been observed. These problems lead to low yields of coupling and purification problems (70SF). It has been reported that the quality of synthetic peptides is higher if the His residue remains protected throughout their assembly (98BP).

Commonly used protecting groups for the imidazole ring include Trityl (triphenylmethyl), Tosyl (p-toluene sulfonyl) and DNP (see Figure 4.1 for the structure). The Tosyl protecting group is removed when HOBt is present in solution (98BP) and is therefore unsuitable for a coupling reaction involving HOBt (Section 4.1.2.3) such as is envisaged. Furthermore, His(Tosyl) may racemize during the

coupling steps especially when using DCC as a coupling reagent (96TA). The Trityl group is also too stable for our purpose, since its removal with TFA (93PC) for example, would concomitantly remove other protecting groups, such as the Boc groups at the amino terminal. Fluoren-9-ylmethoxycarbonyl (Fmoc)-protected His, although commercially available and reported to improve crystallization (93PC), is not suitable for conventional coupling with carbodiimide of amino acids or peptides in the presence of HOBt, because it is too labile under the basic conditions required for such coupling to form new peptide bonds.

The DNP-protected His is stable enough under the conditions of the conventional carbodiimide coupling reactions, and can be removed by reagents such as thiophenols (98BP, 96TA, 70SF), TBAF (98BP) and by NH_4OH or NaOH treatments (98BP, 93PC, 96TA). Details of these approaches are outlined in the Results and Discussion section. The major disadvantage of using the DNP group is that the products obtained after deprotection are yellow in color due to the presence of residual DNP, which is an intense yellow color and is difficult to remove completely (96TA).

4.2 EXPERIMENTAL

4.2.1 Sources of Chemicals

All chemicals used were reagent grade and were used without further purification unless stated below. The solvents and reagents were obtained as follows: Methyl phenyl ether (Anisole) and sodium hydrogen carbonate ($NaHCO_3$) were obtained from the Fisher Scientific Company (Fair Lawn, U.S.A). Chloroform ($CHCl_3$), diethylether ($(C_2H_5)_2O$), methanol (CH_3OH), ammonia (NH_3) solution (28 – 30 %), Magnesium sulfate($MgSO_4$), acetic acid (CH_3COOH) and citric acid ($COOHCH_2C(OH)(COOH)CH_2COOH$) were obtained from BDH Chemicals, (Toronto, Canada). 1-Ethyl-3(3-dimethylaminopropyl) carbodiimide hydrochloride (EDC) was obtained from Calbiochem-Advanced ChemTech (Louisville, USA). Hydrogen bromide (HBr, 30 wt % solution in acetic acid), 99% Trifluoroacetic acid (TFA), 99.5%

triethylamine ($(C_2H_5)_3N$), N-Hydroxybenzotriazole (HOBt) and Charcoal were obtained from Aldrich Chemical Company Inc. (Milwaukee, USA). DSS was from Merck Sharp and Dohme of Canada Limited (Montreal, Canada). Tetramethylsilane (TMS) was obtained from MSD Isotopes-Merck Frosst Canada Inc. (Montreal, Canada). The perdeuterated solvents deuterium oxide (D_2O, 99.9 %), chloroform ($CDCl_3$, 99.8 %), and methanol (CD_3OD, 99.8 %) were obtained from Cambridge Isotope Laboratories (Andover, USA). Methylsulfoxide (DMSO-d_6, 99.9 %) was obtained from Aldrich Chemical Company Inc. (Milwaukee, USA). The protected amino acids were also obtained as follows: Boc-His(DNP)-OH.isopropanol was obtained from Calbiochem-Novabiochem (La Jolla, USA). H-Lys(Z).HCl, Boc-Thr(Bzl) and Z-Asp(OBzl)-OH were all obtained from Calbiochem, Advanced ChemTech (Louisville, USA). The full names or structures of the protecting groups, Z, Boc and Bzl can be found in the abbreviation page and Section 4.1.2.

4.2.2 Instrumental Measurements

Optical rotations were measured using a Rudolph Instruments DigiPol DP781 at 589 nm (c = 1 g/100 ml), d = 100.00 mm) in methanol. Fast-atom bombardment mass spectra (FAB MS) in positive ion mode were collected on a VG Analytical 70 VSE mass spectrometer. A cesium ion gun was used to direct a beam of fast ions (Cs^+) on metal target coated with a glycerol or m-nitrobenzyl alcohol (NBA) matrix in which the sample has been dissolved. The operating pressure of the ion source was typically ~ 10^{-5} Torr and the ions were accelerated at 28 – 30 kV. Elemental analyses for C, H and N were performed using a Perkin Elmer 2400 elemental analyzer. Thin layer chromatographic (TLC) was carried out on a precoated silica gel TLC plates (Merck, 60 F_{254} 2.5 x 5.0 cm, 0.25 mm layer thickness) and elution with a suitable solvent system. Materials were detected by visualization under a UV lamp and/or heating the plates gently on a bunsen flame to mark the spots for R_f calculations. Column chromatography for sample cleanups was performed on silica gel, Merck grade of mesh size 230 – 400. High performance liquid chromatography (HPLC) analysis was carried out on a Hewlett Packard 1050 series liquid chromatograph, equipped with a diode array UV detector

(wavelength range 190 - 600 nm), degasser, and Hypersil ODS column (5 μM particle size silica, 200 mm x 4.6 mm internal diameter), equipped with an in-line filter. A linear gradient elution [CH_3CN:H_2O, (25:75) – pure CH_3CN] over 35 minutes at a flow rate of 1.0 ml min^{-1} was used. The samples for HPLC analysis were prepared by dissolving 1 mg of sample in 1 ml of water (Section 2.2.1) or HPLC grade acetonitrile and filtering through a Pasteur pipette plugged with cotton.

NMR measurements were performed on a Bruker AM 300 spectrometer at frequencies of 300.13 MHz and 75.47 MHz for ^1H and ^{13}C NMR, respectively. ^1H and ^{13}C NMR chemical shifts in $CDCl_3$ and D_2O are reported in ppm relative to TMS or DSS respectively. The ^1H NMR signals were measured relative to the residual solvent signal of $CHCl_3$ at 7.27 ppm or of HOD at 4.80 ppm respectively, and the ^{13}C NMR signals measured relative to the residual solvent signal of $CHCl_3$ at 77.23 ppm in $CDCl_3$, or relative to internal DSS at 0.00 ppm in D_2O. Multiplicity is indicated by one or more of the following: s (singlet), d (doublet), dd (doublet of a doublet), t (triplet), q (quartet), m (multiplet), br (broad); the list of coupling constants (J) corresponds to the order of multiplicity assignment. All NMR assignments are based on ^1H COSY and $^{13}C/^1H$ J-modulated spectra (87D, 87SH) and on the basis of the consistency within a series of similar structures, comparing with commercially available starting materials or other simpler starting materials that had been previously assigned unambiguously. See Section 4.2.3 for the assignments of the peaks and detailed discussions of the logic behind these.

^1H NMR spectra in aqueous solutions were acquired using the binomial composite "1-3-3-1" sequence for water suppression (83H). DSS was added to these samples as a chemical shift reference. The probe of the NMR instrument was thermostated at 25°C.

4.2.3 Peptide Synthesis

4.2.3.1 Synthesis of His-Lys

The synthesis of His-Lys is outlined in Figure 4.2. Standard procedures for peptide synthesis as discussed in Section 4.1.2 were followed, with some modifications as detailed below.

a) Preparation of Boc-His(DNP)-Lys(Z)-OBzl ***(1)***

Refer to Figure 4.2. Coupling of Boc-His(DNP)OH.iPrOH (959 mg, 1.99 mmol) to Lys(Z)OBzl.HCl (962 mg, 2.4 mmol) to give a yellow solid **1** in 94 % yield (1.453 g, 1.88 mmol) was achieved by employing traditional peptide techniques using EDC (472 mg, 1.2 mmol) and HOBt (330 mg, 1.2 mmol) as coupling reagents (84BB) in about 20 mL chloroform. The reaction was allowed to proceed overnight. The reaction solution was then washed consecutively with 50 mL of saturated sodium bicarbonate, 50 mL of 10 % citric acid, 50 mL of saturated sodium bicarbonate, and 50 mL distilled water. The organic phase was dried by anhydrous $MgSO_4$, filtered, and finally rotary evaporated to obtain a crude yellow product. TLC analysis with 90:8:2 $CHCl_3$: MeOH:AcOH as eluent showed two spots : R_f= 0.6 and R_f= 0.1. The former was identified by ^{1}H-NMR to be the required product (see below for the NMR characterization). By using the same solvent system as for the TLC, the final product was purified by column chromatography. TLC of the isolated product as expected showed a single spot with R_f= 0.6. Upon the injection of this into the HPLC, only one HPLC peak was observed. The selection of the solvent system for both the column chromatography and the TLC was based on a prior TLC assessment of different solvent systems (varying polarity) to obtain the optimum spot separations of the constituent species. Details of results are in the Results and Discussion section.

Molecular Mass (g mol^{-1}) for $C_{38}H_{43}N_7O_{11}$: calculated 773.8; found (FAB MS) 773.3. Elemental Analysis (%): calculated C, 58.99; H, 5.60; N, 12.67; found C, 58.94; H, 5.50; N, 12.42. ^{1}H NMR (δ in ppm , $CDCl_3$): 8.76 (1H, d, J_{HH} = 2.4 Hz, aromatic proton DNP), 8.43-8.47 (1H, dd, J_{HH} = 2.4 and 8.7 Hz, aromatic proton DNP),

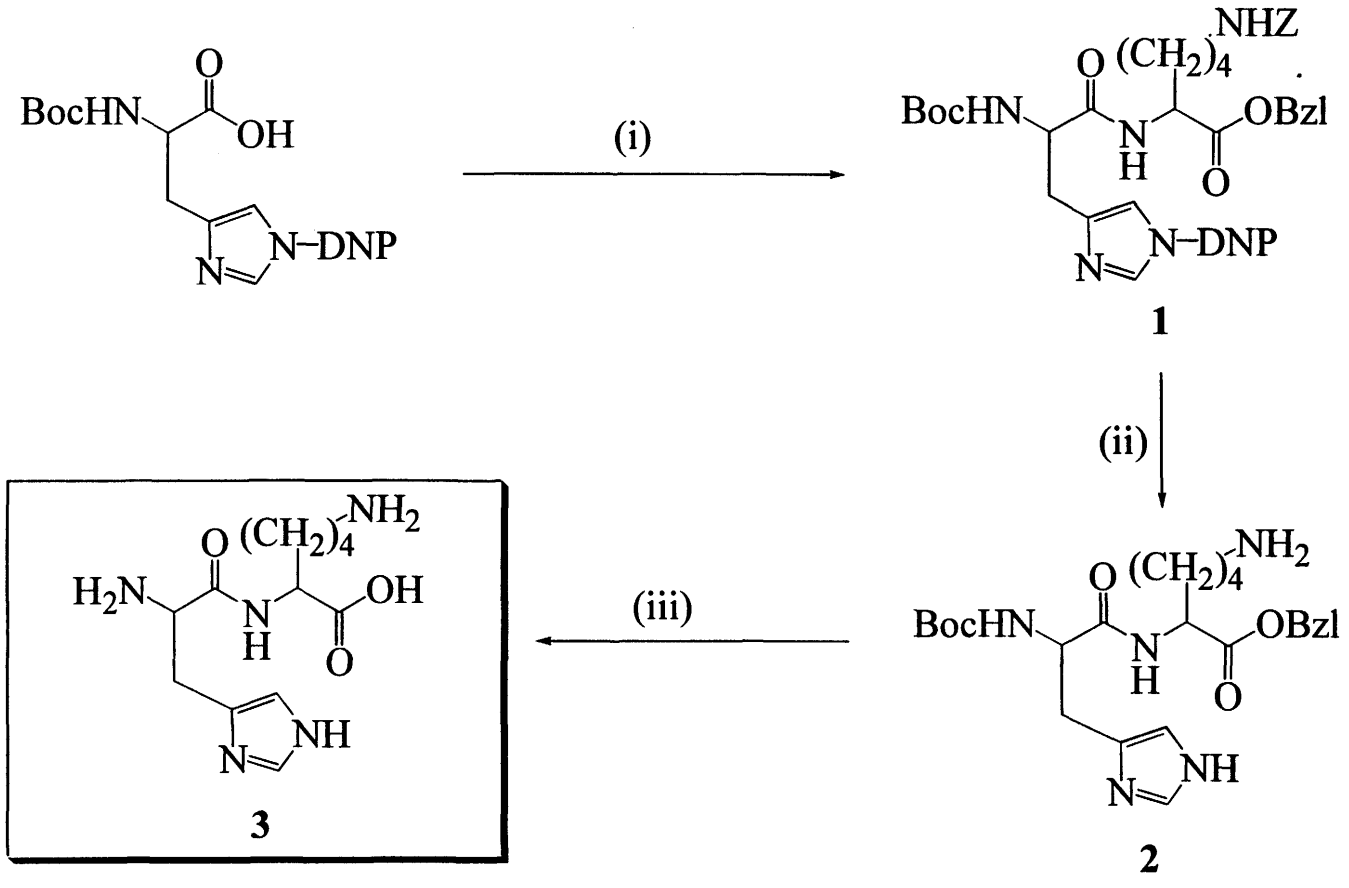

Figure 4.2: Synthetic approach for His-Lys (i) HOBt/$CHCl_3$/0°C, EDC, H-Lys(Z)-OBzl. HCl/ Et_3N (95%) (ii) NH_3/MeOH/35 °C (73 %) (iii) HBr/AcOH (73%).

7.57-7.60 (1H,d, J_{HH} = 8.7 Hz, aromatic proton DNP), 7.55 (1H, s, imidazole) 7.22-7.33 (10H, m, aromatic H of Ph), 6.83 (1H, s, imidazole), 6.06-6.08 (1H, d, J_{NH} = 7.3 Hz, Boc N*H*), 5.02-5.14 (4H, m, 2(OCH_2Ph)), 4.84 (1H, m, Z-N*H*), 4.49-4.53 (2H, m, overlapping signals of α-C*H* of His and α-C*H* Lys), 2.89-3.18 (4H, m, overlapping signals β-CH_2 of His and ε-CH_2 of Lys), 1.57-1.77 (2H, m, β-CH_2 of Lys), 1.42 (9H, s, Boc CH_3), 1.21-1.35 (2H, m, δ-CH_2 of Lys) and 0.84 (2H, m, γ-CH_2 of Lys). For the ^{13}C NMR (δ in ppm, $CDCl_3$), all the peaks were singlets. 172.0, 171.6, 156.6, 155.8 (all C=O), 146.8 (quaternary C of DNP), 144.2, (quaternary C of DNP), 140.4 (quaternary C of DNP), 136.7 (quaternary C of imidazole), 135.5 (quaternary C of Ph), 135.2 (quaternary C of Ph), 129.3 (methine C of DNP), 128.8-128.2 (overlapping signals of 10 methine C of Ph and 2 methine C of DNP), 121.4 (methine C of imidazole), 117.7 (methine C of imidazole), 80.3 (quaternary C of Boc), 67.1 (OCH$_2$Ph), 66.7 (OCH$_2$Ph), 54.2 (methine C), 52.2 (methine C), 40.7 (methylene C), 31.9 (methylene C), 30.3 (methylene C), 29.2 (methylene C), 28.5 (3 methyl Cs of Boc) and 22.3 (methylene C).

b) Preparation of Boc-His-Lys-OBzl ***(2)***

Refer to Figure 4.2. The DNP group attached to the imidazole ring of His can be removed by treatment with concentrated aqueous NH_3/ dioxane 1:1 at room temperature for 17 hr or at 55 °C for 6 hr (98BP). This approach was modified by substituting dioxane with methanol and varying some conditions for the simultaneous removal of both DNP and Z protecting groups of **(1),** as follows. 60 mL of concentrated aqueous NH_3 (28 %) and 60 mL methanol mixture was added to compound **1** (4.232g, 5.5mmol). The reaction slurry was stirred at about 35 °C for 24 hr, and became a solution, which was then evaporated to dryness. The resulting solid was redissolved in a sufficient quantity of a solvent mixture 90:8:2 $CHCl_3$: MeOH: AcOH and passed through a column containing a 12 cm plug of silica. The same solvent was used as eluent to remove the intense coloration due to residual unreacted DNP. The product **2**, which was more polar and therefore retained on the plug, was obtained by eluting with neat methanol and further purified by column chromatography (silica 200-400 mesh, $CHCl_3$: MeOH (2:1), R_f = 0.52) in 73 % yield. The compound was a yellow solid. ^{1}H NMR

(δ in ppm , D_2O): 8.50 (1H, s imidazole) 7.40 (5H, s, aromatic H of Ph), 7.23 (1H, s, imidazole), 5.09 (2H, s, -OCH_2Ph), 4.37 (1H, m, α-C*H* of His), 4.26 (1H, m, α-C*H* of Lys), 2.99-3.14 (4H, m, overlapping signals β-CH_2 of His and ε-CH_2 of Lys), 1.71 (2H, m, β-CH_2 of Lys), 1.50 (2H, m, δ-CH_2 of Lys) 1.35 (11H, s, overlapping signal of Boc CH_3 and γ-CH_2 of Lys).

c) Preparation of His-Lys ***(3)***

Refer to Figure 4.2. The standard HBr/AcOH procedure (84BB, 76BK, 76P) was used to remove simultaneously the Boc and Bzl protecting groups of compound **2.** Anisole was added as a scavenger of the resulting benzylium ions (76BK). Details are as follows. Compound **2** (~ 0.7 g) was dissolved first in AcOH (8 mL) + anisole (1 mL) and treated with 8 mL of a solution of HBr in AcOH (30%). After overnight stirring with gentle heating at ~ 35 ^{0}C on a magnetic stirrer (with a temperature control), the solution was diluted with ~ 200 mL diethylether and the solid hydrobromide salt was isolated by decantation. The crude product obtained was dissolved in ~ 10 mL of methanol, 1 – 2 spatula charcoal added, and the solution stirred for about 5 min to remove residual color from the sample. The sample was filtered through a cotton plugged glass funnel. The filtrate was rotary evaporated almost to dryness and diluted with about 100 mL $CHCl_3$ to isolate the solid product by decantation. This trituration procedure was repeated by dissolving the sample in just a sufficient amount of methanol and diluted this time with 100 mL diethyl ether. The product was finally rotary evaporated to obtain the off-white dipeptide, His-Lys **3** in 73 % yield. The purity was assessed by HPLC analysis on a C-18 column employing CH_3CN /H_2O gradient elution which showed a single peak. Molecular Mass (g mol^{-1}) for $C_{12}H_{21}N_5O_3$: Calc. 283.3320; found (FAB MS) 283.1653. $[\alpha]^{27} = -2.2^o$. Elemental Analysis based on the formula: $[C_{12}H_{21}N_5O_3]^-[NH_4]^+.3HBr.$ 1/2MeOH Calc. C, 26.85; H, 4.96 ; N, 15.03. Found C, 27.06; H, 4.84; N, 15.16. ^{1}H NMR (δ in ppm , D_2O): 8.72 (1H, d, C-2 *H*, J_{HH} = 1.3 Hz) 7.46 (1H, s, imidazole), 4.36–4.41(2H, m, overlapping signals of α-C*H* of His and α-C*H* of Lys), 3.39-3.50 (2H, m, β-CH_2 of His), 3.01 (2H, t, J_{HH} = 7.6 Hz, ε-CH_2 of Lys), 1.76-1.87 (2H, m, β-CH_2 of Lys), 1.66-1.74 (2H, m, δ-CH_2 of Lys) 1.43-1.51 (2H, m,

γ-CH_2 of Lys). ^{13}C NMR (δ in ppm, D_2O) 178.4 (C=O carboxylate), 170.5 (C=O of amide), 137.0, (methine of the imidazole), 128.1 (quaternary C of imidazole), 121.4 (methine C of imidazole), 56.2 (methine C) and 54.5 (methine C), 41.8 (methylene C), 33.1 (methylene C) , 28.9 (methylene C), 28.7 (methylene C) and 24.6 (methylene C).

4.2.3.2 Syntheses of Thr(Ac)-His-Lys and of Thr-His-Lys

These are outlined in Figure 4.3.

a) Preparation of Boc-Thr(Bzl)-His(DNP)-Lys(Z)-OBzl ***(4)***.

The product **1** (1.453 g, 1.88 mmol) was Boc-deprotected by adding neat TFA (~2 mL) for about 20 min. Argon gas was then passed through the solution to remove excess TFA remaining. The residue was dissolved in 5 mL dichloromethane and ~ 2 mL triethylamine added to render the solution basic.

Coupling of the Boc-Thr(Bzl)-OH (0.465 g, 1.5 mmol) to the Boc deprotected product of **1** was achieved as outlined in Section 4.2.3.1a using EDC (0.34 g, 1.88 mmol) as coupling reagent in conjunction with HOBt (0.2541 g, 1.88 mmol). Pure product was obtained in 94 % yield by the same process as described for the protected dipeptide (Section 4.2.3.1a). Purity was assessed by TLC, using the solvent mixture 90:8:2 $CHCl_3$:MeOH:AcOH as the eluent (R_f = 0.58). HPLC analysis (CH_3CN /H_2O gradient) showed a single peak. Molecular mass (g mol^{-1}) for $C_{49}H_{56}N_8O_{13}$: Calc. 965.0 found (FAB mass spectroscopy) 964.4. Elemental Analysis based on the formula $C_{49}H_{56}N_8O_{13}$.0.3 CH_3COOH: Calc. C, 60.24; H, 5.74; N,11.40. Found C, 60.22; H, 5.26; N, 11.23. ^{1}H NMR (δ in ppm, $CHCl_3$): 8.79 (1H, d, J_{HH} = 2.4 Hz, aromatic H of DNP), 8.47 (1H, dd, J_{HH} = 2.4 and 8.7 Hz, aromatic H of DNP), 8.06 (1H, d, J_{NH}= 7.6 Hz, N*H* of His), 7.57 (1H, d, J_{HH} = 8.7 Hz, aromatic H of DNP), 7.21-7.43 (17H, overlapping signals of N*H* of Lys, 15 aromatic H of Ph and 1H of imidazole), 6.79 (1H, s, imidazole), 5.63 (1H, d, J_{NH} = 6.5 Hz, Boc N*H*), 5.06-5.18 (5H, m, overlapping signals of 2(OCH_2Ph) and Z-Lys N*H*), 4.88 (1H, m, α-C*H* of His), 4.51-4.64 (3H, m, overlapping signal of 1(OCH_2Ph), and α-C*H* of Lys), 4.36 (1H, α-C*H* of Thr),

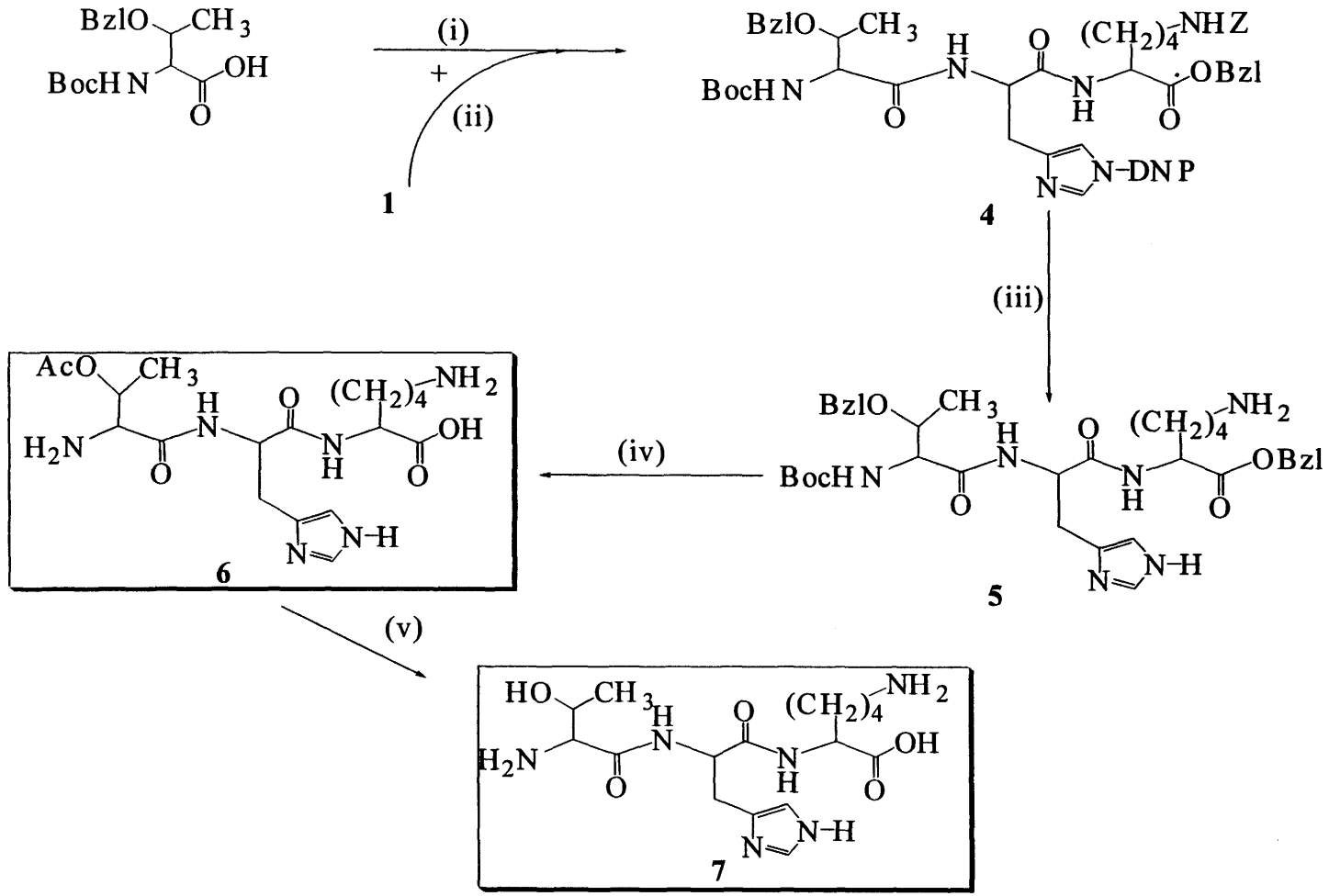

Figure 4.3: Synthetic approach for Thr-His-Lys. (i) HOBt/$CHCl_3$/0°C, EDC (ii) TFA/30min,$CHCl_3$/Et_3N (94 %) (iii) NH_3/MeOH/35°C (73%) (iv) HBr/AcOH (74%) (v) NaOH/35°C/pH ~ 10.5.

4.17 (1H, β-C*H* of Thr), 2.90-3.24 (4H, m, overlapping signals of β-CH_2 of His, and ε-CH_2 of Lys), 1.21-1.75 (18H, m, overlapping signals of β-CH_2 of Lys, 9H of Boc CH_3), δ-CH_2 of Lys, γ-CH_2 of Lys and γ-CH_3 of Thr). ^{13}C NMR (δ in ppm, $CDCl_3$): 171.8, 170.8, 170.3, 156.6, 156.0 (5C=O), 146.8 (quaternary C of DNP), 144.1 (quaternary C of DNP (C-NO_2)), 140.1, 138.3,136.8,135.6, 135.0 (5 ternary aromatic C), 129.3 (methine aromatic C), 128.7-128.1 (overlapping signals of 15 aromatic carbons of Ph and a methine aromatic C), 121.4 (methine aromatic C), 117.7(methine aromatic C), 80.3 (ternary C of Boc), 75.2 (ternary C of Thr), 71.5, 67.0, 66.6 (3 methylene C of OCH_2Ph), 58.2 (methine C), 52.8 (methine C) and 52.3 (methine C), 40.7 (methylene C), 31.7 (methylene C), 29.5 (methylene C), 29.2 (methylene C), 28.4 (3CH_3 of Boc) and 22.4 (methylene C) and 15.8 (CH_3 of Thr).

b) Preparation of Boc-Thr(Bzl)-His-Lys-OBzl ***(5).***

See Figure 4.3. Simultaneous removal of the DNP and Z protecting groups of **4** was accomplished as described above (Section 4.2.3.1) to obtain the solid **5**. The compound was purified by column chromatography (R_f = 0.68, $CHCl_3$: MeOH, 2:1) to obtain a yield of 73 %. ^{1}H NMR (δ in ppm, $CDCl_3$): 8.63 (1H, N*H*), 7.52 (1H, s, imidazole C*H*), 7.29-7.41 (overlapping signals of 10H aromatic H of Ph), 6.91 (2H, overlapping signals NH of Lys and imidazole CH), 6.62(1H, imidazole NH), 6.06 (1H, Boc NH), 5.68(1H, C^{α} H of Thr), 5.13 (2H, 2(OCH_2Ph), 4.48(1H, α-CH of His), 4.27-4.265 (3H, m, overlapping signals of 2H, OCH_2Ph and 1H, m, α-C*H* of Lys), 4.06 (1H, β-C*H* of Thr), 2.92-3.34 (4H, overlapping signals of, β-CH_2 of His & ε-CH_2 of Lys), 1.38 (9H, s, Boc CH_3s), and 1.29 (3H: γ-C*H*s of Thr). The ^{1}H-NMR data was assumed as convincing enough to establish the formation of this intermediate **5** and hence no further analysis was performed on the product before proceeding to the next stage in the synthesis as described in Section 4.2.3.2c below.

c) Preparation of Thr(Ac)-His-Lys ***(6)***

See Figure 4.3. The Boc and the two Bzl protecting groups of compound **5** (0.6 g dissolved in ~ 16 mL AcOH and 2 mL anisole) were removed by treatment with ~ 18 mL of 30 % HBr in AcOH solution. During the treatment, an acetyl group was

introduced to the Thr side chain to give compound **6** in 74 % yield. The purification of the compound was the same as described earlier (Section 4.2.3.1c). HPLC analysis (CH_3CN /H_2O gradient) showed a single peak. Molecular mass (g mol^{-1}) for $C_{18}H_{30}N_6O_6$: Calc. 426.4740; found (FAB mass spectroscopy) 426.2476. $[\alpha]^{29} = -2.5^{o}$. Elemental Analysis based on the formula: $[C_{16}H_{27}N_6O_5]^-[NH_4]^+.3HBr.MeOH$ Calc. C, 31.77; H, 5.19; N, 13.65. Found C, 31.81; H, 4.98; N, 13.67. ^{1}H NMR (δ in ppm, D_2O): 8.64 (1H, d, J_{HH} = 1.2 Hz, imidazole,) 7.33 (1H, s , imidazole), 5.36 (1H, doublet of quartet, J_{HH} = 2.3, J_{HH} = 6.6 Hz, β-C*H* of Thr), 4.75 (1H, α-C*H* of Thr overlapping with residual H_2O signal), 4.22-4.30 (2H, m, overlapping signals of α-C*H* of His and α-C*H* of Lys), 3.35-3.23 (2H, m, β-CH_2 of His), 3.00 (2H, t, ε-CH_2 of Lys, J_{HH} = 7.3 Hz), 1.86-1.64 (4H, m, overlapping signals of β-CH_2 of Lys and δ-CH_2 of Lys), 1.51-1.37 (5H, m, overlapping signals of γ-CH_2 of Lys and 3H, d, J_{HH} = 6.6 Hz, γ-CH_3 of Thr). ^{13}C NMR (δ in ppm, D_2O): 177.2, 173.4, 171.8, 168.8 (4C=O), 134.8, (tertiary C imidazole), 128.9 (methane C of the imidazole), 118.7 (methine C imidazole), 70.0, 57.3, 54.8, 53.7 (4 methine C), 40.4, 31.6, 27.7, 27.5, 23.3 (5 methylene C), 18.1(*C*H_3 of -OCO*C*H_3), 7.2(γ-CH_3 of Thr).

b) Preparation of Thr-His-Lys (7)

See Figure 4.3. The acetyl group introduced in (c) above was removed by adding 0.1 **M** NaOH to compound **6** (~0.2 g) dissolved in MeOH (2.5 mL) to adjust the pH to about 10.5, and stirring. The reaction was allowed to proceed overnight. The crude product was purified by column chromatography (R_f = 0.14, MeOH: $CHCl_3$: 8 % NH_3, 51:34:15). The isolated product was rotary evaporated almost to dryness, leaving about 1 mL of the solution. About 1 mL of concentrated HCl was added to the solution, to obtain the hydrochloride form of the peptide, and the solution evaporated to dryness. The solid obtained was dissolved in a small amount (~ 1mL) of MeOH and filtered through a cotton plugged Pasteur pipette. The filtrate was then triturated with $CHCl_3$ and then with diethyl ether. Molecular mass (g mol^{-1}) for $C_{16}H_{28}N_6O_5$: Calc. 384.4370; found (FAB MS) 384.22193. ^{1}H NMR (δ in ppm, D_2O): 8.65 (1H, d, J_{HH} = 1.2 Hz, imidazole), 7.37 (1H, s, imidazole), 4.77- 4.87 (overlapping signals of the residual H_2O

and 1H from α-C*H* of His), 4.32-4.37 (1H, m, α- C*H* of Lys), 4.14- 4.18 (1H, m, β-C*H* of Thr), 3.94 (1H, d, J_{HH} = 6.0 Hz, α-C*H* of Thr), 3.25-3.30 (2H, m, β-CH_2 of His), 3.00 (2H, t, ε-CH_2 of Lys, J_{HH} = 7.5 Hz), 1.68-1.89 (4H, m, overlapping signals of β-CH_2 of Lys and δ-CH_2 of Lys), 1.41-1.49 (5H, m, γ-CH_2 of Lys) and 1.31 (3H, d, J_{HH} = 6.4 Hz, γ-CH_3 of Thr). ^{13}C NMR (δ in ppm, D_2O) 180.8, 173.9, 173.4, (3C=O), 137.9, (tertiary C imidazole), 133.3 (methine C of imidazole), 120.2 (methine C imidazole), 69.9, 61.6, 57.6, 56.0 (4 methine C), 41.8, 33.5, 30.5, 28.7, 27.8 (5 methylene C), 21.1 (γ -CH_3 of Thr).

4.2.3.3 Synthesis of Asp-Thr(Ac)-His-Lys.

This is outlined in Figure 4.4. Procedures for the peptide synthesis were the same to those described in Section 4.2.3.2 for the synthesis of Thr(Ac)-His-Lys.

a) Preparation of Z-Asp-Thr(Bzl)-His(DNP)-Lys(Z)-OBzl ***(8)***

After Boc-deprotection of **4** with TFA, it was coupled to Z-Asp(OBzl)-OH with HOBt/EDC. Pure product **8** was obtained in 82 % yield.

The purity was assessed by TLC, using the solvent mixture 90:8:2 $CHCl_3$:MeOH:AcOH as the eluent (R_f = 0.58). HPLC analysis (CH_3CN/H_2O gradient) showed a single peak. Molecular mass (g mol^{-1}) for $C_{49}H_{56}N_8O_{13}$: Calc. 1204.24 found (FAB MS) 1204.46. ^{1}H NMR (δ in ppm, $CHCl_3$): 8.78 (1H, d, d J_{HH} = 1.8 Hz, 10.6 Hz, aromatic H of DNP), 8.43-8.50 (1H, m), aromatic H of DNP), 8.26 (1H, d, J_{NH} = 7.4 Hz, N*H* of His), 8.16 (1H, d, J_{NH} = 8.5 Hz, N*H* of Asp) 7.57(1H, d, J_{HH} = 8.8 Hz, aromatic H of DNP), 7.19-7.47 (26H, 25 aromatic H of Ph and 1H imidazole), 6.77 (1H, s, imidazole), 6.57 (1H, d, J_{NH} = 6.5 Hz, N*H* of Thr), 5.92 (1H, d, J_{NH}= 8.7 Hz, N*H* of Lys), 5.03-5.19 (9H, m, overlapping signals of 4(OCH_2Ph) and 1H, Z-Lys NH), 4.86 (2H, m, α-C*H* of His and α-C*H* of Asp), 4.43-4.63 (4H, m, overlapping signal of 1(OCH_2Ph), α-C*H* of Lys, α-C*H* of Thr), 4.27 (1H, β-C*H* of Thr), 2.92-3.24 (6H, m, overlapping signals of β-CH_2 of His, β-CH_2 of Asp and εCH_2 of Lys), 1.57-1.62

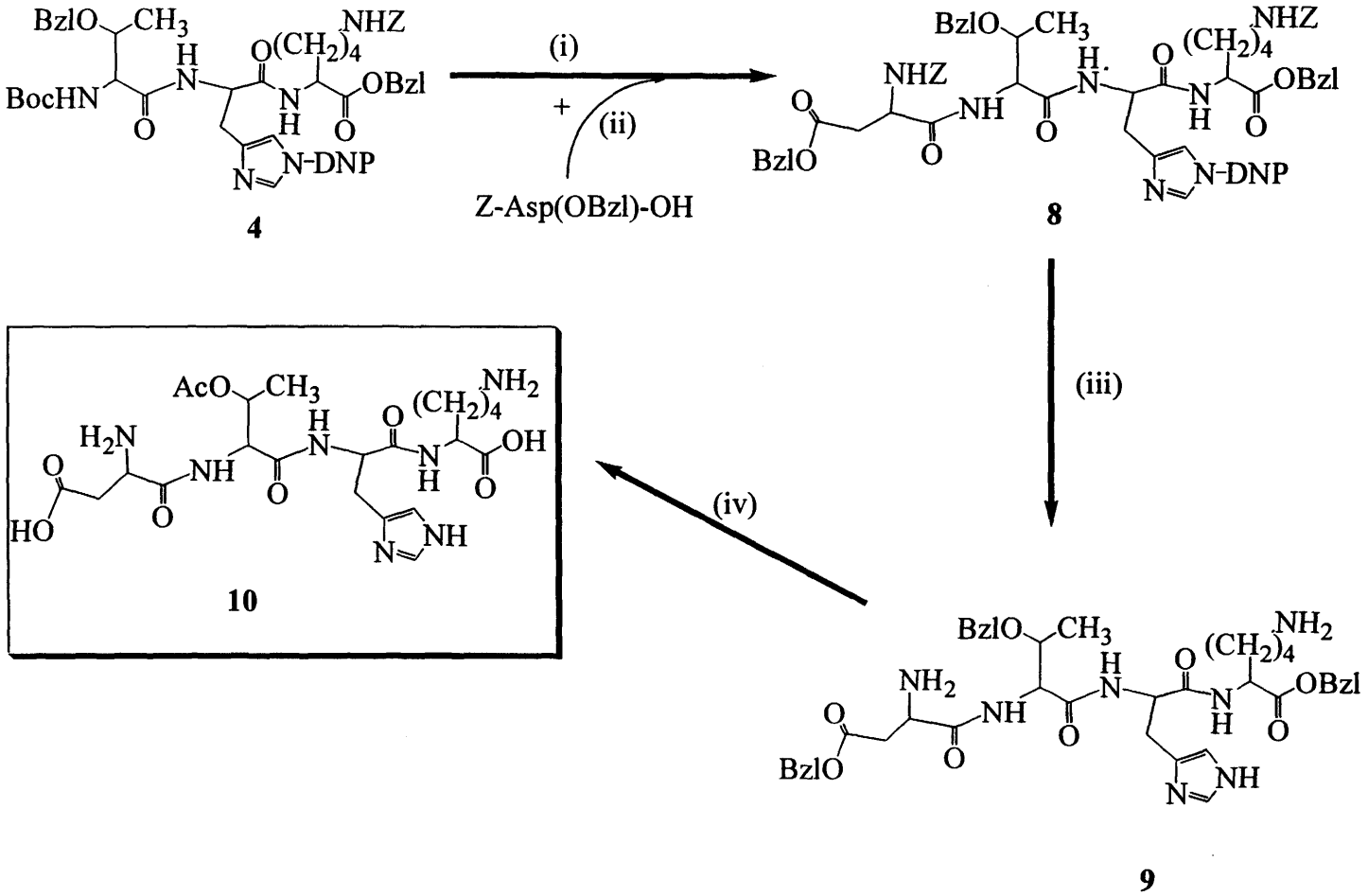

Figure 4.4: Synthetic approach for Thr-His-Lys. (i) TFA/30min,$CHCl_3/Et_3N$ (ii) HOBt/$CHCl_3$/0°C, EDC (82 %) (iii) NH_3/MeOH/35 °C (51%) (iv) HBr/AcOH (60%).

(2H, m, β-CH_2 of Lys), 1.34-1.37 (2H, m, γ-CH_2 of Lys), 1.09-1.27(5H, m, overlapping signals of δ-CH_2 of Lys and γ-CH_3 of Thr). ^{13}C NMR (δ in ppm, $CDCl_3$): 171.9, 171.8, 171.1, 170.8, 169.8, 156.6, 156.3 (7C=O), 146.7 (quaternary C of DNP), 143.9 (quaternary C of DNP (C-NO_2)), 140.4, 138.4,136.9,136.1, 135.7, 135.4, 135.2 (7 ternary aromatic C), 128.7-127.6 (overlapping signals of 27 methine aromatic carbons), 121.6 (methine aromatic C), 117.8(methine aromatic C), 117.6(methine aromatic C), 74.4 (methine β-C of Thr), 74.0 (methine C), 71.5, 67.7, 67.3, 67.1, 66.6 (5 methylene C of O*C*H_2Ph), 52.9 (methine C), 52.4 (methine C) and 51.6 (methine C), 40.9 (methylene C), 36.2 (methylene C), 31.7 (methylene C) , 29.3 (methylene C), 28.7 (methylene C), and 22.6 (methylene C) and 16.6 (CH_3 of Thr).

b) Preparation of Asp-Thr(Ac)-His-Lys ***(10)***

See Figure 4.4. Simultaneous removal of the DNP and Z protecting groups of **8** was accomplished as described earlier (Section 4.2.3.2b) to obtain the solid **9**. The compound was purified by column chromatography (R_f = 0.6, $CHCl_3$: MeOH, 2:1); final yield was 51%. The three Bzl protecting groups of compound **9** were removed by HBr/AcOH treatment. During the treatment, an acetyl-protecting group was introduced to the Thr side chain to give compound **10.** The purification of the compound was the same as described earlier (Section 4.2.3.2c). The final yield was 60%. HPLC analysis (CH_3CN /H_2O gradient) showed a single peak. Molecular mass (g mol^{-1}) for $C_{22}H_{35}N_7O_9$: Calc. 541.56; found (FAB MS) 541.29. Elemental Analysis based on the formula: $[C_{22}H_{41}N_8O_9Br_3]$.1/3 CH_3OH.2/5 CH_3OOH. (The CH_3 signals of CH_3OH and CH_3OOH were both observed in the ^{1}H-NMR spectrum in D_2O and H_2O and their actual values determined by spreadsheet calculations.) Calc. C, 33.23; H, 5.29; N, 13.42. Found C, 33.31; H, 5.15; N, 13.82. ^{1}H NMR (δ in ppm, D_2O): 8.62 (1H, d, J_{HH} = 1.2 Hz, imidazole), 7.28 (1H, s, imidazole), 5.30 (1H, doublet of quartet, J_{HH} = 3.5 Hz, J_{HH} = 6.5 Hz, β-C*H* of Thr), 4.68-7.73 (1H, α-C*H* of Asp and α-C*H* of His overlapping with residual H_2O signal), 4.48 (1H, d, J_{HH} = 3.5 Hz, α-C*H* of Thr), 4.28 (1H, dd, J_{HH} = 2.5 Hz, J_{HH} = 6.0 Hz, α-C*H* of Lys), 3.32-3.09 (4H, m, overlapping signals of β- CH_2 of His and Asp), 2.99 (2H, t, ε-CH_2 of Lys, J_{HH} = 7.6 Hz), 2.03 (3H, s,

CH_3C=O(Thr)), 1.88-1.63 (4H, m, overlapping signals of β-CH_2 of Lys and δ-CH_2 of Lys), 1.49-1.34 (2H, m, γ-CH_2 of Lys), 1.26 (3H, d, J_{HH}= 6.5 Hz, γ-CH_3 of Thr). The amide NH, aromatic NH, and the ammonium protons were detected in water as follows: ^{1}H NMR (δ in ppm, in H_2O) 8.75 (1H, d, J_{NH} = 7.7 Hz, NH of Lys,) 8.42 (1H, d, J_{NH} = 7.6 Hz, His NH), 8.37 (1H, d, J_{NH} = 6.5 Hz, NH of Thr), 7.69 (1H, bs, N1- (Im)), 7.54 (ε-NH_3^+ of Lys) and 7.13 (1H, N3-H(Im)). ^{13}C NMR (δ in ppm, D_2O): 178.8, 177.3, 175.4, 173.8, 173.7 (5C=O), 136.1, (tertiary C of Im), 130.9 (methine C of Im), 119.8 (methine C of Im), 72.7, 59.6, 56.0, 54.8 (4 methine C), 2(41.7), 33.0, 2(28.8), 24.7(6 methylene C), 23.0(CH_3 of -OCOCH_3), 19.0(γ-CH_3 of Thr).

4.3 RESULTS AND DISCUSSION

4.3.1 The Synthesis of Histidine-containing Peptides

All the peptides prepared contain the His residue and therefore the imidazole ring. As discussed in Section 4.1.2.4, this must be protected during coupling. Amongst the commonly used protecting groups for the imidazole ring (Section 4.1.2), DNP was chosen for these studies, as this is stable enough under the conditions used for the conventional coupling with carbodiimide of amino acids or peptides in the presence of HOBt. Initially, three reagents for DNP removal were tried: thiophenol (98BP, 70SF), TBAF (98BP), and ammonia (98BP, 93PC). All 3 reagents could remove the DNP group to a significant extent (monitoring by TLC). However, a cleaner product (after purification by column chromatography) was obtained for the ammonia treatment. All three products contained intense residual colors, purple for TBAF treatment and yellow for both thiophenol and ammonia treatment. However, due to increased polarity of the products after the DNP-deprotection, causing the retardation of the desired product on the silica column, the residual color was largely washed out after passage through the column.

The ammonia treatment used in this study had the additional advantage of cleaving the Z groups simultaneously with the DNP. Initial attempts to remove the Bzl

protecting group from the side chain –OH of Thr by hydrogenation, even at moderate pressures (60 psi, 2 days, Pd/C catalyst, MeOH as solvent), were unsuccessful. It has been reported previously that the presence of amine functions inhibits O-benzyl group hydrogenolysis (84CB). The use of HBr/AcOH removed the benzyl protection but, as expected, introduced an acetyl group to the Thr side chain. This could be removed by base hydrolysis, but the yield was poor. This approach is therefore not recommended for large-scale synthesis of His-Lys.

The order of removing the protecting groups proved very important in obtaining the desired products. Initial attempts to deprotect the Z groups of the dipeptide and tripeptide first by hydrogenolysis, followed by the removal of DNP were not on the whole successful. Although hydrogenation was successful, subsequent DNP removal gave numerous products as observed when monitored by TLC and eluted with the solvent system MeOH/$CHCl_3$/8% NH_3 (51:34:15). None of these was the desired product, as observed from the NMR spectra. However, when the DNP group of the dipeptide was removed first, followed by either hydrogenolysis or HBr/AcOH treatment, the desired product was obtained as the major product in each case. The latter led to the complete deprotection of the peptide at that stage, whereas the former required further treatment to remove the Boc group too. Hence in this study, the order adopted for removing the protecting groups of all the peptides was as follows; DNP, Z, Bzl and lastly the Boc group. It was apparent that the key step in obtaining purer products of higher yields was the complete removal of the DNP and the cleaning of this product. TLC could easily monitor the removal of the DNP.

Coupling of the protected amino acids yielded the desired protected dipeptides, tripeptide and tripeptide in high yields; 95, 94 and 82 % respectively (Figures 4.2, 4.3 and 4.4). The purification procedures outlined in Section 4.2.3 were rigorously used to obtain a single HPLC peak for each of the peptide in its fully protected stage, as well as the final stage of the synthesis (see Table 4.1 for their retention times, t_r).

Table 4.1: The retention time (t_r) of His-containing peptides recorded on HPLC

Sample label	Compound	t_r (min)	Solvent
1	Boc-His(DNP)-Lys(Z)-OBzl	36.20	CH_3CN
3	His-Lys	1.94	H_2O
4	Boc-Thr(Bzl)-His(DNP)-Lys(Z)-OBzl	38.43	CH_3CN
6	Thr(Ac)-His-Lys	1.68	H_2O
8	Z-Asp(Bzl)-Thr(Bzl)-His(DNP)-Lys(Z)-OBzl	36.25	CH_3CN
10	Asp-Thr(Ac)-His-Lys	1.62	H_2O

Full ^1H and ^{13}C NMR assignments for these peptides are provided in the experimental section. ^1H COSY spectra were very useful in providing unequivocal assignments for the ^1H NMR spectra of the peptides, especially for the tetrapeptide **8** and the tripeptide **4**. The latter is shown by way of example in Figure 4.5. The COSY plot shows a weak scalar coupling of proton marked 1 with the proton 2 (designated by an arrow in Figure 4.5). This is consistent with the assignment of peak 1(δ = 8.79, 1H, d, J = 2.4 Hz) and peak 2 (δ = 8.47, 1H, dd, J = 2.4 and 8.7 Hz) of the 1-D ^1H NMR to the aromatic protons of DNP, as marked accordingly in the structure shown in Figure 4.5. Peak 1, which is between the two electron withdrawing nitro groups of DNP, absorbs at a lower field, and the weak coupling observed in the COSY spectrum is marked by the small coupling constant (J = 2.4 Hz) observed in both peaks.

The plot also shows a stronger scalar coupling of peak 2 with peak 3 (marked a). This confirms the assignment of peak 3 (δ = 7.57, 1H, d, J = 8.7 Hz) to the other CH proton of DNP (marked accordingly as 3 in the structure). This stronger coupling has the same J value of 8.7 Hz for both peaks 2 and 3. Proton 2 therefore couples with both 1 and 3; the larger J coupling between 2 and 3 signifies the proximity of the proton 2 to that of 3 as compared to the proton 1. No scalar coupling was observed between peaks 4 and 5, which is consistent with the 1-D spectrum, where these peaks were observed each as a singlet. These two peaks were assigned to the imidazole CH protons.

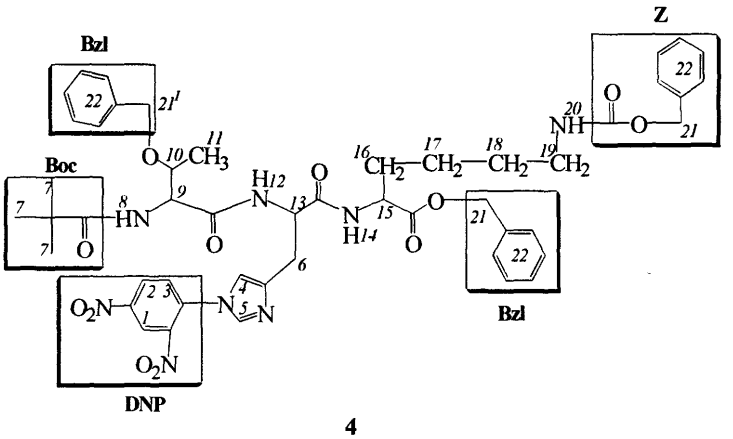

4

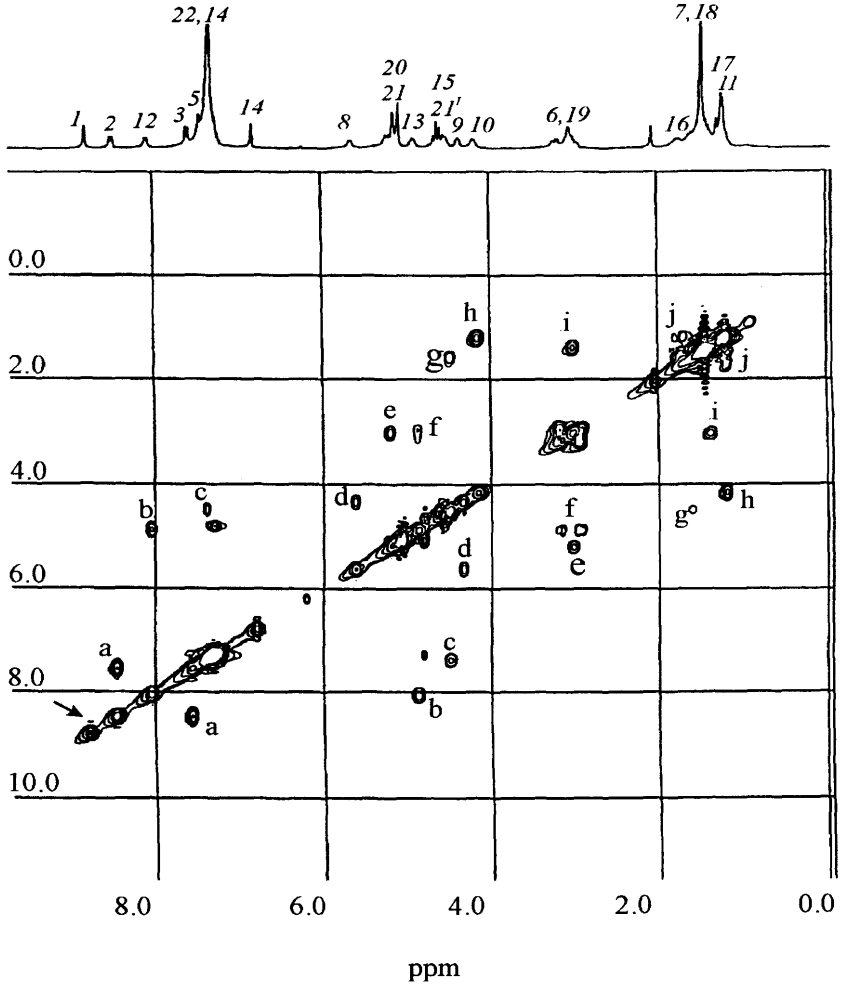

Figure 4.5: Structure and ^{1}H COSY spectrum of Boc-Thr(Bzl)-His(DNP)-Lys(Z)-OBzl **(4)** See text for experimental details and analysis.

The assignment was mainly based on the consistency observed between the starting materials Boc-His(DNP)-OH (see Section 4.2.3.1), Boc-His(DNP)-Lys(Z)-OBzl **(1)** (Section 4.2.3.2) and the compound 4. The ^{1}H-NMR of the commercially available Boc-His(DNP)-OH shows two singlets at 7.87 and 6.88 ppm assignable to the two imidazole CH protons. The one at the lower field can be assigned to the imidazole CH sandwiched between the two-nitro groups on the imidazole. These protons were also observed as singlet peaks in the ^{1}H-NMR ($CDCl_3$) for Boc-His(DNP)-Lys(Z)-OBzl **(1)** at δ = 7.55 ppm and 6.83 ppm and assigned respectively to the same protons. These peaks were also observed at δ = 7.43 ppm and 6.79 ppm for the compound **4** (Figure 4.5) and therefore assigned accordingly to the two imidazole CH protons. Peak 6, assigned to the β-CH_2 of His, couples accordingly with the CH proton 13 (marked f). The Boc CH_3 protons (peak 7) are well known to absorb around 1.44 ppm (Section 4.2.3.2a). Peak 8, assigned to Boc NH, accordingly couples with peak 9 (i.e. α-CH of Thr). The expected coupling between peak 9 and peak 10 (β-CH of Thr), though not very distinct due to the complexity of the spectrum (Figure 4.5), is still discernable. The assignment of 10 to β-CH of Thr is confirmed by its coupling with γ-CH_3 of Thr, peak 11 (marked h). Peak 12, assigned to His-NH, couples, as expected, with His α-CH (peak 13) (marked b). Peak 13, as discussed earlier, couples also with peak 6 (i.e His α-CH_2). The scalar coupling marked c indicates a coupling between the only remaining unassigned CH, i.e Lys α-CH (peak 15) and presumably Lys-NH 'buried" under the aromatic peaks at δ = 7.21 – 7.43 ppm (see Section 4.2.3.2a). This assignment is confirmed by the scalar coupling of peak 15 with 16 (i.e. Lys β-CH_2), marked g. The expected scalar couplings between Lys β-CH_2 (peak 16) and Lys γ-CH_2 (peak 17), between Lys γ-CH_2 and Lys δ-CH_2 (peak 18) and between Lys δ-CH_2 and Lys ε-CH_2 (peak 19) are marked respectively as j, k, and l. Accordingly, there was a scalar coupling between peak 19 and 20 (i.e. ε-NH of Lys). This proton overlapped with the OCH_2Ph peaks at δ = 5.06 - 5.18 ppm.

The ^{13}C/^{1}H J-modulated NMR spectra were also very helpful in assigning the ^{13}C NMR spectra. Figures 4.6 shows the ^{13}C/^{1}H J-modulated NMR spectra

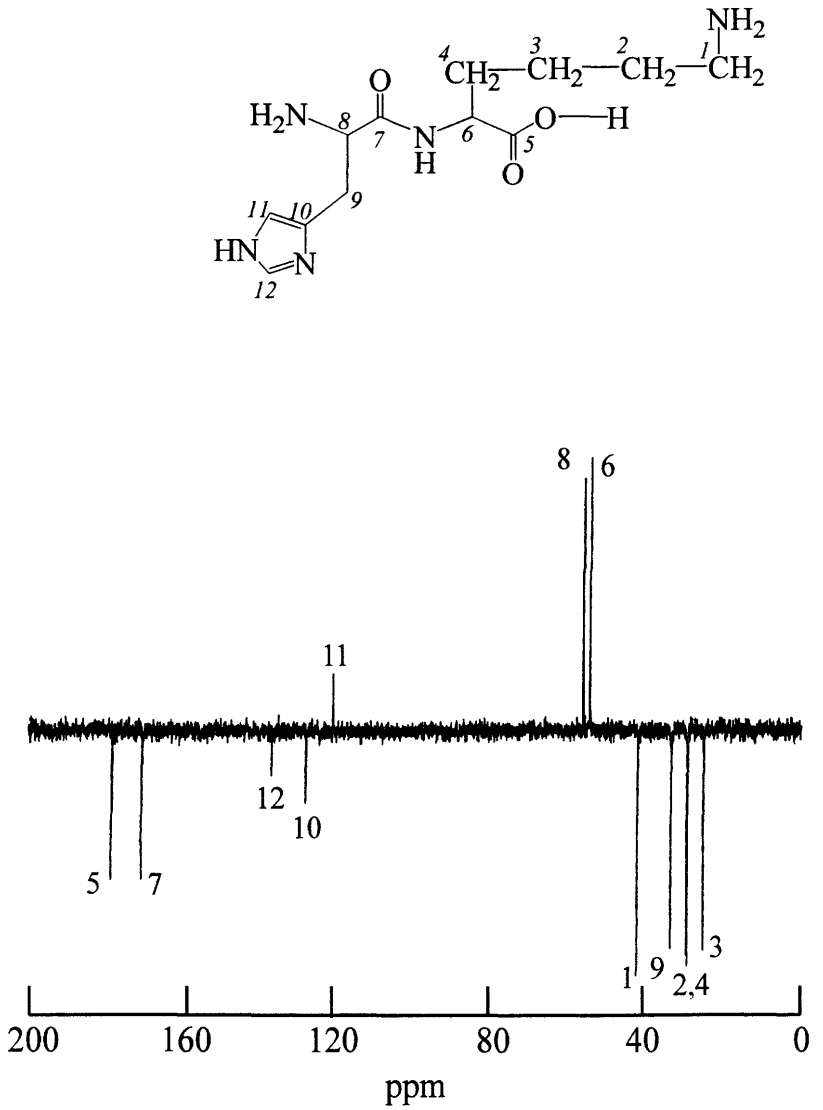

Figure 4.6: Structures and $^{13}C/^{1}H$ J-modulated spectra of His-Lys **(3)**. Spin echo delay time = 0.007 sec. See text for experimental details and analysis.

obtained for His-Lys (**3**) in D_2O at a spin echo delay time of 0.007 secs. The J-modulated spectra show all methylene (CH_2) and quaternary (C) carbons pointing downwards and the methine (CH) and methyl (CH_3) carbons upwards. The spectrum for His-Lys (**3**) shows two quaternary C in the range 160 – 180 ppm signifying the two (C=O) groups. Since the carbon labeled 5 (178.4 ppm) is the C=O of a carboxylic acid, it would be expected to absorb at a lower field (170.5 ppm) than the carbon labeled 7 (i.e. amide C=O). Two methine carbons of **3** were observed at 56.2 ppm and 54.5 ppm (pointing upwards). These were assigned respectively to CH of His (peak 8) and CH of

Lys (peak 6) respectively. The CH of His being under the influence of the (C=O), NH_2, and that of the imidazole group will absorb more downfield than the CH of Lys. The five methylene carbons as expected, all pointed downwards. The specific assignments of the methylene carbons shown in Figure 4.6 were based on the impact of electron withdrawing groups on these carbons. Stronger electron withdrawing groups cause a carbon to be more deshielded, hence absorbing at lower field. The ε-CH_2 (peak 1), for instance, being directly attached to the ε-NH_2 of Lys, is more downfield (δ = 41.8 ppm) than the other methylene carbons. The γ-CH_2 of Lys is at a higher field (δ = 24.6 ppm) than the other methylene protons, since it is more remote from any of the electron withdrawing groups. The β-CH_2 of His attached directly to the imidazole ring is at a higher field (δ = 33.1 ppm) then both β-CH_2 of Lys and δ-CH_2 of Lys, which is in almost the same chemical environment.

The $^{13}C/^{1}H$ J-modulated NMR spectrum of Thr(Ac)-His-Lys (Figure 4.7) showed all the carbon peaks identical to those of His-Lys, and other series absent in His-Lys. Hence, two additional C=O groups are observed pointing downwards. Two additional methine carbons are observed pointing upwards and lastly two methyl groups pointing upwards.

The structure of the imidazole group in **3** suggests the presence of two methine carbons and 1 quaternary carbon and therefore the $^{13}C/^{1}H$ J-modulated NMR spectrum is expected to show two peaks pointing upwards and one downwards. This was not the case for the spectra of both His-Lys (shown in Figures 4.6) and Thr(Ac)-His-Lys (not shown) at the usual spin echo delay time of 0.007 sec. Rather, two peaks pointed downwards ($\delta \sim$ 137 ppm and $\delta \sim$128 ppm) and only one pointed upwards ($\delta \sim$ 121 ppm). Further investigation, by running a non-^{1}H-decoupled ^{13}C- NMR spectrum on the Thr(Ac)-His-Lys sample, showed the peak at $\delta \sim$ 137 ppm (peak 12) as a doublet (d) with a high coupling constant (J_{CH} = 167.3 Hz). Subsequently, by reducing the spin echo delay time to 0.0059 sec the expected $^{13}C/^{1}H$ J-modulated NMR spectrum (Figure 4.7) which is consistent with the structure **6** was obtained.

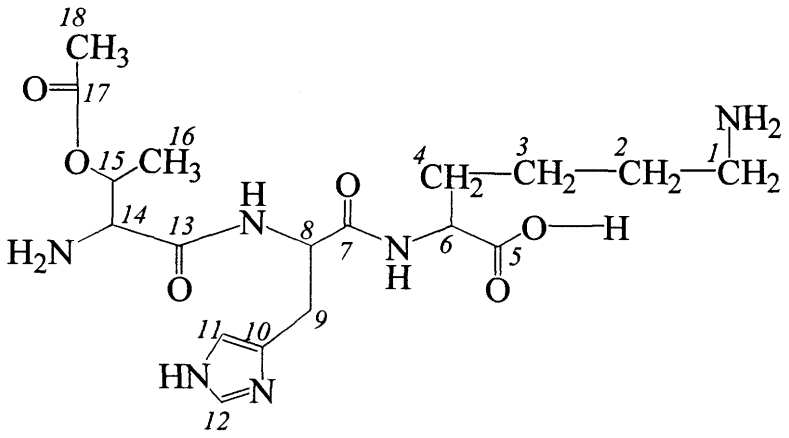

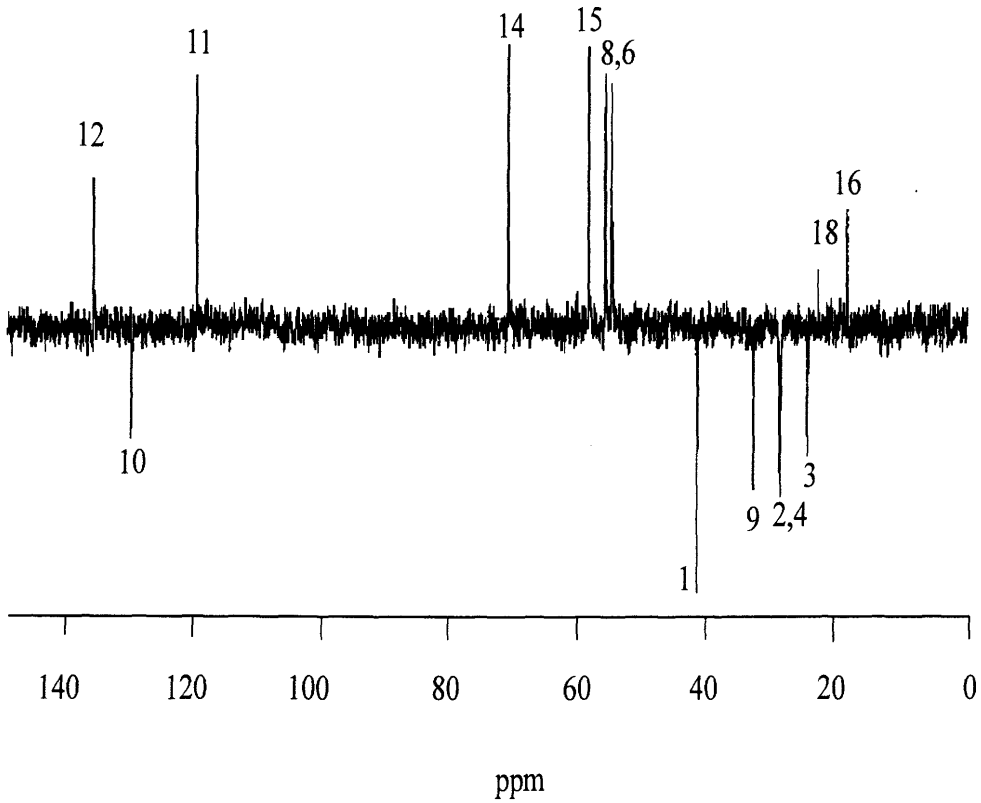

Figure 4.7: Structures and $^{13}C/^{1}H$ J-modulated spectra of Thr(Ac)-His-Lys **(6)**. Spin echo delay time = 0.0059 sec. See text for experimental details and analysis.

Agreements between calculated and found molecular masses by Mass Spectrocopy (FAB) and between calculated and found elemental analyses (C, H, and N) were good, after incorporation in some cases of methanol or acetic acid into the molecular formula. (These substances could be clearly seen in the NMR spectra in such cases.) Removal of acetic acid from **4**, **8**, and **10** proved difficult even after vacuum drying for a prolonged period. The level of acetic acid was confirmed by modeling on Microsoft Excel spreadsheet®. By using the goal seek functions of the program the number of moles of acetic, given initially an arbitrary value in the molecular formula of the compound, was varied to fit the calculated C, H, and N values to the corresponding experimental values. The principle for the fitting is the same as described in Section 2.3.3.

5. PROTON AND COPPER(II) COMPLEXATION STUDIES OF HISTIDINE-CONTAINING PEPTIDES IN AQUEOUS SOLUTION

5.1 INTRODUCTION

As has been discussed in Section 1.7, differences in the N-terminal of various serum albumins affect their ability to bind Cu(II). The N-termini of various serum albumins can either bind strongly to Cu(II), (Bovine serum albumin, BSA, Human Serum Albumin, HSA and Rat Serum Albumin, RSA whose amino acid sequence are respectively Asp-Thr-His-Lys, Asp-Ala-His-Lys, and Glu-Ala-His-Lys) or have little or no ability to bind Cu(II) (Canine Serum Albumin, CSA and Pig Serum Albumin, PSA whose amino acid sequence are respectively Glu-Ala-Tyr-Lys and Asp-Thr-Tyr-Lys). The difference in affinity of the N-termini of these two sets of serum albumins for Cu(II) is attributed to a conserved His at the third position from the α-amino terminal (i.e. (His-3) in BSA, HSA and RSA effecting strong binding to Cu(II). Unlike these serum albumins, CSA and PSA have a tyrosine residue in the third position in place of the His residue (84MR, 87WM). These serum albumins therefore lose their potential to bind Cu(II) as strongly as the His-3 containing albumins (96AC).

Early reports concerning the binding of Cu(II) to BSA or to peptide models (Sections 1.7 and 1.8) also suggested the involvement of the α-amino nitrogen atom of Asp, the two intervening peptide bond nitrogen atoms of Asp-Thr-His and the imidazole nitrogen atom (N-3) which is on the His-3 (67PB, 67SB, 68BS). A square planar BSA-Cu(II) complex was proposed (67SB). Similarly, early reports on studies to investigate the binding of Cu(II) to HSA and its peptide models led to the same hypothesized coordination mode as suggested for BSA (68SW, 71LK, 71AS, 78KL).

See Section 1.7 for details. The techniques used in these old studies were predominantly potentiometry, and visible and optical rotatory dispersion spectroscopy.

However, some later studies with HSA peptide models have pointed also to the involvement of the O of the Asp β-carboxylate side chain, in addition to the four nitrogen atoms above (80LS, 84MR), giving a penta-coordinated structure involving the four N atoms in a square planar coordination to Cu(II) and an axial coordination from the β-carboxylate O of Asp. The techniques used in these studies were 1–D ^{1}H and ^{13}C NMR spectroscopy. As discussed in Section 1.11.2, NMR spectroscopy provides more information on structures of the complexes as well as binding sites than potentiometry and visible spectroscopy, which were used in the older studies above.

A more recent study on the binding of Cu(II) to both HSA and BSA, using both one-dimensional and two-dimensional ^{1}H NMR also led to proposed square planar coordination with ligands of α-NH_2 of Asp-1, the two deprotonated NHs of Ala-2 (HSA) or Thr-2 (BSA) and His-3 and the imidazole of His-3 (94ST). In addition, results suggested a conformation where the Lys side chain lies over the His ring in the albumin-Cu complexes in both cases, but did not indicate the involvement of the β-carboxylate group in the coordination. Recent studies of Cu(II) binding to BSA peptide models, as performed in the case of HSA, are absent from the literature, and thus the issue as to whether or not the β- carboxylate group is also involved in BSA coordination to Cu(II) is still a matter of conjecture.

Understanding the role played by BSA in the transport of Cu(II) in blood requires detailed solution chemistry studies of the structures and the stabilities of the complexes formed in solution. The use of small model peptides has proven valuable in elucidating structural features that contribute to the formation of such metallo-complexes. These models have the advantage of being easier to study than the real species, but should be selected with care to enable reasonable extrapolation of the results to the real protein. Both the structure and the function of the protein should be jointly considered in the selection of such protein models (See Section 1.8.1 for details).

A good BSA model peptide for Cu(II) complexation should mimic the N-terminal amino acid sequence. Cu(II) complexation studies to BSA peptide models in the literature, as started above, are old. Furthermore, the peptic digests of BSA which were used in these old studies do not lend themselves to thorough scrutiny of the role of each amino acid in the BSA-Cu(II) complexation. Small peptide models involving the conserved His-Lys sequence would be good models for BSA considering the well established unique role of His in BSA complexation to Cu(II) and the suggested membrane binding role associated with Lys in promoting the biological activity of Cu complexes of His-Lys containing peptides (see Section 1.9).

Although some compilations of acid dissociation constants (K_a's) and Cu(II) complex stability constants (K_f's) for different His-containing peptides, including His-Lys-containing peptides, have been published (see Sections 1.8 and 1.10 for some references), results from different authors often disagree, and the conditions used may not lend themselves to meaningful biological application.

For instance, Lau and Sarkar (81LS) and May et al. (83MW) have both studied and reported the complexation of Gly-His-Lys to Cu(II). However the identity and the number of species and the measured formation constants determined in these two studies differ significantly from each other, as shown in Table 5.1.

Lau and Sarkar's study was based mostly on a potentiometric approach, complemented by spectrophotometric and equilibrium dialysis methods. May et al. also used the potentiometric method for their study. Differences in the results of the two studies have been attributed by May et al. to the use of more dilute experimental solutions in the case of Lau and Sarkar, despite the difference in temperature between these two studies (37°C versus 25°C). Error propagation analysis by May et al. suggests that potentiometric determinations using concentrations less than about 1 m**M** are prone to be unreliable. It has already been noted that potentiometric methods do not provide as much information as NMR spectroscopy (see Section 1.11.2 for details). NMR has commonly been used for the determination of complex structures when the metal ion is

Table 5.1: Comparison of formation constant data for Gly-His-Lys as obtained by Lau and Sarkar (81LS, 25°C, I = 0.15 **M** [NaCl]) and by May et al. (83MW, 37° C, I = 0.15 **M** [NaCl]). $\beta_{pqr} = [MpL_qH_r]/[M]^p[L]^q[H]^r$ (L = Gly-His-Lys, M= Cu(II)).

p	q	r	log β (81LS)	log β (83MW)
0	1	1	10.44	10.09
0	1	2	18.37	17.47
0	1	3	24.90	23.25
0	1	4	27.81	27.05
0	1	5	[a]-	29.02
1	1	0	16.44	14.83
1	1	-1	7.48	5.87
1	1	-2	-3.74	-4.50
2	1	-1	-	13.95
1	2	2	38.18	34.76
1	2	1	30.83	27.38
1	2	0	21.43	-
1	2	-1	10.76	-
1	2	-2	1.08	-

a. A dash (-) means that this species, according to these authors, does not exist

diamagnetic (eg. 84RRa) but rarely for paramagnetic ions like Cu(II). This is attributable to lack of sensitivity arising from the line broadening resulting from complexation of the paramagnetic species. However, advantage can sometimes be taken of this line broadening to obtain valuable structural information (see Sections 1.12.5 and 1.12.6).

^{1}H NMR experiments for the determination of acid dissociation constants of His-containing peptides, such as His-Lys, and the formation constants with Zn^{2+}, have

been reported in D_2O (84RRa), but these may well be substantially different in H_2O. Since the interactions involving BSA being mimicked here with His-containing peptides occur in aqueous (H_2O) media, studies in H_2O would be more relevant than in D_2O.

In this chapter, solution chemistry studies of the acid-base and Cu(II) complexation chemistry of the peptides His-Lys, Thr(Ac)-His- Lys and Asp-Thr(Ac)-His-Lys in aqueous (H_2O) solution are discussed. The synthesis and characterization of these peptides were previously outlined in Chapter 4. The techniques employed in this study are ^1H NMR and UV/visible spectroscopies.

5.2 EXPERIMENTAL

5.2.1 Sources of Chemicals

Unless otherwise specified, chemicals were purchased as detailed in Sections 3.2.1 and 4.2.1. Potassium nitrate (KNO_3) was obtained from BDH Chemicals (Toronto, Canada). The peptides His-Lys, Thr(Ac)-His-Lys and Asp-Thr(Ac)-His-Lys were synthesized and characterized as described in Section 4.2.3.

5.2.2 Instrumental Measurements

The pH measurements were all made with either an Accu-pHast standard combination glass body pH electrode (Fisher Catalogue No. 13-620-296) or an MI-412 micro-combination pH probe (Microelectrodes, Inc. (Bedford, USA) and a FisherAccumet (model 925) pH meter. The micro-pH probe was used for pH measurements directly in the 5 mm NMR tubes. These electrodes were calibrated as discussed in Section 3.2.3.

All the ^1H NMR experiments were conducted in non-deuterated aqueous solutions. The spectra were acquired using the binomial composite "1-3-3-1" sequence for water suppression (83H) (See Section 1.12.1). DSS was added to these samples as a

chemical shift reference. The probe of the NMR instrument was also thermostated at 25°C.

UV/visible absorption spectra were recorded with an S2000 Ocean Optics Inc. spectrometer (Dunedin, USA) over the range 370-800nm, using 1cm cuvettes. The procedure for the collection of the spectral data is outlined in Section 2.2.4.

5.2.3 Preparation of Solutions for UV/visible Spectral Measurements

For the three His-containing peptides His-Lys, Thr(Ac)-His-Lys and Asp-Thr(Ac)-His-Lys, stock solutions containing 15.6 m**M**, 12.0 m**M** and 3.0 m**M,** respectively, were made using deionized and distilled water. 3 other stock solutions containing 15.6 m**M** His-Lys and 15.6 m**M** of Cu(II), 12.0 m**M** Thr(Ac)-His-Lys and 12.0 m**M** of Cu (II), and 3.0 m**M** Asp-Thr(Ac)-His-Lys and 3.0 m**M** of Cu(II) (i.e. 1:1 peptide:Cu(II) mixtures) were also prepared in water.

The pH of about 3.5 mL of the 1:1 peptide and Cu(II) mixture was adjusted incrementally from ~3 to 12 by adding small quantities (a few μL) of concentrated NaOH (between 2 and 10 **M**). The use of the concentrated NaOH minimizes the error due to dilution.

5.2.4 Preparations of Solutions for NMR Measurements

All aqueous solutions used in this study were prepared using deionized and distilled water. Solution preparation and pH measurements were carried out at 25 ± 1°C. The solutions for all the NMR analysis were prepared with the exclusion of oxygen by passing a stream of nitrogen gas, as oxygen is paramagnetic and could therefore affect NMR spectral behavior (87D). The headspace in each NMR tube was also flushed with a stream of nitrogen gas after the tube was filled (98A, 98RA).

Ionic strengths for the solutions used for K_a studies were adjusted to 0.2 **M** using KNO_3. The solutions used to study the interaction between Cu(II) and the peptides were prepared in a phosphate buffer (pH 7.0 and ionic strength 0.2 **M**) prepared from Na_2HPO_4 and KH_2PO_4 (94C). A stock solution of 0.2 **M** Cu(II) in 0.2 **M** KNO_3 was prepared by weighing accurately 49.9360 g Cu(II)SO_4 and 20.2200 g KNO_3 in separate beakers, dissolving each with some water, transferring quantitatively into a 1 L volumetric flask and diluting to volume.

5.2.4.1 Protonation Studies

0.0031 g of His-Lys was weighed directly into standard 5 mm flat-bottomed NMR tubes and dissolved with 0.5 mL pH 7.0 phosphate buffer to make approximately 10 m**M** His-Lys solution. The pH of the solution was initially adjusted to approximately pH 1 with concentrated HNO_3(aq). The pH was then gradually adjusted to higher values by the addition of concentrated solutions of NaOH, at intervals of approximate 0.4, until reaching a pH value of ~ 13 (i.e. ~ 30 data points). The ^{1}H NMR spectrum was collected after each addition of NaOH (i.e. at each pH).

For Thr(Ac)-His-Lys, 0.0036 g of the peptide was weighed and treated as described for His-Lys above within the pH range 3 to 13 at intervals of approximately 0.4 pH units. With the tetrapeptide, Asp-Thr(Ac)-His-Lys the weight taken was 0.0045 g. This was subjected to the same treatment as described for the di- and tri-peptide, at the usual pH interval of approximately 0.4 within the pH range 1 to 13.

5.2.4.2 Cu(II) Complexation Studies at pH 7

The calculated weight of each of the peptides (based on their molecular weights) to obtain approximately 5 - 6 μmoles of the peptide was accurately weighed (i.e. 0.0029 g His-Lys, 0.0041 g Thr(Ac)-His-Lys and 0.0040 g Asp-Thr(Ac)-His-Lys) directly into a 5 mm NMR tube and dissolved with 0.5 mL of buffer 7 phosphate solution to make approximately 10 m**M** peptide solution. Incremental amounts of the

stock Cu(II) solution (0.2 **M**) were spiked into this peptide solution. Several series of solutions were thereby made for the measurement of the chemical shifts and bandwidths of the various proton signals of the His-containing peptides as a function of [Cu(II)]. The stock 0.2 **M** Cu(II) solution was initially added in small volumes (i.e. 1 – 5 μL) to the peptide solution to collect more data points up to approximately 0.5 : 1 reaction mixture of Cu(II) and the peptide. However, the added volumes had to be increased to 15 μl and 25 μl to obtain higher Cu(II):peptide mole ratios of approximately 1:1 and 2:1, respectively.

5.2.5 Calculations of pKa and Species Chemical Shift values

All calculations were performed using an IBM-standard 133 MHz Pentium microcomputer. Data analysis was performed using Microsoft Excel® spreadsheet program, and *SigmaPlot*® (Jandel Corp., CA, USA), a non-linear least squares data analysis and plotting program, as described previously (98RA, 98A, 01QK). See also Section 1.4.

5.3 RESULTS AND DISCUSSION

5.3.1 Acid Dissociation Constants for His-Lys

Figure 5.1 shows ^{1}H NMR chemical shift data for an approximately 10 m**M** solution of His-Lys as a function of pH. The equilibra involved are fast on the NMR time scale, since sharp resonances are seen, with chemical shifts corresponding to the population-weighted average of those for individual species. Extremely slow equilibria on the NMR time scale would give separate spectra for the various species present. At higher pH, the exchange is somewhat slower, as shown by the observed significant line broadening, but it is still in the fast-exchange regimen. In the fast exchange regimen the observed chemical shift δ_{obs} is the average of those of the individual species, weighted by their relative amounts (98RA); i.e.,

$$\delta_{obs} = \delta_{H_3L}\alpha_{H_3L} + \delta_{H_2L}\alpha_{H_2L} + \delta_{HL}\alpha_{HL} + \delta_L\alpha_L$$

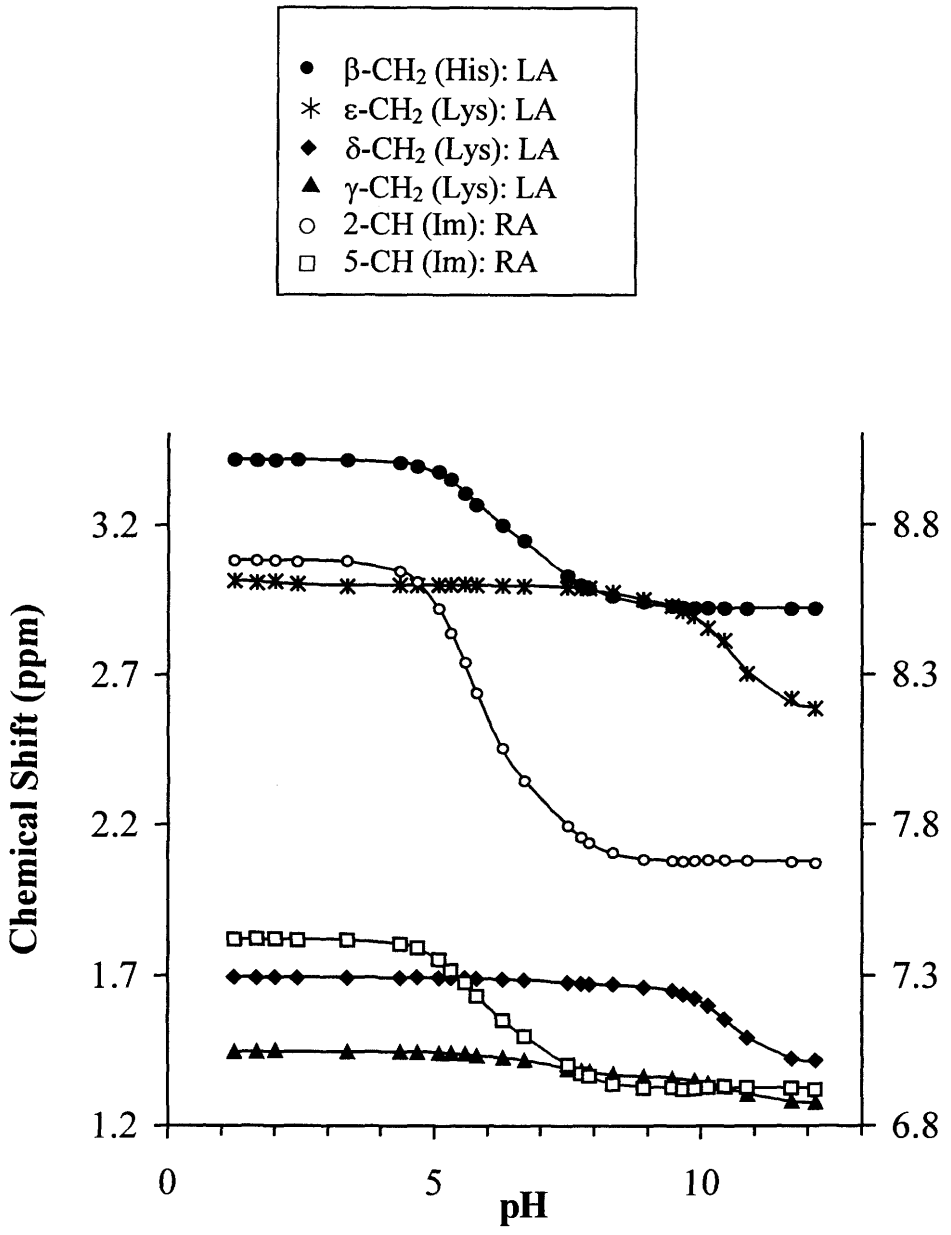

Figure 5.1: ^{1}H chemical shifts of various His and Lys protons in His-Lys as a function of pH in aqueous (H_2O) solution. Symbols represent experimental data and lines values calculated from modeling. RA and LA refer to the right and left chemical shift (y) axes respectively, and Im to the imidazole ring of Histidine.

where δ_x is the chemical shift of a given species x, and α its mole fraction. For clarity, charges have been omitted from the equation. L refers to the "fully deprotonated" His-Lys species. Deprotonation of the N-1(Im) group occurs at extremely high pH (87L) and hence can be neglected. The fourth protonation, to form the H_4L species,

similarly occurs only at very low pH (84RRa). Over a physiologically relevant pH range, α for both of these species is effectively zero. For these reasons, these groups were neglected in the model system for the determination of the acid dissociation constants.

The titration curves of imidazole CH protons in Figure 5.1 each show a decrease in chemical shift as pH increases through the point of inflexion, signifying the deprotonation of the imidazolium group as the pH increases. Beyond pH ~ 8, the chemical shifts of the signals of the imidazole protons remain constant, suggesting that the deprotonation of the imidazolium group is complete. In contrast, significant changes in the chemical shifts of the Lys ε-CH_2 and Lys δ-CH_2 protons are only observed beyond ~ pH 9, suggesting that the deprotonation of ε-Lys ammonium group is observed only beyond this pH. Thus, the imidazolium group is completely deprotonated before titration of the ε-Lys ammonium group. A similar comparison of the Lys ε-CH_2 and Lys δ-CH_2 data with that for the His β-CH_2 protons indicates that the α-ammonium group is fully deprotonated before titration of the ε-Lys ammonium group. However, data for the two imidazole CH protons and the His β-CH_2 protons seem to suggest overlap of the pH regions over which the imidazolium and the His ammonium groups deprotonate. It is well known that imidazolium and peptide α-ammonium groups deprotonate over the same pH range (77RG, 96GH).

From the NMR titration data, the macroscopic stepwise acid-dissociation constants K_{a1}, K_{a2} and K_{a3} can also be evaluated. These constants are related to the various fractions of species as follows:

$$\alpha_{H_3L} = \frac{H^3}{D}; \quad \alpha_{H_2L} = \frac{K_{a1}.H^2}{D}; \quad \alpha_{HL} = \frac{K_{a1}.K_{a2}.H}{D}; \quad \alpha_L = \frac{K_{a1}.K_{a2}.K_{a3}}{D}; \quad \text{where}$$

$$D = (H^3 + H^2.K_{a1} + H.K_{a1}.K_{a2} + K_{a1}.K_{a2}.K_{a3}) \text{ and } \quad H = \text{antilog}(-pH) \sim a_{H+} \quad \textbf{(5.1)}$$

Non-linear regression analysis of the data readily extracts the chemical shifts for the individual species as well as the values of K_{a1}, K_{a2} and K_{a3}. This "full" model is rarely required in practice. The protonation sites are widely separated in the molecule. If a protonation occurs at a site remote to the NMR site being observed, there may be no resultant chemical shift change. In that case, the K_a for that protonation process may be deleted from the model for that data set.

Such an analysis was performed for each chemical shift curve, except where peak overlap made this impossible. The resultant fits to experimental values are shown in Figure 5.1. Figure 5.2 shows the pK_a values thus obtained. Also shown in parentheses are the changes in the chemical shifts observed during the protonation process governed by a given pK_a. The size of this change is a measure of the sensitivity with which the observed NMR chemical shift "senses" that process.

The chemical shift changes for the imidazole CH protons (Figures 5.1 and 5.2) clearly indicate that these are "sensing" deprotonation first at the imidazole N-3 ($pK_{a1} \sim 5.6$) and then at the protonated N-terminal amino group ($pK_{a2} \sim 7.3$). These processes are also "sensed" by the β-CH_2 protons of His, except that the sizes of the chemical shift changes involved are different, in the manner expected. The chemical shift changes observed for the pK_{a3} process ($pK_{a3} \sim 10.6$) increase down the Lys side chain (from β to ε positions), confirming that this is ocurring at the protonated Lys ε-NH_2 . The δ- and γ-Lys protons also "sense" the imidazolinium and protonated N-terminal amino group deprotonations (although with small chemical shift changes). Since the deprotonating sites are several bonds away from the site of observation, this suggests a "through-space" effect, probably a conformation where the Lys chain lies over the His ring. The identity of the process with $pK_a \sim 8.4$ is not clear. It is sensed consistently in **both** side chains, by the His β-CH_2 and Lys ε-CH_2 protons. It is not an artifact of the fitting procedure, nor is it an impurity. Although peptides generally adopt a relatively large number of conformers of comparative stability (88RPa), it is possible that in this case the existence of two or more stable conformers is affecting results.

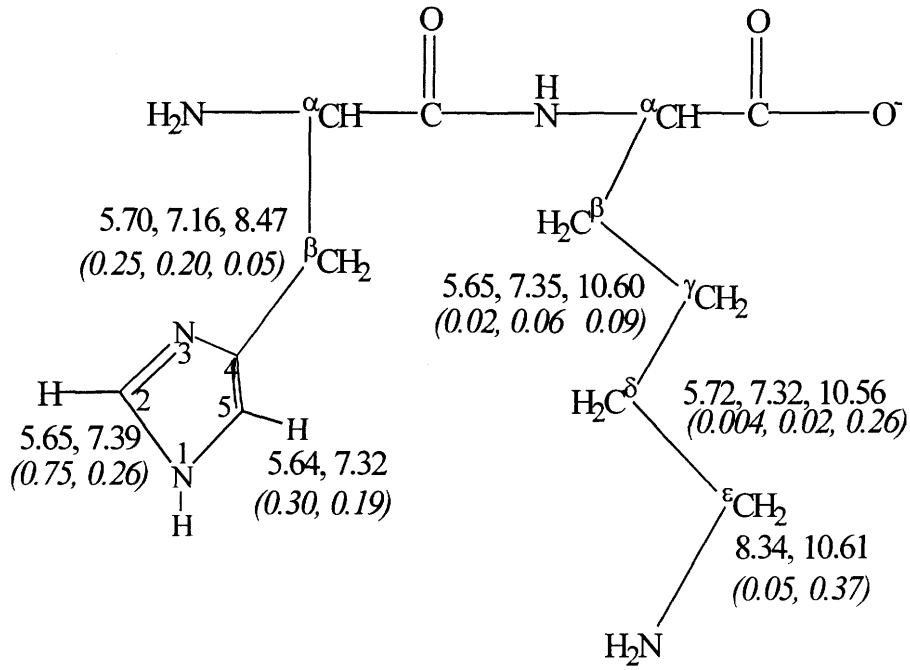

Figure 5.2: Calculated pK_a values and (in parentheses) changes in chemical shift (ppm) upon protonation for various ^1H resonances of His-Lys. The fully deprotonated structure is shown.

Averaged values for pK_{a1}, pK_{a2} and pK_{a3}, weighted by the magnitude of the chemical shift change in each case, are 5.67 ± 0.04, 7.30 ± 0.08, and 10.59 ± 0.03 respectively. The distribution of acid-base species as a function of pH for His-Lys, based on these pK_a values and using Equations 5.1, is shown in Figure 5.3. Values previously measured for His-Lys in D_2O and at a temperature of 37°C were 5.63, 7.29 and 10.09 (84RRa). Despite the difference in temperature and solvents, the values of pK_{a1} and pK_{a2} agree well. The discrepancy in the pK_{a3} values requires further discussion. There are various differences between H_2O and D_2O that may influence the measured pK_a values of solutes in these two solvents: 1) The autoionization constant of D_2O, pK_w^D, is 14.95 (~ 1 pK units larger than H_2O) (01L); 2) There is a slight difference in the dielectric constants of the two solvents, that of H_2O being ~ 1% larger than that of D_2O (95H). This change in dielectric constant, although small, may have a significant effect on solute behavior, particularly for charged species (95H); 3) There is also a considerable increase in both viscosity and density (~ 11% increase) and a consequent decrease in ionic mobility on going from H_2O to D_2O (95H, 01L).

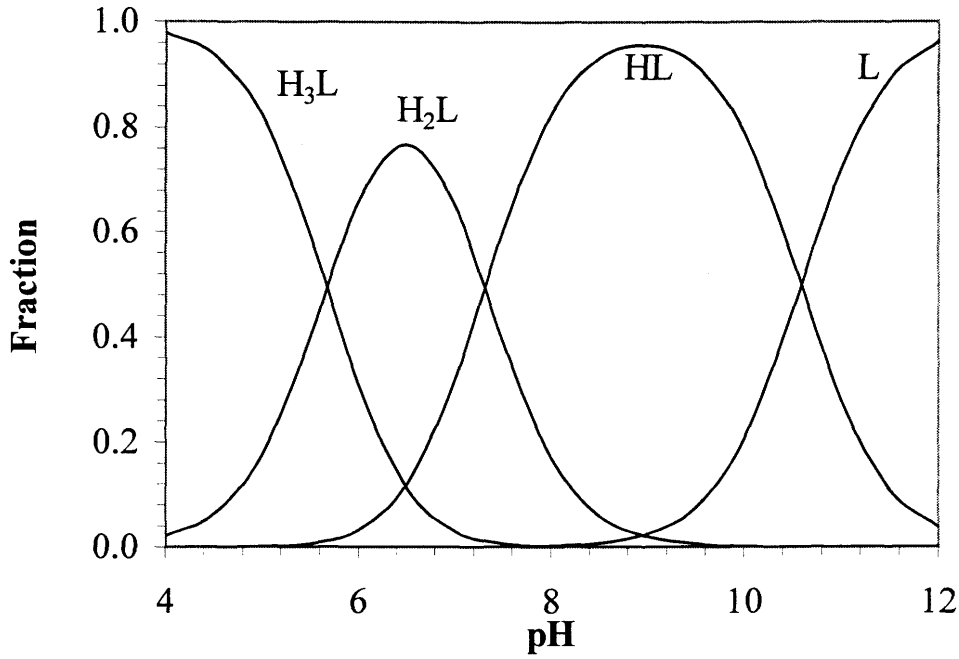

Figure 5.3: pH dependence of the fractional concentrations of the various acid-base forms of His-Lys at 25°C in 0.2 **M** KNO_3 solution.

Observed differences for pK_a values in the two solvents have also been previously observed to be larger for higher values of pK_a (88RP). This was attributed mainly to the differing acidities of the two solvents. Furthermore, a linear free energy relationship between ΔpK_a of the two solvents and pK_a in water for a series of closely related simple carboxylic acids, simple amines and amino acids can be developed, predicting the observed trend that the differences between the pK_a values in the two solvents increase with increasing pK_a values (95H).

5.3.2 Acid Dissociation Constants for Thr(Ac)-His-Lys

Non-linear regression analysis was used to calculate the also chemical shifts of the individual species and the corresponding pK_a values of Thr(Ac)-His-Lys from the ^1H NMR chemical shift data as a function of pH. Changes in the chemical shifts of these species and the calculated macroscopic pK_a values are presented in Figure 5.4. The ionisation scheme for this system is the same as that for His-Lys; although the molecule

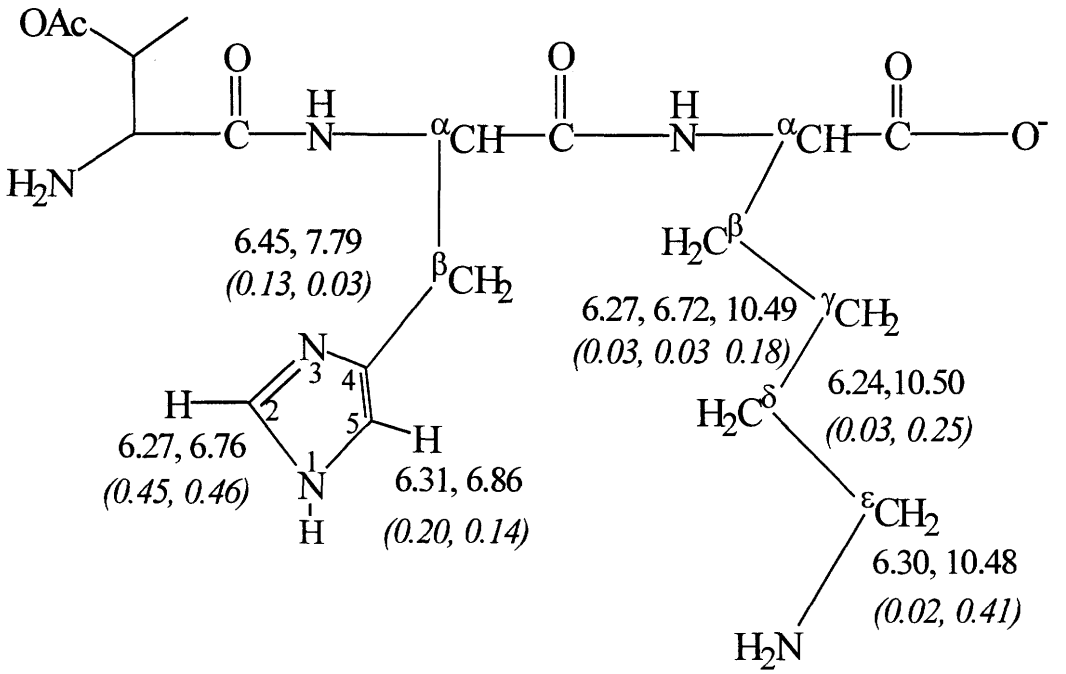

Figure 5.4: Calculated pK_a values and (in parentheses) changes in chemical shift (ppm) upon protonation for various ^1H resonances of Thr(Ac)-His-Lys. The fully deprotonated structure is shown.

under consideration is now a tripeptide, the added Thr residue has its side chain –OH group protected and hence contributes no additional acid-base functionality (see Figures 5.2 and 5.4 for the structures of the two peptides). Weighted mean values for pK_{a1}, pK_{a2} and pK_{a3} are 6.31 ± 0.07, 6.78 ± 0.07 and 10.49 ± 0.01 respectively. The resultant species distribution of Thr(Ac)-His-Lys as a function of pH is shown in Figure 5.5. As observed for His-Lys, the identity of the process with pKa ~ 7.8 is not clear and is neglected in the figure. As for His-Lys, this was "sensed" by the His β-CH_2 protons.

There appear to be no previously reported pK_a values in the literature for Thr(Ac)-His-Lys, nor for the fully deprotected tripeptide Thr-His-Lys. The proton complexation of the tripeptide Gly-His-Lys has however been extensively studied both by potentiometry (81LS, 83MW, 84RRa, 85RR, 85DA) and by ^1H NMR (77RG, 85DA). The values of pK_{a1}, pK_{a2} and pK_{a3} at 25°C and an ionic strength of 0.1**M**, critically selected by Martell et al. (98MS) are 6.50, 7.91 and 10.51 respectively. The pK_{a1} and more so the pK_{a3}, representing the protonation of Im (N-3) and ε-Lys nitrogen,

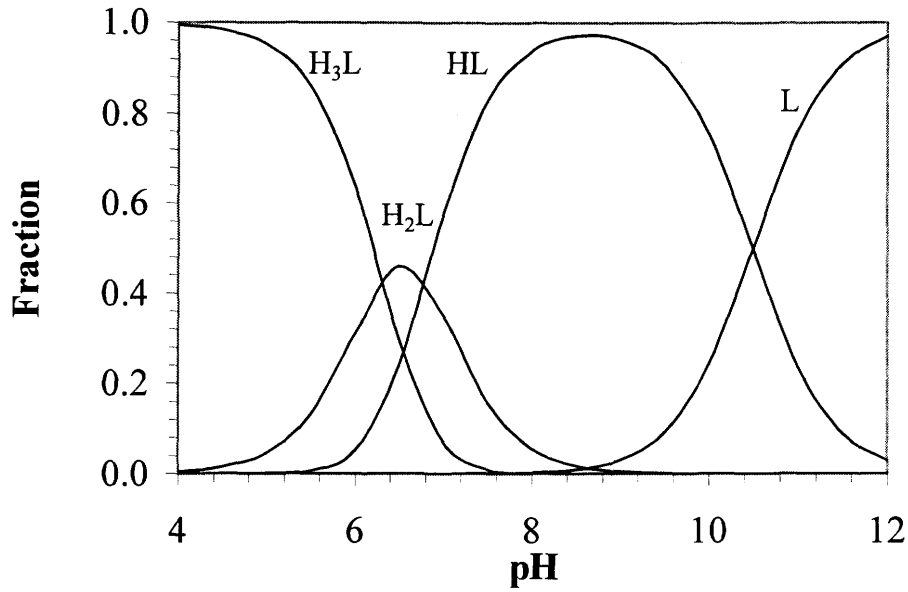

Figure 5.5: pH dependence of the fractional concentrations of the various acid-base forms of Thr(Ac)-His-Lys at 25°C in 0.2**M** KNO_3 solution.

agree well with that of Thr(Ac)-His-Lys in this study, despite the difference in the ionic strength of the solutions. As expected, the pK_{a2} value reported for Gly-His-Lys (i.e., for the protonated terminal amino group) was significantly different for Thr(Ac)-His-Lys.

5.3.3 Acid Dissociation Constants for Asp-Thr(Ac)-His-Lys

The analysis of the ^1H NMR chemical shift data of Asp-Thr(Ac)-His-Lys as a function of pH is similar to that detailed in Section 5.3.1:

$$\delta_{obs} = \delta_{H_4L}\alpha_{H_4L} + \delta_{H_3L}\alpha_{H_3L} + \delta_{H_2L}\alpha_{H_2L} + \delta_{HL}\alpha_{HL} + \delta_L\alpha_L$$

where δ_x is the chemical shift of a given species x, and α its mole fraction. L refers to the "fully deprotonated" Asp-Thr(Ac)-His-Lys species as shown in Figure 5.6. The deprotonation of the N-1(Im) group and the fifth protonation, to form an H_5L species (protonation of the C-terminal carboxylate) can be neglected for the same reasons already given in Section 5.3.1. See Figure 5.6 for details of the ionization scheme assumed for Asp-Thr(Ac)-His-Lys in solution. The fraction of each of the peptide

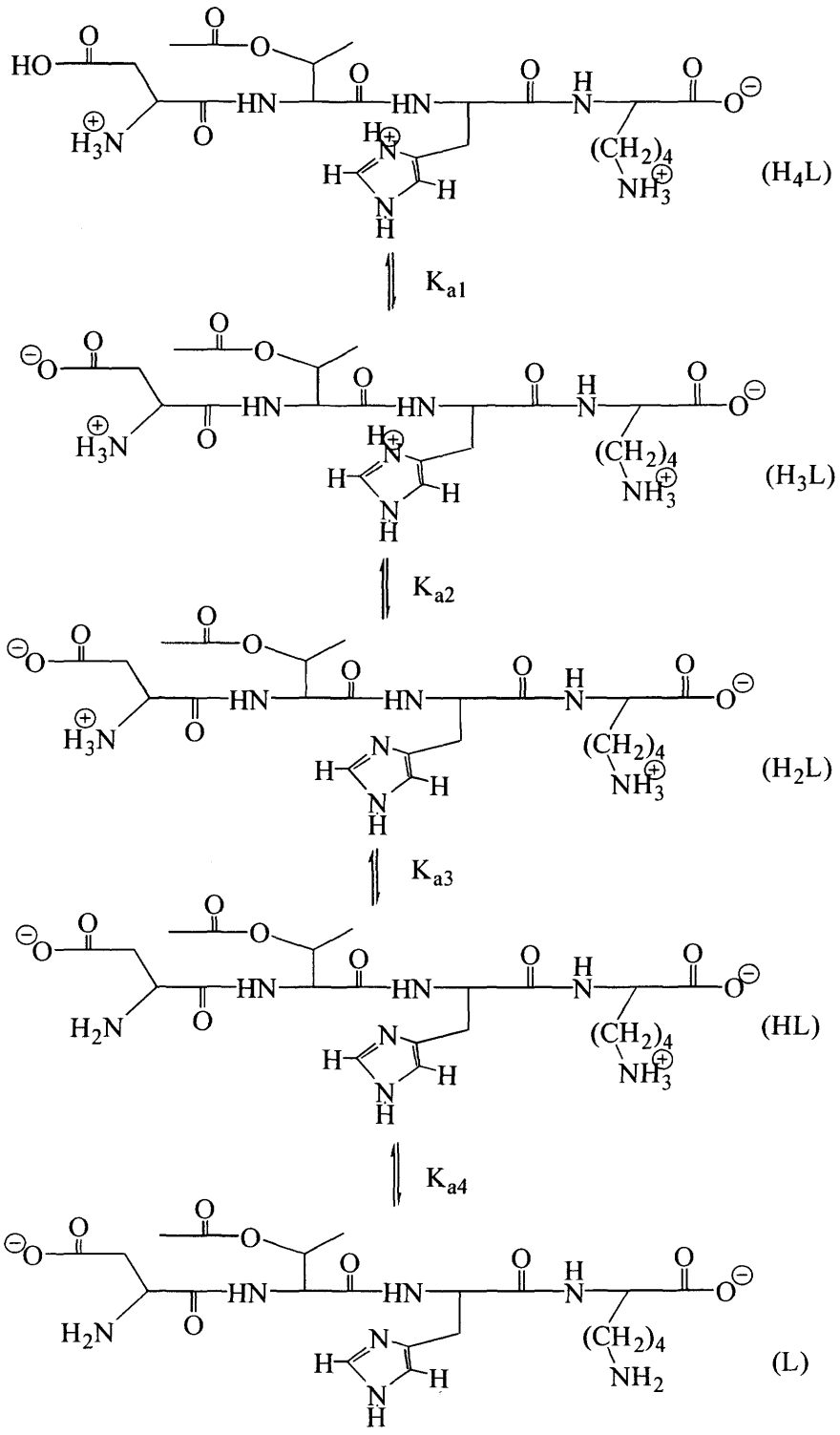

Figure 5.6: Acid-base scheme for Asp-Thr(Ac)-His-Lys.

species at a particular pH is given by the Equations 5.2:

$$\alpha_{H_4L} = H^4 / D;\ \alpha_{H_3L} = K_{a1}H^3 / D;\ \alpha_{H_2L} = K_{a1}K_{a2}H^2 / D;$$

$$\alpha_{HL} = K_{a1}K_{a2}K_{a3}H / D;\ \alpha_{L} = K_{a1}K_2K_3K_{a4} / D$$

where

$D = (H^4 + H^3.K_{a1} + H^2.K_{a1}.K_{a2} + H.K_{a1}.K_{a2}.K_{a3} + K_{a1}.K_{a2}.K_{a3}\ K_{a4})$ and

$$H = \text{antilog}(-pH) \sim a_{H+} \qquad \textbf{(5.2)}$$

See Figure 5.7 for the K_a values and the changes in the chemical shifts during the deprotonation process governed by a given pK_a.

The chemical shift changes for the imidazole CH protons (Figure 5.7) clearly indicate that these are "sensing" the state of protonation at the imidazole N3 (pK_{a2} ~ 6.5). This process was also "sensed" by the β-CH_2 of His and the NH of Im N1, except that the sizes of the chemical shift changes involved are different, in the manner expected. The NH of Im N1 and the β-CH_2 of His sense the state of protonation of the N-terminal amino group (pK_{a3} ~ 8.7), although the sensitivity of the latter is very small. A third protonation is "sensed" by the NH of Im N1 at a lower pKa value of (~5.0). This process is also sensed by the CH_3 protons of the acetyl protecting group on the Thr residue. The most likely protonation site is that of the β-COOH of Asp. Since the acetyl CH_3 protons are several bonds away from the protonation site, this suggests a conformation where the Asp and the Thr side chains lie in close proximity. This also accounts for how the NH- Im(N1) proton, several bonds away from this site, also senses this process. The chemical shift changes observed for the pK_{a4} process (pK_{a4} ~ 10.6) increase down the Lys side chain (from β to ε positions) as also observed for His-Lys and Thr(Ac)-His-Lys (Sections 5.3.1 and 5.3.2), confirming that this is the protonated Lys ε-NH_2 deprotonation.

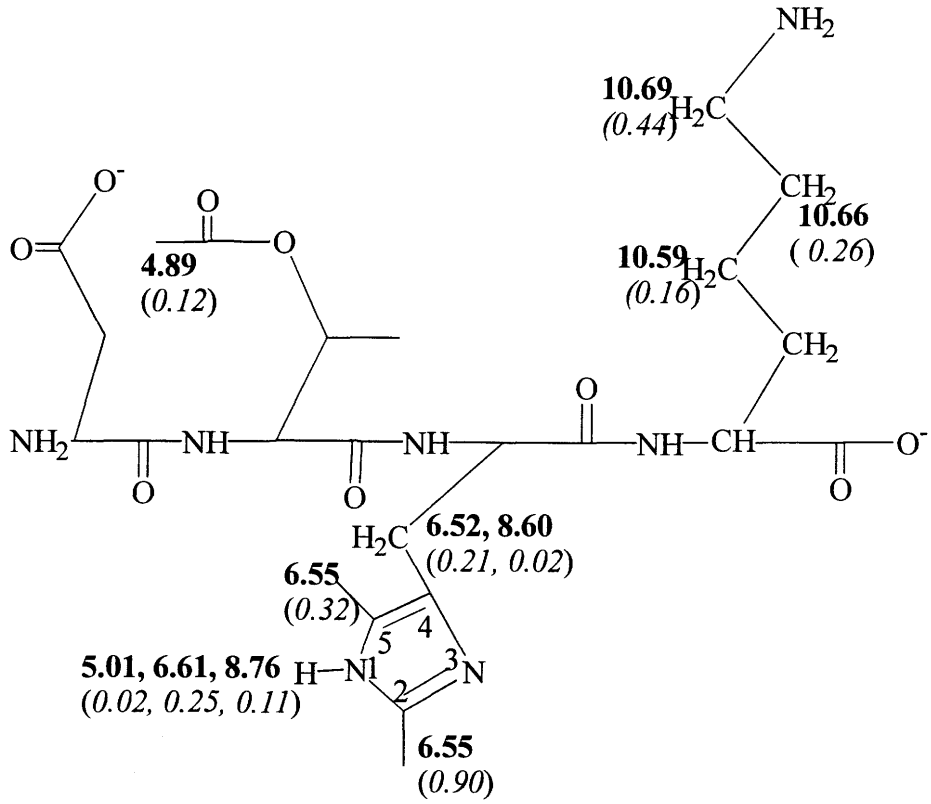

Figure 5.7: Calculated pK_a values and (in parentheses) changes in chemical shift (ppm) upon protonation for various ^1H resonances of Asp-Thr(Ac)-His-Lys. The fully deprotonated structure is shown.

Weighted average values for pK_{a1}, pK_{a2} , pK_{a3} and pK_{a4} are 4.91 ± 0.06, 6.55 ± 0.03, 8.74 ± 0.06 and 10.66 ± 0.04 respectively. The resultant acid-base speciation of Asp-Thr(Ac)-His-Lys as a function of pH is shown in Figure 5.8. The dominant species under physiological pH are H_3L and H_2L. Both of these species have the terminal amino group protonated. It is only beyond pH 8 that the fraction of the HL species (possessing a deprotonated terminal amino group) is significant.

The pK_a for the ionization of the β-carboxylate is somewhat higher than those reported for most Asp containing peptides, which have typical pK_a values < 4 (78IS). There are however a few longer peptide chains with pK_avalues > 4; for example, Asp-Arg-Val-Tyr-Ile-His-Pro-Phe has COOH (Asp) pK_a= 4.67 (95BJ).

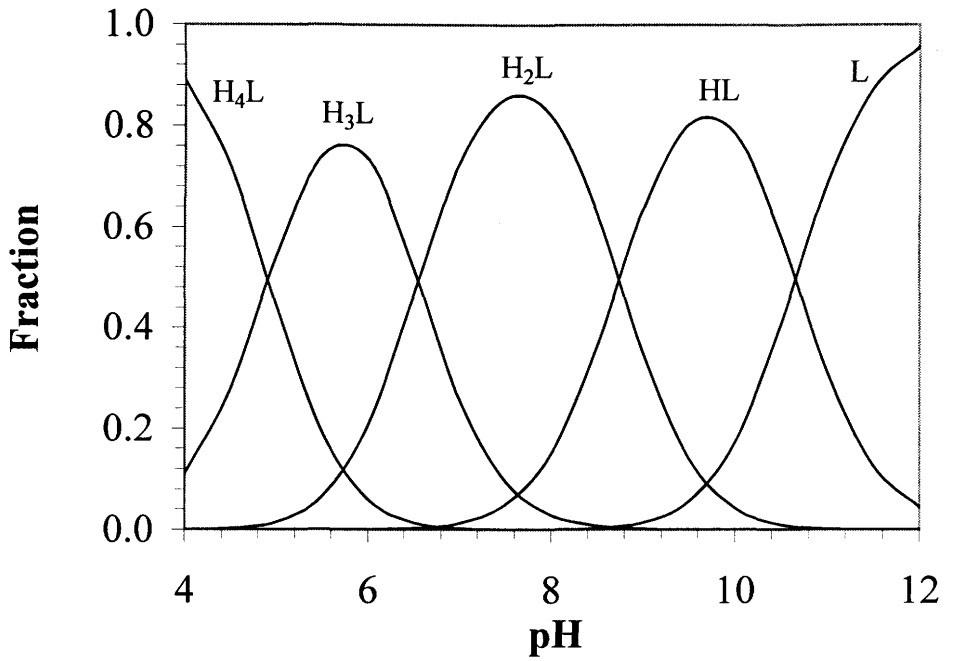

Figure 5.8: pH dependence of the fractional concentrations of the various acid-base forms of Asp-Thr(Ac)-His-Lys at 25°C in 0.2 **M** KNO_3 solution.

5.3.4 Comparison of the pK_as of His-Lys, Thr(Ac)-His-Lys and Asp-Thr(Ac)-His-Lys

Numerous pK_a values for His-containing dipeptides (93SF, 00BC, 85RR, 84RRa), tripeptides (93SF, 83MW, 81LS, 85RR, 84RR, 84RRa) and tetrapeptides or higher chain peptides (93SF, 93BN, 90PP, 00VS) have been reported. See Table 5.2. Reports for peptides containing the His-Lys chain seem to be confined to the dipeptide His-Lys (RRa) and the tripeptide Gly-His-Lys (81LS, 83MW, 84RRa, 85RR, 85DA, 77RG), which were discussed above (Section 5.3.2).

Since even minor changes in the amino sequence can lead to significant changes in the acid-base behavior of a peptide it is difficult to make any meaningful comparison with pK_as of other peptides in the literature. Noteworthy, however, are the significant differences between the pK_a's observed for the protonated α-amino group in the dipeptide His-Lys(~7.3), the tripeptide Thr(Ac)-His-Lys (~6.8) and the tetrapeptide

Table 5.2: Imidazole pK_a values of His-containing peptides

Peptide	His position relative to α-NH_2 terminal	pK_a (Im N-3)	Ref
His-Lys	1	5.66	This study
His-Ala	1	5.90	97TH
His-Gly	1	5.39	97TH
His-Gly-Gly	1	5.52	97UH
His-His-Gly-Gly	1	5.6	97UH
	2	6.3	97UH
Gly-His-Gly-His	2	6.00	93BN
Gly-His	2	6.61	97TH
Ala-His	2	6.58	97TH
Gly-His-Gly	2	6.63	97UH
		6.62	77RG
		6.35	93BN
Gly-His-Lys	2	6.6	77RG
Thr(Ac)-His-Lys	2	6.31	This study
Gly-Gly-His	3	6.64	93BN
	3	6.82	00VS
Asp-Thr(Ac)-His-Lys	3	6.6	This study
Gly-His-Gly-His	4	6.95	93BN
Ala-Gly-Gly-His	4	6.89	90PP
Ala-Gly-Pro-His	4	6.80	90PP
Gly-Gly-Gly-His	4	6.86	00VS
Ala-Gly-Gly-His-Ome	4	6.62	90PP
Gly-Gly-Gly-Gly-His	5	6.93	00VS
Asp-Arg-Val-Tyr-Ileu-His	6	7.13	95BK

Asp-Thr(Ac)-His-Lys (~8.7), which would certainly influence their relative metal binding abilities. See Section 5.3.5 to 5.3.8 for discussions on Cu(II) binding to these peptides. The basicity of a group depends on the protonation state of the other acid-base site of the molecule, which can interact electrostatically with the group (74YA, 91NR).

The lower pK_a value for the dipeptide as compared to the tetrapeptide may therefore be expected due to a stronger interaction between the amino group and the adjacent imidazole group as compared to the interaction between the β-carboxylate and the amino group. The imidazole and the terminal carboxylate groups are too remote from the amino group to interact significantly with it. The lower pK_a observed for the protonated α-amino group of the tripeptide than both the dipeptide and tetrapeptide cannot be similarly explained, since in the absence of any group in close proximity to the α-amino for any meaningful interaction, the pK_a should rather increase. Perhaps the tripeptide adopts a conformation that hinders the deprotonation of the $\alpha\text{-}NH_3^+$.

There were also differences in the pK_as of the protonated imidazole N3 groups for His-Lys (~ 5.7), Thr(Ac)-His-Lys (~ 6.3) and Asp-Thr(Ac)-His-Lys (~ 6.6). It appears that the closer this group is to the terminal amino group the lower the pK_a. This trend also seems to hold in almost all instances in the literature (Table 5.2). Generally at position 1, the imidazolium pK_a ranges from 5.5-5.7, at position 2 from 6.3-6.8, at position 3 from 6.6-6.8, and at position 4 and beyond the pK_a is > 6.8.

The pK_as for ε-Lys deprotonation for the 3 peptides (10.59, 10.49 and 10.66 for the di-, tri- and tetra-peptides) are not substantially different from each other.

5.3.5 Cu(II) Complexation Studies of His-Lys

5.3.5.1 UV/visible Spectra

The UV/visible spectra of a solution containing a 1:1 mixture of Cu(II) and His-Lys at a concentration of 15.6 m**M** are shown as a function of pH in Figure 5.9.

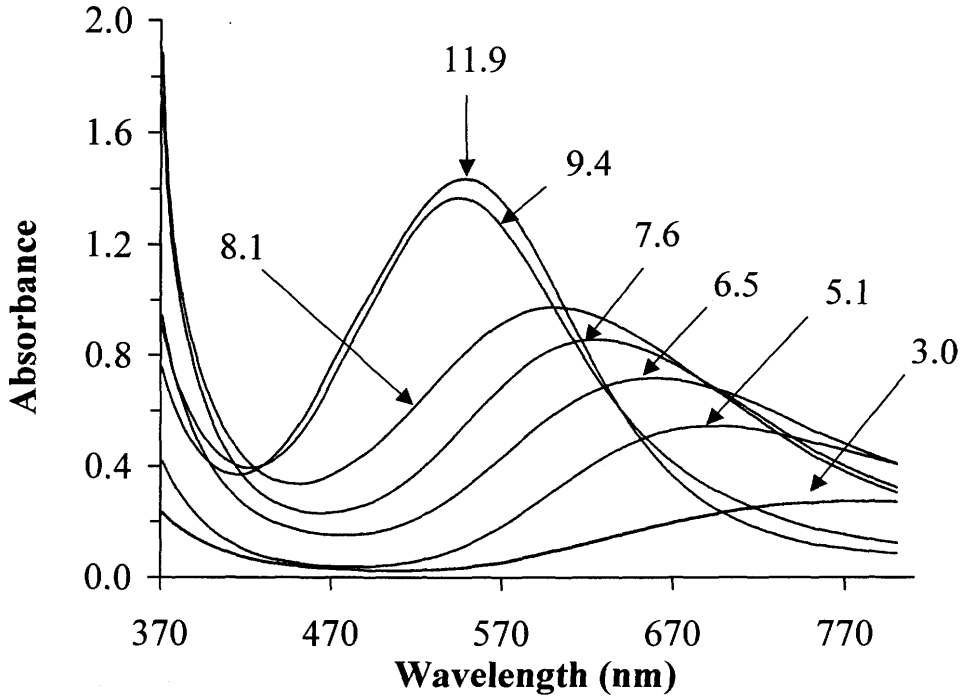

Figure 5.9: UV/visible spectra of a 15.6 mM 1:1 mixture of His-Lys and Cu(II) at various pH values (shown on figure).

Billo's empirical equation (74B) can be used to propose structures for the possible complexes formed in mixtures of Cu(II) and His-Lys, based on the observed λ_{max} value in visible absorption spectrophotometry:

$$\lambda_{max} = 10^3 / \sum_i n_i \nu_i \qquad \textbf{(5.3)}$$

where n_i is the number of donor atoms of type i in the complex ($\sum n = 4$). The coefficient ν_i (in μm^{-1}) is the corresponding ligand-field contribution of that donor atom. Table 5.3 gives the coefficients ν for various donor atoms as calculated by different investigators.

According to Equation 5.3, the replacement of water molecules by oxygen or nitrogen donors in Cu(II) should shift λ_{max} towards lower values, the effect of the nitrogen donors being more marked. In Figure 5.12, there is a progressive apparent shift of the λ_{max} of the various peaks to shorter wavelengths as pH increases, an indication of

Table 5.3: Calculated ligand field contributions ν (in μm^{-1}) from various donor groups to Cu(II) as reported by different investigators.

	References		
Donor atoms	74B	99PD	01MM
peptide N	0.485	0.495	0.494
amino N	0.453	0.450	0.460
Imidazole N	0.43	0.427	0.434
carboxylate O	0.342	0.353	0.346
O of H_2O	0.301	0.39	-
hydroxyl O	0.301	0.296	0.294
carbonyl O	0.301	-	0.294

the involvement of oxygen or nitrogen atoms in complex formation. The observed maximum can be used together with other information about the coordinating groups that are available to bind to a Cu(II) center to construct a ligand set that would produce the observed spectral maximum (99CP). Based on the selected set of coordinated ligands, it is also possible to make an intelligent guess as to the stoichiometry of the complex formed.

All possible logical permutations (~ 120) of the donor groups listed in Table 5.3 that will sum up to four (assuming square planar complexes) were entered and calculated in an Excel® spreadsheet and matched with the observed λ_{max} at different pH values to choose the likely coordination set of donor atoms. Table 5.4 summarizes the possible donor atoms for the various complex species at different pH values, based on closeness of the experimental λ_{max} to the calculated values. All the three calculated λ_{max} (i.e. 685, 689 and 687 nm) using the different coefficients in Table 5.3 for a coordination mode involving 2 imidazole nitrogen and 2 H_2O molecules are consistent

Table 5.4: Experimental and calculated λ_{max} values based on the different ν values as referenced in brackets, together with possible donor atoms for mixture of 1:1 His-Lys and Cu(II) at different pH values. λ_{max} in nm and ε_{max} in $dm^3\ mol^{-1}cm^{-1}$.

pH	Possible Donor atoms	Expt. λ_{max}	ε_{max}	Cal. λ_{max} (74B)	Cal. λ_{max} (99PD)	Cal. λ_{max} (01MM)
5.05	$2N_{im}$, $2H_2O$	685	35	684	689	687
6.47	$1N^-$, $1N_{im}$, $2H_2O$	660	46	659	659	660
7.55	$1N^-$, $1N_{im}$, $1H_2O$, 1OH	624	55	659[b]	621	-
7.55	$1N^-$, $1N_{im}$, $2COO^-$	624	55	625	614	617
8.10	$1N^-$, $1NH_2$, $1N_{im}$, $1H_2O$,	601	63	599	599	595
11.94	$1N^-$, $2NH_2$, $1N_{im}$,	548	92	549	549	541

b – The values of the coefficient ν reported do not differentiate H_2O contribution from that of –OH.

with the experimental λ_{max} at 685 nm at pH ~5 (Table 5.4). A stable Cu(II) complex of bis(imidazol-2-yl) as ligand has been reported to be formed in acid medium with the coordination of two imidazole nitrogen atoms, whose absorption spectra has λ_{max} around 680 nm (00VS).

Calculated λ_{max} values for the coordination mode involving 1 peptide N, 1carboxylate and 2 H_2O, i.e. 700, 692, 700 nm using the respective coefficients from 74B, 99PD and 01MM are also close to the observed λ_{max} (see Table 5.4.). However, this coordination mode does not seem likely, since metal ion induced deprotonation and coordination of amide nitrogen are well known to occur only after the initial coordination of an amino group (00VS). Also in the case of His-peptides, the metal induced deprotonation and amide N coordination occurs only after the initial coordination of the imidazole N (90PP), but ***not*** of carboxylate groups nor, of course, H_2O.

These calculations all suggest that the initial binding site of the peptide to Cu(II) is an imidazole N. In the presence of both a terminal amino group and a His residue, the N-3 of the imidazole ring of the His residue has been reported to be the primary anchoring site for Cu(II) coordination (90PP). The predicted coordination mode is consistent with the formation of a (His-Lys)-Cu(II) complex of stoichiometry 1:2 (i.e a $(H_2L)_2Cu$ complex), since two imidazole N groups are required to coordinate to one Cu(II) center as predicted by the calculations shown in Table 5.4. The proposed coordination scheme as pH is increased from ~ 5 to 12 for the complexation of His-Lys to Cu(II), based on the discussion above, is summarized in Figure 5.10. Figure 5.10a shows the proposed structure of the complex at pH ~ 5.

This initial binding of the imidazole N group serves as an "anchor" that facilitates the deprotonation and the coordination of Cu(II) to the peptide N, with displacement of the peptide N proton, as pH is increased to about 6.5 (90PP). A new complex species $(H_2LH_{-1})Cu$ is then formed (Figure 5.10b), where H_{-1} indicates loss of

a proton from the peptide moiety and Cu(II) is coordinated via the imidazole N, a deprotonated peptide nitrogen (N^-) and to two H_2O molecules.

Increasing the pH to about 7.6 could form two possible species, each maintaining the coordination of the two nitrogen donors (peptide N and the imidazole N) of the $(H_2LH_{-1})Cu$ species, but either having the two weakly bonded H_2O molecules replaced with 2 carboxylate groups, or replacing one of the coordinated water molecule with an -OH as a result of a proton lost from the water molecule, to form a complex species $(H_2LH_{-1})OHCu$. See Figure 5.10c. The latter seems to be more plausible, since the –COOH group is completely deprotonated above pH 6 and hence there appears to be no reason why it would not coordinate at pH ~ 6.5 but would at a higher pH).

As the pH is increased up to pH 8.1 the apparent λ_{max} gradually decreases to 601 nm, in good agreement with a calculated value of ~599 nm for coordination by 1 amino N, 1 peptide N, 1 imidazole N and 1 oxygen of H_2O. This coordination is consistent, with that between Cu(II) and the dominant species at pH ~ 8 (i.e HL- see Figure 5.3) to form a $(HLH_{-1})Cu$ complex (Figure 5.10d). 1:1 complex formation is assumed here, since the donor atoms indicated from the calculations to coordinate one Cu(II) are all derivable from a single His-Lys to form a chelate which is therefore expected to be more stable than a 2:1 peptide:Cu(II) complex. At extremely high pH (e.g. pH ~12) the ε-Lys N becomes involved as the weak coordination with H_2O is replaced with this group. The observed λ_{max} = 549 nm at pH 11.9 (Figure 5.9) agrees closely with the calculated value of ~ 549 nm for 2 amino N, 1 amide N and 1 imidazole N (Table 5.4). Note that at that high pH, the dominant species is L and all removable protons including that on ε-Lys NH_3^+ are absent (see Figure 5.3). The complex thus formed is most likely $(LH_{-1})Cu$. See Figure 5.10e.

5.3.5.2 ^1H NMR Studies at pH 7

Figure 5.11 shows the ^1H NMR spectra obtained at pH 7.0 for a 10 m**M** His-Lys aqueous solution as different amounts of Cu(II) are added. The maximum Cu(II)

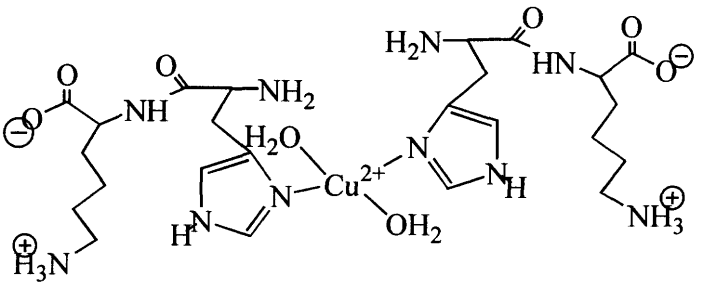

(a) = $(H_2L)_2Cu$

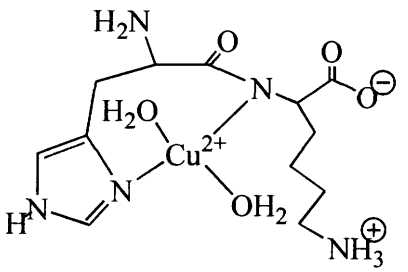

(b) = $(H_2LH_{-1})Cu$

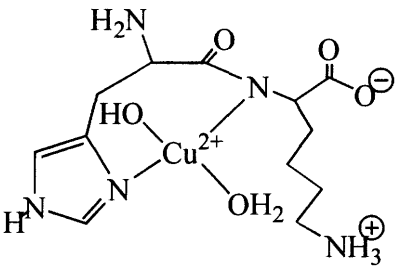

(c) = $(H_2LH_{-1})OHCu$

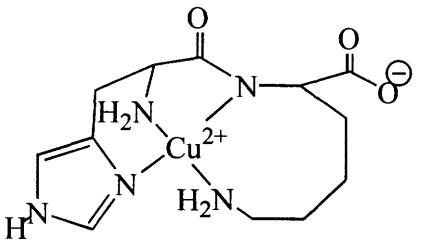

(e) = $(LH_{-1})Cu$

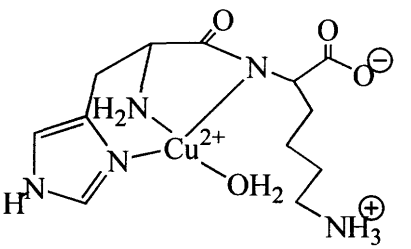

(d) = $(HLH_{-1})Cu$

Figure 5.10: Proposed structures of complexes formed from His-Lys and Cu(II) reaction mixtures in aqueous solutions at approximate pH values of (a) 5 (b) 6.5 (c) 7.6 d) 8 and (e) 11.9.

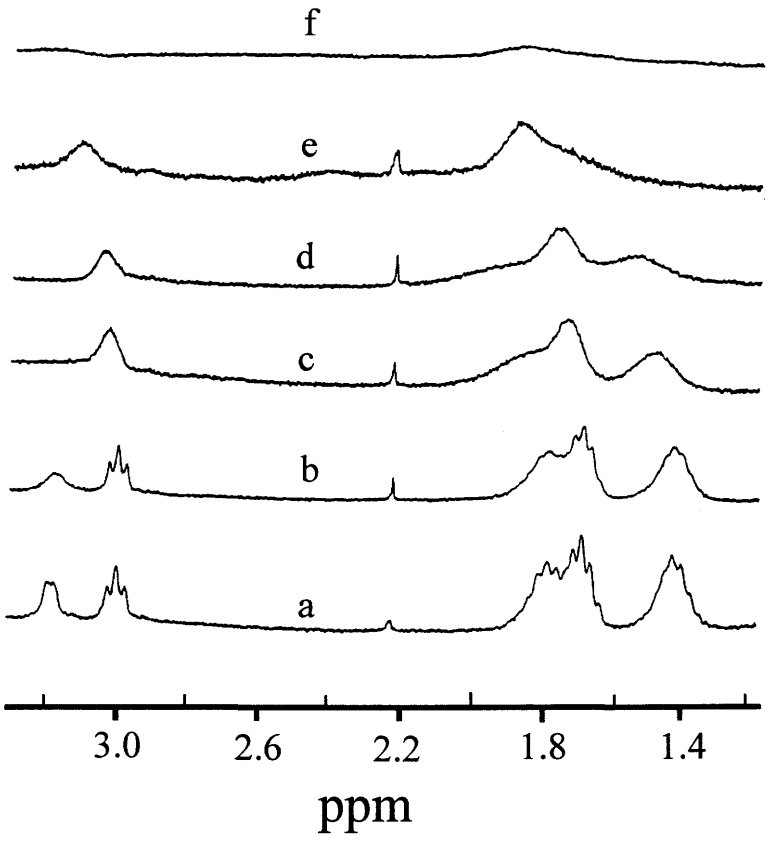

Figure 5.11: ^{1}H NMR spectra at pH 7.0 of His-Lys (10 mM) . with Cu(II) added at concentrations of (a) 0.0 mM (b) 0.1 mM (c) 1.1 mM (d) 2.1 mM (e) 9.6 mM (f) 18.2 mM.

concentration possible is limited by the paramagnetic nature of the Cu(II) ion, which gives rise to efficient NMR relaxation and hence very broad resonances. If, as is the case here, fast exchange pertains, then if too high a proportion of a ligand is complexed to Cu(II), the averaged resonances are so broad as to be unobservable. However, as discussed in Sections 1.12.5 and 1.12.6, the severity of this broadening for a given resonance can give an indication of the spatial proximity of the paramagnetic ion to the nucleus being observed.

The His β-CH_2 signal, at a chemical shift of ~ 3.2 ppm, disappears when about a tenth of an equivalent of Cu(II) is added to His-Lys (Figure 5.11). At this level of added Cu(II), the imidazole C2-H signal (8.03 ppm) is also barely visible. However, the

imidazole C5-H proton signal (7.16 ppm) does not completely disappear until about a fifth of an equivalent of Cu(II) is added. The earlier disappearance of the His β-CH_2 signal suggests the involvement of another coordination site close to His β-CH_2 protons (i.e. the amino N and/or the peptide N) in addition to the N-3 imidazole coordination to Cu(II). Line broadening effects decrease down the Lys chain; the most effective line broadening is observed for the β-Lys protons, followed by the γ-Lys protons and to a much lesser extent the δ- and ε-Lys protons. This suggests that the ε-NH_2 of Lys is not involved in Cu(II) complexation, but that complexation occurs at the amide N atom and/or the carboxylate site. Considering the preference of Cu(II) for N donors over O donors (87H), and the fact that carboxylate coordination would result in an implausible 8-membered ring, coordination via the amide N to form a 6-membered ring seems to be more likely (Figure 5.10d). This coordination environment has been reported for Cu(II) complexation to many His-containing dipeptide including HisPhe, HisTyr, HisMet, HisAla, HisVal and HisLys (85RR, 87SP, 90B). Alternatively, coordination to both sites could be involved, yielding a 6-membered ring (involving the amide N) and a 5-membered ring (involving the carboxylate), as shown in Figure 5.12.

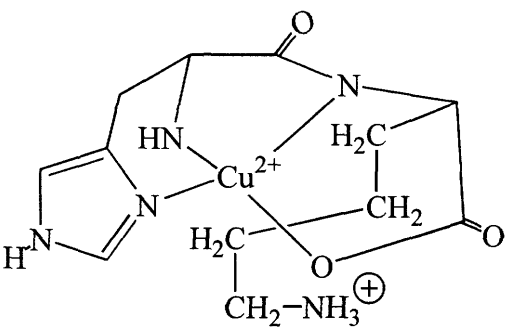

$(HLH_{-1})Cu$

Figure 5.12: Possible alternative structure of the His-Lys $(HL)H_{-1}Cu$ complex .

The unpaired electron of the Cu(II) ion also produces a large local magnetic field at all nuclei in its vicinity (98RA), leading to substantial changes in chemical shifts (see Section 1.12.5). The chemical shifts of the Lys protons δ-CH_2, ε-CH_2, γ-CH_2 of His-Lys at pH 7 as increasing amounts of Cu(II) are added are shown in Figure 5.13.

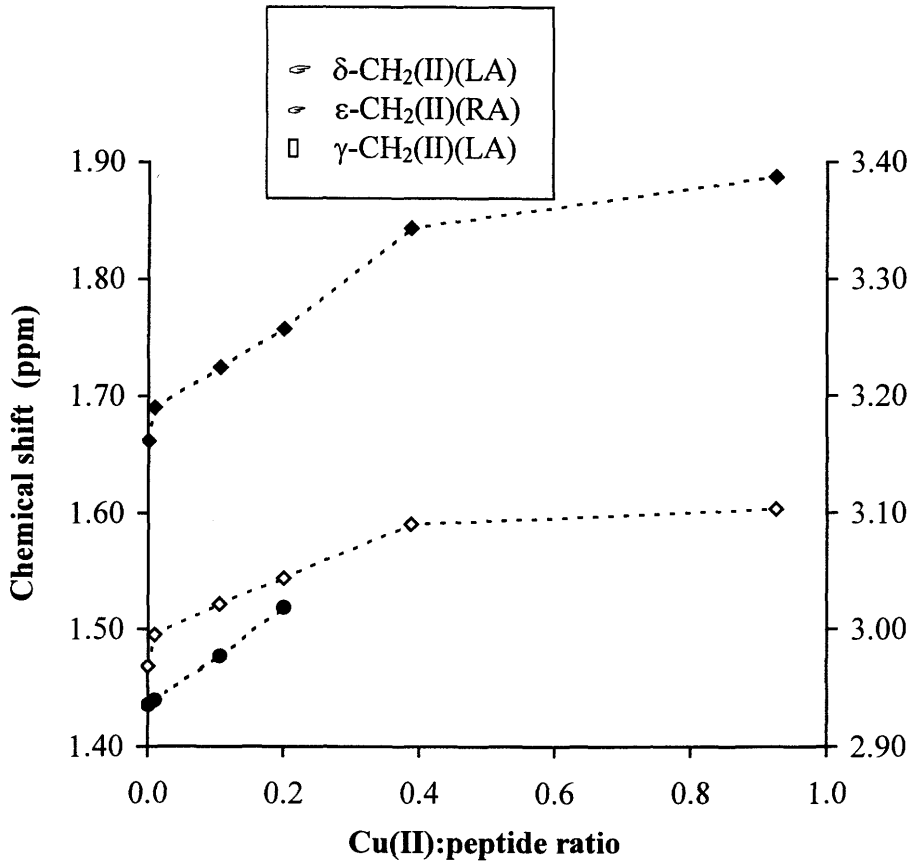

Figure 5.13: Lys γ-, δ-, and ε-CH_2 chemical shifts of 10 m**M** aqueous His-Lys solution containing various amounts of Cu(II) as a function of the Cu(II):peptide ratio. The nomenclature for the protons is as for Figure 5.3 and the text. RA and LA refer to right and left chemical shift (y) axes respectively.

The chemical shift changes decrease down the Lys side chain. Clearly, the ε-NH_2 of Lys is not involved in Cu(II) complexation at pH 7.

5.3.5.3 Proposed Structure based on both NMR and UV/visible spectroscopy at pH 7

The UV/ visible study suggests the involvement of 1 imidazole, 1 peptide N^-, $2H_2O$ with Cu(II) coordination at pH 6.5, and at pH 7.6 the same coordination is implied with the exception that one of the waters is deprotonated. At pH 7 the NMR results suggest 1 imidazole and the peptide N-, with obviously no information about the water molecules. Thus, it seems clear from both the NMR studies and the visible

spectroscopic studies above (Sections 5.3.4.1 and 5.3.4.2) that at pH 7, the coordination involves the imidazole group and the peptide N on the ligand and two water molecules, one of which is partially deprotonated. Possible involvement of the carboxylate group, suggested based on the NMR studies (Section 5.3.4.2) but regarded as implausible, can be conclusively ruled out based on the visible absorption data. Calculations based on this coordination mode using the coefficients by 74B, 99PD and 01MM give λ_{max} values of 585, 577, and 580 nm respectively, which are all far smaller than the observed value of 624 nm.

5.3.6 Cu(II) Complexation to Thr(Ac)-His-Lys

5.3.6.1 UV/visible Spectra

The UV/visible spectra of a 12.0 m**M,** 1:1 mixture of and Thr(Ac)-His-Lys and Cu(II) in the pH range 2.7 to 11.9 are shown in Figure 5.14.

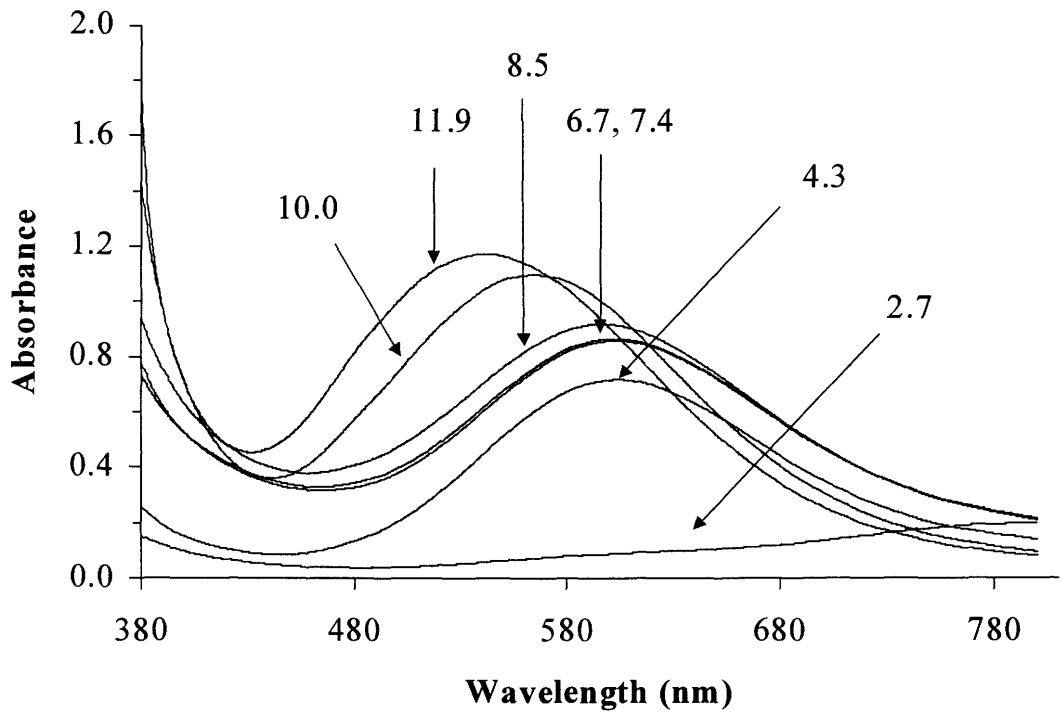

Figure 5.14: The UV/visible absorption spectra of 12.0 m**M** 1:1 mixtures of Thr(Ac)-His-Lys and Cu(II) at various pH values (shown on Figure).

Unlike the His-Lys system (Section 5.3.4.1), as the pH increases from 4.3 to 8.5 the observed λ_{max} stays practically the same, i.e. 600 ? 5nm. This value is in excellent agreement with the predicted values of 599 nm (74B, 99PD) and 595 nm (01MM) for coordination by 1 amino N, 1 amide N, 1 imidazole N and 1 oxygen atom of either COOH or H_2O. This suggests the simultaneous binding of these donor atoms to Cu(II) for Thr(Ac)-His-Lys, in contrast to the successive deprotonation and subsequent binding of each of the ligand for His-Lys as pH increases from ~ 4 to 8. One major species, $(HLH_{-1})Cu$, seem to be formed between pH 4.3 to 8.5 (Figure 5.15a) with the maximum absorptivity (ε_{max} = 77 dm^3 mol^{-1} cm^{-1}) occurring at pH ~8.5.

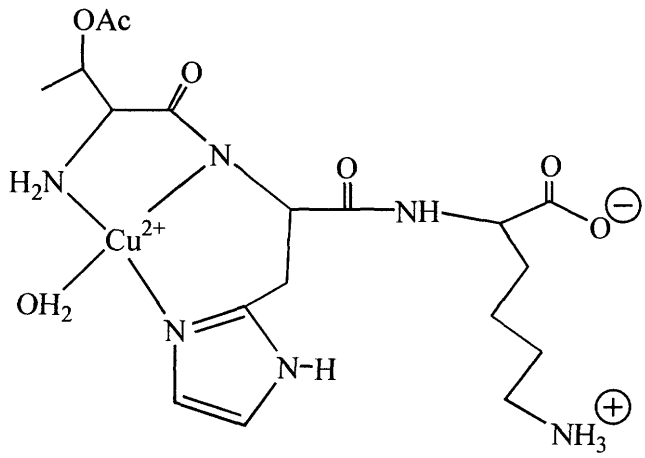

(a) = $(HLH_{-1})Cu$

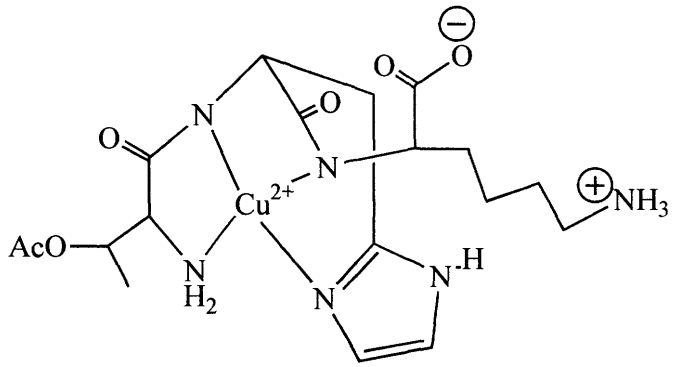

(b) = $(HLH_{-2})Cu$

Figure 5.15: Proposed structures of Thr(Ac)-His-Lys-Cu(II) complexes formed at (a) pH 4 – 8.5 (b) pH > 8.5.

The above observation is in accord with the difference in the acid-base speciation of the two peptides (compare Figure 5.5 to Figure 5.3). Unlike His-Lys, the pK_a values for Thr(Ac)-His-Lys signifying the protonation of the imidazolium group and the α-ammonium groups are very close, 6.31 and 6.78 respectively as compared to 5.63 and 7.27 for His-Lys (Sections 5.3.1 and 5.3.2). Thus, the HL-containing species in Thr(Ac)-His-Lys are formed in significant amounts over a wide pH range of ~ 5 to 12 and dominate all the other species over a wider pH range of ~ 7 to 11 (Figure 5.5). The dominance of H_2L in His-Lys for the pH range ~5.5 to 7, however limits the pH range where HL is dominant (Figure 5.3). Thus unlike Thr(Ac)-His-Lys, as pH is increased from ~ 4 to 8, different species predominate, and these in preference over the minor ones form different and more Cu(II) complexes with the various His-Lys species.

Beyond pH 8.5 for the Thr(Ac)-His-Lys case, there is deprotonation of the other NH to allow a coordination mode involving 2 amide N atoms, 1 amino N, 1 imidazole N (Figure 5.15b) whose predicted λ_{max} = 540 nm (74B) is in agreement with the observed λ_{max} 541 nm. This type of bonding has also been observed in an X-ray study of Cu(II)-Gly-Gly-His-N-methylamide (76CC).

5.3.6.2 ^{1}H NMR Studies at pH 7

The same trend in chemical shifts is observed for (Thr(Ac)-His-Lys) and Cu(II) complexation at pH 7 as was observed for the His-Lys counterpart (Section 5.3.4.2), but the changes in chemical shifts for the various protons was smaller. The smaller changes in chemical shift suggest weaker interaction between Thr(Ac)-His-Lys and Cu(II) ions than His-Lys and Cu(II) ions at pH 7. This conclusion is supported by the observation that the imidazole CH protons are less affected by line broadening in the case of Thr(Ac)-His-Lys than the His-Lys.

Further, the Lys protons were all observable even when an excess amount of Cu(II) was added to Thr(Ac)-His-Lys. This clearly indicates the non-involvement of both the carboxylate and the His-Lys amide N in the Cu(II) coordination at neutral pH.

The amide N implied in the Cu(II) coordination from the visible absorption spectra (Section 5.3.5.1) is therefore the Thr-His peptide N (the one closer to β-His and better suited for coordination to Cu(II)).

The above suggests the structure shown in Figure 5.15a for the (Thr(Ac)-His-Lys)-Cu complex species, $(HLH_{-1})Cu$ at pH 7. This structure is consistent with the pronounced paramagnetic broadening effects observed for the His β-CH_2 protons, and the relatively minor chemical shift changes observed for the Lys protons. This tridentate coordination of Thr(Ac)-His-Lys to Cu(II) is similar to the proposed structure of (His-Lys)-Cu in Figure 5.10d. It is also consistent with the observations that the chemical shifts of Lys protons in the latter are more affected than in the former, whereas the His β-CH_2 signals in both cases are affected similarly.

5.3.7 Comparison of the Coordination Modes of (His-Lys)-Cu and (Thr(Ac)-His- Lys)-Cu

Despite the proposal above for the coordination of His-Lys and Thr(Ac)-His-Lys to Cu(II) at neutral pH, the proposed structures (Figure 5.10d and Figure 5.15a) do not fully account for the differences observed in the broadening of the imidazole CH protons, as well as differences in the chemical shift behavior of the Lys protons as Cu(II) is added to the two peptides. Although it was concluded above that the binding was stronger in the His-Lys case, the mode of coordination in the two structures is identical. Perhaps the Thr-side chain introduces some steric hindrance, thereby weakening the coordination with Cu(II) in the case of Thr(Ac)-His-Lys.

5.3.8 Cu(II) Complexation to Asp-Thr(Ac)-His-Lys

5.3.8.1 UV/visible Spectra

The visible spectra of 3.0 m**M** 1:1 mixture of Cu(II) and Asp-Thr(Ac)-His-Lys in the pH range 2.80 to 12.20 is shown in Figure 5.16. Table 5.5 is a summary of the possible donor atoms for the various species at different pH values, based on

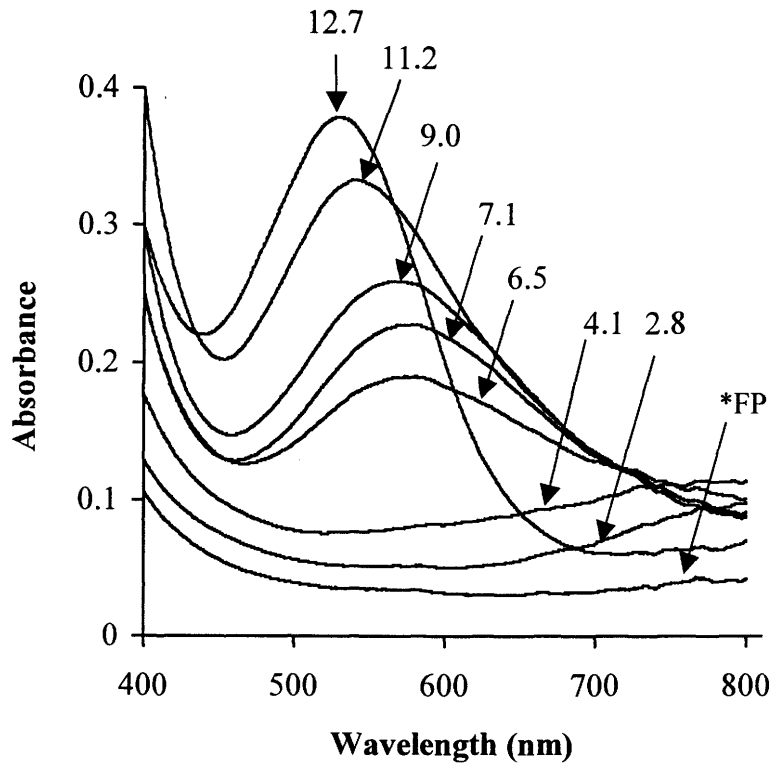

Figure 5.16: The UV/visible absorption spectra of 1:1 (Asp-Thr(Ac)-His-Lys):Cu(II) mixture of concentration 3.0 mM at various pH values between 2.80 and 12.7. *FP refers to visible spectra of "free peptide" at pH ~ 3.

experimental and calculated λ_{max} (Equation 5.3 and Table 5.3). There is generally, a good agreement between the observed and all the calculated λ_{max} for the various species. The almost featureless spectra obtained between pH 2.8 and pH 4.0 indicates no significant coordination of Asp-Thr(Ac)-His-Lys to Cu(II). Between pH 6.5 to 9 broad peaks at λ_{max} 576 ± 8 nm are observed for bright blue aqueous solutions which are due to coordination of O and /or N-donor groups to Cu(II). The average predicted λ_{max} for the visible absorption spectra using Equation 5.3 and coefficients obtained from the three different sources (Table 5.5) when the coordinating groups are an amino, a peptide N-, a carboxylate and a N(3)-imidazole nitrogen is about 581nm, in good agreement with the experimental value of 581 nm. The species so formed reaches its maximum absorptivity (ε = 86 dm^3 $mol^{-1}cm^{-1}$) at pH ~ 9. There is then a gradual blue shift as the pH of the solution is increased above 9, an indication of the involvement of more

Table 5.5: Experimental and calculated λ_{max} values based on the different ν values as referenced in brackets, together with possible donor atoms for mixture of 1:1 Cu(II) and Asp-Thr(Ac)-His-Lys at different pH values. λ_{max} in nm and ε_{max} in $dm^3\ mol^{-1}cm^{-1}$.

pH	Possible Donor atoms	Expt. λ_{max}	ε_{max}	Cal. λ_{max} (74B)	Cal. λ_{max} (99PD)	Cal. λ_{max} (01MM)
6.5	$1N^-$, $1NH_2$, $1N_{im}$, COO^-	581	63	585	577	580
7.09	$1N^-$, $1NH_2$, $1N_{im}$, COO^-	576	76	585	577	580
	or					
7.09	$2N^-$, $1N_{im}$, COO^-	576	76	574	565	567
9.0	$2N^-$, $1N_{im}$, COO^-	569	86	574	565	567
11.2	$2N^-$, $1NH_2$, $1N_{im}$,	541	112	539	536	531
12.7	$2N^-$, $1NH_2$, $1N_{im}$,	530	126			

nitrogen atoms in the coordination to form another species (purple in color). The formation of this species seems to be complete (maximal absorptivity) when the pH = 11.2. The λ_{max} of the species is 541 nm and the absorptivity is 112 $dm^3\ mol^{-1}\ cm^{-1}$. This value agrees very well with a calculated one of 539 nm (Table 5.5) for the coordinating groups of two dissociated peptide, 1 amino and N(3)-imidazole nitrogens.

5.3.8.2 ^1H NMR Studies at pH 7

Paramagnetic linebroadening

Figure 5.17 (b to g) shows the ^1H NMR spectra for the amide protons, ammonium protons and aromatic proton region obtained from a phosphate buffer solution at pH 7.0 of a 9.6 m**M** Asp-Thr(Ac)-His-Lys aqueous solution as different amounts of Cu(II) are added . Figure 5.17a shows the ^1H NMR spectra of these peaks in water adjusted with a concentrated HNO_3 to a pH of ~ 3.0, and demonstrates the substantial shift in the chemical shifts of some of the resonances as the pH changes from ~ 3 to 7. Figure 5.17a shows the ^1H NMR spectra of these peaks in water adjusted with a concentrated HNO_3 to a pH f ~ 3.0, and demonstrates the substantial shift in the chemical shifts of some of the resonances as the pH changes from ~ 3 to 7.

The disappearance of the imidazole C-2 signal, at a chemical shift of ~ 8.1 ppm, and of the His β-CH_2 proton signal, at a chemical shift of ~ 3.2 ppm, when about a fifth of an equivalent of Cu(II) is added (Figure 5.17e) is due to the paramagnetic broadening effect (Sections 5.3.4.2 and 5.3.5.2). Although there is substantial reduction of the intensity of the imidazole C5-H peak at ~7.12 ppm under these conditions, indicating some proximity to the paramagnetic Cu(II), this signal and the imidazole N1-H were both recognizable even at a peptide:Cu(II) ratio of 1:1. These observations support the idea that N3 and not N1 is the binding site for the imidazole group in this complex.

Furthermore, the spectra before adding any Cu(II) in both non-buffered aqueous solution (Figure 5.17a) and in buffer 7 solution (Figure 5.17b), and peak integrations, indicate the presence of another resonance (Im N3-H) overlapping with the C5-Im at a

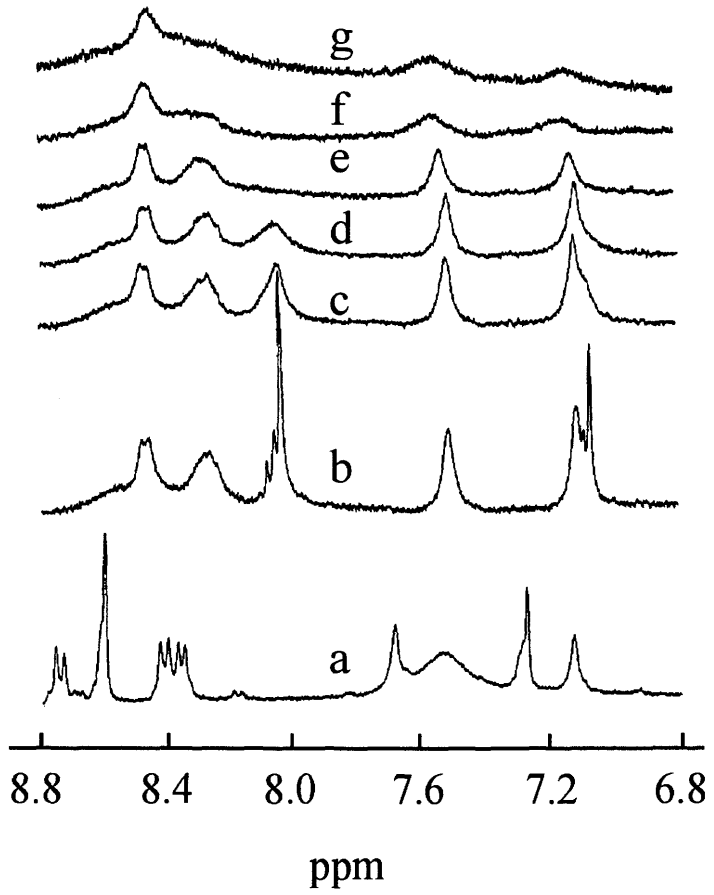

Figure 5.17: Effect of increasing Cu (II) concentration on the ^{1}H NMR spectrum of 9.6 m**M** Asp-Thr(Ac)-His-Lys.(a) "Free" peptide in water (pH ~ 2.8), (b) 0.00 mole equivalent Cu(II), (c) 0.01 mole equivalent Cu(II), (d) 0.05 mole equivalent Cu(II), (e) 0.18 mole equivalent Cu(II), (f) 0.37 mole equivalent Cu(II), (g) 0.92 mole equivalent Cu(II). (b) through (g) are in buffer solution of pH 7.

chemical shift of ~7.12. The Im N3 peak broadens out immediately on adding the initial amount of Cu(II) and also shifts downfield to make it barely recognizable, being buried under C5-Im (see Figure 5.17c). This further supports the idea of Cu(II) binding initially to Im N-3.

At Cu(II):peptide ratios > 1:1, the overlapping signals of the Thr- and His-amide NH completely disappear. This could either be due to the removal of these protons, or as a result of paramagnetic broadening, or both. In either case, this indicates binding of Cu(II) to both amide Ns. By contrast, the Lys amide NH signal, at a chemical

shift of 8.5 ppm was still visible at ~ 1:1 stoichiometry (Figure 5.17g) and even at a two-fold excess of Cu(II) over peptide it was still present (not shown). Consistent with this, the well resolved doublet due to the γ-Thr CH_3 protons also broadens out gradually upon the initial addition of Cu(II), to result in a broad singlet when about a third of an equivalent of Cu(II) has been added.

Chemical Shifts

Figure 5.18 shows the chemical shifts of the C-2 imidazole and β-His CH_2 protons as Cu(II) is added. The chemical shift changes as a function of the Cu/peptide ratio are both linear with correlation coefficients of 1.00 for the C-2 imidazole protons and 0.98 for the β-His CH_2 protons. Although the C-2 imidazole proton is closer to the N-3(Im) than the β-His protons, the changes in the chemical shifts are comparable. This suggests the involvement of another coordinating site proximal to the β-His CH_2 protons (i.e. the His-amide NH). This is confirmed by the fact that the His-amide NH experiences substantial chemical shift changes, even more than for the C-5 imidazole proton.

As shown in Figure 5.19, the chemical shift of the CH_3CO-Thr protons are more affected upon adding Cu(II) than the γ-CH_3-Thr protons. The observed changes cannot plausibly be attributed to Thr peptide N coordination, since these protons are several bonds away. A through space interaction with a binding site in close proximity i.e. COOH (Asp) is implied. Note from Section 5.3.3 that the acid-base behavior of the free peptide indicates a conformation where the CH_3CO-Thr protons are in close proximity to the COOH (Asp).

Note that the above arguments do not preclude the possible binding of Cu(II) also to the Thr amide N.

The delayed initial rise for both curves a and b in Figure 5.19 seem to suggest that some other activity than the Cu(II) complexation occurs at low Cu:peptide ratio. The abrupt tailing off for curve b at a Cu:peptide ratio of 0.5 (i.e. peptide:Cu ratio of

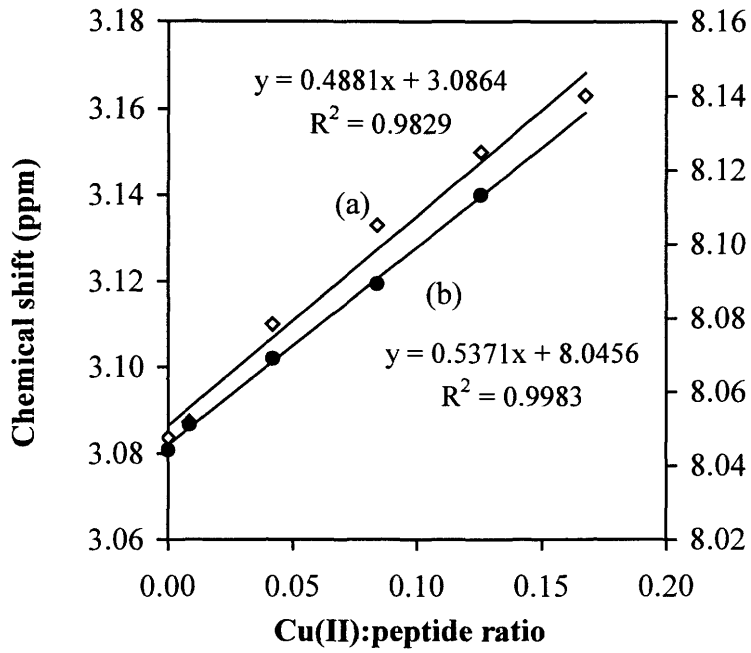

Figure 5.18: Chemical shifts of (a) β-His CH_2 (left axis) (b) Imidazole C2-H (right axis) of 9.6 mM Asp-Thr(Ac)-His-Lys as a function of Cu(II):peptide ratio.

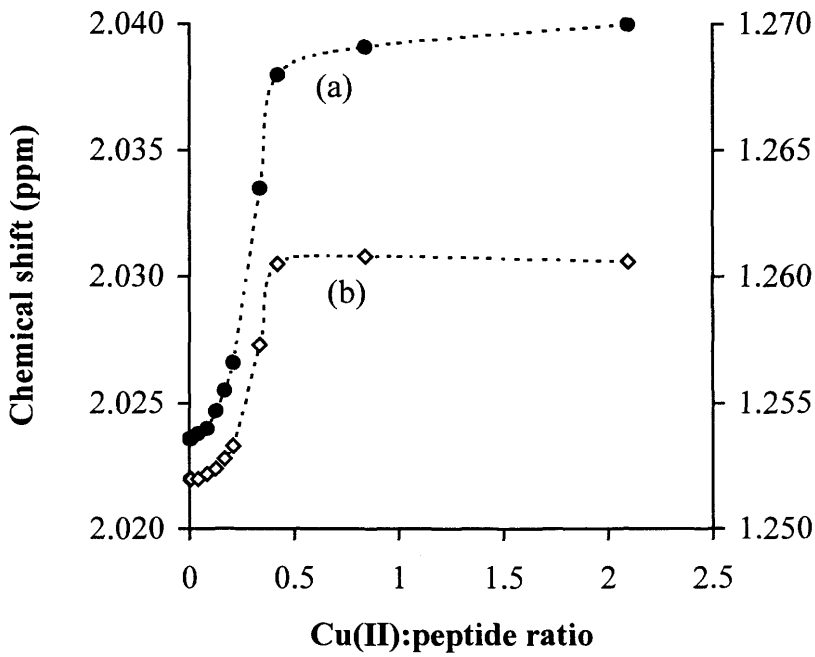

Figure 5.19: Observed changes in the chemical shift of (a) CH_3CO-Thr (left axis) (b) Thr γ-CH_3 (right axis) of Asp-Thr(Ac)-His-Lys (8.7 mM) as a function of Cu(II):peptide ratio.

2:1) seem to suggest a possible formation of a peptide-Cu complex of stoichiometry 2:1. In Figure 5.20b and to a lesser extent Figure 5.19a, two stages of the curves can be observed, an initial steep slope up to Cu:peptide ratio of 0.5 and a second stage where the slope is more gradual up to a Cu:peptide ratio of 1 at which occurs abrupt tailing off of the curve. These two curves therefore support the formation of 2:1 peptide-Cu complex at low Cu(II) concentrations, which is replaced to 1:1 as Cu(II) concentration increases.

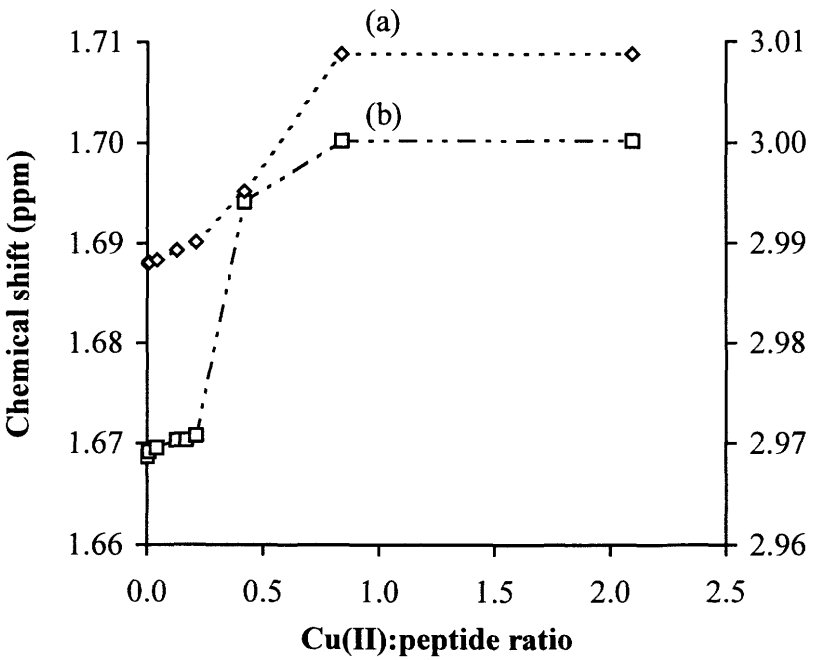

Figure 5.20: Chemical shifts of (a) ε-Lys (right axis) and (b) δ-Lys (left axis) protons of Asp-Thr(Ac)-His-Lys (8.7 m**M**) as a function of Cu(II):peptide ratio

Since the δ-CH_2 protons of the peptide display larger chemical shift changes as Cu(II) is added than the ε-CH_2 protons, it appears that the ε-NH_2 of Lys is not involved in Cu(II) complexation at pH 7. An earlier report which observed similar changes in chemical shift of Lys protons as Cu(II) was added to both BSA and HSA, attributed such changes to a conformation where the Lys ring lie over the imidazole ring of His (94ST). There was also no indication of the involvement of the Lys amide N in the complexation.

5.3.8.3 Proposed Structures of the Complexes of Cu(II) with Asp-Thr(Ac)-His-Lys

Despite the similarities in the amino acid sequence, HSA models cannot effectively model the activity of BSA, since "minor" changes such as replacing Ala with Thr can lead to differences in their coordination ability. For instance, the pK_as for the β-carboxylate, the imidazole and the amino groups were measured to be 2.98, 6.66 and 7.73 for the HSA model Asp-Ala-His-N-methylamide as compared to 4.91, 6.55, and 8.74 for the BSA model Asp-Thr(Ac)-His-Lys in this study. The difference in the pK_a values for the β-COO^- and α-amino protons are very substantial and would therefore result in a significant difference in their species distribution with respect to pH. The complex species that would be formed would therefore also be expected to differ significantly.

The ^{1}H-NMR data clearly indicate the involvement in Cu(II) binding of the N-3 His nitrogen, the amide nitrogens of His and Thr and another site closer to the Thr-side chain (the β-carboxylate and/or the α-amino nitrogen). The β-carboxylate seems to be the more likely site, since the CH_3CO-Thr protons that sense the Cu(II) coordination at this site, sense the β-carboxylate and **not** the α-amino when the free peptide is deprotonated. The ε-amino N of Lys is clearly not involved.

The visible absorption data of Asp-Thr(Ac)-His-Lys and Cu(II) mixtures at pH 7.1 display a broad absorption maximum centered at 576 nm, whose closest predicted (averaged) λ_{max} based on the three coefficients in Table 5.3 are respectively 581 and 569 nm for the two possible coordination modes {N^-, $1NH_2$, $1N_{im}$, $1COO^-$} and {$2N^-$, $1N_{im}$, $1COO^-$}(see Table 5.5 for details). Since the involvement of the imidazolium, carboxylate, and the amide nitrogens of His and Thr are clearly indicated by both the NMR and visible spectroscopic studies at pH ~ 7, the latter coordination is implied at that pH value. Nevertheless, the former coordination also needs further consideration, since the NMR study, in fact, did not rule out the possibility of the involvement of the α-NH_2, but rather suggested its remote involvement (Section 5.3.6.2). The observed λ_{max} (581 nm) at pH 6.5 is in excellent agreement with a

predicted value of 580 nm for {1 N^-, 1 NH_2, 1 N_{im}, 1COO^-} coordination (01MM), whilst the value observed at pH 9 (569 nm) is in excellent agreement with a predicted value of 567 nm for {2 N^-, 1 N_{im}, 1COO^-} coordination (01 MM). See Table 5.5. This suggests that the visible absorption spectra observed at approximately pH 7 is due to an equilibrium mixture of these two species.

Since pK_{a3} of Asp-Thr(Ac)-His-Lys is 8.7 (this involves deprotonation at N-terminal amino group; see Section 5.3.3), H_2L is the dominant species in the pH range of ~ 6.5 to 9 (Figure 5.8). As pH is increased through the vicinity of pK_{a3}, competition by protons for the α-amino coordinating site becomes less effective making it easier for Cu(II) to bind this site. At pH > 6.5, a simultaneous binding of Cu(II) to the imidazole N-3 nitrogen, carboxylate, a deprotonated peptide N, and the α-amino group to form a $(HLH_{-1})Cu$ complex species is therefore possible, as shown in Figure 5.21a. Further increase in pH value towards 9 can cause Cu(II)-induced deprotonation of the second amide NH bond (82SM), that is Thr amide-NH, and lead to the formation of the $(HLH_{-2})Cu$ complex species, as shown in Figure 5.21b. Both these species, $(HLH_{-1})Cu$ and $(HLH_{-2})Cu$, involve the coordination of the carboxylate group to Cu(II), in agreement with previous ^{13}C NMR findings by Lussac and Sarkar (80LS) for the HSA model , Cu-Asp-Gly-His-N-methylamide complex system between pH 4 and 6. (See Section 1.8.2).

Between pH values 9 and 11 where HL and L are the dominant species for the free peptide (Figure 5.8) the weaker coordination by the carboxylate group is replaced with the α-amino group to form the $(LH_{-2})Cu$ species, with the 4N coordination involving the α-amino group, 2 peptide N- and the Im N-3, as shown in Figure 5.21c). This results in a visible absorption band with λ_{max} = 541 nm, consistent with theoretical prediction of 539 nm (74B) for such coordination (Table 5.5). The studies of the Cu-Asp-Gly-His-N-methylamide complex system as a model of HSA suggested the same coordination environment as the $(LH_{-2})Cu$ species (Figure 5.21) but at a lower pH, between 6 to 10.

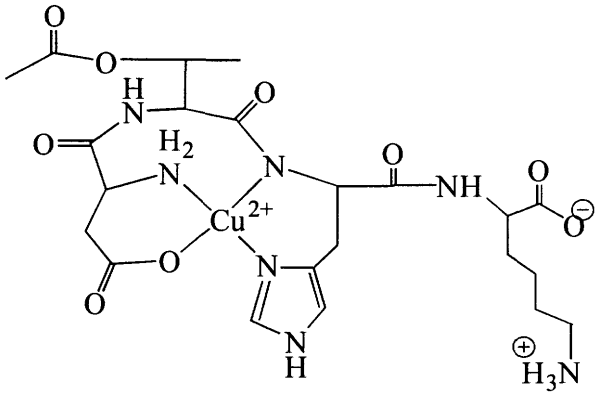

(a) = $(HLH_{-1})Cu$

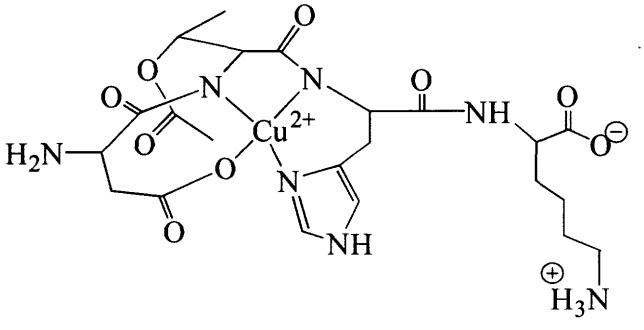

(b) = $(HLH_{-2})Cu$

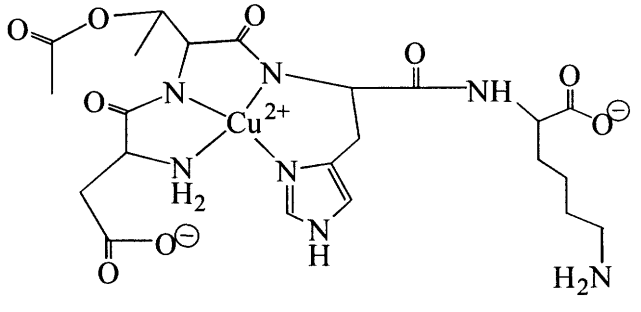

(c) = $(LH_{-2})Cu$

Figure 5.21: Possible structures of (Asp-Thr(Ac)-His-Lys)-Cu(II) complexes at pH (a) 6.5 (b) 9 (c) 11.2

5.3.8.4 Binding Strength of Cu(II) to AspThr(Ac)-His-Lys

The NMR chemical shift of the imidazole C5-H proton of Asp-Thr(Ac)-His-Lys (9.6 mM) in a buffer solution of 7 was measured as a function of [Cu(II)] (Figure 5.22).

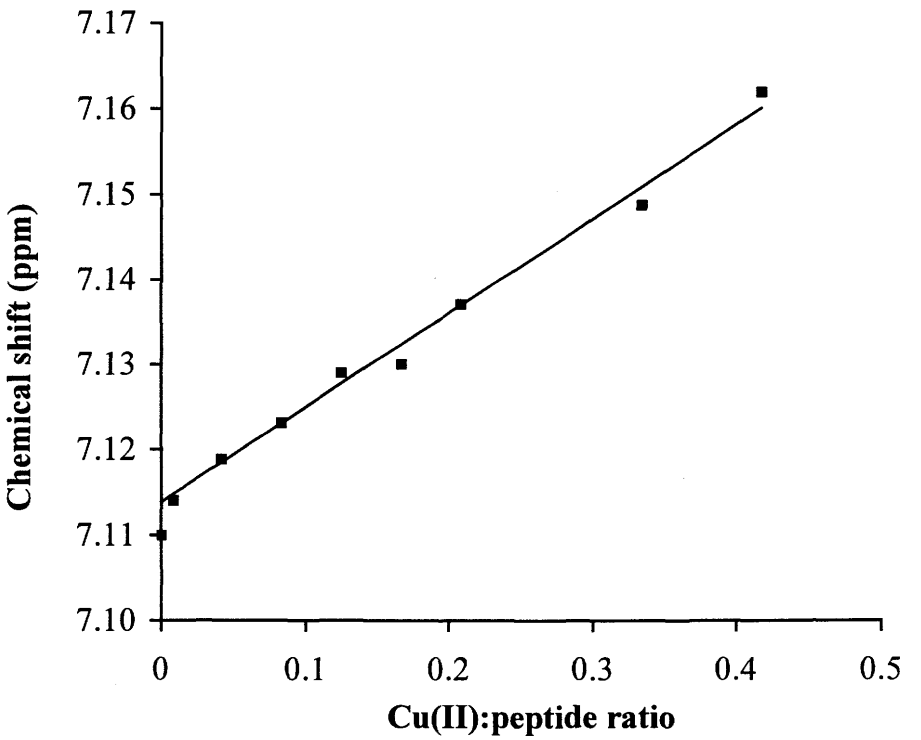

Figure 5.22: Observed and predicted chemical shifts of the Im C-5 proton of Asp-Thr(Ac)-His-Lys in a buffer solution of pH 7 as a function of the Cu(II): peptide ratio. The solid line is predicted based on the model described in the text (Section 5.3.8.4).

The equilibria involved in the (Asp-Thr(Ac)-His-Lys)-Cu(II) aqueous system at pH 7 can be expressed as follows:

$$H_3L \rightleftharpoons H_2L \quad K_{a1}$$

$$H_2L \rightleftharpoons HL \quad K_{a2}$$

$$HL \rightleftharpoons (HLH_{-X})Cu \quad K_{f1}$$

As discussed in Section 5.3.6.3, the two main Cu(II)- complexed species of Asp-Thr(Ac)-His-Lys ($(HLH_{-1})Cu$ and $(HLH_{-2})Cu$ both involve the HL species of the peptide; since the difference between the two is the loss of a proton, with a value of a pKa connecting the two, at any given pH the ratio of the two is constant. Hence for simplicity these two species are treated as one composite species, $(HLH_{-x})Cu$. Only one averaged chemical shift, δ_{obs} , is actually observed for each resonance, indicating that exchange between free and Cu(II)-complexed Asp-Thr(Ac)-His-Lys species is fast on the NMR timescale. The observed chemical shift in each case is therefore the average of those of the individual species, weighted by their relative amounts:

$$\delta_{obs} = \delta_{H3L}\alpha_{H3L} + \delta_{H2L}\alpha_{H2L} + \delta_{HL}\alpha_{HL} + \delta_{CuHLHx}\alpha_{Cu(HLHx)} \quad \textbf{(5.4)}$$

where δ_x refers to the chemical shift of a given species x, and α_x its mole fraction. α values can be calculated from the acid dissociation constants, formation constants and the pH values of the solutions. The pH in this case is constant at 7.0. The calculation is done using the formulae in the equations shown in Appendix I: As derived in Appendix I, the quadratic Equation 5.5 can be obtained and solved for [Cu] at equilibrium for each data point:

$$[Cu]^2.K_f + [Cu]\{1/\alpha_{HL} + K_f(C_L - C_{Cu})\} - C_{cu}/\alpha_{HL} = 0 \quad \textbf{(5.5)}$$

Since the chemical shifts and the acid dissociation constants of free Asp-Thr(Ac)-His-Lys were determined in Section 5.3.3, the only unknown parameters in Equations 5.4 and 5.5 are the formation constant and the chemical shifts of the $HLH_{-x}Cu$ complex species. The non-linear least squares regression analysis described in Section 5.3 can be used to fit the predicted chemical shift to the observed chemical shift in an attempt to extract the chemical shifts and the formation constant of the HLCu complex species. The resultant fit of predicted to experimental values are shown in Figure 5.22. The predicted fit was found not to depend on the value of K_f. The linearity of the relationship (Figures 5.22) suggested that the equilibrium lay well to right for the complexation of Cu(II) to the tetrapeptide at pH 7. As discussed in Chapter 3, if the

binding is sufficiently strong, then the mole fraction of complexed formed (i.e.αHLCu) is simply proportional to the amount of Cu added.

An alternative approach to estimating strength of binding is to set up a competition for Cu(II) by the peptide and another ligand of established formation constant. Such competition was carried out between Asp-Thr(Ac)-His-Lys and Lysine, by observing the chemical shift changes of Im C5-H as increasing amounts of Cu(II) were added to the peptide, in the presence and absence of 1.25 mole equivalents of Lys (Figure 5.23). In the absence of any interaction between the Lys and the tetrapeptide, the chemical shift of the Im C5-H proton of the peptide should be the same in the presence or absence of the Lys when no Cu(II) has been added. This is not the case in Figure 5.23, suggesting some interaction between the Lys and the peptide, perhaps hydrogen-bonding interaction.

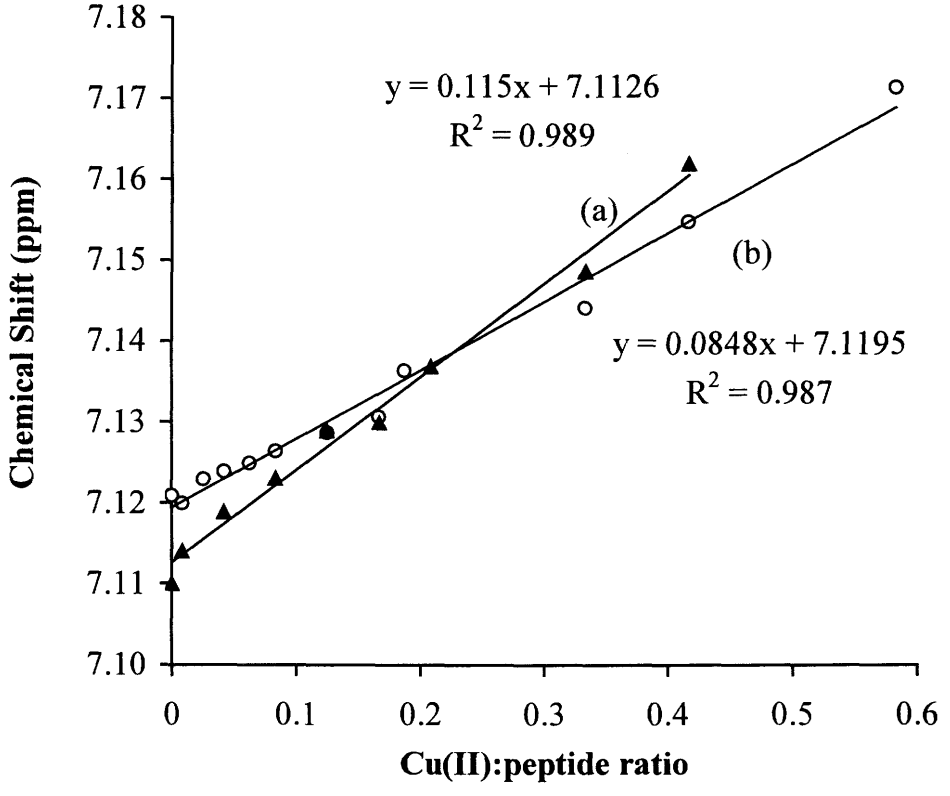

Figure 5.23: Chemical shift of the Im C5-H resonance of 9.7 mM Asp-Thr(Ac)-His-Lys in the presence and absence of 1.25 mole equivalent of Lys as increasing amounts of Cu(II) were added.

As expected, the chemical shift in both the presence and absence of Lys increases monotonically. The presence of Lys decreases the slope from 0.115 to 0.085, indicating that Lys competes with Asp-Thr(Ac)-His-Lys for Cu(II) and that the latter exhibits 3.5 (i.e. (0.085*1.25)/(0.115-0.085) fold stronger binding to Cu(II) than does Lys. (This is only true assuming no ternary complexation between Lys, the peptide and Cu(II) occurs). Cu(II) complexation to Lys has been well studied by Dr. Reid's research group over a pH range of 2-13 (96AR, 98RA). The dominant species at neutral pH is CuL_2H_2 with a $\log\beta = 35.90$ formation constant (96AR). The formation constant of (HLHx)Cu complex species of the (Asp-Thr(Ac)-His-Lys)-Cu system at pH 7.0 is therefore $\log\beta = 36.45$ (i.e 35.90 + log 3.54).

5.4 CONCLUSIONS

As part of the broad objective of investigating interactions between Cu(II), TMs, and BSA, the acid-base behavior of the BSA model peptides His-Lys, Thr(Ac)-His-Lys, Asp-Thr(Ac)-His-Lys was studied by ^{1}H NMR, and Cu(II) complexation by both ^{1}H NMR and visible spectroscopy. Despite the paramagnetic nature of Cu(II) ions, solution ^{1}H NMR studies proved very insightful in elucidating the binding sites and the relative strengths of Cu (II) binding to these peptides. Complemented by some visible absorption data, this study proposed structures for Cu(II)-HisLys, Cu(II)-Thr(Ac)-His-Lys and Cu(II)-Asp-Thr(Ac)-His-Lys systems in solution at different pH values.

Asp-Thr(Ac)-His-Lys coordinates with Cu(II) at neutral pH to form a square planar complex involving the His imidazole N3, the Thr and His amide nitrogens and the β-carboxylate oxygen. The well known proposal of a square planar complex involving the α-amino nitrogen, the two amide nitrogens and ImN3 occurs at higher pH. The binding of Cu(II) to Asp-Thr(Ac)-His-Lys is approximately 3.5 times stronger than that to Lys at neutral pH. These findings should serve as basic information for understanding BSA-Cu(II) and (His-containing peptide)-Cu interactions in biological systems.

6. TERNARY COMPLEXATION BETWEEN SMALL PEPTIDE MODELS, Cu(II) and THIOMOLYBDATES

6.1 INTRODUCTION

As discussed in Section 1.5.2.2, bovine serum albumin (BSA), Cu(II) and TM3 are known to participate in a three-way (tripartite) interaction. In the studies described in Section 3.3.3 this was confirmed, and the interaction was demonstrated to extend to the other TMs, especially TM4.

This tripartite interaction is of considerable biochemical relevance, since TMs prevent Cu(II) absorption in ruminants by forming polymeric and/ or insoluble products which are not absorbable. In the presence of albumin, however, this polymerization is prevented, as evidenced by the soluble nature of the ternary complex involving albumin in aqueous solutions (see Section 3.3.3). Also, Cu(II) removed from the storage organs in both ruminants (87WM, 91S) and non-ruminants like rats (98OS) and humans (00CO) is thought to form a BSA-Cu-TM complex. However, the active site on the albumin where this interaction occurs, and the details of what is actually occurring, are unknown. Some ideas based purely on conjecture have been reported in the literature and were discussed in Section 1.5.2.2.

TMs can react with thiols (RSH, where R is any alkyl group), as discussed in Section 1.2.5, and hence it might seem possible for TMs to bind the only free cysteine –SH group on albumin in a similar fashion. Closer examination rules out this possibility, since there is no difference in the interaction of TM4 with commercially available cysteine-protected BSA or normal BSA (87CLa). The idea of possible covalent disulfide formation (sulfur from TM bonding with S from the free cysteine-SH

group on albumin) had also been ruled out in the past for the same reason (87CLa). Furthermore, the interaction between TM and albumin-Cu is affected substantially by pH and ionic strength, suggesting that the binding to albumin is ionic (87CLa, 87WM) and not covalent as is expected for a disulfide bond formation.

This chapter reports investigations into tripartite interactions involving BSA, Cu(II) and TMs, using peptide models to represent BSA. The dipeptide His-Lys, whose synthesis and characterization was described in Chapter 4, and which was used as a simple BSA model in Chapter 5 for Cu(II) complexation studies, was the main model used to test whether the N-terminal of albumin is or is not involved in the interaction. The techniques used for the studies were ^{1}H NMR and UV/visible spectroscopy. To see if the findings from the His-Lys studies held for His-containing peptides in general, some experiments were also conducted using the other two peptide models of BSA discussed in Chapters 4 and 5 (i.e. Thr(Ac)-His-Lys and Asp-Thr(Ac)-His-Lys).

6.2 EXPERIMENTAL

6.2.1 Sources of Chemicals

L-histidine was obtained from Sigma Chemical Co. (St. Louis, USA). All other reagents were obtained as detailed in Sections 4.2.3 and 5.2.1. The TM salts $(NH_4)_2MoS_4$, Cs_2MoOS_3 and $(NH_4)_2\ MoO_2S_2$ were synthesized and characterized as described in Chapter 2.

6.2.2 Instrumental Measurements

The elemental analyses and the NMR measurements were performed as described in Sections 2.2.4 and Section 5.2.2 respectively. UV/visible spectra were also measured as in Section 5.2.2, but with a Cary model 100 recording spectrophotometer at 1 nm intervals over the wavelength range 230 to 700 nm. For quantitative studies, data were recorded at 1 nm intervals for the wavelength range 236 to 600 nm.

6.2.3 Preparation of Solutions for UV/visible Spectrophotometry Measurements

2.5 mL portions of a 2 x 10^{-4} **M** 1:1 His-Lys:Cu(II) stock solution were pipetted into a series of 5.0 mL volumetric flasks. Different amounts (0, 5, 10, 15, and 25 μL) of a 2 x 10^{-2} **M** stock solution of the relevant TM were pipetted into flasks to make solutions containing His-Lys, Cu(II) and TM with mole ratios 1:1:0, 1:1:0.2, 1:1:0.4, 1:1:0.6 and 1:1:1 respectively. Each flask was filled to the mark with a mixed phosphate buffer of pH 7.0 and ionic strength 0.2 **M** and shaken. The pH 7.0 buffer solution was used as solvent throughout these studies and was prepared as outlined in Section 3.2.2.

The UV/visible spectrum was taken for each solution as described in Section 6.2.2, 60 min after adding the TM. The TMs (TM2, TM3 and TM4) react at different rates with Cu(II) to form insoluble products, as discussed in Section 3.3.1. This was also observed for these experiments involving peptide-Cu complexes. Hence, the delay of 1 hr prior to spectral measurement was selected as a "compromise" time to allow a significant completion of the reaction involving the various TMs (see Section 6.2.4 for details), whilst at the same time avoiding the precipitation of the resulting products. Even within the 1 hr period, solutions that contained TM4 of concentrations higher than 6 x 10^{-5} **M** in the reaction mixture formed fine precipitates, and therefore their spectra were not used for any quantitative assessment. Although TM3 and TM2 in their relevant reaction mixtures, at the concentration of 6 x 10^{-5} **M**, did not form any insoluble product visible to the naked eye within the 1 hr period (they formed the insoluble products later- see Section 6.3.1 for details), the spectra data obtained for the reaction mixtures containing these TMs, at concentrations greater or equal to the value above, were also not used for quantitative assessment.

6.2.4 Preparation of Solutions for NMR Measurements

A stock 0.2 **M** Cu(II) solution was prepared by dissolving 4.9937 g of $CuSO_4.5H_2O$ in 0.2 **M** KNO_3, diluting to volume in a 100 mL volumetric flask. Freshly prepared 2.00 x 10^{-2} **M** TM2, TM3 and TM4 were made by dissolving accurately

0.00528 g, 0.00948 g and 0.00520 g of $(NH_4)_2MoO_2S_2.2H_2O$, $(Cs)_2MoOS_3$ and $(NH_4)_2MoS_4$ respectively in 1 mL of a mixed pH 7.0 phosphate buffer, ionic strength 0.2 **M**, prepared as outlined in Table 3.2 (Section 3.2.2). The exclusion of oxygen was ensured as discussed in Section 5.2.4. DSS was added to each sample as a chemical shift reference. Three types of NMR experiments were performed as outlined below in Sections 6.2.4.1, 6.2.4.2, and 6.2.4.3:

6.2.4.1 Monitoring the reaction as a function of Time

To prepare a reaction mixture of His-Lys, Cu(II) and TM2 of approximate ratio 13: 1:1, 0.00642 g (11.48 μmol) of His-Lys was weighed directly into a standard 5 mm flat-bottomed NMR tube and dissolved in 0.5 mL of buffer 7 solution. 4.4 μL of the stock 0.2 **M** Cu(II) was added to the dissolved His-Lys solution in the NMR tube. 1 mole TM2 equivalent of Cu(II) (44 μL of 2.00×10^{-2} **M** TM2) was added to the contents of the NMR tube. The same quantities and procedure were followed to prepare an approximately 13: 1: 1 reaction mixture of His-Lys, Cu(II) and TM3. For the reaction involving TM4, two different reaction mixtures of approximate ratios 11:1:1 and 26:1:1 were prepared. The mixtures in the NMR tubes were prepared from 0.0027 g (4.83 μmol) His-Lys, 2.2 μL of 0.2 **M** Cu(II) and 22 μL of 2.00×10^{-2} **M** TM4 for the former ratio and 0.00637 g (11.39 μmol) His-Lys, 2.2 μL of 0.2 **M** Cu(II) and 22 μL of 2.00×10^{-2} **M** TM4 for the latter. The ^{1}H-NMR spectrum of each of the resulting reaction solutions was monitored at approximate times of 0, 5, 10, 15, 30, 45, 60, 120, 180, 240 min after the addition of the relevant TM. The actual recorded times have been specified in Section 6.3.2.

The same procedure as above was used to prepare reaction mixtures of Thr(Ac)-His-Lys, Cu(II) and TM (TM2, TM3 or TM4) of approximate ratio 13:1:1. For each TM, 0.0084 g of Thr(Ac)-His-Lys, 4.4 μL of 0.2 **M** Cu(II) and 44 μL of 2.00×10^{-2} **M** of the relevant TM were mixed in an NMR tube as outlined above.

6.2.4.2 The Stoichiometry of Cu(II):TM4 for the reaction

To evaluate the Cu(II):TM4 stoichiometry of reaction in the ternary reaction involving His-Lys, 0.00571 g (10.21 μmol) of His-Lys was weighed directly into a standard 5 mm NMR tube and dissolved with 0.5 mL pH 7.0 buffer solution. 2 μL of 0.2 **M** (0.4 μmol) Cu(II) solution was added. Different reaction mixtures of different Cu(II):TM4 ratios, but in the fixed reaction amount (moles) of the peptide, were prepared in the same NMR tube by spiking in succession to the content of the NMR tube, at 1 hr interval, a relevant volume of 2×10^{-2} **M** TM4. In this case, 4 μL, 2 μL, 4 μL, 4 μL, 4 μL, 4 μL, and 10 μL, of the TM solution were spiked in succession to obtain a cumulative (total) volume of 0 μL, 4 μL, 6 μL, 10 μL, 14 μL, 18 μL, 22 μL, and 32 μL of the TM solution in the resulting reaction mixture. The time interval of 1 hr between each addition was to ensure that the reaction had essentially come to completion at each stage of the addition, as suggested by the observations in experiment (1) above (see Section 6.3.2. for details).

To evaluate the Cu(II):TM4 stoichiometry in the ternary reaction involving Asp-Thr(Ac)-His-Lys, the same procedure was followed. 0.00667 g (8.0 μmol) of Asp-Thr(Ac)-His-Lys was dissolved in 0.5 mL pH 7.0 buffer solution, and 1.63 μL of 0.2 **M** (0.326 μmol) Cu(II) solution added. 2×10^{-2} **M** TM4 were added in succession such that the resulting reaction mixtures at the various stages contained 0 μL, 5 μL, 8 μL, 15 μL and 25 μL of the TM solutions.

6.2.4.3 The Involvement of Peptides

The third experiment was performed to determine the involvement of the peptide in the tripartite interaction between His-Lys, Cu(II) and TM4. Two separate solutions (A and B) each containing the same amount of peptide and of equal total volume of solution, but in the presence of Cu(II) and TM4 (A) or their absence (B), were prepared as follows.

(A) 0.0057 g of His-Lys was weighed accurately directly into a 5 mm NMR tube. 0.4 mL of pH 7.0 buffer was added to dissolve the peptide. 4 μL of 0.2 **M** Cu(II) was added to the His-Lys solution to form a pale blue solution. 50 μL of 2.00 x 10^{-2} **M** TM4 was then added to obtain a reaction mixture of His-Lys, Cu(II) and TM4 of ratio 12.74:1:1.25. The solution was shaken to dissolve the His-Lys. 7μL of a diluted DSS solution was added to the NMR tube.

(B) The same procedure as (A), except that 0.454 mL pH 7.0 buffer was added in place of the Cu(II) and TM4 solutions, to ensure that the total volumes of the two solutions were equal and that the concentrations of the peptide in the two reacting mixtures were the same.

The spectrum of each of the two solutions was taken immediately on adding TM4 (where applicable) as well as 30 min and 20 hr after the TM4 addition. The integrals of the various His-Lys signals for solution A, at the three different times, were determined, and normalized to that of the DSS signal at 0 ppm. The same process was followed for solution B and the corresponding integral values compared.

6.2.5 Sample Preparations for Elemental Analyses

The procedure for obtaining solid products for the ternary interactions between His-Lys, Cu(II) and TM4 was as follows: 0.02066 g (37.0 μmol) His-Lys was weighed directly into a 5 mL glass vial and dissolved with about 0.4 mL of pH 7.0 phosphate buffer. In a drop wise fashion with occasional shaking, about 1 mole equivalent of Cu(II), i.e., 0.185 mL 0.2 **M** stock solution, was added. A TM4 solution containing 0.0095 g (36.5 μmol) TM4 in ~ 2 to 3 mL pH 7.0 phosphate buffer was added, and the mixture stirred magnetically for 20 to 30 min and then allowed to stand for about 8 hr. The mixture was centrifuged and the supernatant decanted. Distilled water was added to the precipitate, the mixture re-centrifuged and the supernatant again decanted. This washing process was repeated three more times. A similar procedure was used in the TM3 and TM2 cases.

Another experiment was conducted for the TM4 case. Exactly 0.185 mL of 0.2 **M** (37.0 μmol) Cu(II) was added to 0.02029 g (36.3 μmol) His-Lys. 0.01015 g (39.0 μmol) of TM4, dissolved in about 1 mL of pH 7.0 buffer solution was added, and the mixture stirred for about 20 min and allowed to stand for about 1 hr. The solid product was washed as described above.

The same product was also obtained by adding exactly 0.416 mL of 0.2 **M** (83.2 μmol) Cu(II) to 0.0126 g (81.2 μmol) of the His-Lys. 0.0228 g (87.6 μmol) of TM4 dissolved in about 2 mL of pH 7.0 buffer solution was added, and the mixture stirred for about 20 to 30 min and allowed to stand for about 8 hr. The washed solid product was obtained as in the two cases above.

6.3 RESULTS AND DISCUSSION

6.3.1 Solubility of the Ternary Complexes

In Sections 6.3.2, 6.3.3 and 6.3.4 the evidence that ternary complexes form between the peptide models, Cu(II) and TMs are provided.

Although the emphasis of this chapter is on interactions in aqueous solution of mixtures of His-containing peptides, Cu(II) and TMs, the complexes formed have very low solubility in water, hence demanding some comments on the solubility of the products. No quantitative study was actually conducted to determine the solubilities of the ternary complexes formed, but some qualitative observations which are of relevance in the understanding of the tripartite interaction involving a peptide, Cu(II) and a TM are presented in this section.

As in the case of the Cu-TM complexes (Chapter 3), these ternary complexes form insoluble products in solutions of high ionic strength. Rates of precipitation were higher in the presence of His and His-containing peptides than in their absence. For instance, for the UV/visible experiment described in Section 6.2.3, the sample

containing His-Lys, Cu(II), and TM3 in the ratio 1:1:1 at a concentration of 1 x 10^{-4} **M**, precipitated in less than 2 hr, whereas a sample containing only 1:1 Cu(II):TM3 at the same concentration precipitated only after 9 days. The same trend was also observed for both TM4 and TM2; the insoluble product was formed sooner after the addition of the TM in the presence of the peptide than in its absence. In the case of TM2, this was especially dramatic; although addition of one mole equivalent of TM2 to 1:1 mixture of His-Lys and Cu(II) (1 x 10^{-4} **M**) could form a precipitate within 24 hr, no such precipitate was observed in the absence of peptide on standing for several days. The precipitation of adduct was fastest for TM4, followed by TM3 and then TM2, as also observed for the interactions between Cu and TM when peptides were absent (Chapter 3).

These results suggest that the presence of the peptide has a significant effect on the formation of the product and/or its coagulation. Ionic strength cannot account for the differences observed in the peptide and non-peptide cases, since the added His-Lys at the concentration used in the study (i.e.1 x 10^{-4} **M**) is not expected to affect the ionic strength of the phosphate buffer solution (~ 0.2 **M**) significantly.

A more plausible explanation for the observations above is that in the presence of the peptide a different process, probably ternary complexation, is taking place. This issue is pursued below.

6.3.2 UV/visible Spectral Studies of Interactions between His-Lys, Cu(II) and TMs

The UV/visible spectra for the solutions described in Section 6.2.3 were obtained for TM2, TM3 and TM4 cases. Figures 6.1 shows the spectrum for the TM2 case. The spectrum for the TM2 alone and the binary Cu-TM2 complex is also included in the figure for comparison. There is no indication at any stage of any TM absorption peaks for the three cases. The spectra of mixtures of His-Lys and Cu(II) have no

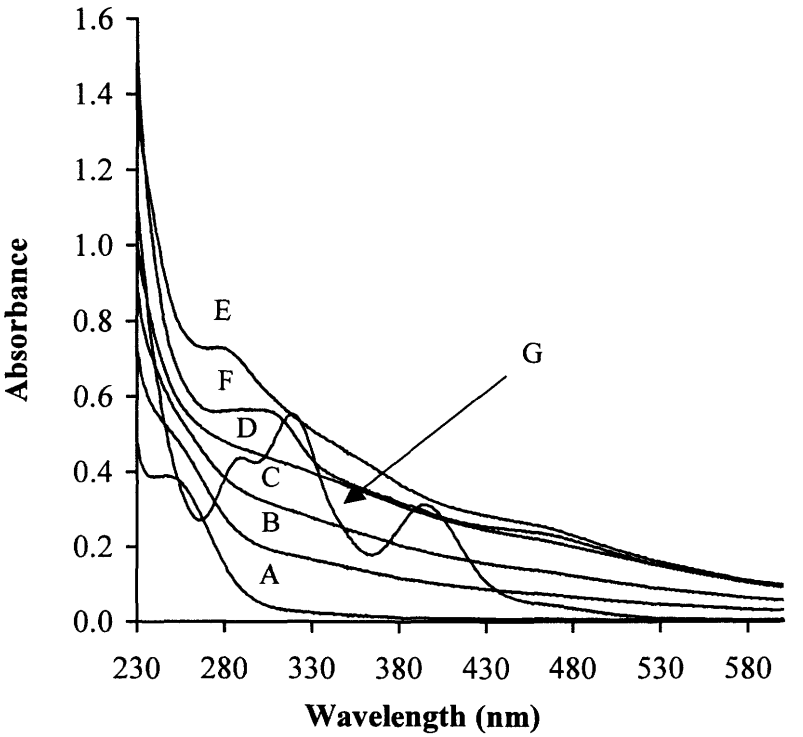

Figure 6.1: The UV/visible spectra of reaction mixtures of His-Lys, Cu(II) and TM2 at various mole ratios. (A) 1:1:0, (B) 1:1:0.2, (C) 1:1:0.4, (D) 1:1: 0.6, (E) 1:1:1 (The His-Lys and the Cu(II) concentration from A through E are each 0.1 m**M**), (F) 1:1 mixture of Cu(II):TM2 and (G) TM2 alone. The TM2 concentration for F and G is also 0.1 m**M**.

significant absorbance between the wavelengths 330 nm and 600 nm (see Figures 6.1); hence, the suppression of the TM (TM2, TM3 and TM4) peaks cannot be attributed to the sum of individual contributions from the TM and some (His-Lys)-Cu(II) interaction. If that was the case, it should be expected that at least within the regions 330 nm and 600 nm, there would be a dominance of the TM absorption peaks and this is not obviously the case as can be seen in Figures 6.1 for the TM2 case as well as both TM3 and TM4 (not shown). The loss of the characteristic peaks of the TMs seems therefore to be due to the complete reaction of a TM when added to equal or excess amounts of His-Lys and Cu(II) mixture.

The spectra obtained for the binding of Cu(II) to the TMs in the presence of the peptide are also quite different from those obtained when the peptide was absent (Compare Figure 6.1 E to F for instance). The formation of a ternary complex species involving the peptide may therefore be implied. This issue is pursed in the subsequent sections of this chapter.

6.3.2.1 Attempted Verification of Ternary Complexation Involving His-Lys, Cu and TM by a Model based on Beer's Law

Since the peptide-Cu complex shows some absorption, especially at wavelengths less than 330 nm (see Figures 6.1), it is necessary to subtract its absorbance from that observed before the absorbance of a ternary complex can be estimated. If Beer's law is obeyed, then, at any given wavelength:

$$A_{obs} = A_{Cupep} + A_{pepCuTM} \quad \textbf{(6.1)}$$

where A is absorbance and obs refers to observed, pepcu to the peptide-Cu(II) complex and pepCuTM to some ternary species. Assuming also that:
(i) the TM is never in excess
(ii) each TM added reacts completely to form complex
(iii) 1 mole equivalent of TM is required to react with the peptide-Cu

then for a cell path length of 1 cm, the following equation can be derived:

$$A_{pepCuTM} = A_{obs} - \varepsilon_{pepCu} \{[pepCu] - [TM]\} \quad \textbf{(6.2)}$$

where ε_{pepCu} is the molar absorptivity for the peptide-Cu complex. [pepCu] and [TM] are the concentrations of the peptide-Cu and the TM respectively. $A_{pepCuTM}$ is the calculated absorbance of the ternary complex, after the absorbance of the peptide-Cu remaining has been subtracted. Applying Equation 6.2 for two different values of [TM], X and Y, gives:

$$^{X}A_{pepCuTM} = {}^{X}A_{obs} - \varepsilon_{pepCu}\{[pepCu] - X\}$$

and $$^{Y}A_{pepCuTM} = {}^{Y}A_{obs} - \varepsilon_{pepCu}\{[pepCu] - Y\}$$

Since, applying Beer's Law to these corrected absorbances for the ternary complex:

$$^{X}A_{pepCuTM} = \varepsilon_{pepCuTM}.X \qquad \text{and} \qquad ^{Y}A_{pepCuTM} = \varepsilon_{pepCuTM}.Y \text{ , then:}$$

$$^{Y*}A_{pepCuTM} = (Y/X).\ ^{X}A_{pepCuTM} \tag{6.3}$$

$^{Y}*A_{pepCuTM}$ is a predicted value of $^{Y}A_{pepCuTM}$. If the model is valid, $^{Y}*A_{pepCuTM}$ and $^{Y}A_{pepCuTM}$ should be equal.

Values of $^{X}A_{pepCuTM}$ and $^{Y}A_{pepCuTM}$ were obtained from the UV/visible data taken at wavelengths every 1 nm from 260 to 600 nm (Section 6.2.2). Discrepancies in some cases were substantial. Various modifications to the model were attempted to see if the "fit" could be improved, varying various parameters, such as the stoichiometry of reaction, to minimise the residual factor R:

$$R = \Sigma_i[(^{Y}*A_{cupepTM})_i - (^{Y}A_{cupepTM})_i]^2 \tag{6.4}$$

where the summation is over all wavelengths i.

However, although some of these procedures did result in improved fits, little confidence is placed in the results. It was observed at high TM concentrations that fine precipitates, presumably of peptide-Cu-TM, could form (see Section 3.3.1), and it is also possible that these were forming even when this was not obvious to the naked eye. The difference in the quality of the fits for the various TMs supports this idea; TM4 yields the greatest discrepancies between $^{Y*}A_{pepCuTM}$ and $^{Y}A_{pepCuTM}$, and as discussed in Section 3.3.1, TM4 forms insoluble products faster than the other TMs.

It is concluded that this approach cannot yield trustworthy, quantitative information about the stoichiometry of the interaction. However, it does support the formation of a ternary complex and also suggests that the added TMs react completely with the excess peptide-Cu. The establishment of the actual stoichiometry of the ternary complex requires further studies by other methods such as NMR (Section 6.3.3) and elemental analysis (Section 6.3.4).

6.3.2.2 Implications of the Calculated UV/visible Spectral data

Table 6.1 gives UV/visible spectral data for the (His-Lys)-Cu-TM ternary complexes calculated from the model described in Section 6.3.2.1. Also in the table are spectral data for different reaction mixtures of Cu(II) and TM.

Table 6.1: Calculated UV/visible spectral data for 1:1:1 (His-Lys)-Cu-TM ternary complexes, and experimentally determined data for Cu(II)-TM reaction system.

Reaction system	λ, nm (10^{-4} ε, $M^{-1}cm^{-1}$)
Cu(II)-TM2 (experimental)	291(0.57)
(His-Lys)-Cu-TM2 (calculated)	297(0.82)
Cu(II)-TM3 (experimental)	447(0.22)
(His-Lys)-Cu-TM3 (calculated)	448(0.40), 326 (shoulder)
Cu(II)-TM4 (experimental)	513(0.33), 357 (shoulder), 306 (0.76)
(His-Lys)-Cu-TM4 (calculated)	511(0.55), 369 (shoulder) 299(1.37)

The closeness of corresponding values suggests that Cu binds somewhat similarly to the TMs in the two situations, for each of the three TMs. However, the significant differences between the molar absorptivities observed in the absence of His-Lys and those observed in its presence are an indication of the influence of the peptide on the binding of Cu to the TMs. (There are small changes in the λ_{max} as well; this issue is pursued further below.)

In all known M-(S)-Mo-S clusters (M = transition metal ion) the TMs ($MoO_{4-n}S_n^{2-}$) coordinate via sulfur to soft cations such as Cu(I), Ag(I) and Au(I). As discussed in Section 1.2.6, the linear polymeric chain structural type necessarily requires one molecule of TM to use four atoms that can bridge two molecules of Cu atoms (i.e. two bridging atoms each for one Cu). Since O^{2-} are hard ligands, and consequently poor in bridging Mo to Cu, it has not been possible to prepare any compound of the linear structural types with TM3, TM2 or TM1 (see Table 1.2). Amongst the TMs, the previously most studied and best understood Cu-(S)-Mo-S systems involve TM4 (Section 1.2.6). For this reason, TM4 studies are those mainly used for comparison with the present findings.

UV/visible bands in known complexes of the type $[M^I (MoO_{4-n}S_n)_2]^{2-}$ (M^I = Fe(II), Co(II), Ni(II), Pd(II), Pt(II)) are such that the positions of the peaks (λ_{max}) are approximately the same as those of the free TMs (81MD). The intensities of the peaks also remain virtually unchanged. Unlike these complexes, the lowest energy band of TM4 (λ_{max} = 468 nm, $\varepsilon = 1.16 \times 10^{-4}$ $M^{-1}cm^{-1}$), which is assigned to the transition $t_1 \rightarrow 2e$ (ν_1) (Section 1.2.2) was red-shifted to 511 nm with reduced intensity in the (His-Lys)-Cu-TM4 complex in this study. This seems to be a particular feature for Cu-(S)-Mo-S cluster systems, (Table 1.4) which display characteristic absorptions in the 472-520 nm area (87Ma, 97ZH, 82CL,83AG, 94LN). The pronounced shift, and the concomitant reduced intensities of the lowest energy band (ν_1), as mentioned above, are actually indicative of the fact that the t_1 orbital (HOMO) of TM4 is more strongly disturbed than the lower energy lying $3t_2$, 2e and $4t_2$ molecular orbitals (81MD). Detailed discussions on the assignment of the electronic transitions of the TMs were provided in Section 1.2.2.

In this study shoulders around 357 nm and 369 nm (Table 6.1) were observed respectively for the reaction mixture of Cu(II) and TM4, and for the computed (His-Lys)-Cu-TM4 ternary complex (obtained by the model described in Section 6.3.2.1). Such shoulders have been reported in the literature, between 338 and 370 nm, for various Cu-(S)-Mo-S cluster compounds, including especially binuclear and

trinuclear species (Table 1.4). The shoulder is attributed to a red shift of the ν_2 band of TM4 at 316 nm, which is assigned in the literature to a promotion of an electron from the $3t_2 \rightarrow 2e$ orbitals (Section 1.2.2). See Figure 1.2 for a molecular orbital scheme that depicts the electronic transitions in TM4. The shift of the ν_2 band is noted to be more pronounced in trinuclear species, e.g. [(phen)Cu(I)S_2MoS_2Cu(I)(phen)] and [(PhS)Cu(I)S_2MoS_2Cu(I)(PhS)]$^{2-}$, where the ν_2 band can be observed at about 375 nm and 370 nm respectively (Table 1.4). Note that both species are also symmetrical. The ν_2 bands for the corresponding asymmetric dinuclear complexes [(phen)Cu(I)S_2MoS_2]$^-$ and [(PhS)Cu(I)S_2MoS_2]$^{2-}$ are observed at 338 nm and 350 nm respectively (Table 1.4) .

These trends are consistent with results from XPS studies of binding energies of constituent atoms of the dinuclear complex [(phen)Cu(I)S_2MoS_2]$^-$ and the trinuclear species [(phen)Cu(I)S_2MoS_2Cu(I)(phen)]. The binding energies obtained for the S(2p) and Cu($2P_{3/2}$) suggested a shift of electron density from Cu(I) to the S of the TM4 group (84SM). Furthermore, the S(2p) binding energy for the trinuclear complex was observed to be lower than that for the dinuclear complex, also consistent with the observation that the bathochromic shift is more pronounced in the trinuclear case. Further, comparison of the spectra of the Cu(II)-TM4 reaction system and the (His-Lys)-Cu-TM4 ternary complex (Table 6.1) indicates larger red-shift of the ν_1 (468 nm) and ν_3 (241) bands of TM4 in the former than the latter. (It should be noted that these bands result from transitions involving the HOMO, t_1 orbital which is a pure S orbital, as discussed in Section 1.2.2 and also shown in Figure 1.2). These indicate stronger coordination of TM4 to Cu(II) in the absence of His-Lys than in its presence. Perhaps there is more pronounced polymerization in the former case. In the binary system, a polymeric Cu(I) derivative is said to be formed, which is composed of chains of edge-sharing CuS_4 and MoS_4 tetrahedra (70Br). Such polymerization of Cu and MoS_4 is inhibited by a variety of ligands, which bind to the Cu (Section 1.2.6). Why the precipitation occurs faster in the presence of the peptide (Section 6.3.1) despite its inhibition of the polymerization is uncertain. Presumably, the kinetics favor the separation from solution of the initially expected, bulkier (His-Lys)-Cu-TM ternary

complex as compared to an "unpolymerized" Cu-TM adduct or partially polymerized Cu-TM cluster.

6.3.3 ^{1}H NMR Studies of His-Lys, Cu(II) and TM Interactions

Figures 6.2 and 6.3 show the ^{1}H NMR spectrum monitored as a function of time on adding 1 m**M** TM4 to a solution containing 1m**M** Cu(II) and 26 m**M** His-Lys. It is clear that with the passage of time, the broad peaks that resulted from the binding of the paramagnetic Cu(II) to His-Lys sharpen and become better resolved due to the added TM4.

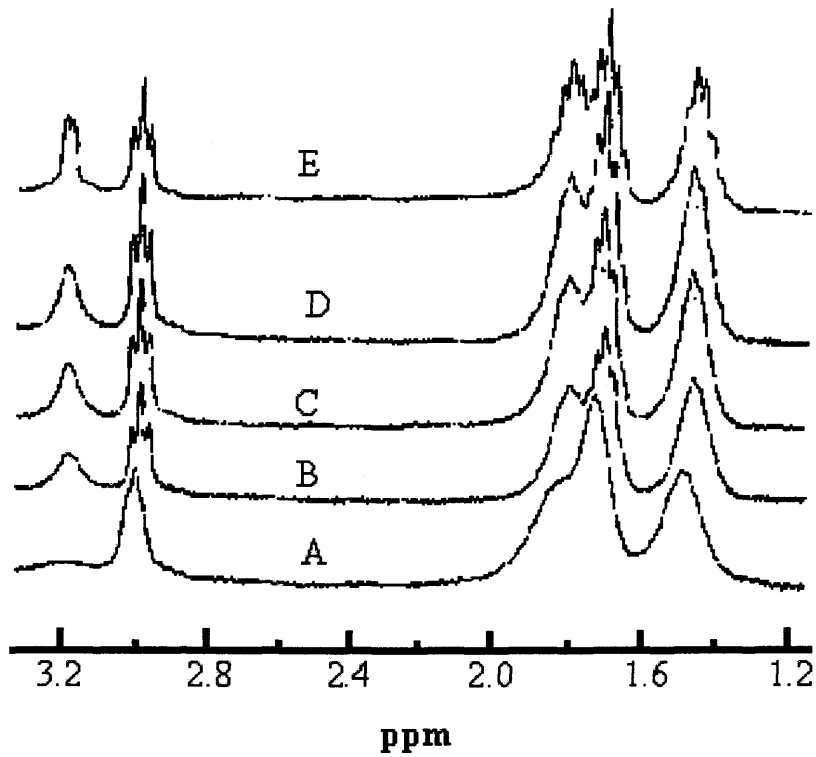

Figure 6.2: ^{1}H NMR spectra showing the Lys side chain CH_2 and His β-CH_2 proton signals of His-Lys at different times after adding 1m**M** TM4 to a solution containing 26 m**M** HisLys and 1m**M** Cu(II) (A) 0 min (B) 6 min (C) 30 min (D) 60 min (E) "Free" peptide in phosphate buffer (pH =7.0).

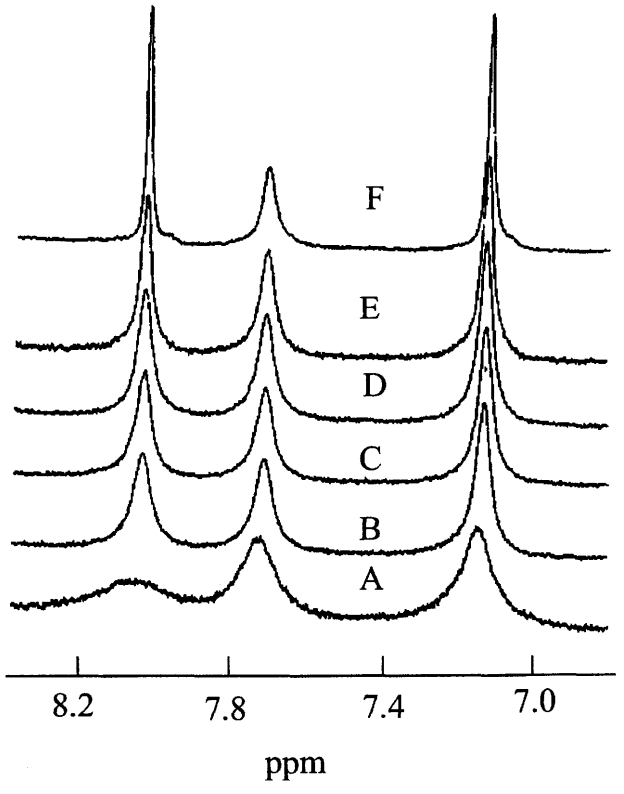

Figure 6.3: ^{1}H NMR spectra showing the Imidazole C2-H, N1-H, and C5-H proton signals of His-Lys at different times after adding 1m**M** TM4 to a solution containing 26 m**M** HisLys and 1m**M** Cu(II) (A) 0 min (B) 6 min (C) 30 min (D) 60 min (E) 120 min and (F) "Free" peptide in a phosphate buffer (pH =7).

Under the assumption that the lineshape in high-resolution NMR spectroscopy is Lorentzian (81WR), the linewidth of the individual His-Lys peptide resonances were calculated from fitted bands of Lorentzian shape to the observed NMR peaks. Errors due to variations in shimming were compensated by subtracting the linewidth of the DSS signal at 0 ppm from the measured linewidth for each signal. These adjusted linewidths were calculated for the individual peaks of the spectrum of His-Lys prior to the addition of Cu(II), immediately on adding the Cu(II) and at different times after adding the TM. Hence, for a particular peak, a linewidth P_A would be determined before adding Cu(II), a different linewidth P_B after adding Cu(II) to excess peptide and a third linewidth P_C after the further addition of the TM to the mixture.

The use of excess ligand over a paramagnetic metal ion to obtain indirect information as employed in this study is valid, provided that there is a fast chemical exchange on the NMR time scale between the free ligand and the bound ligand molecule, as discussed in Section 1.12.5. This condition is normally met by multidentate ligands (Section 1.12.5), of which peptides, including those used in this study, are good examples. The observed linewidths are therefore the population-weighted averages of the linewidths of the "free" peptide, P_A, of the Cu(II):peptide complex, (determined in Chapter 5 as having 1:1 stoichiometry) and possibly also of a ternary complex.

Some assumptions are made here. Either the TM strips off the Cu(II) to form the polymeric Cu-TM4 adduct and "free" peptide, or, a ternary complex is formed in which the Cu(II) is reduced to Cu(I). Subtraction of the contribution of free His-Lys from the observed linewidth yields the linewidth contribution due to the Cu(II) still bound to His-Lys (i.e. the paramagnetic broadening) after adding TM. This was calculated using Equation (6.5) as a percentage excess line broadening (ELB):

$$\% \text{ ELB} = 100*(P_c-P_A)/(P_B-P_A) \qquad \textbf{(6.5)}$$

% ELB is the excess line broadening over that of "free" peptide, which represents the paramagnetic line broadening due to Cu(II) still bound to the peptide after TM has been added, expressed as a percentage of excess linebroadening observed before TM addition.

Not all peaks gave acceptable data. Very broad peaks have poor signal to noise ratio and hence one cannot measure their linewidth precisely. This was the case for the Im C2-H and the His β-CH_2 peaks. Precision in measuring very small amounts of linebroadening is also very poor, and hence peaks further away from the Cu(II) binding site of the peptides gave unacceptable data (see Sections 5.3.5.2, 5.3.6.2 and 5.3.8.2). In almost all cases the Im C5-H peak was found to be the most reliable signal for such calculations.

6.3.3.1 Monitoring the reaction as a function of Time

Figure 6.4 shows the calculated excess linebroadening as a function of time when TM2 and TM3 were added to Cu(II) in aqueous solution (~1.8 m**M**), in the presence of excess His-Lys, such that the ratio of (His-Lys):Cu(II):TM was 13:1:1 (See Section 6.2.4.1 for experimental details).

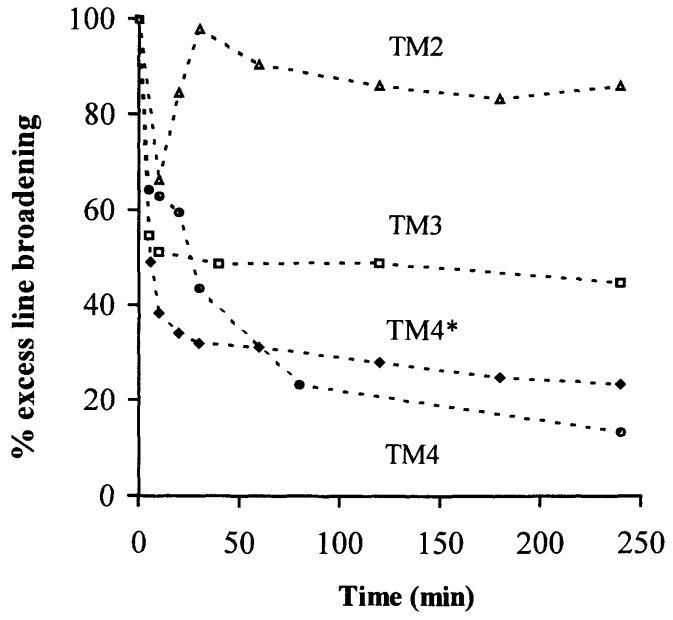

Figure 6.4: Percentage of excess line broadening of His-Lys resonances as a function of time after TM4 is added to reaction mixture of peptide and Cu(II). [Cu(II)] = 1.8 m**M**. The initial reaction ratio for the case of TM2 and TM3 was 13:1:1 peptide:Cu(II):TM. TM4 indicates a peptide:Cu(II):TM4 = 11:1:1; TM4* a peptide:Cu(II):TM4 ratio of 26:1:1.

The figure also contains data for two cases where TM4 was added to Cu(II) aqueous solution (~ 0.9 m**M**) in the presence of two different amounts of His-Lys, both in excess over Cu(II). The two resulting solutions after the TM addition contained 11:1:1 and 26:1:1 (His-Lys):Cu:TM4 ratios.

The line sharpening effect due to added TM4 is also exhibited by TM3 and TM2, but is most pronounced for TM4. However, the figure suggests that the reactions with TM2 and TM3 terminate earlier than that for TM4, as evidenced by a continuous decline of the excess line broadening even beyond 1 hr in the case of TM4, but not for the other TMs. This cannot be due to faster kinetics in the TM2 or TM3 cases, since it was concluded from the UV/visible studies that the rates of precipitation of the TM adducts are in the order TM4 > TM3 > TM2 (Section 6.3.1). Rather, the reason may in part be linked with the relative instability of TM2 and TM3 in aqueous solutions as compared to TM4 (Section 2.3.8) and hence their inability to persist in solution to continue the reaction.

It is also possible that the TM4 adduct is involved in a further reaction (possibly polymerization) which is terminated in the case of the other TMs. Oxygen atoms in TMs have been said only to act as terminal groups in Cu-(S)-Mo-S clusters (94HL); in other words, their presence prevents further polymerization. On the other hand, a single TM4 moiety can form dinuclear, trinuclear, tetranuclear, pentanuclear, hexanuclear, heptanuclear etc. species step by step when it coordinates with Cu atoms (94HL). It may therefore be this polymerization that accounts for the gradual but steady decline in the excess line broadening with the passage of time (Figure 6.4). Note that the oxidation state of Cu in almost all such cases has been reported as +1, not paramagnetic +2 state (Table 1.3). See below for further discussion of the polymerization process.

It is difficult to assign any definite reason for the unusual pattern for the TM2 reaction in the early stages. This does not seem to be an error in the measurements since it was reproducible and was also observable for both TM3 and TM4 when their concentration in the reaction mixture was small. Perhaps three different steps occur for the interaction of Cu(II) complexes with TMs, as can be deduced from the 3 stages for the TM2 case - a sudden decrease in linewidth, then an abrupt increase, and then a gradual decrease. The first reaction step may involve a fast redox reaction, possibly the formal reduction of Cu(II) to Cu(I) by the TMs. In that case, such reaction may be reversible, the forward direction (i.e. Cu(II) $\rightarrow$ Cu(I)) being less favored by increasing

amount of O in the TM. TM2 which contains two oxygen atoms per molecule would show less tendency to reduce Cu(II) to Cu(I). Thus, TM2 would have relatively more of the Cu(II)-peptide complex still in solution, and consequently show broader linewidth peaks for the peptide signals as compared to TM3 and TM4 (Figure 6.4).

The second step may involve TM binding to the complexed Cu (now at least partially in the +1 state). The proportion of each state will be dependent on the particular TM; the increasing proportion of the +1 state will be in the order TM4 > TM3 > TM2. The sudden change from a lesser broadening linewidth trend to broader linewidths in the early stages after adding TM2 may be due to slow molecular tumbling as a result of the involvement of more peptide molecules to form bulkier initial ternary complex which may have the Cu still dominantly in the + 2 state. The consequence of this slow molecular tumbling is the line broadening as explained in more details in Section 6.3.3.3. For the case of TM4, which favors the formation of Cu(I), there will be less involvement of the peptide in the formation of the ternary complex, so it is reasonable that the complex so formed initially may have a smaller nuclearity (e.g. a binuclear or a trinuclear complex).

For instance, a binuclear, peptide-Cu(I)-TM complex (**A**) might be formed from the second reaction step, and could polymerize in the third and final step of the reaction process to increase its nuclearity and form, for example a tetranuclear complex (**B**), as shown in Scheme I below. In the process, some peptide may be lost as also shown in Scheme I. Note that the original N or O Cu(II) binding sites of the peptide will have less affinity for the Cu(I) reduced state. Thus, these sites will be bound only loosely, if at all, to the Cu(I) and can be replaced by S ligands from TMs.

By changing the (His-Lys):Cu(II):TM4 mole ratio from 11:1:1 to 26:1:1 the less linebroadening effect of TM4 was more gradual (Figure 6.4). It appears that the presence of the peptide inhibits whatever process is causing the gradual less linebroadening.

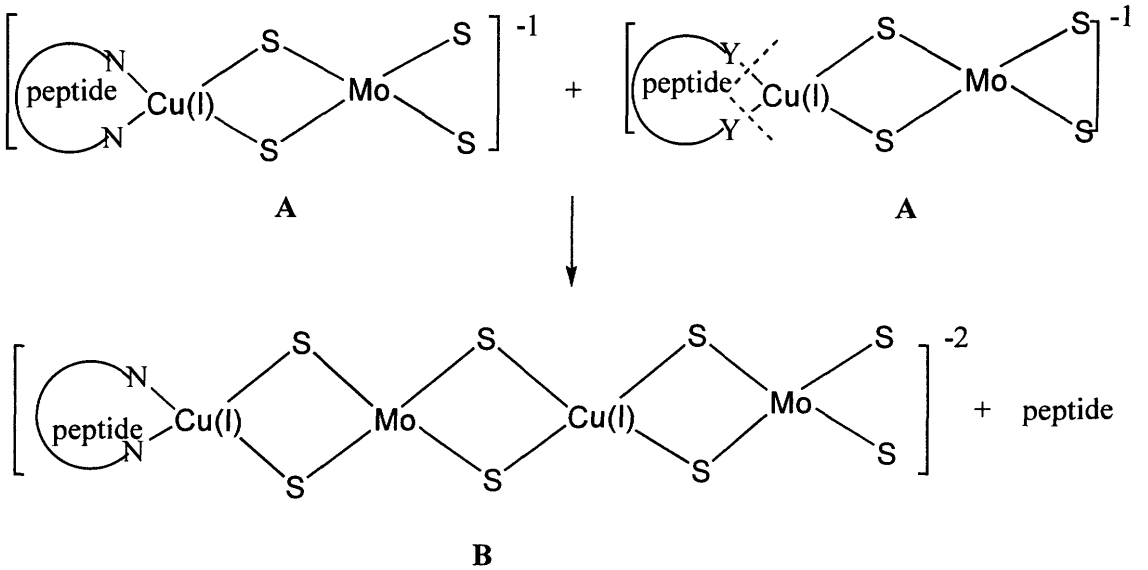

B

Scheme I

However, the presence of the peptide favors the early precipitation of the reaction product (Section 6.3.1). In Section 6.3.2 an attempt was made to explain this apparent contradiction.

An explanation for the less linebroadening effects arising from the addition of TMs to (His-Lys)-Cu(II) must account for these observations. There are three possibilities:

1. Stripping of Cu(II) from the peptide to form the polymeric Cu-TM adduct (70BR, 94LN) leaving the "free" peptide in solution.
2. Formation of a ternary complex between TMs, Cu, and His-Lys with the Cu in the +1 state. The structure of such a ternary complex may be similar to that described above for systems containing 1,10-phenanthroline as co-ligands in Cu-TM systems, or as shown in the scheme above.
3. TM acting as a reducing agent, by donating electrons via the S atoms to form a (His-Lys)-Cu(I) complex.

It is difficult to judge between these hypotheses based only on the results discussed thus far, but it seems clear from Figures 6.2, 6.3 and 6.4 that the reaction between TM and

(His-Lys)-Cu(II) is generally slow, needing at least 1 hr to ensure completion of the reaction. As discussed earlier, in an attempt to explain the unusual behavior of TM2 in Figure 6.4, the last two mechanisms may be involved somehow in the overall reaction.

6.3.3.2 The Stoichiometric ratio of Cu(II):TM4 for the reaction

The Cu:Mo stoichiometry in Cu-(S)-Mo-S clusters has not been settled in the literature (Section 1.2.6). Compounds with between 1 and 6 Cu for each Mo have been identified in the literature (Table 1.2) when co-ligands are present in the reaction mixtures. This wide variation in stoichiometry has been attributed to the reaction conditions, for instance the ratios of the starting reactants and the nature of the solvent (00L). Conditions in any *in vitro* experiment used to speculate about the actual stoichiometry of the ternary complex formed between peptide (or protein), Cu(II) and TM *in vivo* should therefore mimic those in the biological fluid very closely. Such conditions include solvent, pH of the solution, ionic strength, and the ratios of the starting materials. Conditions chosen in these studies are outlined in Section 6.2.4.2.

Figure 6.5 shows part of the ^{1}H NMR spectra (from 1.0 to 3.5 ppm) observed as incremental amounts of TM4 are added to a solution containing 1 m**M** Cu(II) and 26 m**M** His-Lys prepared from a mixed phosphate buffer of pH 7.0 and ionic strength 0.2 **M**. Addition of the TM gives sharpening of the broad initial peaks resulting from the presence of the paramagnetic Cu(II). This is observed for all the proton signals (those for the imidazole protons are not shown but display similar behaviour). The effects are, however, more pronounced on the signals in the proximity of the Cu(II) binding sites (Section 5.3.4). Hence, the His β-CH_2 resonance, which disappears completely on complexing His-Lys with Cu(II) (Figure 6.5A) gradually reappears, (Figure 6.5 B-D), initially as a broad peak, and subsequently as a doublet due to resolution of the coupling to the His α-CH (Figure 6.5E). Similarly, Lys β-CH_2 which is initially barely recognizable, and the poorly resolved broad signals of the other Lys side chains signals (i.e. Lys γ-CH_2, Lys δ-CH_2, and Lys ε-CH_2) in the Cu-(His-Lys) complex

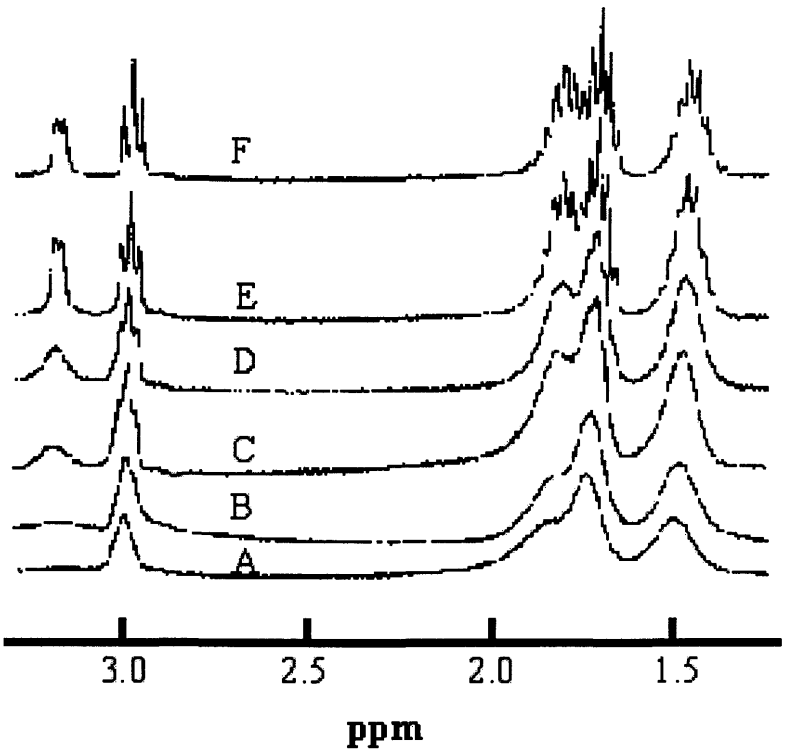

Figure 6.5: ^{1}H NMR spectra showing the Lys side chain CH_2 and His β-CH_2 protons signals of His-Lys as different amounts of TM4 are added to a solution containing 26 m**M** His-Lys and 1 m**M** Cu(II). (A) No TM4 added. (B)-(E) TM4 added to give TM4:Cu(II) ratios of (B) 0.3:1 (C) 0.9:1 (D) 1.1:1 (E) 1.5:1. (F) His-Lys alone (no Cu(II) or TM4). All spectra collected in phosphate buffer (pH =7.0 and ionic strength 0.2 **M**).

(Figure 6.5A) become well resolved at a TM4:Cu(II) ratio of 1.5:1 (Figure 6.5E), with no significant difference in linewidth from uncomplexed His-Lys (Figure 6.5F). It should be immediately pointed out that this ratio (1.5:1) should *not* be taken as the reaction stoichiometry for TM4:Cu; an excess of TM may be required to drive the reaction to completion. This is discussed at greater length later in this section.

The chemical shift changes observed for the Im C2-H and C5-H signals upon adding TM4 are shown in Figure 6.6. The trends are similar, although more pronounced for the former than the latter. Although the nature of these curves in the figure is unexpected, it was reproducible. However, the Lys side chain protons display a steady

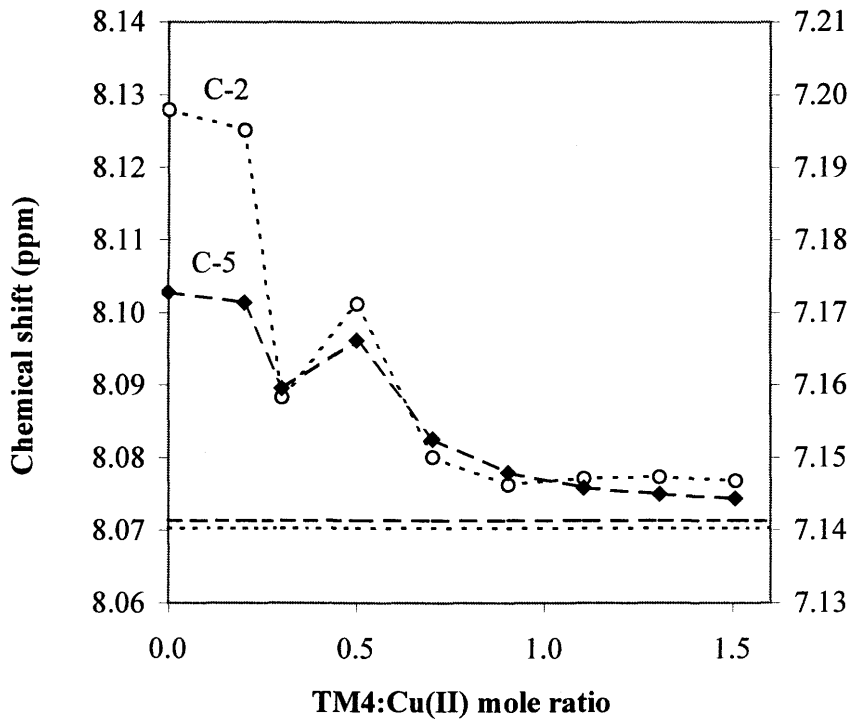

Figure 6.6: Chemical shifts of the imidazole C5-H protons (right axis) and C2-H protons (left axis) as TM4 is added to a solution containing (His-Lys):Cu(II) with mole ratio 27.5:1. Initial Cu(II) concentration was 1 m**M**. The horizontal dotted and dashed lines represent the chemical shifts of the C2-H and C5-H signals respectively, for uncomplexed peptide in a solution buffered at pH 7.0.

decline of the chemical shifts as shown in Figures 6.7 for γ-CH_2 Lys. As mentioned above (Section 6.3.3.1), there appear to be three different steps involved in the interaction between His-Lys, Cu(II) and TM, and the first of these may involve a fast and reversible Cu(II)/Cu(I) redox reaction. The data seem to suggest that this activity occurs near the Cu(II) binding site, and hence the Im C-H protons sense it but the Lys signals, which are remote from the Cu(II) binding site, do not.

The suggested stripping of Cu(II) by TM from the peptide (Section 6.3.3.1) to form a Cu-TM adduct (with no His-Lys as part of the complex) as a possibility to account for the His-Lys, Cu(II) and TM interaction, seems unlikely since the chemical shift for the "free" peptide is different from that of the final product even on adding an excess of the TM.

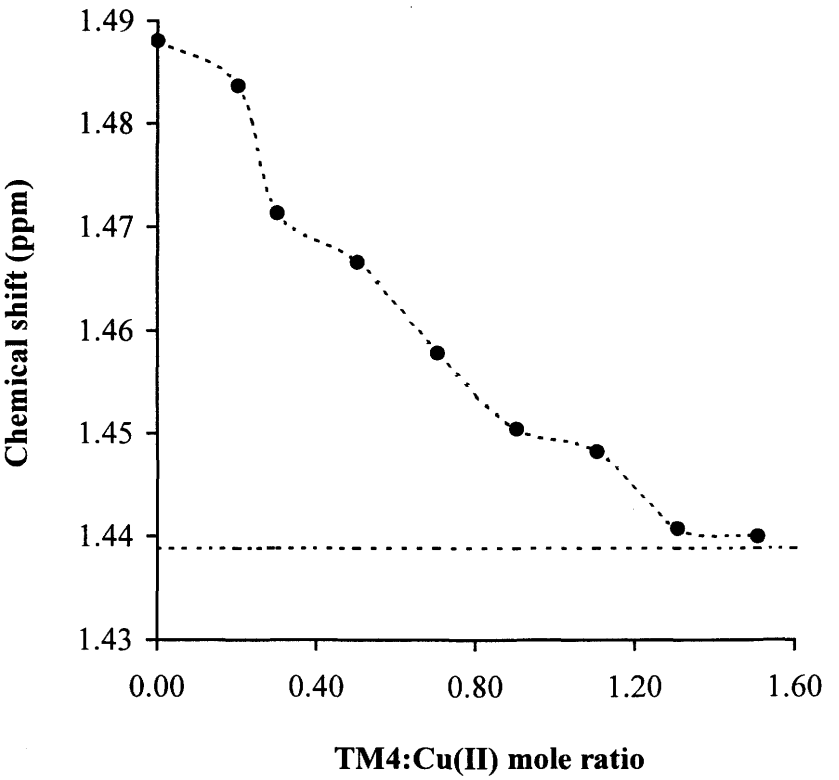

Figure 6.7: Chemical shift of the Lys γ-CH_2 protons as TM4 is added to (His-Lys):Cu(II) solution of ratio 27.5:1. Initial Cu(II) concentration was 1 m**M**. The horizontal line represents the chemical shift of the Lys γ-CH_2 signal for uncomplexed peptide in a solution buffered at pH 7.

Presumably, the binding of the TM to the peptide-Cu(II) complex could cause the weakening and the breaking of the Cu(I)-N^- (amide) bond, whilst maintaining the binding to imidazole N-3 nitrogen and the terminal amino nitrogen, as shown for compound **A** in Scheme I. In so doing, there would be rearrangement of the coordination environment to favor the usual tetrahedral coordination for Cu(I) complexes. This would create a coordination environment where the Lys side chain becomes even more remote from the Cu binding site, and hence senses activities at the Cu binding site less efficiently than the imidazole protons. On the other hand, the imidazole signals are *more* prone to sense changes at the Cu binding site as a result of the ternary complexation.

There is literature support for the proposal above; reduction of Cu(II) to Cu(I) in the presence of thiometallates like WS_4^{2-} and MoS_4^{2-} (TM4) is well known (Section 1.2.6). Recall also the well-known preference of Cu(I) for soft ligands like the S atoms from the TMs (Section 1.2.6) rather than the alternative N^- (amide N) or the O^- (carboxylate) which were coordinated originally to the Cu(II) (see Section 5.3.4). As shown in Scheme 1, the structure(s) of the resultant ternary complex(es) may be similar to those observed for the heterometal complexes of the aromatic diimines-Cu-thiometalate systems $[LCu(\mu\text{-}S)_2M(\mu\text{-}S)_2]$ and $[LCu(\mu\text{-}S)_2M(\mu\text{-}S)_2CuL]$ (M= Mo, W and L= 2,2'-bipyridine(bpy), 1,10-phenanthroline (phen)) (84SM, 87PM, 87PMa, 90SS).

The results in Figures 6.6 and 6.7 show that approximately constant chemical shifts are observed beyond a TM4:Cu ratio of ~1.2:1, suggesting that the stoichiometry of the complex is 1:1, and that the slight excess of TM4 over Cu(II) is only required to drive the reaction to completion. It should also be recalled from the introductory part of Section 6.3.3, that the Im C5-H peak was found to be the most reliable signal for quantitative studies. From Figure 6.6, it can be seen that the chemical shift for this resonance actually stays practically constant from all TM4:Cu ratios beyond ~ 0.9.

6.3.3.3 The Involvement of Peptide in Ternary Complexation

To obtain direct information to confirm that His-Lys participates in ternary complexation, the ^1H NMR spectra of two sets of solutions, each containing the same amount of the peptide (20 m**M**), but in the absence and the presence of Cu(II) (1.6 m**M**) and TM4 (2 m**M**), were monitored over a period of time. The excess of 0.4 m**M** TM4 over the Cu(II) concentration used in this study was to enable the reaction to go to completion, as discussed in Section 6.3.3.2. Results are shown in Figure 6.8. By determining the peak areas of individual ^1H NMR signals of the His-Lys peptide in each set of solutions, as shown in Figure 6.8 for Im C5-H peak (p1) and Im C2-H peak (p2), the amount of His-Lys utilized could be obtained by simple proportion. Averaging the results from these two peaks 20 hr after adding the reaction

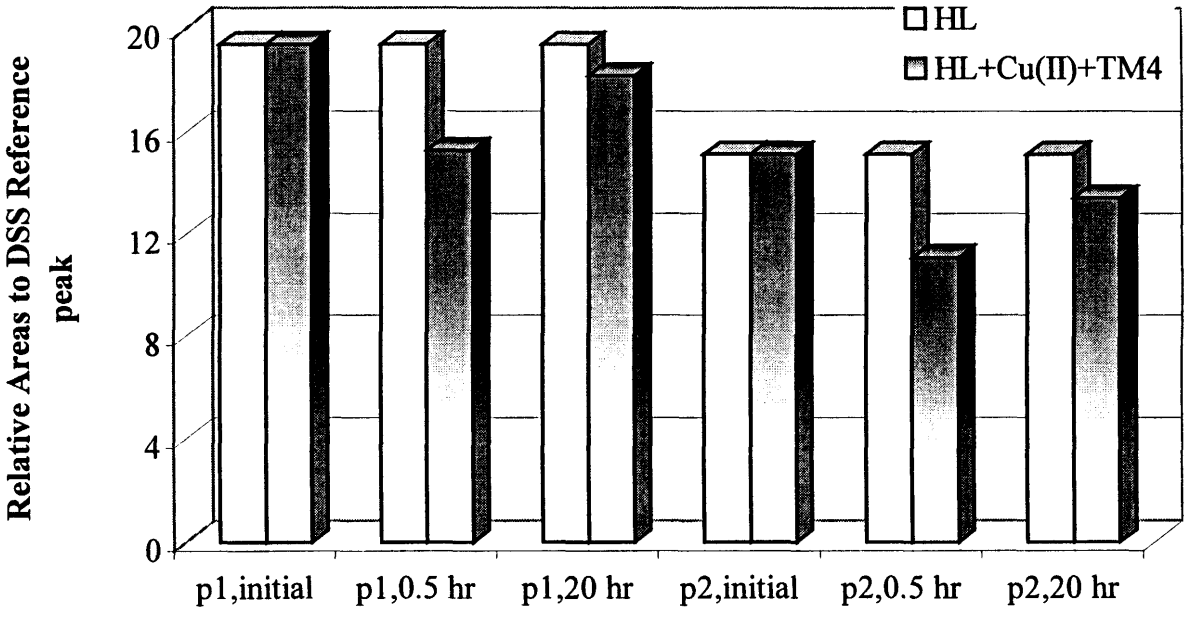

Figure 6.8: Relative areas under Im C5-H peak (p1) and Im C2-H peak (p2) of HL (His-Lys) (20mM) in the presence and absence of 1.6 mM Cu(II) and 2 mM TM4, initially and at various times after mixing the reactants.

mixtures, a concentration of 18.2 m**M** His-Lys was found to be still present in solution as compared to the initial concentration of 20.0 m**M.** This shows that approximately 1 mole equivalent of the peptide is required to form the insoluble product that precipitated in the NMR tube after 20 hr. This product may be a 1:1:1 ternary complex involving the peptide His-Lys, Cu and TM4.

However, results obtained only 30 min after mixing are substantially different from those at 20 hr. The concentration of the peptide remaining in solution after this time was only 15.2 m**M**, indicating that ~ 3 equivalents of the peptide were unavailable to be detected in solution. There is apparently an initial product utilizing relatively more peptide, which is lost as the reaction proceeds. This initial product containing 3 equivalents of the peptide per Mo could possibly be a polymeric product, whose molecular tumbling is slow and whose ^{1}H NMR signals therefore have short T_2 relaxation times; spin diffusion leads to short lifetimes for individual spin states and these lead in turn to broad lines (87SH). If this indeed is the case, then the selective linebroadening of the imidazole resonance will have contributions from two sources after the formation of the initial polymeric species: paramagnetic linebroadening due to Cu(II) binding and linebroadening due to the short T_2 values associated with the polymeric species. This is consistent with what is observed in Figure 6.4, where addition of TM2 leads initially to linesharpening, and later to linebroadening, again probably after the formation of the polymeric species.

Is there chemical precedence in the literature to support the formation of the polymeric species so described? There are examples in the literature of polymeric Cu-(S)-Mo-S clusters, which, in addition to μ_2-S bridging, have the involvement of co-ligands such as CN^-, SCN^-, Cl^-, and Br^- in bridging core units (Section 1.2.6). A bulkier bidentate ligand, dihydrobis(3,5-dimethylpyrazoyl) borate (Bp) has also been reported (01BH) as a bridging ligand in $[EtN]_2[(Bp)Cu^IMoS_4Cu^I_2(m\text{-}Bp)_2Cu^I_2MoS_4Cu^I(Bp)]$, which crystallizes as a centrosymmetric dimeric anion. These complexes involve varied ligand:Cu:TM ratios e.g. of 3:2:1 (CN:Cu:TM4), 4:2:1 (X(Cl, Br): Cu:TM4) and 2:2:1

(Bp:Cu:TM4) (81MD, 83NF, 87G, 01BH). A characteristic feature of these polymeric species is the involvement of more Cu and co-ligand in the stoichiometry, as expected for the initial polymeric species discussed in the preceding paragraph. There is therefore the real possibility of forming similar polymeric species , under conditions when a small amount of TM is added to excess peptide-Cu(II), or ***initially*** on adding TM to peptide-Cu(II) complexes (even at equivalent ratios).

6.3.4 Attempts to Characterize the solid Ternary Complexes formed from (His-Lys)-Cu-TM and His-Cu-TM reaction Systems

Elemental analyses for C, H, N, Mo and Cu were performed for the solid product obtained from the interactions of His-Lys, Cu(II) and TM, and of His, Cu(II) and TM4 as described in Section 6.2.5. Results, shown in Table 6.2, clearly indicate the presence of His-Lys or His in the solids obtained. (The inclusion of Histidine in this study was to ascertain whether this amino acid is also involved in a similar reaction with Cu(II) and TM.)

The presence of some peptides and amino acids such as His have been observed previously in complexes resulting from the addition of TM4 to their Cu(II) complexes, but were regarded as impurities. Hence their presence in the first place was avoided completely for fear of "contaminating" the final products (86LP). Being aware of this caution from the literature, the final products were well washed with distilled water to prevent any such possible residual contamination that could be present due to improper washing (Section 6.2.5). The ^{1}H NMR studies discussed in Section 6.3.3.3 suggest that His-Lys is an integral part of the insoluble ternary complex which precipitates from the interaction between Cu(II), His-Lys and TM4. The C, H, N analyses performed on the solid products indicate significant levels of these elements (Table 6.2), which cannot be due to residual contamination, again suggesting the involvement of the peptide in the complexation. More detailed discussion is presented below.

The calculated empirical formulae for the solids obtained for the reaction between His-Lys, Cu(II) and TM4 which were allowed to proceed for 1 hr and 8 hr are

$C_{12}H_{25}N_6Mo_2Cu_3$ and $C_{12}H_{25}N_6Mo_2Cu_{3.7}$ respectively. The empirical formulae from the elemental analysis data for these two preparations indicate a peptide to Mo ratio of 1:2 even though the percentage compositions of the elements analyzed in the two cases were different (Table 6.2). The Cu level was not constant for the two preparations. Attempts to synthesize complexes involving His, Cys, and other amino acids have resulted in such varied stoichiometry (84SM). Such variations, dependent on the nature of the precipitation conditions, have also been observed for the interaction involving Fe(II), TM4 andH_2O (87MD).

The empirical formula for the solid product obtained from the reaction of Cu(II), His and TM4 was $C_6H_{11}N_3Mo_2Cu_{3.7}$, similar to that for the His-Lys case for the same time period of 8 hr (i.e., approximately 1 peptide or amino acid:4 Cu:2 Mo).

Table 6.2: Relative masses of the elements C, H, N, Mo, Cu (C = 10 .0) based on the experimentally determined elemental compositions of the insoluble reaction products of different ternary mixtures and the calculated relative masses of these elements (in parenthesis) based on the empirical formulae cited in the text

Reacting System	C	H	N	Mo	Cu
Cu-TM4 (1hr)	10.0	1.6	5.7	12.8	12.8
	(10.0)	(1.8)	(5.8)	(13.3)	(13.2)
(His-Lys)-Cu-TM4 (8hr)	10.0	1.9	5.6	13.8	16.8
	(10.0)	(1.8)	(5.8)	(13.3)	(16.3)
His-Cu-TM4 (8hr)	10.0	1.6	6.3	27.5	32.1
	(10.0)	(1.5)	(6.4)	(27.9)	(32.6)
(His-Lys)-Cu-TM3 (8hr)	10.0	1.8	5.6	9.4	18.4
	(10.0)	(1.7)	(5.8)	(9.3)	(18.5)
(His-Lys)-Cu-TM2 (8hr)	10.0	1.8	5.6	7.9	20.5
	(10.0)	(1.7)	(5.8)	(8.0)	(20.3)

Although the ^1H NMR solution chemistry studies (Section 6.3.3.3) seem to suggest a stoichiometry of 1:1:1 (His-Lys):Cu(II):TM4, the empirical formulae above seem to suggest the involvement of 2 moles of TM4, and at least 3 moles of Cu(II) per peptide, depending on the procedure for the precipitation. These various stoichiometries are all consistent with some complexes of linear structures observed for different Cu-(S)-Mo-S cluster systems and reported in various review papers (81MD, 84SM, 87MD). Figure 6.9 shows some linear structures, which are consistent with the elemental analysis data presented above.

The empirical formulae for the (His-Lys)-Cu-TM3 and (HisLys)-Cu-TM2 were found to be $(C_{12}H_{25}N_6)_5Mo_7Cu_{21}$ and $(C_{12}H_{25}N_6)_5Mo_6Cu_{23}$. These are not consistent with possible empirical formulae for Cu-(S)-Mo-S clusters of linear structures. Indeed, the formula for the TM2 analogue is more consistent with complexes containing the core Cu_3MoX_4 (X= O, or S) for cubane-like clusters (87MD, 81MD, 84SM, 83AG).

Due to the amorphous nature of the Cu-TM adducts, extended x-ray absorption fine structure spectroscopy (EXAFS), near edge x-ray absorption fine structure spectroscopy (NEXAFS) and x-ray photoelectron spectroscopy (XPS) have been used to characterize the Cu-TM4 adducts, rather than x-ray crystallography. Such methods are valuable in providing information about the binding environment around atoms such as Mo, Cu and S.

Attempts were made by Dr. S.G. Urquhart (Department of Chemistry, University of Saskatchewan) to measure S 1s EXAFs spectrum using the S Kα (2308 eV) fluorescence yield, but the Mo Lα_2 (2289 eV) was too close in energy to permit resolution of the fluorescence signals for the S and Mo core edges. However, the S 1s NEXAFS spectra of TM3 and TM4 samples, and of the same Cu-TM3, Cu-TM4 and His-Cu-TM4 samples used for the elemental analysis, were successfully measured by Dr. Urquhart. The S 1s spectra of the TM compounds show a first peak, which is nearly the same energy (2472 eV) for TM3, TM4, and Cu-TM3 but that in

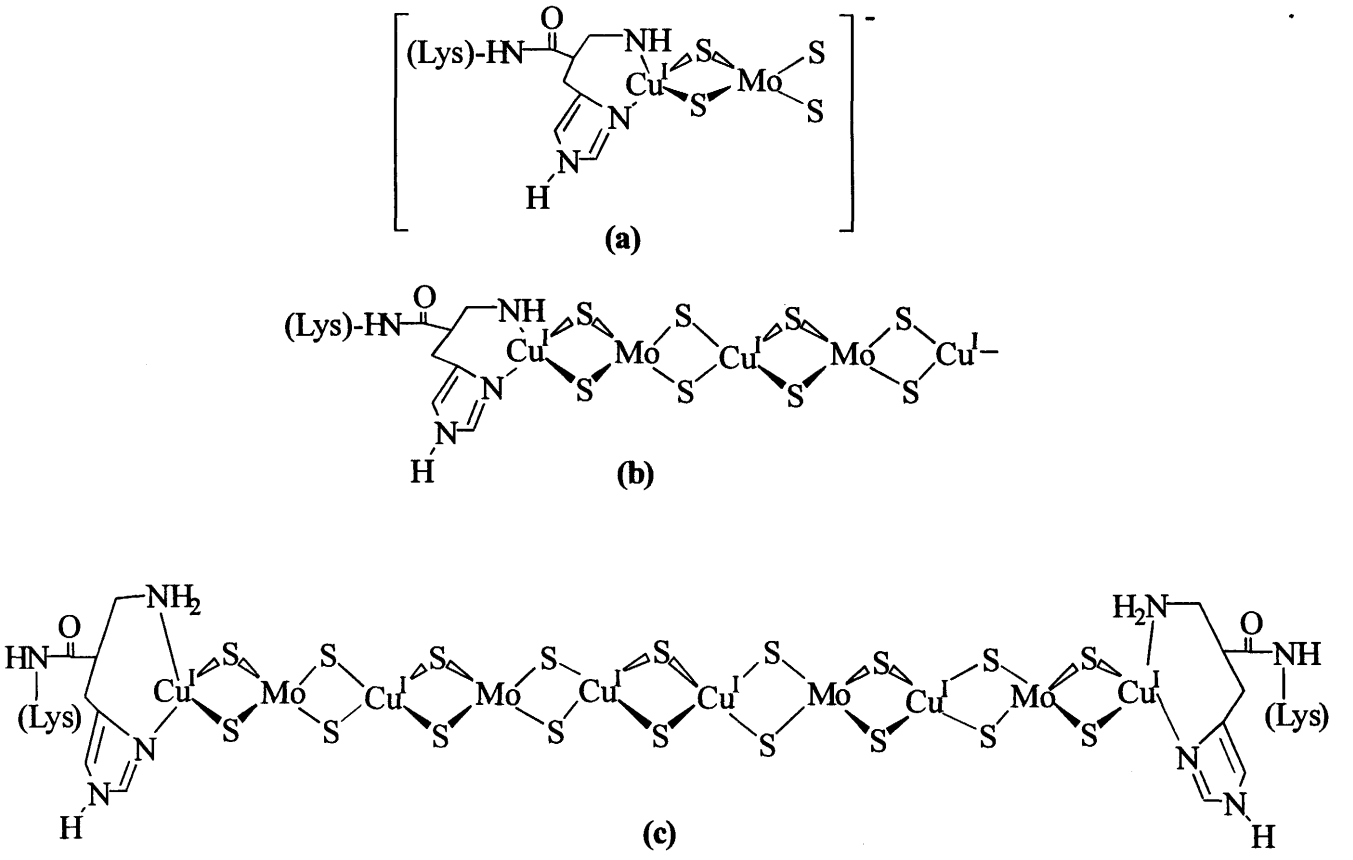

Figure 6.9: Possible structures of the ternary complex(es) of (His-Lys)-Cu-TM4. (See Section 3.3.4 of text for details)

Cu-TM4 (2493eV) and His-Cu-TM4 is shifted to higher energy, which suggests that the S atoms are more strongly involved in bonding to the Cu atom in these species than in Cu-TM3. Perhaps the strong S-Cu bonding is an indicative of a higher degree of polymerization in the Cu-TM4 adduct than the Cu-TM3 adduct. The Mo $2p_{3/2}$ and $Mo2p_{1/2}$ NEXAFs spectra of the four species mentioned were also measured. The NEXAFs spectra from these two different core edges are nearly identical, except for the displaced energy scale. The Mo $2p_{3/2}$ peaks of Cu-TM4 and His-Cu-TM4 were at slightly lower energy than the TM4 species, leaving room for speculation that Mo becomes less electronegative when TM4 is bound to Cu(II) (in either the amino acid chelated form or simply as a hydrated ion).

6.3.5 Interactions between other His-containing Peptides, Cu(II) and TM4

The ^{1}H NMR studies of the interactions between the His-containing peptides Thr(Ac)-His-Lys, and Asp-Thr(Ac)-His-Lys with Cu(II) and TMs give similar results to those observed for the dipeptide His-Lys (Section 6.3.3.1 and 6.3.3.2). Figure 6.10 shows part of the ^{1}H-NMR spectrum (1-3.5 ppm) for a 1:1 Cu(II):TM4 reaction mixture in the presence of excess Thr(Ac)-His-Lys, as a function of time. Reduced Line broadening is observed as was previously observed for the His-Lys case (Section 6.3.3.1) but the chemical shift changes were less pronounced.

Figure 6.10 clearly shows that the addition of TM4 affects the reduced line broadening of the His β-CH_2 and the Thr side chain protons (i.e. γ-CH_3 and the acetyl protons) of the tripeptide to a greater extent than the Lys side chain protons of the peptide. In Chapter 5, the amino terminal N, His amide N^-, and Im N3 were identified as the Cu(II) binding site for Thr(Ac)-His-Lys. It is therefore reasonable that the His β-CH_2 and the Thr γ-CH_3, being in close proximity to this binding site, sense changes that occur at this site more than those protons remote from the site.

Prior to the addition of TM4, the binding of Cu(II) to the peptide causes the broadening of the peaks from protons that are close to the binding site. The addition of

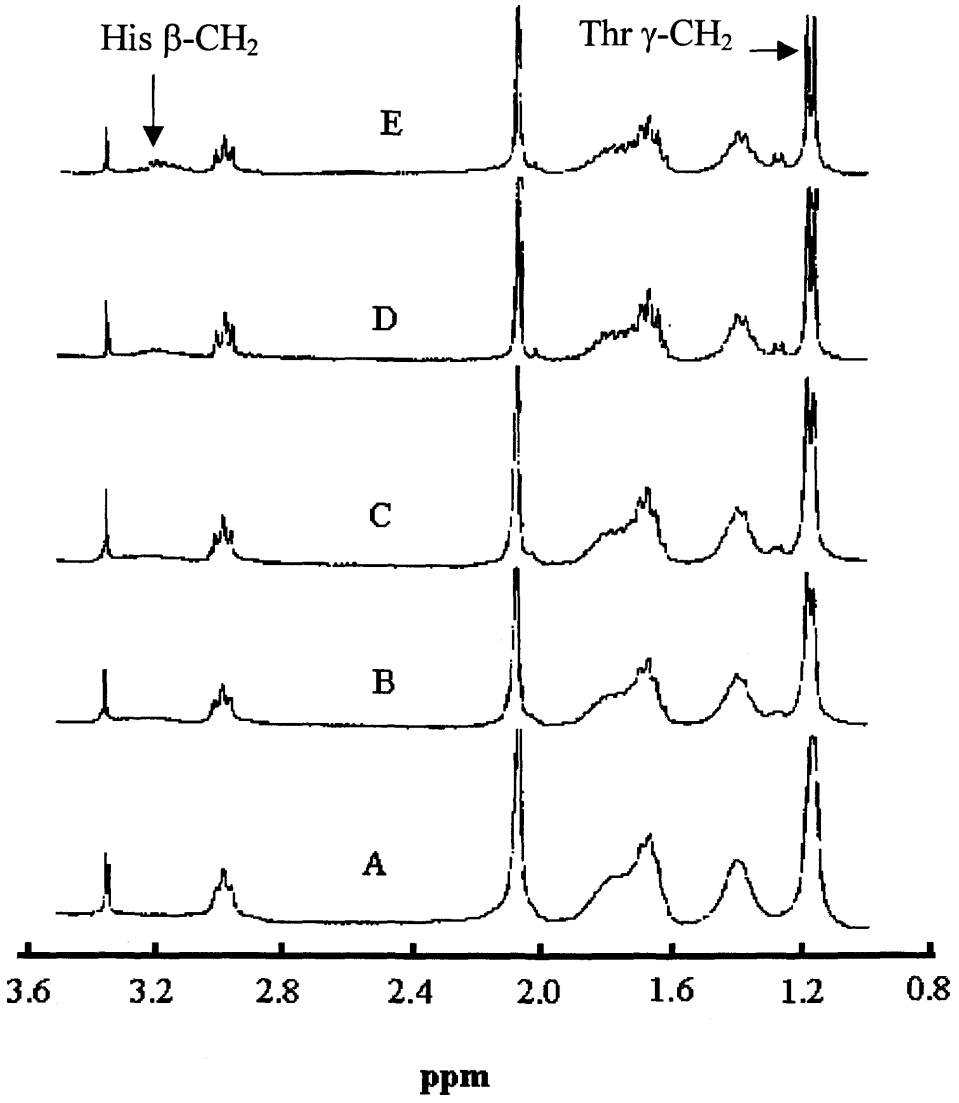

Figure 6.10: Lys side chain CH_2 and His β-CH_2 proton chemical shifts of Thr(Ac)-His-Lys at different times after adding 1 m**M** TM4 to a solution containing 13 m**M** Thr(Ac)-HisLys and 1m**M** Cu(II) (A) 0 min (B) 10 min (C) 60 min (D) 5 days (E) Thr(Ac)-His-Lys alone (no Cu(II) or TM4). pH =7.0 (phosphate buffer) for all spectra.

the TM to either strip the Cu from the peptide or convert the paramagnetic Cu(II) to Cu(I) when still bound to the peptide will cause significant changes to those signals that are near the Cu binding site, as observed in the figure. As discussed in Section 6.3.3.2 for the case of His-Lys, the idea of stripping the Cu is unlikely. As was also the case for His-Lys, the impact of TM4 on reducing linebroadening of Cu(II) bound peptide was more marked than that for TM3; TM2 had even less effect.

The reduced linebroadening effect was also significant for the tetrapeptide Asp-Thr(Ac)-His-Lys case, as exemplified in Figure 5.11 for the Im C5-H peaks when TM4 is added to the peptide.

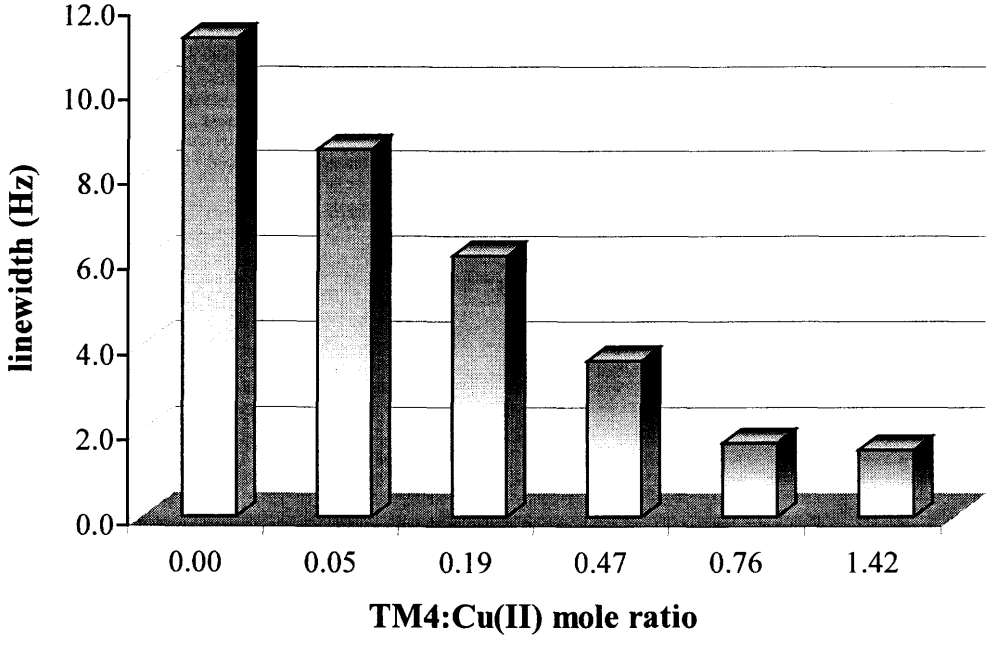

Figure 6.11: Linewidth (Hz) of the Imidazole C5-H proton in a (Asp-Thr(Ac)-His-Lys):Cu(II):TM4 solution of ratio 24.5:1:x as a function of the TM4:Cu(II) ratio (i.e., x). Initial Cu(II) concentration was 1m**M**.

6.3.6 Biological Implications

In Section 3.3.3, it was demonstrated that mixtures of BSA, Cu(II) and TM form ternary complexes. It is therefore interesting to compare the UV/visible data collected there to those collected for the (His-Lys)-Cu-TM model system. Understanding of the similarities or the differences in these two systems will contribute significantly in addressing the issue of how BSA gets involved in ternary complexation with TMs and Cu, an issue unclear in the literature and left unresolved in Chapter 3 of this thesis.

The red shifts of both the ν_1 and ν_2 bands observed for the Cu(II) and TM4 and His-Lys, Cu(II) and TM4 systems, as discussed in Section 6.3.2, are observed also for the ternary interactions of the BSA, Cu(II) and TM4 system (Section 3.3.3.1) at the same pH (7.0) as used in this chapter (Section 6.2.3). Since the observed peaks in the Cu-TM and (His-Lys)-Cu-TM systems were attributed to electronic transitions characteristic of Cu-(S)-Mo-S clusters, it can be inferred that TM4 is bound to Cu in the albumin via its S atoms. The smaller shift as compared to the (His-Lys)-Cu-TM4 system and more so, the Cu-TM4 system is a probable indication of a weaker Cu-(S)-Mo-S interaction in the presence of the protein. The presence of the protein will presumably prevent the polymerization of the Cu-TM adduct. The red-shift of the unreacted TM3 band at 396 nm (Table 2.1), observed for both the Cu(II)-TM3 and the (His-Lys)-Cu(II)-TM3 reaction systems (to 447 and 448 nm respectively) (Table 6.1), was also observed for the BSA-Cu-TM3 systems by Wood and Mason (87WM), and confirmed in Section 3.3.3.2 at a wavelength of 420 nm in a solution of pH ~7. This shift is significantly less than those of the Cu(II)-TM3 and the (His-Lys)-Cu(II)-TM3 reacting systems as is the case for the TM4 analogue. This confirms the inhibitory role the BSA plays in preventing cluster formation of Cu-TMs in general.

Another issue of paramount significance to biological systems is the oxidation state of Cu ions in these Cu-(S)-Mo-S cluster system, since the metabolic activity of copper is believed to be facilitated when it is present in the Cu(I) state rather than the Cu(II) (84SM). Also, in many copper proteins, especially those containing thionein

bound copper, the formal oxidation state of copper is believed to be +1 (Section 1.5). Do these copper ions maintain their original oxidation state of +2, or change it via some redox reaction? The latter seems to be the case for many reported cases for Cu(II) interaction with TM4 where Cu(I) complexes are formed (Table 1.3). Increasing the oxygen content of the TM ligand reduces its capability of performing such reduction (87MD) as well as the formation of polymeric species. The enhanced capability of TM4 over the oxythiomolybdates of reducing Cu(II) to Cu(I) appears to be the primary reason for its unique antagonistic role in effecting Cu deficiency in biological systems.

6.4 CONCLUSIONS

From the results presented here, it is clear that ternary complexes which are poorly soluble in water are formed from the interactions between His-Lys, Cu(II) and TMs. Elemental analysis indicates that Histidine as an amino acid is also involved and the ternary complexation may generally involve His-containing peptides since two other His-containing peptides, Thr(Ac)-His-Lys and Asp-Thr(Ac)-His-Lys, gave similar ^{1}H-NMR results. There was not enough information to come to a definite conclusion about the structures of these solids. However, the overall results seem to suggest a core unit where the peptide or the amino acid binds Cu in the +1 state via the terminal amino N, the imidazole N-3, and two S atoms from a thiomolybdate (particularly TM4). There may then be a subsequent involvement of more Cu and TM in forming polymeric species. The elemental analysis data seem to suggest a different type of polymeric species for the TM3 and TM2 complexes from that formed in the TM4 case, which is likely to be linear, involving alternating Mo and Cu centers.

7. SUMMARY, BIOLOGICAL IMPLICATIONS, AND SUGGESTIONS FOR FURTHER WORK

7.1 SUMMARY

Although the synthesis of TMs dates back to the early nineteenth century and various workers have reported preparation of one or more of the TMs in aqueous-soluble form, the preparation of samples of all four by a single synthetic route has been lacking. TM1 in particular has been said to be difficult to isolate. The presence of this anion has hitherto been mainly inferred from analysis of aqueous reaction mixtures containing low S: Mo ratios.

In this study, the synthesis of all four TMs by a single synthetic route using $(NH_4)_2S$ as the sulfide source was achieved. TM1 was obtained as the cesium salt, the first time the preparation of this salt in pure form has been reported.

Detailed characterization of the TM products to ascertain their purity had also been previously lacking. Assessment of the purity of these products had typically been based either on elemental analysis or on comparison of the measured UV/visible spectra to any of those available in the literature. However, neither of these approaches is discriminating enough to determine the degree of mutual cross-contamination of the various TMs. In this work, the actual amount of TMs in synthesized samples, as well as the expected absorptivities of each pure TM at several wavelengths, were calculated using a computer model based on a non-linear least squares approach to fit the acquired UV/visible spectral data. The intensities of ^{95}Mo NMR signals could also be used to determine the level of cross-contamination of the various TMs, but with lower precision. Discrepancies in some properties of the TMs described in the literature can

now be ascribed to differences in purity of the TM samples prepared and used by different researchers.

The purity assessment method was also used to assess the effectiveness of preparative column chromatography on Sephadex G-25 at purifying synthesized TMs. The findings in the study support Sephadex G-25 treatment for purifying TMs, with the exception of TM1. The model was also used to determine the levels of TMs in aqueous solutions that mimic those in the rumen.

It was therefore now possible to perform meaningful studies of the solution chemistry of the individual TMs, and their interactions with Cu(II) ions in simple aqueous solutions. These interactions were found to form insoluble products; formation of these was favored by increased ionic strength and reduced pH. The effect of these factors on precipitation was most pronounced for TM4, followed by TM3, TM2, and then TM1. This type of interaction was identified as being kinetically rather than thermodynamically controlled. Both S^{2-} and EDTA compete to some extent with TMs for Cu(II) when they are allowed to react first with the Cu(II) before the TM is added, or when they are added simultaneously with the TMs in solution. However, once Cu(II) reacts with the TMs, neither S^{2-} nor EDTA can strip off the Cu even with a large excess. This is attributed to polymerization of the Cu-TM adduct.

Further experiments were conducted to examine the 3-way interaction between BSA, Cu(II) and TM3 suggested by Wood and Mason (1987). UV/visible spectrophotometric results confirm that this occurs. Ternary complexation occurs for TM3, TM4 and probably TM2. Interestingly, ternary BSA-Cu-TM complex(es) appear soluble in aqueous solution, unlike the Cu-TM complex. The ternary complexes were very stable to acids and the influence of known ligands. Acidification to pH < 2 for several weeks does not lead to the formation of insoluble products as observed in the case of Cu-TM. The UV/visible spectra observed are characteristic of those for Cu-Mo-S complexes, suggesting that the TMs in the ternary complexes are bound directly to the Cu, which also is bound to the proteins.

To examine the possible involvement of the N-terminal amino acid sequence in these ternary interactions, some His-containing peptides were synthesized, characterized and used as BSA models to study their acid-base and Cu(II) complexation behavior, and ternary interactions with TMs and Cu(II). The peptides His-Lys, Thr(Ac)-His-Lys and Asp-Thr(Ac)-His-Lys were synthesized employing traditional peptide synthesis techniques, using water-soluble carbodiimide (EDC) and HOBt as coupling reagents.

Proton NMR spectra of the three peptides were monitored in H_2O solution as a function of pH and added Cu(II) concentration. The spectra were acquired using the binomial composite "1-3-3-1" sequence for water suppression. Reliable K_a values for these peptides were established. Probable binding sites of Cu(II) and the relative strengths of binding to these peptides were elucidated.

It was shown that ternary complexation involving these peptides, Cu(II) and TMs does occur. It was not possible to come to a definitive conclusion with regards to the structure of these ternary complexes, but there was ample evidence to suggest the formation of polymeric species, probably of linear structure for the peptide-Cu-TM4 clusters. The structure and perhaps the strength of the peptide-Cu-TM3 and peptide-Cu-TM2 clusters may be comparable but the TM4 analogue was distinctly different in almost all, if not all the experiments in this study.

7.2 BIOLOGICAL IMPLICATIONS OF THE STUDY

As discussed in Section 1.5, the biochemical relevance of Cu at trace level in living systems cannot be overemphasized and its deficiency causes many diseases. Deficiency can be caused by inadequate Cu intake (**primary Cu deficiency**) or by the presence of an antagonist in the diet (**secondary Cu deficiency**) (Section 1.5.2).

A variety of substances can cause secondary deficiency. The TMs are some of the most potent of these. Considerable experimental evidence supports the hypothesis that TMs are formed in the rumen. These, particularly TM4, react with Cu(II) and

render it unavailable. However, the chemical basis of the interaction between TMs and both dietary and systemic Cu remains unclear. Feed studies have been largely unsuccessful in defining the quantitative effects of dietary Mo and S sources upon the absorption and retention of Cu by ruminants. There were many apparent contradictions in the literature.

These contradictions can be ascribed partly to a previously lacking unambiguous determination of the purity of authentic synthesized TMs. Different TMs may have very different properties and their cross-contamination is a real possibility, so mixtures can give ambiguous results. Using information obtained from the solution chemistry studies in these thesis and those of others, an attempt will now be made to resolve at least some of the apparent contradictions in the literature in this area.

Much of the literature in this area was presented and discussed in detail in Chapter 1; this material will only be summarised here.

7.2.1 TM Formation in the Rumen

Which TM or TMs can be formed in the rumen has long been an issue of contention in the literature. The controversy over the presence or absence of TM4 is particularly significant, because this is the only form that has been shown to affect rats and sheep to the extent of inducing signs of Cu deficiency or of decreased Cu absorption.

Various feed studies in cattle and sheep have detected radioactive labeled TM2 and TM3 (but not TM4) in the blood of animals, which were originally given the TM in the rumen. Earlier solution experiments also could not detect the presence of TM4 on mixing S^{2-} and MoO_4^{2-} at lower S:Mo ratios. This has led to the conclusion by some that TM4 is not formed in the rumen. Others have detected the characteristic absorption spectrum of TM4 in rumen liquor. The levels of Mo and S used in these studies,

however, have been criticized as being above their normal levels. A detailed discussion on this controversy is provided in Section 1.5.2.1.

It can be noted at the outset that the inability to detect TM4 (or any other TM) spectrophotometrically in rumen fluids at normal dietary Mo levels does not necessarily mean that it is absent. High background absorbances may make such measurements difficult. Bray et al.(1982 a & b) were successful in detecting TMs in an artificial rumen system at low Mo levels (4 – 12 mg L^{-1}), by using an oxidative treatment to remove the background interference. Prior to such treatment the TMs could not be measured. For similar reasons, in the present work levels of all the TMs formed at an S: Mo ratio of 22:1 could be measured, after reaction of the buffer system used with some of the excess $(NH_4)_2S$ to remove the intense yellow color of the solution. By contrast, TMs could not be detected even in solutions with higher S: Mo ratios in solutions where the high background absorbance persisted (Sections 2.2.11 and 2.3.9).

Prediction of the particular TM or TMs to be found in the rumen requires extensive knowledge of the conditions in the rumen that can influence the formation and the stability of the TMs, such as the levels, relative proportions and the actual chemical states of Mo, S, and Cu, and the ambient pH and temperature.

Calculations of the S:Mo mole ratios based on dietary information on S and Mo (in grams) from a survey of feed studies on Mo/S/Cu antagonism shows that there is considerable variance in the dietary S:Mo ratios, from as low as 3.2:1 (81ME) to as high as ~ 18,000:1 (97GC). It is necessary to explore in detail what absolute, and relative, levels of S and Mo are most relevant. Under normal agricultural conditions, forages usually contain 2.0 – 4.5 g total sulfur kg^{-1} (DM) with extreme values of 0.2 - 21.1 g kg^{-1} (DM) possible (87BD). The total S^{2-} concentration in rumen liquor of ewes, 2 hr after been given inorganic supplement and organic supplement, to correspond to the proportions found in a herbage containing total S = 4 g kg^{-1}, was found to be 24 mg L^{-1} (i.e. 7.5 x 10^{-4} **M**) (74S). This figure is an underestimate of the actual total sulfide concentration formed in the rumen, because it disregards any

interactions between Mo (molybdate), Cu(II) and other species with S^{2-}. However, it can be used as a basis to estimate S^{2-} levels in the rumen from dietary S intake. If 4 g kg^{-1} dietary S can produce 7.5×10^{-4} **M** S^{2-} in the rumen, then using simple proportion as a first approximation, the observed extreme dietary S value of 21.1 g kg^{-1} (87BD) can be estimated to produce approximately 4.0×10^{-3} **M** S^{2-} in the rumen when the animals under study are subjected to similar conditions.

Higher levels of dietary S appear to be a condition necessary for observing the clinical signs of Cu deficiency in ruminants (87Ga). For example, in some South Australian pastures the continued widespread occurrence of Cu deficiency in sheep and cattle has been attributed largely to the presence in pastures of weeds with unusually high S contents (83MR, 87DL). Cu deficiency has also been reported in three-to-four month-old Simmental calves consuming water high in SO_4^{2-} (1.9 g L^{-1}, ~ 0.06 **M**) (92SC). Even after considering the dilution that will occur in the rumen, the levels of sulfide in the rumen of the calves will be expected to be far in excess over "normal" S level in the rumen (i.e. 7.5×10^{-4} **M** (74S)). Micro-organisms in rumen digesta produce large quantities of S^{2-} by metabolic reduction of inorganic SO_4^{2-} (76GN). A maximum concentration of 97 mg L^{-1} S^{2-} (~ 3×10^{-3} **M**) was found in the rumen when 2.25 g L^{-1} (0.07 **M**) of S as SO_4^{2-} was given (66H, 56A).

The residence time of S^{2-} in the rumen of sheep has been observed to depend on MoO_4^{2-}. In its presence a residence time of about 107 min has been reported for sheep (76GN). With an infusion of 0.52 mmol MoO_4^{2-} daily, the absorption of sulfide from the rumen is decreased by 20 mmol day^{-1} (76GN). The amount of S^{2-} retained in the rumen as a result of this may presumably, represent the level of S^{2-} required to drive the interaction with MoO_4^{2-} to form TMs in this instance. In that case, the concentration ratio of the retained S^{2-} to the MoO_4^{2-}, ~40:1, represents what was required for the formation of TMs in the rumen.

Solution chemistry studies of the formation of TMs from MoO_4^{2-} and S^{2-} salts in aqueous media under conditions which simulate the fluid phase in the rumen were

carried out by Clarke and Laurie (80CL) and also in this study, employing a more rigorous approach in determining the TM levels (Sections 2.2.11 and 2.3.9). The concentration of MoO_4^{2-} in both studies was of the order of 1 x 10^{-4} **M**, a level deemed to be intermediate for the Mo levels reported in animal rumens (80CL, 79GS). Clarke and Laurie (80CL) observed that at S:Mo ratios ≤ 3:1 the reaction did not proceed beyond the TM1 stage. At ratios 5:1-10:1, the reaction proceeded as far as TM2. With S:Mo ≥ 10:1 the formation of TM2 was very rapid, followed by the conversion to TM3 with subsequent partial conversion to the TM4. Only at a very high S: Mo ratio (300:1) was the conversion to TM4 complete. These authors therefore concluded that under physiological conditions TM2 and TM3 form more readily than TM4, and that TM4 formation *in vivo* would occur only after a relatively long period of time and at higher S:Mo ratios. At the time of that study, detailed solution chemistry studies on the individual and specific potency of each of the TMs as antagonists to Cu(II) had not been conducted. It was therefore difficult for Clarke and Laurie 1980 (80CL) to envisage why, for instance, they should accord 20% TM4 formation any special significance with regard to TM interactions with Cu.

In Section 2.3.9, a similar study was conducted, at a S:Mo ratio of 22:1, but calculating the actual levels of each TM as a function of time. During the period from 90 min to 150 min after mixing Na_2MoO_4 and NH_4S as reactants, TM2 and TM3 levels remained almost constant at ~ 28% and ~ 48% of the total Mo species respectively, with a gradual decline in TM1 level and a concomitant buildup of TM4 level. Although the formation of TM4 under these conditions was slow, it was detectable within 30 min, and constituted 18% of the total at the mean S^{2-} residence time (107 min) and 30% within 2 hr. As discussed earlier, the S^{2-} concentration of 2.2 x 10^{-3} **M** used in the study, though higher than a normal value reported in literature (74S) is a plausible value for the rumen fluid of TM-affected ruminants.

It has been argued that the TM2 or TM3 initially formed in the rumen might react with, for example, Cu(II) ions, thus preventing the formation of TM4 (82M). However, at pH > 5, the reactions between Cu(II) and TM3, TM2 or TM1 (to form

insoluble polymeric Cu-TM adducts) are relatively slow compared to that between Cu(II) and TM4 (Section 3.3.1). Furthermore, although the UV/visible spectra indicate some reaction between Cu(II) and each of the TMs within 20 min (Section 3.3.1), the time taken for the initially formed Cu-TM adduct to polymerize into the insoluble products where Cu is more tightly bonded to the TM is so long for the TM1, TM2 and TM3 cases (Section 3.3.1) that it would permit a wide variety of competition reactions between Cu(II)/Cu(I), oxy-TMs (TM1, TM2 or TM3) and sulfides.

For the purposes of discussion, these competition reactions can be divided into two basic categories:

(1) Competition from sulfides with Cu ions for the initially formed oxy-TM. In this case, when the sulfide concentration is very high as compared to that of the Cu ion present in the reaction mixture, competition will favor the sulfide reaction with the oxy-TMs to form TM4, which will in turn rapidly, react with the Cu ion to form eventually the polymeric insoluble Cu-TM4. This idea has some support from the literature. Using TM3 and Cu(I) salts as starting materials, and adding excess Li_2S into the reaction solution after the precursor Cu-TM3 had been formed, it was shown that there existed transformation from TM3 to TM4 in the reaction solution, and there were many kinds of intermediate products before the formation of the final stable product (98GS).

(2) Competition from sulfides with oxy-TM for the Cu ion. It was clearly demonstrated in Section 3.3.1 that increasing amount of S^{2-} inhibits the reaction of TM3 with Cu(II) by forming most likely insoluble CuS. This implies that even in the presence of Cu(II), once the S^{2-} concentration is extremely high, as to be expected in a rumen, TM4 formation is possible because of the initial formation of CuS, permitting further displacement of oxygen atoms on the oxy-TMs by sulfur atoms to form TM4. Once the TM4 is formed, it can react with CuS to form the Cu-TM4 polymeric and insoluble product as discussed in Section 3.3.1.

Local conditions that sometimes prevail in the rumen, such as longer residence time of S^{2-}, lower pH, warmer temperature and increased residence times for the TMs in the rumen all favor the formation of TM4. Examples are cited in the literature of such conditions, as follows:

1. Ingested SO_4^{2-}, which is easily converted to S^{2-} in the rumen, may take as long as 3 to 5 hr to disappear from the rumen (53LW). Anderson (56A), on studying the observed sulfate disappearance and the corresponding S^{2-} production in the rumen of sheep, noticed that the period of observing the peak S^{2-} concentration depended on the amount of SO_4^{2-} ingested. At high concentration (2.25 g L^{-1} of S as SO_4^{2-}), peak S^{2-} concentration was observed about 5 hr after the sheep had been fed the SO_4^{2-}.

2. Lower pH results under concentrate feeding, or when ruminant diets contain much soluble carbohydrates and starch (66H). Note that higher S containing TMs are relatively more stable than the lower ones at low pH (see Section 2.3.8).

3. Rumen temperature may also rise as high as 41°C (66H).

4. The incubation period used for most in *vitro* studies to simulate ruminal disappearance of the feed molybdate is longer than 16 hrs (83EM, 87PW); If this time also represents the residence time of TMs in the rumen then it is so long that even in the absence of excessive amount of S^{2-}, any of the lower S-containing TMs formed in the rumen (TM3, TM2, and TM1) would be expected to reapportion the S ligands on the Mo centres to give the more stable mixture of TM4 and TM0 (molybdate) as discussed in Section 2.3.8.

It can be concluded that a significant amount of TM4 is formed under relevant conditions in the rumen, especially for ruminants that are prone to Mo/S induced copper deficiency. It appears that all the TMs can be formed to some extent in the rumen depending on the S:Mo ratio. However, their persistence in a particular situation depends on the pH, temperature, their residence time, and most importantly the excess

S^{2-} in the rumen. In cases of lower pH, higher temperature, longer residence time of both TMs and S^{2-} and higher S/Mo ratios the TM4 has the advantage over TM1, TM2, and TM3.

7.2.2 Interaction of TMs with Cu in the Gastrointestinal Tract

Solution chemistry studies of the interactions between Cu(II) and TMs indicate initially the formation of stable but soluble substances. These then polymerise to give stable and insoluble polymers, which would be unavailable for metabolic functions. These insoluble products have been found to be mostly polymeric Cu-Mo-S clusters with the Cu in the +1 state (Section 1.2.6).

The initial soluble Cu-TM4 adduct involves such strong binding that it does not exchange Cu ions with even moderately strongly binding ligands like EDTA (100-fold more in concentration) (Section 3.3.1.3). In the presence of His and His-containing peptides such as His-Lys, similar polymeric species involving these biological ligands were found (Section 6.3.3). Hence, the use of amino acid-Cu chelates would not have any advantage over the inorganic Cu(II) salts in the presence of TMs. This complexation involving His and His-containing peptides may not be limited only to these, but may also occur with other amino acids and peptides having side chains with soft ligand atoms such as N and S which would bind Cu(I), as was shown in Figure 6.16.

Decreasing pH and increasing ionic strength favor the formation of the polymeric, insoluble Cu-TM adducts. Hence at low pH (~2), all the TMs form precipitates with Cu(II) (see Section 3.3.2). Since most of Cu absorption in sheep, for example, occurs in the abomasum (pH ~2), small intestines and the colon (96WS) this may explain how TMs reduce Cu absorption, especially TM4 which forms the precipitate at the fastest rate. This is supported by the radioactive labeling studies by Price et al. (87PW): acidification of rumen digesta to mimic passage from rumen to

duodenum, as can be visualized in the schematic diagram shown in Figure 1.5, resulted in the precipitation and coagulation of suspended solids.

Price et al.'s proposition that TMs are "released" in the abomasum (87PW, 91S), because trace amounts of TM2 and TM3 (only 0.5% of the total radioactivity) were detected in the liquid phase of digesta from the duodenum, does not seem likely. Whether Cu(II) is present or absent, the solution chemistry studies discussed in Section 3.3.1 and those earlier (80CL, 82CL, 86LP) do not support this proposition. In the presence of Cu(II), the low pH that pertains in the abomasum would rather favor the formation of the insoluble polymeric Cu-TM adducts. The small amount of TM observed by Price et al. could simply represent Cu-TM2 and Cu-TM3 left in the liquid phase (possibly as ternary complexes with proteins) after the bulk of these species had precipitated. In the absence of Cu(II) and at such low pH values, the TMs will also be degraded quickly to form insoluble solids like MoS_3 (86KM) or MoS_2 (80HM, 92BC).

16 hr after injecting $^{99}MoO_4^{2-}$ in the rumen, Price et al. (87PW) also observed that ^{99}Mo-labelled species in the rumen fluid was present mainly in the solid phase. The ^{99}Mo-labelled species were displaced from the digesta solid by exchange with unlabelled TM4 and the individual species $^{99}MoO_4^{2-}$ (^{99}TM0), $^{99}MoSO_3^{2-}$ (^{99}TM1), $^{99}MoS_2O_2^{2-}$ (^{99}TM2), $^{99}MoS_3O^{2-}$ (^{99}TM3), and $^{99}MoS_4^{2-}$ (^{99}TM4) identified from their characteristic elution profile after separation by chromatography on Sephadex G25 columns. The ^{99}Mo-labelled species in the digesta solid were predominantly ^{99}TM3 (41%) and ^{99}TM4 (34%) as determined from the relative of the areas of the characteristic peaks that are eluted after separation by Sephadex. It was assumed in the study that the association of ^{99}TM with the solid phase of the rumen fluid, which could be displaced by excess unlabelled TM4, was due to the "binding" of the ^{99}TM with some components in the solid phase.

This observation led to the suggestion that although TMs *per se* are unstable in acid solution, and therefore unlikely to escape hydrolysis in the abomasum, they can "bind" with protozoa, bacteria, proteins and other macromolecules in the solid phase of

the rumen liquor to confer stability upon them (91S, 87AG). This hypothesis has since been embraced by many others (87Ga, 90M, 97GC).

However, this hypothesis is inconsistent with the findings in this study, as well as several observations elsewhere in the literature. Perhaps the pervasive notion of TM binding to protozoa, bacteria etc. stems from the fact that TMs have been found bound to plasma albumin (82ML, 84HL, 85HW) and that such interactions have confirmation from solution chemistry studies (87WM, 87CLa). See also Section 3.3.2.1. However, the products formed from TM-Albumin interactions under moderate conditions, for both *in vivo* and *in vitro* studies, are found in the liquid (not the solid) phase of the matrix. The binding between TMs and albumin are also weak and ionic, with no indication of covalent bonding. More importantly, there is no evidence of this binding at pH $\leq$ 3 and at such low pH the TMs are all degraded to form brown precipitates, presumably MoS_3 or MoS_2, even in the presence of BSA (Section 3.3.2.1).

Application of Price et al.'s displacement procedure (97PW), discussed above, to a ^{99}Mo-labeled "Cu(I)-TM4 complex", a crimson-red insoluble complex CuS_2MoS_2Cu formed by the reaction of aqueous TM4 with excess of CuI_2, revealed that ^{99}TM4 in the complex was completely exchangeable with unlabelled TM4 (87PW). Hence, their observation of ^{99}TM displacement in the solid of the rumen, duodenal and ileal digesta by unlabelled TM4 does not preclude the formation of insoluble Cu-TMs. In fact, Price's group (85PC) had earlier shown that available Cu was "associated" mainly with the solid phase on increasing dietary Mo intake. This is probably due to the formation of the insoluble Cu-TM. Furthermore, the elution profiles of ^{99}Mo species in the rumen solid digesta of Cu-treated or untreated sheep were the same after the usual displacement of ^{99}TM in the solid phase of the rumen with unlabelled TM and passage through Sephadex G25 column. This is what would be expected, since the available Cu would already be in the form of Cu-TM adduct. The dietary ratio of Cu:Mo in the grass fed to the sheep in the Price *et al.* study (87PW) was 1.5:1 (i.e. > 1); a ratio which will favor the complete reaction of the TM with the available Cu(II) ions to form Cu-TM. (Detailed discussions on the stoichiometric relationships between Cu and Mo are given

below). "Free" TM should therefore not be expected in the liquid phase of the rumen digesta, and this was precisely what was observed.

Deciding which TM(s) is/are responsible for Mo-induced Cu deficiency rests on the joint consideration of the S:Mo and the Cu:Mo ratios. Judgments in the literature based only on the dietary level of Mo are partly responsible for the controversy in this field. As rightly stated by Gawthorne (87Ga), it is particular values of these *ratios*, rather than of the absolute concentrations of the elements Mo, S and Cu, that can result in Mo-induced copper deficiency.

The presence or absence of TM4 in blood plasma, for instance, will depend on the amount formed in the rumen relative to the amount of Cu(II) present. An excess of TM4 over Cu(II) can result in TM4 absorption to the plasma; otherwise, TM4 will be absent. This is probably why TM4 has been reported as present in blood in some studies (91S, 89GB, 82ML, 88O), but absent from the blood in others (82ML, 84HL, 85HW). For instance, when a sheep is fed a diet containing 6.0 mg Cu kg^{-1} and 6.2 mg Mo kg^{-1} (essentially as TM4) and 4.3 g S kg^{-1} representing a TM4:Cu molar ratio of approximately 0.7:1, only trace amounts of TM4 was found in the blood (87PW). On the other hand, a sheep on a daily diet containing a total of 5.29 mg Cu, 0.71 mg Mo and 2.84 g S showed appreciable quantities of ^{99}Mo present in the blood, five minutes after placing ^{99}Mo-labeled TM4 (20 mg Mo) in the rumen. The TM4: Cu ratio in this sheep after the addition of ^{99}Mo-labeled TM4 will be greater than 2.5. Although sulfides have significant influence on the interaction between Cu(II) and TM as discussed in Chapter 3, and their formation from the dietary S sources is also unquestionable, the observed effects in the two studied sheep above are mainly due to the difference in dietary TM4: Mo ratio and not the difference in the dietary S. The daily food intake of sheep is on the average more than 1 kg, and therefore the dietary S intake in the former sheep (with only a trace TM4 in blood) was more than in the latter. It would therefore be that this increased level of S should indirectly increase the absorption of TM4 from the rumen to the blood as a consequence of a possible interaction between the Cu ions

and sulfides freeing the TMs from interaction with the Cu ions. The contrary is rather observed.

The usual presence of TM3 and TM2 in blood plasma may be due to their relatively slower reactivity with Cu(II) ions as compared to TM4. In a typical rumen mixture of TMs (TM4, TM3 and TM2) in the presence of Cu (II), TM3 and TM2 would therefore be absorbed as they traverse in the intestinal tract towards the abomasum. TM3 is the more likely because of its relative stability over TM2. The preponderance of TM2 and TM3 in the blood does not therefore preclude the formation of TM4 in the rumen.

All the TMs can be absorbed into the blood and lead to the appearance in plasma of a Cu- and Mo- containing fraction, which is associated with albumin and is insoluble in 5% trichloroacetic acid (TCA) (83EM). It has also been observed in rats that both the absorption of TM4 and the subsequent presence of the TCA-insoluble Cu- and Mo-containing product, which is associated with albumin in plasma, are eliminated if dietary Cu is increased. However, similar increases in dietary Cu do not influence the absorption of TM2 and TM3 or the presence of the TCA-insoluble Cu- and Mo-containing product in plasma (83EM). Although these studies were with rats rather than with ruminants, they still support the idea that TM4 is a more potent binding agent for Cu(II) and therefore its absorption is prevented, whereas the absorption of TM2 and TM3 is permitted. As demonstrated in Section 3.3.1, the kinetics of the reaction between Cu(II) and TMs favor the higher forms of TMs. Hence, at comparable levels of these TMs in the rumen, TM4 (or TM3) are the more likely candidates for the formation of the insoluble polymeric complex which renders both Cu and TM4 unavailable for absorption.

In Chapter 3, it was demonstrated that the stoichiometry for the interaction of Cu(II) with TM (TM2, TM3 and TM4) is 1:1 (Section 3.3.1). It was also demonstrated in that chapter that under pH conditions that simulate passage of fluid from the rumen to the abomasum (see Figure 1.5), there is the formation of an insoluble 1:1 Cu-TM

complex for any of the four TMs. Although the stoichiometry for Cu(II) and TM3, and Cu(II) and TM4 interactions is indeed 1:1, as observed earlier by Clarke and Laurie (82CL), at pH ~7 in aqueous solution, a higher Cu(II):Mo ratio (1.5 to 1.6 for Cu-TM4 (86LP,98EH,00L) is required to drive the reaction to completeness. This higher ratio should not, however, be confused with the actual stoichiometry (1:1) of the reaction in the absence of other ligands. Nevertheless, in Chapter 6, it was clear that His and His containing peptide are involved in a 3-way interaction to form ternary complexes whose stoichiometry appears different from the 2-way interaction between Cu(II) and TM. Although the stoichiometry was not established with certainty, the Cu:Mo ratio for the ternary complexes formed between Cu(II), His-Lys (or His) and TM4 seem to be in the range 1.5:1 to 2:1 (Section 6.3.4).
Sarkar and Mishra (84SM) in reacting CuS with TM4 in a varied reacting ratios of 1:1, 2:1, 3:1 and 4:1 in the presence of o-phenanthroline has also observed a varied stoichiometry for the resulting product but observed a general tendency for the formation of a 2:1 (Cu:Mo) stoichiometric product.

Dietary Cu:Mo ratios should therefore probably exceed 1.5 to allow the effective absorption of Cu(II) in cases where there are no co-ligands (Section 1.2.4) that can form ternary complexes with Cu and TM in the rumen. On the other hand, when such co-ligands are present, higher dietary Cu:Mo ratios, probably exceeding 2.0, would be required for the effective absorption of Cu(II). It had earlier been determined in some feed studies (89GB, 71MM) that a Cu:Mo ratio of less than 2.0 is likely to cause Cu deficiency in cattle.

In the light of the above discussions, the observation of TM3 and TM2 (and not TM4) in the plasma of sheep and cattle infused with molybdate (82ML, 87WM, 84HL, 85HW) should not be surprising. Although the dietary S:Mo ratios in these studies were approximately 300:1, it is important to note that the S administered in the diet was in the elemental form (poor solubility in water), and hence the actual HS^- : Mo ratio in the rumen would be well below this. With a Mo:Cu ratio of 1.8:1 in some of these studies (84HL, 85HW), about 56 % of the TM formed in the rumen is predicted to react

with Cu(II) to form the insoluble Cu-TMs, assuming no 3-way complexation occurs. If such complexes do form, about 28 % of the TM will participate in their formation. The Cu-TM or the coligand-Cu-TM formed would be mostly as Cu-TM4 or coligand-Cu-TM4, with probably a small amount of TM3 analogs. The unreacted TM3 and TM2 will be absorbed prior to the abomasum (82M).

Once this issue of how the stoichiometry of Cu:Mo:S and other co-ligands affect Cu(II) or TM absorption is resolved, it is possible to explain many diverse observations in the animal science literature, such as the following:

1. Ruminants grazing on England pastures containing 14 to 108 ppm Mo, and on New Zealand pastures containing 7 to 16 ppm Mo both develop similar debilitating diarrhea and signs of copper deficiency (87Ga). (Because the Mo: Cu ratio in both cases was > 3:1.)
2. The continuous feeding of a semi-purified diet, high in S but low in Mo, decreased Cu availability in sheep more than did once daily feeding (91S). (Because the former increased rumen sulfide over the latter (91S)).
3. TM4 was absent or only in trace amounts in blood plasma despite its existence almost exclusively in this form in rumen digesta or when TM4 is injected directly into the rumen (87PW). (Because the Cu: Mo ratio in that study was 1.5:1 (> 1).) However, diets containing both TM4 and MoO_4^{2-} and S^{2-} in rats cause a decline in ceruloplasmin (Section 1.5.2.1) activity (81ME). (Because the Cu:Mo ratios are respectively 1: 2.63 and 1:7.7 i.e. both ratios are < 1.)

To summarize: When the dietary S:Mo ratio is high enough, TMs (including a substantial amount of TM4) will form. Cu-TM4 will preferentially be formed from the TM interaction with Cu(II). Alternatively, coligand-Cu-TM4 will be formed when co-ligands that can engage in 3-way interactions are present. The analogs of the other TMs are less probable, since theTM4 products are formed most rapidly. Both Cu-TM and Cu-coligand-TM adducts are polymeric and insoluble, and hence are not absorbed but

are excreted in the feces. TM4 in excess of Cu(II) could be absorbed, as could the other TMs, from the rumen or perhaps from the omasum.

7.2.3 Interaction of TMs with Cu in the Blood or other Tissues

After uptake in the gut, Cu is bound by albumin and to a lesser extent by certain amino acids such as His, Thr and Gln. Cu is then transported as Cu-albumin or Cu-amino acid complexes to the liver and other tissues where the Cu species are taken up rapidly (80B, 87Ha).

7.2.3.1 TM Effects on Plasma Copper and some Tissues

TM2, TM3 (82ML, 84HL, 85HL) and TM4 (91S, 89GB, 89GL, 83EM, 88O) have all been observed to be bound to albumin in the plasma of different ruminants; i.e. sheep, cattle and deer. The main site for the absorption of TM intact is presumably the rumen, since the low pH in the abomasum will cause the break down of the TMs to the Mo sulfides such as MoS_2 and MoS_3 (Section 1.2.3).

There is general agreement in the literature, for both *in vitro* and feed studies, that ternary albumin-Cu-TM complexes are formed (Section 1.5.2.2). (See also Section 3.3.2.2). However, authors disagree about the actual mechanism involved *in vivo.* The Cu in this ternary complex which involves albumin, precipitates with the protein upon acidification with 5% TCA (91S, 82ML, 87PW). TCA is normally used to determine total blood Cu by precipitating the proteins, leaving the Cu behind in soluble form (75DD).

From the studies reported in Chapter 3, it appears that two possible modes of action could account for the ternary complex(es) found in the plasma of animals:

1. Binding of Cu to albumin after absorption (89GL) and the subsequent transport of the Cu by albumin in the blood circulation, followed by interaction with TMs newly absorbed into the blood (Figure 7.1). Uptake of Cu by liver and kidney is

thereby prevented. (Once Cu is digested its further uptake is normally controlled by the albumin circulating in the blood, which presumably delivers the Cu to the liver (91FW).

2. Binding of a TM to albumin or other proteins after its absorption from the GI tract whilst in transit from the rumen to the abomasum. Albumin or other proteins in this TM-bound form may then be transported to the liver and other tissues, where previously stored Cu or Cu from various enzymes can be removed in the form of a ternary complex (Figure 7.1), causing various systemic effects.

The studies with the BSA peptide model compounds reported in Chapter 6 gave results consistent with Hypothesis 1, i.e., the formation of a (BSA or peptide)-Cu-TM ternary complex. These studies did not, however, indicate any interactions between TMs and the peptides to support Hypothesis 2, although such interactions were observed for BSA itself and TM3 or TM4. Such binding, if it occurs at all, must occur at a different site than the amino terminal. In the presence of Cu(II) however, a relocation from this site to the Cu(II) binding site (i.e. the amino terminal) is possible.

A third hypothesis, of a binding of a "soluble Cu-TM complex" to albumin in the blood (00OC) seems implausible since the addition of BSA to a Cu-TM mixture does not in fact prevent the formation of the insoluble Cu-TM adduct (see Section 3.3.2.2). It is also unlikely that transported TM4 in the blood circulation will be present in the "free" (non-protein bound) form to form Cu-TMs, unless it is in high excess over the concentration of albumin, which is about 0.7 m**M** (97HS). In that instance, competition of unbound TMs with TM-BSA for Cu(II) could be possible. This may explain the observation of insoluble Cu-TM4 in the liver of rats given an overdose of TM4 (00OC). However, this situation seems highly improbable for ruminants.

Are other proteins in the blood also involved in similar three way interactions? There is no direct evidence of other proteins interacting in the same way as albumin. However, the observation of a high molecular weight Cu and TM bound proteins of

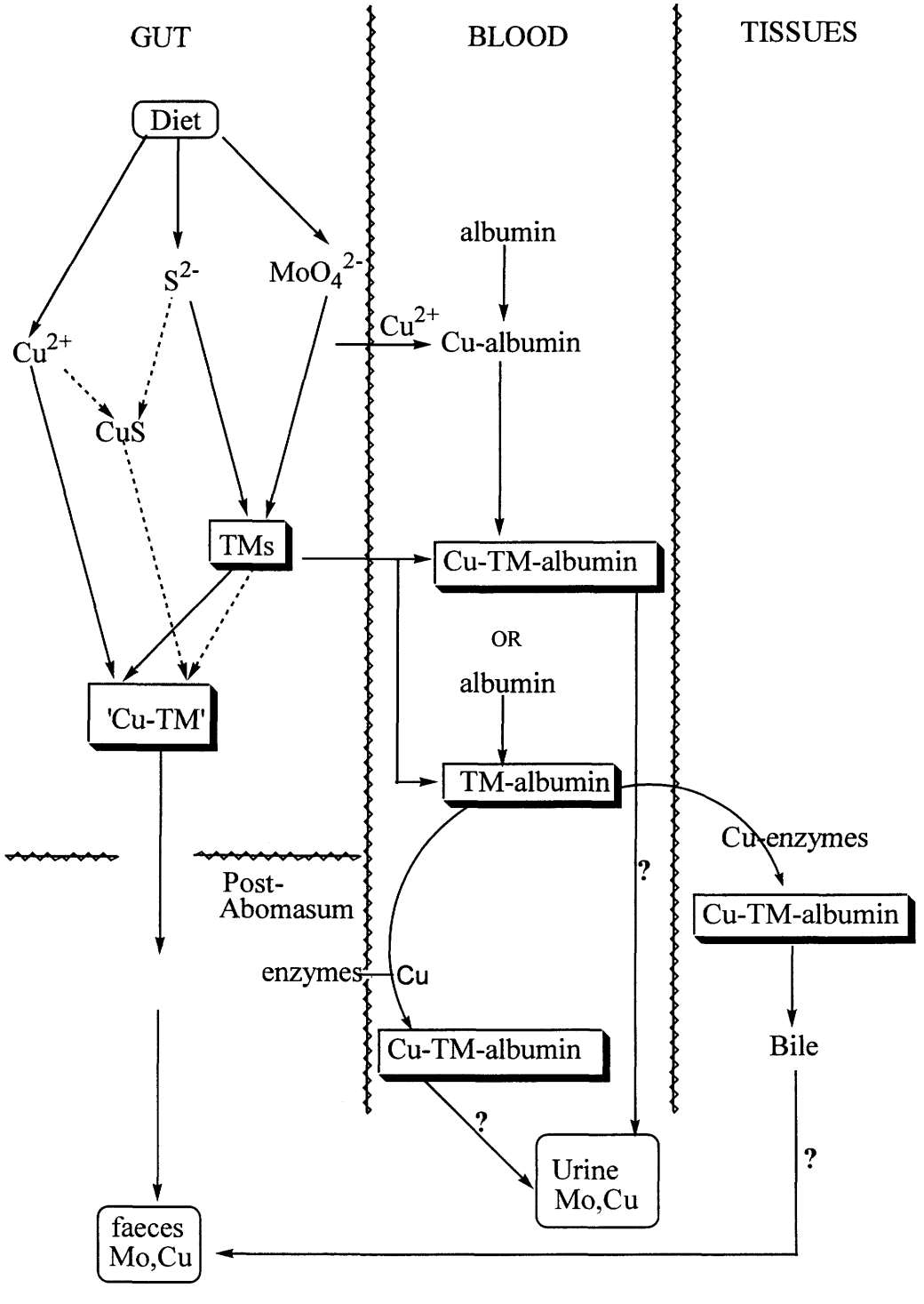

Figure 7.1: Proposed scheme for the interaction of copper, molybdenum, and sulfur compounds in the gut, blood and other tissues of ruminants.

MW ~90,000 Daltons in the liver of sheep (80NS), ~ 100,000 Daltons from extracts of the livers and kidneys of rats and sheep (87AG) and other observations like these, seem to suggest the involvement of at least one more protein of MW ~ 90,000 (87Ga). Also in plasma, a significant proportion of Mo was found to be bound, probably to the same protein (MW ~ 90,000 Daltons) in sheep supplemented with Mo and considerable amounts of sulfate (78BY).

There is no experimental evidence in the literature to suggest that proteins such as ceruloplasmin (Cp), superoxide dismutase (SOD) and Metallothionein (MT) are involved in the 3-way interaction. Albumin bound TMs or "free TMs" may strip off "loosely" bound Cu in these proteins to form Cu-TM. There is ample evidence in the literature to support the idea that TMs "strip" Cu from MT (87AG, 88WM, 89GB, 96OO,98OS, 00OC). TM4 and TM2 have been reported to displace Cu from both SOD and Cp in rats; the displaced Cu was said to be found in the plasma in the form of albumin-Cu-TM complexes (99OK).

7.2.3.2. Excretion of the BSA-Cu-TM Complex

Pharmacological doses (5.4 to 62.5 mg Mo) of ^{99}Mo labeled TM2, TM3 and TM4 injected intravenously in sheep (83ML) showed initial rapid and extensive hydrolysis to what was presumed to be molybdate, which was rapidly excreted in urine over the first 15 min post injection. Thereafter the residual radioactivity in the blood was mainly in TCA-insoluble forms, presumably as ternary albumin-Cu-TM complexes (containing ^{99}Mo-TM2, ^{99}Mo-TM3 and ^{99}Mo-TM4), which were slowly cleared from the blood, with a half- life of about 30 hr for TM2 and 40 hr for TM3 and TM4. When [^{185} W] trithiotungstate is also injected intravenously to both sheep and cattle, it is found to circulate in plasma bound to proteins, mainly albumin as also discussed for [^{99}Mo] TM above (94ML). The studies with sheep showed that the final fate included hydrolysis and excretion of label in urine as [^{185} W] tungstate (89MM). These observations have formed the basis for the suggestion, by analogy with the metabolism of thiotungstates, that albumin-Cu-TM complexes could eventually be hydrolyzed and

their constituent Mo excreted in urine, with the previously complexed Cu simultaneously released (91S); the fate of this Cu was not indicated.

However, the solution chemistry studies in Chapter 3 do not support this hypothesis. Even at pH < 2, there was no evidence of the hydrolysis of albumin-Cu-TM for several weeks (Section 3.3.3.1). The studies in Chapter 2 suggest that it is probably rather unreacted TMs that undergo such hydrolysis. Excess albumin-TM or "free" TM over Cu in the blood is a real possibility, at least initially before any interaction with Cu from any other tissues. It is likely, therefore, that the decrease of the ^{99} labeled Mo from the blood to the urine is due to the hydrolysis of albumin-TM or "free" TM and ***not*** of albumin-Cu-TM.

Since the solution chemistry studies discussed in Chapter 3 do not support the hydrolysis of Cu-albumin-TM presumed to occur from earlier feed studies with sheep and cattle (89MM, 91S), a question that should be addressed is how this ternary product might be excreted. Radio-labeled Cu injected into sheep has been found excreted together with Mo in the urine (89GL, 89GLa), suggesting that Cu and Mo may be together in an excreted compound in the urine. In the ternary complex (albumin-Cu-TM), albumin may serve as the vehicle by which Cu and TM are transferred to the kidney to accumulate therein (89GB). Albumin is slowly degraded in kidney tubule cells (89Ga). It is possible that the degradation of albumin, even when bound to Cu and TM, can still proceed to form a lower molecular weight species containing Cu-TM, and that this degraded form is what is passed through the urine. In this case the degraded albumin could be reabsorbed to eventually replenish what was lost. Since albumin degradation is slow, this hypothesis explains why TM treated animals have been found with increased urinary Cu in studies that are long-term (88ML, 89GL, 89GLa) but not in those that are short-term (88ML, 91S). Perhaps a similar mechanism of protein degradation of the 3-way complex (Cu-protein-TM) occurs in the bile, which is known to be a major TM-induced Cu excretory route (89GB, 89GL).

In summary, it is concluded that TMs could render Cu non-bioavailable in cattle and other ruminants by three means:

a) *by causing impaired intestinal absorption of Cu.* This is achieved by the formation of stable and polymeric compounds, which are insoluble in the high ionic strength rumen liquor, and in the very low pH (~2) liquor, during transit to the intestine.

b) *by preventing Cu uptake to the storage compartment of the liver by absorbed TMs.* This is achieved by interaction of TMs with Cu-albumin in the blood circulating system.

c) *by altering the distribution of Cu in tissues.* This can be achieved only when the TM to Cu(II) mole ratio in the GI tract is greater than unity and perhaps greater than 2 when low molecular weight co-ligands such as His and His-containing peptides are present in the gastrointestinal tract. The TM is bound to a BSA or to other proteins, and in those forms can remove Cu in many tissues (eg. liver, kidney, etc) to form the soluble, stable ternary complex. By this means, Cu is removed from the liver and other organs.

7.3 FUTURE WORK

Although the solution chemistry studies outlined in this thesis provide considerable insight into many of the controversial results from animal studies concerning the formation of TMs in the rumen, a more conclusive method should consider direct UV/visible measurement of the TMs of actual rumen liquor once background signals problems are addressed. Such studies could also be used to track the TMs further down the digestive tract.

The studies presented in this thesis have shown that ^{1}H NMR is a sensitive, reliable and informative method for the study of the acid-base behavior of peptides of various chain lengths. The NMR approach also proved very useful in providing structural information about the Cu complexes. However, the paramagnetic behavior of Cu(II) did not lend itself easily to quantitative measurement of the concentrations of

Cu(II) complexes and hence of their formation constants. Potentiometric techniques are, however, well known for their improved precision over NMR techniques especially for paramagnetic species, and will therefore provide more reliable K_f values.

It is obvious that a complete understanding of how TMs bind Cu(II), in the presence or absence of peptides and proteins, would involve consideration of redox chemistry. Electrochemical studies would throw more light on these interactions and help to explain how TMs prevent the absorption and the utilization of Cu(II).

Understanding of the mechanism for the formation of the ternary albumin-Cu-TM complex is still lacking. Further studies along the lines of those described in the thesis utilizing different amino acids and peptides would help to test the generality of the involvement of amino acids and peptides in the ternary complexation. More thorough studies (e.g. EXAFs, NEXAFs, XPS etc.) and more detailed elemental analyses on the solid products of the ternary complexation is required to obtain definite structural information on the complex. The use of ^{95} Mo NMR may also help in defining the nature and strength of the interaction between TMs and albumin, and of ternary complexation.

REFERENCES

1826B J.J. Berzelius, *Poggendorffs Ann. Phys. Chem.*, *7*, 262 (1826).

1826Ba J.J. Berzelius, *Poggendorffs Ann. Phys. Chem.*, *8*, 269 (1826).

22M J.W. Mellor, '*A Comprehensive Treatise on Inorganic and Theoretical Chemistry*', Vol IX, Longmans, London, 1922.

53LW G.P. Lofgreen, W.C. Weir and J.F. Wilson, *J. Anim. Sci.*, *12*, 347 (1953).

56A C.M. Anderson, *New Zealand J. Sci. Technol.*, *A37*, 379 (1956).

61BT J.C. Bernard and G. Tridot, *Bull. Soc. Chim. France*, 810 (1961).

61BTa J.C. Bernard and G. Tridot, *Bull. Soc. Chim. France*, 818 (1961).

61FP A.A. Frost and R.G. Pearson, '*Kinetics and Mechanism*', 2nd Edn, J. Wiley and Sons, New York (1961).

61RR F.J.C. Rossotti and H. Rossotti, *'The Determination of Stability Constants'*, Mc Graw-Hill, New York (1961).

62D C.W. Davies, '*Ion Association*', Butterworth, London (1962).

64SS H. Schäfer, G. Schäfer and A. Weiss, *Z. Naturforsch. B*, *19*, 76 (1964).

65FS H.C. Freeman and J.T. Szymanski, *Chem. Commun.*, 598 (1965).

65W W.E. Wenworth, *J. Chem. Ed.*, *42*, 96 (1965).

66H R.E. Hungate, *'The Rumen and its Microbes'*, Academica Press, New York (1966).

67BF J.F. Blount, K.A. Fraser, H.C. Freeman, J.T. Szymanski and C-H. Wang, *Acta Crystallogr.*, *22*, 396 (1967).

67PB T. Peters Jr. and F.A. Blumenstock, *J. Biol. Chem.*, *242*, 1574 (1967).

67SB W.T. Shearer, R.A. Bradshaw and F.R.N. Gurd, *J. Biol. Chem.*, *242*, 5451 (1967).

68BS R.A. Bradshaw, W.T. Shearer and F.R.N. Gurd, *J. Biol. Chem.*, *243*, 3817 (1968).

68G W.B. Guenther, '*Quantitative Chemistry: Measurements and Equilibrium*', Addison-Wesley Publishing Company, Reading (1968).

68MD A. Müller, E. Diemann, B. Krebs and M.J.F. Leroy, *Angew. Chem. Int. Ed. Engl.*, *7*, 817 (1968).

68SJ R.S. Saxena, M.C. Jain and M.L. Mittal, *Austr. J. Chem.*, *21*, 91 (1968).

68SW B. Sarkar and Y. Wigfield, *Can. J. Biochem.*, *46*, 601 (1968).

69AR P.J. Aymonino, A.C. Ranade, E. Diemann and A. Müller, *Z. Anorg. Allg. Chem.*, *371*, 300 (1969).

69MD A. Müller, E. Diemann and U. Heidborn, *Z. Anorg. Allg. Chem.*, *371*, 136 (1969).

70BR W.P. Binnie, M.J. Redman and W.J. Mallio, *Inorg. Chem.*, *9*, 1449 (1970).

70IB M. Ihnat and R. Bersohn, *Biochem.*, *9*, 4555 (1970).

70KM B. Krebs, A. Müller and E. Kindler, *Z. Naturforsch B*, *25*, 222 (1970).

70KMa A. Kay and P.C.H. Mitchell, *J. Chem. Soc. A.*, 2421 (1970).

70MD A. Müller, E. Diemann and E. J. Baran, *Z. Anorg. Allg. Chem.*, *375*, 87 (1970).

70RJ G.C.K. Roberts and O. Jardetzky, *Adv. Protein Chem.*, *24*, 447 (1970).

70SM W. Stumm and J.J. Morgan, '*Aquatic Chemistry*', J. Wiley and Sons, New York (1970).

70SF S. Shaltiel and M. Fridkin, *Biochem.*, *9*, 5122 (1970).

71AS D.W. Appleton and B. Sarkar, *J. Biol. Chem.*, *246*, 5040 (1971).

71LK S-J. Lau, T.P.A. Kruck and B. Sarkar, *J. Biol. Chem.*, *246* 5938 (1971).

71MM J.E. Miltimore and J.L. Mason, *Can. J. Anim. Sci. 51*, 193 (1971).

72MM A. Müller and R. Menge, *Z. Anorg. Allg. Chem.*, *393*, 259 (1972).

72OS R. Österberg, B. Sjöberg, and R. Söderquist, *Acta Chem., Scand., 26*, 4184 (1972).

73B R.G. Bates, *'Determination of pH: Theory and Practice'*, J. Wiley and Sons, New York (1973).

73DM E. Diemann and A. Müller, *Coord. Chem., Rev., 10*, 79 (1973).

73H N.W. Hanson *'Official Standardised and Recommended Methods of Analysis'*, Heffers, Cambridge (1973).

73LC J. Lapasset, N. Chezeau and P. Belougne., *Acta Crystallogr. B, 29*, 3087 (1973).

73MH G.N. La Mar, W.D. Horrocks, Jr. and R.H. Holm, *'NMR of Paramagnetic Molecules, Principles and Application'*, Academic Press, New York (1973).

74AY H. Aiba, A. Yokoyama and H. Tanaka, *Bull. Chem. Soc. Japan, 47*, 136 (1974).

74B E.J. Billo, *Inorg. and Nucl. Chem. Lett., 10*, 613 (1974).

74DS J.W. Dixon and B. Sarkar, *J. Biol. Chem., 249*, 5872 (1974).

74LK S-J. Lau, T.P.A. Kruck and B. Sarkar, *J. Biol. Chem., 249*, 5878 (1974).

74S N. F. Suttle, *Br. J. Nutr., 32*, 559 (1974).

74YA A. Yokoyama, H. Aiba and H. Tanaka, *Bull. Chem. Soc. Japan, 47*, 112 (1974).

75DD A.T. Dick, D.W. Dewey and J.M. Gawthorne, *J. Agric. Sci., 85*, 567 (1975).

76BK M. Bondansky, Y.S. Klausner and M.A. Ondetti, *'Peptide Synthesis'*, Wiley, New York (1976).

76CC N. Camerman, A. Camerman and B. Sarkar, *Can. J. Chem., 54*, 1309 (1976).

76EM W.G. Espersen and R.B. Martin, *J. Amer. Chem. Soc., 98*, 40 (1976).

76GN J. M. Gawthorne and C. J. Nader, *Br. J. Nutr.*, **35**, 11 (1976).

76KL T. P. A. Kruck, S. Lau and B. Sarkar, *Can. J. Chem., 54*, 1300 (1976).

76LC J. Lapasset, N. Chezeau and P. Belouge, *Acta Crystallogr. B, 32*, 3087 (1976).

76LN O. Lutz, P. Nolle and P. Kroneck, *Z. Naturforsch A, 31*, 454 (1976).

76P G.R. Pettit, '*Synthetic Peptides*', Vol. 4, Elsevier, Amsterdam (1976).

76W K. Wüthrich, '*NMR in Biological Research*', North-Holland, Amsterdam (1976).

77LN O. Lutz, P. Nolle and P. Kroneck, *Z. Naturforsch A, 32*, 505 (1977).

77LNa O. Lutz, P. Nolle and P. Kroneck, *Z. Phys. A, 282*, 157 (1977).

77OS V.R. Ott, D.S. Swieter and F.A. Schultz, *Inorg. Chem., 16*, 2538 (1977).

77RG D.L. Rabenstein, M.S. Greenberg and C. A. Evans, *Biochem., 16*, 977 (1977).

77U E. J. Underwood, '*Trace Elements in Human and Animal Nutrition*', 4th Edn., J. Wiley and Sons, New York (1977).

77VV R.R. Vold and R. Vold, *J. Magn. Reson., 19*, 365 (1977).

78BY I. Bremmer and B.W. Young, *Br. J. Nutr., 39*, 325 (1978).

78IL K.S. Iyer, S-J. Lau, S.H. Laurie and B. Sarkar, *Biochem. J.*, **169**, 61 (1978).

78M J. Mason, *Vet. Sci. Comm., 2*, 85 (1978).

78MN A. Müller, W.O. Nolte, and B. Krebs, *Angew. Chem., Int. Ed. Engl., 17*, 279 (1978).

78SK I. Sóvágó, T. Kiss and A. Gergely, *J. Chem. Soc. Dalton Trans.*, 964 (1978).

78Z W.G. Zumft, *Eur. J. Biochem., 91*, 345 (1978).

79GS N.D. Grace and N.F. Suttle, *Br. J. Nutr., 41*, 125 (1979).

79RM W. Ritter, A. Müller, A. Neumann, W. Bäther and R.C. Sharma, *Angew. Chem. Int. Ed. Engl., 18*, 530 (1979).

79WL K. M. Weber, D.D. Leaver and A.G. Wedd, *Br. J. Nutr., 41*, 403 (1979).

80B I. Bremmer, in *'Biological Roles of Copper (Ciba Foundation Symposium 79'*, C. F. Mills ed., Excerpta Medica, Amsterdam (1980) p. 23.

80CL N.J. Clarke and S.H. Laurie, *J. Inorg. Biochem.*, *12*, 37 (1980).

80CP K.P. Callahan, P.A. Piliero, *Inorg. Chem.*, *19*, 2619 (1980).

80HS M.A. Harmer and A.G. Sykes, *Inorg. Chem.*, *19*, 2881 (1980).

80LS J-P. Laussac and B. Sarkar, *J. Biol. Chem.*, *255*, 7563 (1980).

80MB A. Müller, H. Bögge, H-G. Tolle, R. Jostes, U. Schmanski and M. Dartmann, *Angew. Chem. Int. Ed. Engl.*, *19*, 654 (1980).

80MD A. Müller, H. Dornfeld, H. Schulze and R.C. Sharma, *Z. Anorg. Allg. Chem.*, *468*, 193 (1980).

80NS G. Norheim, N.E. Søli, A. Frøslie and M. Mjør-Grimsrud, *Acta Vet. Scand. 21*, 428 (1980).

80PF L. Pickart, J.H. Freedman, W.J. Loker, J. Peisach, C.M. Perkins, R.E. Stenkamps and B. Weistein, Nature, *288*, 715 (1980).

80S N.F. Suttle, *Proc. Nutr. Soc.*, *39*, 63A (1980).

81GP S.F. Gheller, P.A. Gazzana, A.F. Masters, R.T.C. Brownlee, M.J. O'Connor and A.G. Wedd, *Inorg. Chim. Acta*, *54*, L131 (1981).

81J R.F. Jameson, 'Metal ions in Biological Systems', Vol. 12, Marcel Dekker, New York (1981).

81L S-J. Lau and B. Sarkar, *J. Chem. Soc. Dalton Trans.*, 491 (1981).

81MD A. Müller, E. Diemann, R. Jostes and H. Bögge, *Angew. Chem. Int. Ed. Engl.*, *20*, 934 (1981).

81MDa A. Müller, M. Dartmann, C. Römer, W. Clegg and G.M. Sheldrick, *Angew. Chem. Int. Ed. Engl.*, *20*, 1060 (1981).

81ME C.F. Mills, T.T. El-Gallad and I. Bremmer, *J. Inorg. Biochem.*, *14*, 163 (1981).

81MEa C.F. Mills, T.T. El-Gallad and I. Bremmer, *J. Inorg. Biochem.*, *14*, 189 (1981).

81WR D. Wolfgang and G. Reinhard, *J. Magn. Reson. 44,* 229 (1981).

82BS J.R. Brown and P. Shockley, in '*Lipid-Protein interactions*', Vol 1, P. Jost and O.H. Griffith eds., J. Wiley and Sons, New York (1982) p.25.

82BSa A.C. Bray, N.F. Suttle and A.C. Field, *Proc. Nutr. Soc. 41*, 66A (1982).

82BSb A.C. Bray, N.F. Suttle and A.C. Field, *Proc. Nutr. Soc. 41*, 67A (1982).

82CL N. J. Clarke and S. H. Laurie, *Inorg. Chim. Acta*, *66*, L35 (1982).

82DS M. Draganjac, E. Simhon, L.T. Chan, M. Kanatzidis, N.C. Baenziger and D. Coucouvanis, *Inorg. Chem. 21*, 3321 (1982).

82FS E. Farkas, I. Sovago and A. Gergely, *J. Chem. Soc. Dalton Trans.*, 2159 (1982).

82M J. Mason, *Ir. Vet. J.*, *36*, 164 (1982).

82MJ A. Müller, W. Jaegermann and J.H. Enemark, *Coord. Chem. Rev.*, *46*, 245 (1982).

82ML J. Mason, M. Lamand and C. A. Kelleher, *J. Comp. Path.*, *92*, 509 (1982).

82MK J. Mason, C.A. Kelleher and J. Letters, *Br. J. Nutr.*, *48*, 391 (1982).

82SF I. Sóvágó, E. Farkas and A. Gergely, *J. Chem. Soc. Dalton Trans*, 2159 (1982).

82SM H. Sigel and R.B. Martin, *Chem. Rev.*, *82*, 385 (1982).

82SMa W. B. Simpson and C.F. Mills, *J. Inorg. Biochem.*, *17*, 155 (1982).

83AG S. R. Acott, C. D. Garner and J. R. Nicholson, *J. Chem. Soc. Dalton Trans.*, 713 (1983).

83AS J.P.S. Arora, R.P. Singh, D. Soam, S.P. Singh and K. Kumar, *Bioelectrochem. Bioenerg.*, *10*, 441 (1983).

83C S. H. Chiou, *J. Biochem. (Tokyo)*, *94*, 1259 (1983).

83DE A. Demaret, A. Ensuque and G. Lapluye, *J. Chim. Phys. Phys.-Chim. Biol.*, *80*, 475 (1983).

83EM T.T. El-Galland, C.F. Mills, I. Bremmer and R. Summers, *J. Inorg. Biochem.*, **18**, 323 (1983).

83H P.J. Hore, *J. Magn. Reson.*, *55*, 283 (1983).

83MB A. Müller, H. Bögge and U. Schmanski, *Inorg. Chim. Acta*, *69*, 5 (1983).

83MD A. Müller, U. Schmanski and T. Schmanski, *Inorg. Chim. Acta, 76*, L245 (1983).

83MF J. W. McDonald, G. D. Friesen, L. D. Rosenhein and W. E. Newton, *Inorg. Chim. Acta.*, *72*, 205 (1983).

83ML J. Mason, M. Lamand and M. Hynes, *J. Inorg. Biochem.*, *19*, 153 (1983).

83MW P. M. May, J. Whittaker and D. R. Williams, *Inorg. Chim. Acta*, *80*, L5 (1983).

83MR R.H. Merry, D.J. Reuter, K.G. Tiller and G.J. Young, *Aust. J. Exp. Agric. Anim. Husb.*, *23*, 24 (1983).

83NF J.R. Nicholson, A.C. Flood, C.D. Garner and W. Clegg, *J. Chem. Soc. Chem. Commun.*, 1179 (1983).

84BB M. Bondansky and A. Bodansky, *'The Peptide Synthesis'*, Springer-Verlag, New York (1984).

84CB B.P. Czech and R.A. Bartsch, *J. Org. Chem.*, *49*, 4076 (1984).

84CBa M.V. Chidambaran, G. Barnes and E. Frienden, *J. Inorg. Biochem.*, *22*, 231 (1984).

84FS E. Farkas, I. Sovago and A. Gergely, *J. Chem. Soc. Dalton Trans.*, 611 (1984).

84GH S.E. Gheller, T.W. Hambley, J.R. Rodgers, R.T.C. Brownlee, M.J. O'Connor, M.R. Snow and A.G. Wedd, *Inorg. Chem.*, *23*, 2519 (1984).

84HL M. Hynes, M. Lamand, G. Montel and J. Mason, *Br. J. Nutr.*, *52*, 149 (1984).

84HV J. Heut and E. Vilkas, *Inorg. Chim. Acta*, *91*, 43 (1984).

84LP S. H. Laurie, D.E. Pratt and J.H.L. Yong, *Inorg. Chim. Acta*, *93*, L57 (1984).

84LS J-P. Laussac and B. Sarkar, *Biochem., 23* 2832 (1984).

84ME M. Minelli, J.H. Enemark, J.R. Nicholson and C.D. Garner, *Inorg. Chem. 23*, 4386 (1984).

84MR D. Müller, D-L. Révérend and B. Sarkar, *J. Inorg. Biochem., 21*, 215 (1984).

84PH W. H. Pan, M. A. Harmer, T.R. Halbert and E.I. Stiefel, *J. Am. Chem. Soc., 106*, 459 (1984).

84RR M.J.A. Rainer and B.M. Rode, *Inorg. Chim. Acta, 92*, 1 (1984).

84RRa M.J.A. Rainer, and B.M. Rode, *Inorg. Chim. Acta, 93*, 109 (1984).

84SM S. Sarkar and S.B.S. Mishra, *Coord. Chem. Rev., 59*, 239 (1984).

85BG S. Bristow, C.D. Garner, S.K. Hagyard, G.A. Morris, J.R. Nicholson and C.F. Mills, *J. Chem. Soc. Chem. Commun.*, 479 (1985).

85BP R.D. Boss and A.I. Popov, *Inorg. Chem., 24*, 3660 (1985).

85CB A.C. Culer, T. Brittain and P.D.W. Boyd, *J. Inorg. Biochem., 24*, 199 (1985).

85DA S.A. Daignault, A.P. Arnold, A.A. Isab and D. L. Rabenstein, *Inorg. Chem., 24*, 3984 (1985).

85E G.E. Ewing, *'Instrumental Methods of Chemical Analysis'*, 5th Edn., McGraw-Hill, New York (1985).

85HW M. Hynes, M. Wood, D. Poole, P. Rogers and J. Mason, *J. Inorg. Biochem., 24*, 279 (1985).

85PC J. Price and J.K. Chester, *Br. J. Nutr., 53*, 323 (1985).

85PH W.-H. Pan, T.R. Halbert, L.L. Huchings and E.I. Stiefel, *J. Chem. Soc., Chem. Commun.*, 927 (1985).

85RR M.J.A. Rainer and B.M. Rode, *Inorg. Chim. Acta, 107*, 127 (1985).

85XM X. Xin, N.L. Morris, G.B. Jameson, M.T. Pope, *Inorg. Chem., 24*, 3482 (1985).

86AF J.M. Arber, A.C. Flood, C.D. Garner, S.S. Hasnain and B.E. Smith, *J. Phys., Colloq.*, *2*, 1159 (1986).

86KM C.A. Kelleher, and J. Mason, *Int. J. Biochem.*, *18*, 629 (1986).

86LP S. H. Laurie, D. E. Pratt and J.B. Raynor, *Inorg. Chim. Acta*, *123*, 193 (1986).

86M J. Mason, *Toxicology*, *42*, 99 (1986).

87A W.M. Allen, in *'Copper in Animals and Man'*, Vol.2, J. McC. Howell and J.M. Gawthorne eds., CRC Press, Boca Raton, Florida (1987) p. 123.

87AG J.D. Allen and J.M. Gawthorne, *Br. J. Nutr.*, *58*, 265 (1987).

87AK R.J. Anglin, D.M. Kurtz Jr., S. Kim and R.A. Jacobson, *Inorg. Chem.*, *26*, 1470 (1987).

87BD R.J. Boila, T.J. Devlin and K.M. Wittenberg, *Can. J. Anim. Sci.*, *67*, 869 (1987).

87BR L.J. Berliner and J. Reuben, *'Biological Magnetic Resonance'*, Vol. 9, Plenum Press, New York (1987).

87C K.A. Connors, *'Binding Constants'*, J. Wiley and Sons, New York (1987).

87CA J. Chandrasekaran, M.A. Ansari and S. Sarkar, *J. Less-Common Met.*, *134*, L23 (1987).

87CL N.J. Clarke and S.H. Laurie, *Inorg. Chim. Acta*, *130*, 79 (1987).

87CLa N.J. Clarke, S.H. Laurie and D.E. Pratt, *Inorg. Chim. Acta* , *138*, 103 (1987).

87D A.E. Derome, *'Modern NMR Techniques for Chemistry Research'*, Pergamon Press, Oxford (1987).

87DL E. Delhaize, J.F. Loneragan and J. Webb, in *'Copper in Animals and Man'*, Vol 1., J.M. Howell and J.M. Gawthorne eds., CRC Press, Boca Raton, Florida (1987) p. 1.

87DM E. Diemann and A. Müller, in *'Comprehensive Coordination Chemistry'*, Vol. 2, G. Wilkinson, R.D. Gillard, and J. McCleverty eds., Pergamon Press, Oxford (1987) p. 559.

87G C. D. Garner, in '*Comprehensive Coordination Chemistry*', Vol. 3, G. Wilkinson, R.D. Gillard, and J. McCleverty eds., Pergamon Press, Oxford (1987) p. 1421.

87Ga J. M. Gawthorne, in '*Copper in Animals and Man*' J. M. Howell and J.M. Gawthorne eds., CRC Press, Boca Raton, Florida (1987) p. 79.

87H B. J. Hathaway, in '*Comprehensive Coordination Chemistry*', Vol. 5, G. Wilkinson, R. D. Gillard and J. McCleverty eds., Pergamon Press, Oxford (1987) p. 533.

87Ha M. N. Hughes, in '*Comprehensive Coordination Chemistry*', Vol. 6, G. Wilkinson, R.D. Gillard and J.A. McCleverty, eds., Pergamon Press, Oxford (1987) p. 541.

87HL H.E. Howard-Lock and C.J.L. Lock, "*Comprehensive Coordination Chemistry*", Vol. 6, G. Wilkinson, R.D. Gillard and J. McCleverty eds., Pergamon Press, Oxford (1987) p. 755.

87L S. H. Laurie, in "*Comprehensive Coordination Chemistry*", Vol. 2., G. Wilkinson, R.D. Gillard and J.A. McCleverty, eds., Pergamon Press, Oxford (1987) p. 740.

87LP C. Livera, L.D. Pettit, M. Bataille, B. Perly, H. Kozlowski and B. Radomska, *J. Chem. Soc. Dalton Trans.*, 661 (1987).

87PM C. Potvin, J.M. Manoli, F. Sêcheresse and S. Marzak, *Inorg. Chim. Acta, 134*, 9 (1987).

87PMa C. Potvin, J.M. Manoli, F. Sêcheresse, and S. Marzak. *Inorg. Chem., 26*, 4370 (1987).

87PW J. Price, M.A. Will, G. Paschaleris, and J.K. Chester, *Br. J. Nutr. 58*, 127 (1987).

87RK B. Radomska, T. Kiss and I. Sóvágó, *J. Chem. Res., Synop, 5,* 156 (1987).

87SH J.K.M. Sanders and B.K. Hunter, '*Modern NMR Spectroscopy*', Oxford University Press, Oxford (1987).

87SP I. Sóvágó and G. Petöcz, *J. Chem. Soc. Dalton Trans.*, 1717 (1987).

87UI J. Udo, N. Ikota, A. Hanaki and K. Koga , *Inorg. Chim. Acta, 135*, 43 (1987).

87V P.J. S. Van Soest, *'Nutritional ecology of the ruminants'*, Comstock Publishing Associates, London (1987).

87WM M. Woods and J. Mason, *J. Inorg. Biochem.*, *30*, 261 (1987).

88CA J. Chandrasekaran, M.A. Ansari and S. Sarkar, *Inorg. Chem.*, *27*, 3663 (1988).

88ML J. Mason, M. Lamand, J.C. Tressol and G. Mulryan, *Br. J. Nutr.*, *59*, 289 (1988).

88MP J. M. Manoli, C. Potvin, F. Secheresse and S. Marzak, *Inorg. Chim. Acta*, *150*, 257 (1988).

88O N.H. Osman, PhD. Thesis, Lincoln College, Canterbury, New Zealand.

88RP R.S. Reid and B. Podányi, *J. Inorg. Biochem.*, *32*,183 (1988).

88RPa R.S. Reid and B. Podányi, *J. Am. Chem. Soc.*, *110*, 3805 (1988).

88VK A. Vogler and H. Kunkely, *Inorg. Chem.*, *27*, 504 (1988).

88W R.C. Weast, ed., *'CRC Handbook of Chemistry and Physics'*, CRC Press, Boca Raton, Florida (1988).

88WM Z.Y. Wang and J. Mason, *J. Inorg. Biochem.*, *33*, 19 (1988).

89EA B.D. El-Issa, A.A. M. Ali and H. Zanati, *Inorg. Chem.*, **28**, 3297 (1989).

89CT D. Coucouvanis, A. Toupadakis, S.-M. Koo and A. Hadjikyriacou, *Polyhedron*, *28*, 1705 (1989).

89GB S.R. Gooneratne, W.T. Buckley and D.A. Christensen, *Can. J. Anim. Sci.*, *69*, 819 (1989).

89GL S.R. Gooneratne, B. Laarveld, R.K. Chaplin, and D.A. Christensen, *Br. J. Nutr.*, *61*, 355 (1989).

89GLa S.R. Gooneratne, B. Laarveld, R.K. Chaplin, and D.A. Christensen, *Br. J. Nutr.*, *61*, 373 (1989).

89MM J. Mason, G. Mulryan, M. Lamand and C.Large, *J. Inorg. Biochem.*, *35*, 115 (1989)

90B K. Burger, *'Biocoordination Chemistry'*, Ellis Horwood, New York (1990).

90BB L. Banci, I. Bertini, P. Caliceti, L.M. Scolato, O. Schiavon and F.M. Veronese, *J. Inorg. Biochem.*, *39*, 149 (1990).

90CB D. Chakraborty and P. K. Bhattacharya, *J. Inorg. Biochem.*, *39*, 1 (1990).

90CH C.L. Coyle, M.A. Harmer, G.N. George, M. Daage and E.I. Stiefel, *Inorg. Chem.*, *29*, 14 (1990).

90M J. Mason, *Ir. Vet. J.*, *43*, 18 (1990)

90NS H. Nakatsuji and M. Sugimoto, *Inorg. Chem.*, *29*, 1221 (1990).

90PP L.D. Pettit, S. Pyburn, W. Bal, H. Kozlowski and M. Bataille, *J. Chem. Soc. Dalton Trans.*, 3565 (1990).

90SS B.R. Srinivason and S. Sarkar , *Inorg. Chem.*, *29*, 3898 (1990).

90TC R. Tauler, J. F. Cid, and E. Casassas, *J. Inorg. Biochem.*, *39*, 277 (1990).

90ZF A. Zgirski and E. Frieden, *J. Inorg. Biochem.*, *39*, 137 (1990).

91DZ P.G. Daniele, O. Zerbinati, V. Zelano, G. Ostacoli, *J. Chem. Soc. Dalton Trans.*, 2711 (1991).

91FW J.J.R. Frausto da Silva and R.J.P. Williams, *'The Biological Chemistry of Elements'*, Clarendon Press, Oxford (1991).

91J J. Jones, *'The Chemical Synthesis of Peptides'*, Clarendon Press, Oxford (1991).

91L M.C. Linder, *'Biochemistry of Copper'*, Plenum Press, New York (1991).

91NR B. Nosal and D.L. Rabenstein, *J. Phys. Chem.*, *95*, 4761 (1991).

91S N.F. Suttle, *Annual Rev. Nutr.*, *11*, 121 (1991).

92BB S.W.A. Bligh, H.A. Boyle, A.B. McEwen, P.J. Sadler and R.H. Woodham, *Biochem. Pharmacol.*, *43*, 137 (1992).

92BC H. Bergmann, B. Czeska, I. Haas, B. Mohsin and K-H. Wander, in *'Gmelins Handbook of Inorganic and Organometallic Chemistry'*, 8th Edn., Supplement Vol B7, G. Czack, H. Katscher, G. Kirschstein and E. Warkentin eds., Springer-Verlag, Berlin (1992).

92CL R. Cao, X. Lei, M. Hong, Z. Huang and H. Liu, *Jiegou Huaxue* **11**, 34 (1992); CA 117:82318f.

92G P. Gans, *'Data Fitting in the Chemical Sciences'*, J. Wiley and Sons, New York (1992).

92SC M.E. Smart, N.F. Cymbaluk and D.A. Christensen, *Can. Vet. J.*, *33*, 163 (1992).

92ST S.B. Sharma and I.N. Tewari, *Synth. React. Inorg. Met.-Org. Chem.*, *22*, 217 (1992).

93BN R.P. Bonomo, F. Bonsignore, E. Conte, G. Impellizzeri, G. Pappalardo, R. Purrello and E. Rizzrelli, J. *Chem Soc. Dalton Trans.*, 1295 (1993).

93MB F-X. Maquart, G. Bellon, B. Cahquor, J. Wegrowski, L.M. Patt, R.E. Trachy, J-C. Monboisse, F. Chastang, P. Birembaut, P. Gillery, and J-P. Borel, *J. Clin. Invest.*, *92*, 2368 (1993).

93PC N.N. Polushin, B-C. Chen, L.W. Anderson and J.S. Cohen, *J. Org. Chem.*, *58*, 4606 (1993).

93SF I. Sóvágó, E. Farkas, C. Bertalan, A. Lebkiri, T. Kowalik-Jankowska, and H. Kozlowki *J. Inorg. Biochem.*, *51*, 715 (1993).

94C G.D. Christian, *'Analytical Chemistry'*, 5th Edn., J. Wiley and Sons, New York (1994).

94GH T. Gajda, B. Henry and J-J. Delpuech, *J. Chem. Soc. Perkin Trans. 2.*, 157 (1994).

94HL H. Hou, J. Lang, J. Li and X. Xin, *Wuji Huaxue Xuebao 10*, 218 (1994); CA 121:314251s.

94LN V. Lakshmanan, K.S. Nagaraja, and M.R. Udupa, *Indian J. Chem.*, *33*, 772 (1994).

94ML A. McQuaid, M. Lamand, and J. Mason, *J. Inorg. Biochem. 53*, 191 (1994).

94STV P.J. Sadler, A. Tucker, and J. H. Viles, *Eur. J. Biochem.*, *220*, 193 (1994).

95B G. Berthon ed., *'Handbook of Metal-Ligand Interactions in Biological Fluids, Bio-inorganic Chemistry'*, Vol.1, Marcel Dekker, New York (1995).

95BK W. Bal, H. Kozlowski, R. Robbins and L.D. Pettit, *Inorg. Chim. Acta, 231*, 7 (1995).

95BJ W. Bal, M. Jezowska-Bojczuk, H. Kozlowski, L. Chruscinki, G. Kupryszewski, B. Witczuk, *J. Inorg. Biochem., 57*, 235 (1995).

95BM I. Bertini, L. Messori and M.S. Viezzoli, in *"Handbook of Metal-Ligand Interactions in Biological Fluids"*, Vol.1, G. Berthon ed., Marcel Dekker Inc., New York (1995) p. 156.

95BW P. M. Boorman, M. Wang and M. Parvez, *J. Chem. Soc. Chem. Commun.* 999 (1995).

95H M. A. Hetherington, Msc. Dissertation, University of Saskatchewan, Saskatchewan (1995)

95HS C. Harford and B. Sarkar, in '*Handbook of Metal-Ligand Interactions in Biological Fluids*' Vol. 1, G. Berthon ed., Marcel Dekker, Inc. New York (1995) p. 405.

95L P.W. Linder, in '*Handbook of Metal-Ligand Interactions in Biological Fluids*', Vol. 1, G. Berthon, ed., Marcel Dekker, Inc. New York (1995) p. 524.

95LW D.J. Leggett and G.G. Wu, in '*Handbook of Metal-Ligand Interactions in Biological Fluids*', Vol. 1, G. Berthon ed., Marcel Dekker, Inc. New York (1995) p. 533.

95MS M.R. McDonald, W.M. Scheper, H.D. Lee and D.W. Margerum, *Inorg. Chem., 34*, 229 (1995).

95RD C.C. Raymond, P.K. Dorhout and S.M. Miller, *Z. Kristallogr., 210*, 775 (1995).

95SO K.T. Suzuki, Y. Ogra and M. Ohmichi,, *J. Trace Elements Med. Biol., 9* 170 (1995).

96AC G. Allen and R. O. Campbell, *Int. J. Peptide Protein Res., 48*, 265 (1996).

96AR M. A. Attaelmannan and R.S. Reid, *J. Inorg. Biochem., 64*, 215 (1996).

96GH T. Gajda, B. Henry, A. Aubry and J-J. Delpuech, *Inorg. Chem. 35*, 586 (1996).

96H J.M. Hollas, *'Modern Spectroscopy'*, 3rd Edn., Wiley, New York (1996).

96HN C. Harford, S. Narindrasorasak and B. Sarkar, *Biochem. 35*, 4271 (1996).

96HW Q. Huang, X.-T. Wu, Q.-M Wang, T.-L. Sheng and J.-X. Lu, *Inorg. Chem., 35*, 893 (1996).

96HX H.-W. Hou, X.-Q. Xin and S. Shi, *Coord. Chem. Rev., 153*, 25 (1996).

96LH X.G. Luo, P.R. Henry, C.B. Ammerman and J.B. Madison, *Anim. Feed Sci. Technol., 57*, 281 (1996).

96OO Y. Ogra, M. Ohmichi and K.T. Suzuki, *Toxicology, 106*, 75 (1996).

96RK J. F. Rusling and T.F. Kumosinski, *'Nonlinear Computer Modeling of Chemical and Biochemical Data'*, Academic Press, San Diego (1996).

96TA J-C. Truffert, U. Asseline, A. Brack, N.T. Thuong, *Tetrahedron, 52*, 3005 (1996).

96TS H. Teruel and A. Sierralta, *Polyhedron, 15*, 2215 (1996).

96WH D. Wu, M. Hong, R. Cao and H. Liu, *Inorg. Chem., 35*, 1080 (1996).

96WS J.D. Ward, J.W. Spears and E.B. Kegley, *J. Dairy Sci., 79*, 127 (1996).

97DH D. Diamond and V.C.A. Hanratty, *'Spreadsheet Applications in Chemistry using Microsoft Excel'*, J. Wiley and Sons, New York (1997).

97GC H. Galbraith, W. Chigwada, J.R. Scaife and W.R. Humphries, *Anim. Feed Sci.Technol., 67*, 83 (1997).

97H E.D. Harris, in *'Handbook of Nutrionally Essential Mineral Elements'* B.L. O'Dell and R.A. Sunde eds., M. Dekker, New York (1997) p.231.

97HS C. Harford and B. Sarkar, *Acc. Chem. Res., 30*, 123 (1997).

97KS W. Kaim and B. Schwederski, *'Bioinorganic Chemistry: Inorganic Elements in the Chemistry of Life'*, J. Wiley and Sons (1997).

97IP P. Ilankumaran, K.R. Prabhu and S. Chandrasekaran, *Synth. Commun., 27*, 4031 (1997).

97L S.G. Lieb, *J. Chem. Ed., 74*, 1008 (1997).

97MF M.R. McDonald, F.C Fredericks and D.W. Margerum, *Inorg. Chem.*, *36*, 3119 (1997).

97SS D. Sellmann and J. Sutter, *Acc. Chem. Res.*, *30*, 460 (1997).

97TH P. Tsiveriotis, N. Hadjiliadis and I. Sóvágó, *J. Chem. Soc. Dalton Trans.*, 4267 (1997).

97UH J. Ueda, A. Hanaki, N. Yoshida and T. Nakajima, *Chem. Pharm. Bull.*, *45*, 1108 (1997).

97ZA T.J. Zielinski and R.D. Allendoerfer, *J. Chem. Ed.*, *74*, 1001 (1997).

97ZH H. Zhu, X. Huang, Y. Deng, D. Wu, C. Chen and Q. Liu, *Inorg. Chim. Acta*, *256*, 29 (1997).

98A M. A. Attaelmannan, PhD dissertation, University of Saskatchewan (1998).

98BJ K. Beck-Piotraschke and H.-D. Jakubbe, *Tetrahedron*, *9*, 1505 (1998).

98BP M. Beltrán, E. Pedroso and A. Grandas, *Tetrahedr. Lett.*, *39*, 4115 (1998).

98C D. Coucouvanis, *Adv. Inorg. Chem.*, *45*, 1 (1998).

98CD R.S. Czernuszewicz, B.C. Dave and J.P. Germanas, in '*Spectroscopic Methods in Bioinorganic Chemistry*', E. I. Solomon and K. O. Hodgson, eds., American Chemical Society Symposium Series # 692, Washington DC (1998) p. 220.

98CM S. Curry, H. Mandelkow, P. Brick and N. Franks, *Nat. Struct. Biol.*, 5, 827 (1998).

98CW S.P. Cramer, H. Wang, C. Bryant, M. Legros, C. Horne, D. Patel, C. Ralston and X. Wang, in "*Spectroscopic Methods in Bioinorganic Chemistry*", E. I. Solomon and K. O. Hodgson, eds., American Chemical Society Symposium Series # 692, Washington DC (1998) p. 154.

98EH T. Ecclestone, I. Harvey, S.H. Laurie, M.C.R. Symons and F.A. Taiwo, *Inorg. Chem. Commun.*, *1*, 460 (1998).

98EL T. Ecclestone, S.H. Laurie, M.C.R. Symons and F.A.Taiwo, *Polyhedron*, *17*, 1435 (1998).

98GD C.A. Grapperhaus and M.Y. Darensburg, *Acc. Chem. Res.*, *31*, 451 (1998).

98GS J. Guo, T. Sheng, Z. Tianlu, W. Wenjian, L. Xintao, P. Lin, Q. Wang, and J. Lu, *Inorg. Chem.*, *37*, 3689 (1998).

98LT J-P. Lang and K. Tatsumi, *Inorg. Chem.*, *37*, 6308 (1998).

98LK J-P. Lang, H. Kawaguchi, S. Ohnishi and K. Tatsumi, *Inorg. Chim. Acta*, *283*, 136 (1998).

98MS A.E. Martell, R.M. Smith and R.J. Motekaitis, "*NIST Standard Reference Database 46: Critically Selected Stability Constants of Metal Complexes Database*", Version 5.0, National Institute of Standards and Technology, Gaithersburg, MD (1998).

98OS Y. Ogra and K.T. Suzuki, *J. Inorg. Biochem.*, *70*, 49 (1998).

98RA R.S. Reid and M.A. Attaelmannan, *J. Inorg. Biochem.*, *69*, 59 (1998).

98W F.A. Walker, in '*Spectroscopic Methods in Bioinorganic Chemistry*', E. I. Solomon and K. O. Hodgson, eds., American Chemical Society Symposium Series # 692, Washington DC (1998) p. 30.

99CP Y. Chen, R. Pasquinelli, M. Ataai, R.R. Koepsel, T.W. Stringfield, R.E. Shepherd, *J. Inorg. Biochem.*, *76*, 211 (1999).

99CW F. A. Cotton, G. Wilkinson, C.A. Murillo and M. Bochmann, 'Advanced Inorganic Chemistry' 6th Edn., J. Wiley and Sons, New York (1999).

99EN J. Ellermeier, C. Näther and W. Bensch, *Acta Crys C.*, *55*, 1748 (1999).

99OH E. Ohyoshi, Y. Hamada, K. Nakata and S. Kohata, *J. Inog. Biochem.*, *75*, 213 (1999).

99OK Y. Ogra, Y. Komada and K.T. Suzuki, *J. Inorg. Biochem.*, *75*, 199 (1999).

99PD E. Prenesti, P.G. Daniele, V. Zelano and M. Gulmini, *Annali di Chim.*, *89*, 1 (1999).

99S B. Sarkar, *Chem. Rev.*, *99*, 2536 (1999).

99SKa S. Sugio, A. Kashima, S. Mochizuki, M. Noda and K. Kobayashi, *Protein Eng.*, *12*, 439 (1999).

99T J.R. Turnlund, in *'Modern Nutrition in Health and Diseases'*, 9th Edn., M.E. Shills, J.A. Olson, M. Shike and A.C. Ross, Lippincott Williams and Wilkins, Philadelphia (1999) p. 241.

00BC S. Bruni, F. Cariati, P.G. Daniele and E. Prenesti, *Spectrochim. Acta A*, *56*, 815 (2000).

00CO D. Coucouvanis, N. Ockwig, G. Brewer and S. Merjver, *"Methods and Compositions for the Protection or Treatment of Cancer"*, Patent # WO0013712, USA (2000).

00EH B.E. Erickson and G. R. Helz, *Geochimica et Cosmochimica Acta*, *64*, 1149 (2000).

00L S.H. Laurie, *Eur. J. Inorg. Chem.*, 2443 (2000).

00OC Y. Ogra, H. Chikusa and K. T. Suzuki, *J. Inorg. Biochem.*, *78* , 123 (2000).

00VS K. Várnagy, J. Szabó, I. Sóvágó, G. Malandrinos, N. Hadjiliadis, D. Sanna and G. Micera, *J. Chem. Soc. Dalton Trans.*, 467 (2000).

01BH C.A. Beheshti, S.M. Hosaini, *Polyhedron*, *20*, 179 (2001).

01KW N.L. Kruhlak, M. Wang, P.M. Boorman, M. Parvez and R. McDonald, *Inorg. Chem.*, *40*, 3141 (2001).

01L D. R. Lide, Ed., *'CRC Handbook of Chemistry and Physics'*, 82nd Edn., CRC Press, Boca Raton, London (2001).

01MM A. Myari, G. Malandrinos, Y. Deligiannakis and J.C. Plakatouras, N. Hadjiliadis, Z. Nagy and I. Sòvágó, *J. Inorg. Biochem.*, *85*, 253 (2001).

01NK R. Nagane, T. Koshigoe, M. Chikira and E. C. Long, *J. Inorg. Biochem.*, *83*, 17 (2001).

01SV B.R. Srinivasan, B.R. Vernekar, K. Beena and K. Nagarajan, *Indian J. Chem. Sec A: Inorg., Bio-inorg., Phys., Theor. Anal. Chem.*, *40A (6)*, 563 (2001).

01T D. Thome, Msc. Dissertation, University of Saskatchewan (2001)

02MH M.E. Merrifield, Z. Huang, P. Kille and M.J. Stillman, *J. Inorg. Biochem.*, *88*, 153 (2002).

02KB S.K. Karathanasis, A.R. Bapat, E. Beer, R.A. Bhat, E. Ferris, M.J. Evans,

J. Zhang, R. Mastroeni and M.S. Scicchitano, Patent # WO 0212470, USA (2002)

APPENDIX I

Derivation of Equation5.5 (see Section 5.3.8.4)

The two main Cu(II)- complexed species of Asp-Thr(Ac)-His-Lys ($(HL)H_{-1}Cu$ and $(HL)H_{-2}Cu$), both involving the HL species of the peptide, can for simplicity be treated as one composite species, $Cu(HL)H_{-x}$ .This is simply called Cu(HL) in the derivation below. In this case, the following reaction scheme is implied:

$$HL \overset{K_{fl}}{\rightleftharpoons} Cu(HL)$$

The mass action equation for the above reaction is

$$K_{fl} = [Cu(HL)]/[Cu][HL] \quad \textbf{(1)}$$

Rearrangement gives

$$[HL] = [Cu(HL)]/([Cu].K_{fl}) \quad \textbf{(2)}$$

From the mass balance equations for the peptide (L), it can also be deduced that

$$[HL] = \{C_L - [Cu(HL)]\}.\alpha_{HL} \quad \textbf{(3)}$$

where C_L is the analytical concentration of the peptide. (Hence, $\{C_L - [Cu(HL)]\}$is the concentration of ligand (in all acid-base forms) not complexed at equilibrium. On multiplying by the fraction of **this**, which is in the HL form, α_{HL}, the concentration at equilibrium of HL results.) Equating the right hand sides of (2) and (3) yields

$$[Cu(HL)]/([Cu].K_{fl}) = \{C_L - [Cu(HL)]\}.\ \alpha_{HL} \quad \textbf{(4)}$$

From the mass balance equation for Cu

$$[Cu(HL)] = C_{Cu} - [Cu] \quad \textbf{(5)}$$

Substituting (5) into (4) (twice) gives

$$\{C_{Cu} - [Cu]\}/\{[Cu].K_{fl}\} = \{C_L - C_{Cu} - [Cu]\}.\ \alpha_{HL} \quad \textbf{(6)}$$

Multipling through Equation 6 by $[Cu]K_{fl}/\alpha_{HL}$ gives

$$\{C_{Cu} - [Cu]\}/\ \alpha_{HL} = \{C_L - C_{Cu} - [Cu]\}.\ [Cu].K_{fl} \quad \textbf{(7)}$$

Grouping of terms in [Cu] generate the quadratic equation in [Cu] (Equation 8 below, which is the same as Equation 5.5).

$$[Cu]^2.K_f + [Cu]\{1/\alpha_{HL} + K_f(C_L\text{-}C_{Cu})\} - C_{cu}/\alpha_{HL} = 0 \quad \textbf{(8)}$$

Note that as K_{fl} tends to infinity, the two terms in α_{HL} become negligible, and Equation 8 reduces to

$$[Cu]^2K_{fl} + [Cu]\{K_{fl}C_L - K_{fl}C_{Cu}\} = 0 \quad \textbf{(9)}$$

Dividing both sides by by $[Cu]K_{fl}$ and rearranging gives

$$[Cu] = C_{Cu} - C_L \quad \textbf{(10)}$$

This confirms that when K_{fl} is large, the behaviour of the system does not depend on the actual value of K_{fl}. This is what was observed; see Section 5.3.8.4.